2015-08-14

Investigating the Effects of Mutant FUS on Stress Response in Amyotrophic Lateral Sclerosis: A Thesis

Laura J. Kaushansky
University of Massachusetts Medical School

INVESTIGATING THE EFFECTS OF MUTANT FUS ON STRESS RESPONSE IN AMYOTROPHIC LATERAL SCLEROSIS

A Thesis Presented

By

LAURA JANE POTHIER KAUSHANSKY

Submitted to the faculty of the

University of Massachusetts Graduate School of Biomedical Sciences, Worcester

In partial fulfillment of the requirement for the degree of

MASTER OF SCIENCE

August 14, 2015

BIOCHEMISTRY AND MOLECULAR PHARMACOLOGY

INVESTIGATING THE EFFECTS OF MUTANT FUS ON STRESS RESPONSE IN AMYOTROPHIC LATERAL SCLEROSIS

A Masters Thesis Presented By Laura Jane Pothier Kaushansky

The signatures of the Dissertation Defense Committee signify Completion and approval as to style and content of the Dissertation

_____
Elisabet Mandon, Ph.D., Member of Committee

_____
Mary Ellen Lane, Ph.D., Member of Committee

The signature of the Chair of the Committee signifies that the written dissertation meets the requirements of the Masters Committee

_____
Eric Baehrecke, Ph.D., Chair of Committee

The signature of the Dean of the Graduate School of Biomedical Sciences signifies that the student has met all graduation requirements of the School

_____
Anthony Carruthers, Ph.D. Dean of the Graduate School of Biomedical Sciences

Biochemistry and Molecular Pharmacology, August 14, 2015

To my husband and lifelong buddy.

ACKNOWLEDGEMENTS

"Put your best foot forward."

I thank my graduate mentor, Daryl, for her guidance and influence over my years in graduate school. Daryl has taught me how to think critically as a scientist and scholar, and her work ethic is a driving inspiration in my everyday life. Her guidance is so broadly applicable that I will try to make choices with her words and actions in mind for the rest of my life. Daryl is not only brilliant, but she is also a bone-deep caring person. During very difficult times, Daryl supported me unflinchingly, even while she gave necessary constructive criticism. It is not always easy to do that on top of running the kind of tight ship that academic science requires of a principle investigator, and I was lucky to have her as a mentor. Her energy and passion inspires me to live by my own values and sail my own ship, and I will never forget the lessons she has bestowed upon me. She is a superstar.

I would also like to thank the members of my TRAC and thesis advisory committee for their mentoring and guidance throughout the years: Dr. Eric Baehrecke, Dr. Elisabet Mandon, Dr. Mary Munson, and Dr. Allan Jacobson. Additionally, thank you to Dr. Victor Ambros for serving on my qualifying exam committee. Your time and guidance is very much appreciated.

"Pro-tip!"

I also thank my lab mates and peers, who have been a source of comfort, encouragement, and perspective through the challenges of graduate school. They understand most of all what it takes to be a graduate student in training, having lived by my side through it, and I would not have learned nearly as much without their company at the bench every day. Thank you to Dr. Desiree Baron, my early morning good friend and always-thoughtful colleague, who supported me with strong doses of both research excitement and heartening family surroundings. Thank you to Drs. Catherine Ward, Reddy Sama and Melissa Rotunno, my surrogate big siblings, whose maturation over the years was a beautiful and inspiring sight to behold. Thank you to Sivakumar Boopathy and Eric Schmidt, my lab brothers, who provided such lovely, amiable company during nights, weekends, and coffee runs. Thank you to Maeve Tischbein, my "little" lab sister who is anything but little in heart and mind and who has been an emotional support more times than I can count. Lastly, thank you to Bill Monis, Marina Paul and Ly-sha Ee, who I was lucky enough to have sat next to during orientation and who will always be my friends. Thank you to the rest of the 6th floor of the Albert Sherman Center, in whom I hold great regard and affection.

~Hurricane Kaushansky~

I thank my wonderful family-in-law, Ken and Lauren, Fran, Alexis and Josh H., and Howie and Colleen, who have provided so much unadulterated intellectual and spiritual support to me over the years. They are all such wonderful people, and they have shown me a bedrock of happy, good-natured, culture-minded, industrious living that my husband and I thrive on. Thank you for loving me, and thank you for raising the guy at the end of this section. ☺

~The Pothier Clan~

I could not have had the gumption to attempt higher education without the unwavering support of my family. I am the descendant of a line of strongly bonded, truly loving, blue-collar Bostonian people. I grew up around over 25 uncles and aunts and at least as many cousins, and I never lacked companionship. From an early age, I was shown by my father Lee, my mother Amy, my two real-life sisters Kerry and Rachel, and more recently from my brothers-in-law Chris and Mathew that I am worthy of pursuing any path I choose, even if it extends beyond the borders of what my family has experienced. Because of the sacrifices my parents made to get us into a good school system, I have lived in and fallen in love with lands on the other side of the earth, experienced the calming ecstasy of comprehending the basics of quantum mechanics, marveled at growing flowers with a world-altering biology lens, read befuddling and heart-arresting literature, sung like a bird at Boston Symphony Hall, met, understood and loved truly “other-worldly” people, saved stories to inspire my nieces and nephews, and had the rare, freeing opportunity to change my mind. Thanks to my parents’ selflessness, my sisters and I were the first generation to go to college, and I am the most advanced educationally of anyone in my extended family. They remind me that this is something to be proud of, and I remind them through my gratitude here that education and career paths are not the only marks of an admirable life. To the electricians, childcare providers, technicians, housewives, secretaries, masons, welders, painters, and the many, many nurturers of my life, I love you all.

“Good morning, pretty lady.”

Finally, and very importantly, I thank my husband Josh. He has steadily seen me through years of hard work, long hours, missed vacations, incomprehensible data-babble, tears of frustration, tears of joy, and the countless conversations in between these moments that have lined my time in graduate school. The entire time, he has loved me for who I am, not for who I might be someday. We have gotten married, restored a house, lost some loved ones, but gained a life together since I started at UMass, and there is no one on Earth who has supported me more than Josh while I have trained. There is no one to whom I am more thankful. I love you, Bub.

ABSTRACT

During stress, eukaryotes regulate protein synthesis in part through formation of cytoplasmic, non-membrane-bound complexes called stress granules (SGs). SGs transiently store signaling proteins and stalled translational complexes in response to stress stimuli (e.g. oxidative insult, DNA damage, temperature shifts and ER dysfunction). The functional outcome of SGs is proper translational regulation and signaling, allowing cells to overcome stress.

The fatal motor neuron disease Amyotrophic Lateral Sclerosis (ALS) develops in an age-related manner and is marked by progressive neuronal death, with cytoplasmic protein aggregation, excitotoxicity and increased oxidative stress as major hallmarks. Fused in Sarcoma/Translocated in Liposarcoma (FUS) is an RNA-binding protein mutated in ALS with roles in RNA and DNA processing. Most ALS-associated FUS mutations cause FUS to aberrantly localize in the cytoplasm due to a disruption in the nuclear localization sequence. Intriguingly, pathological inclusions in human FUS-ALS cases contain aggregated FUS as well as several SG-associated proteins. Further, cytoplasmic mutant FUS incorporates into SGs, which increases SG volume and number, delays SG assembly, accelerates SG disassembly, and alters SG dynamics.

I posit that mutant FUS association with stress granules is a toxic gain-of-function in ALS that alters the function of SGs by interaction with SG components. Here, I show that mutant FUS incorporates in to SGs via its C-terminal RGG motifs, the methylation of which is not required for this localization. Further, I identify protein interactions specific to full-length mutant FUS under stress conditions that are potentially capable of interacting with FUS in SGs. Finally, I demonstrate a potential change in the protein composition of SGs upon incorporation of mutant FUS. These findings advance the field of ALS and SG biology, thereby providing groundwork for future investigation.

TABLE OF CONTENTS

LIST OF TABLES

CHAPTER III

APPENDIX I

LIST OF FIGURES

CHAPTER I

CHAPTER II

LIST OF THIRD PARTY COPYRIGHTED MATERIAL

The following chapter contains material that was reproduced from Journals:

	Publisher
CHAPTER III	BioMed Central

The following appendices were reproduced from journals: No permission required:

	Publisher	**License number**
APPENDIX III	John Wiley and Sons	3335921094006
APPENDIX IV	BioMed Central	n/a

LIST OF ABBREVIATIONS

AdOx – Adenosine-2',3'-dialdehyde
ALS – Amyotrophic lateral sclerosis
ER – Endoplasmic reticulum
EWS – Ewing sarcoma
FALS – Familial amyotrophic lateral sclerosis
FET – FUS, EWS, TAF15
FTLD – Frontotemporal lobar degeneration
FUS or FUS/TLS – Fused in sarcoma/Translocated in liposarcoma
Gly-rich – Glycine-rich
G3BP – GTPase activating protein (SH3 domain) binding protein 1
hnRNP – Heterogeneous ribonuclear protein
LMN – Lower motor neuron
NLS – Nuclear localization signal
PB – P-body
PFN1 – Profilin 1
PRMT – Protein methyl arginine transferase
QGSY – Glutamine-glycine-serine-tyrosine-rich
RRM – RNA recognition motif
RGG – Arginine-glycine-glycine
SALS – Sporadic amyotrophic lateral sclerosis
SDS-PAGE – Sodium dodecyl sulfate-polyacrylamide gel electrophoresis
SOD1 – Cu/Zn superoxide dismutase 1
SA – Sodium arsenite
TAF15 or TAFII68 – TATA box binding protein associated factor 68 kDa
TARDBP or TDP-43 – Transactive response DNA binding protein 43
TET – TLS, EWS, TAF15
TIAR – TIA1-related protein
UMN – Upper motor neuron
ZF – Zinc-finger domain

Proteomics hits:
ATXN2 – Ataxin-2
UBP10 – Ubiquitin carboxyl-terminal hydrolase 10
NUFP2 – Nuclear fragile X mental retardation-interacting protein 2
F120A – Constitutive coactivator of PPAR-gamma-like protein 1
RHOA – Transforming protein RhoA
PUM1 – Pumilio homolog 1
LARP1 – La-related protein 1
PURB – Transcriptional activator protein Pur-beta
RENT1 – Regulator of nonsense transcripts 1
CYC – Cytochrome c

MCTS1 – Malignant T-cell-amplified sequence 1
PHS – Pterin-4-alpha-carbinolamine dehydratase
YTHD3 – YTH domain-containing family protein 3
UBP2L – Ubiquitin-associated protein 2-like
FA98A – Protein FAM98A
ERF3A – Eukaryotic peptide chain release factor GTP-binding subunit ERF3A
FMR1 – Fragile X mental retardation protein 1
FXR1 – Fragile X mental retardation syndrome-related protein 1
FXR2 – Fragile X mental retardation syndrome-related protein 2
MOV10 – Putative helicase MOV-10
ATX2L – Ataxin-2-like protein
MSI1H – RNA-binding protein Musashi homolog 1
MSI2H – RNA-binding protein Musashi homolog 2
G3BP2 – Ras GTPase-activating protein-binding protein 2
PURA – Transcriptional activator protein Pur-alpha
IF2B2 – Insulin-like growth factor 2 mRNA-binding protein 2
IF2B3 – Insulin-like growth factor 2 mRNA-binding protein 3
G3BP1 – Ras GTPase-activating protein-binding protein 1
IF2B1 – Insulin-like growth factor 2 mRNA-binding protein 1
PABP4 – Polyadenylate-binding protein 4
YBOX1 – Nuclease-sensitive element-binding protein 1n

PREFACE

Parts of this dissertation appeared in:

Baron, D. M. *et al.* Amyotrophic lateral sclerosis-linked FUS/TLS alters stress granule assembly and dynamics. *Molecular Neurodegeneration* **8,** 1–1(2013).

Parts of this dissertation appeared in:

Sama, R. R. *et al.* FUS/TLS assembles into stress granules and is a prosurvival factor during hyperosmolar stress. *Journal of Cellular Physiology* (2013). doi:10.1002/jcp.24395

CHAPTER I:

INTRODUCTION

AMYOTROPHIC LATERAL SCLEROSIS

Discovery and Clinical Symptoms

Amyotrophic lateral sclerosis (ALS), commonly known as Lou Gehrig's disease, was first described in the 19th century as a progressive and fatal neurodegenerative disease of the motor system (Charcot and Joffroy, 1869). Clinically, ALS is characterized by cumulative neurological deterioration of motor neurons. ALS varies in age of onset, site of disease onset, and rate of disease progression. The disease presents in one of the following ways: (a) *limb onset*, eventually affecting both the brain stem (upper motor neuron; UMN) and spinal cord (lower motor neuron; LMN); (b) *bulbar onset*, presenting with initial speech and swallowing impairments followed by limb features later in the course of the disease; (c) *primary lateral sclerosis*, with exclusive UMN involvement throughout disease duration; and (d) *progressive muscular atrophy*, with exclusive LMN involvement throughout disease duration (Traxinger et al., 2013). Patients most often present as limb onset (~70%) or bulbar onset (~25%), and a minority present with initial trunk or respiratory involvement (~5%) (Kiernan et al., 2011). Less typical presentations include weight loss, muscle fasciculation without weakness, unintentional laugher or crying, and frontal lobe-based cognitive dysfunction (Ferguson and Elman, 2007). Despite the clinical heterogeneity, half

of diagnosed patients die from complications of respiratory failure within 30 months of symptom onset, and ~20% die within 5-10 years. Median survival duration of ALS patients is 3–5 years. Bulbar onset, early respiratory presentation and older age at onset are associated with reduced survival, whereas limb onset disease and younger age at presentation are predictors of longer survival (Talbot, 2009).

Incidence and Distribution

There are 1 to 2 new cases of ALS per 100,000 people, with a total of ~5 per 100,000 total cases, each year in the United States. To put this math in perspective, the rate implies that 500,000 people alive in the U.S. today will someday die of ALS (Sreedharan and Brown, 2013).

The worldwide incidence of ALS is not known (Alappat, 2007), but ALS in Europe occurs at a rate 2.16 per 100,000 person-years based on population studies. The lifetime risk of ALS is 1:400 for women and 1:350 for men, and the peak age of onset is 58–63 years for SALS disease and 47–52 years for FALS disease. ALS presentation in people diminishes beyond 80 years of age, in contrast to Alzheimer's disease (Logroscino et al., 2010).

Environmental Risk Factors

Several environmental risk factors exist for ALS. For example, disease manifestation in adulthood may be driven, in part, by early life exposure to

infection. Evidence from a Swedish case-control study showed that exposure to younger siblings, and thus more frequent viral exposure, put people at a significantly increased risk of developing ALS (Fang et al., 2008).

Other environmental risk factors for ALS during developing years also exist, such as repeated exposure to physical impact. Specifically, participation in high impact sports increases the likelihood of developing ALS, as retrograde studies of Italian and British football players reveal (Chio et al., 2005; Harwood et al., 2009; Wicks et al., 2007). Active duty in the armed forces in the United States also correlates a higher incidence of ALS (Kasarskis et al., 2009).

In addition to internal stressors resulting from infection or injury, external toxin exposure is also linked to ALS. Cigarette smoking has a dose-dependent effect on the development of ALS (Gallo et al., 2009). Another neurotoxin, β-methyl-amino-L-alanine, was found in high concentrations in the brains of patients during a co-epidemic of ALS and Parkinson's on the island of Guam. This crisis was driven by consumption of flying foxes, which feed on cycad seeds enriched with the toxic amino acid derivative (Cox and Sacks, 2002). These studies therefore suggest a failure of recovery from toxic stress conditions as a potential risk factor for developing ALS.

Genetic Contributions

Like many other neurodegenerative diseases, the degenerating neurons of ALS patients are characterized by the accumulation of protein aggregates (Forman et al., 2004). Though the precise mechanisms of ALS pathogenesis are

still unknown, evidence implicates the disruption of molecular pathways by many genetic factors. As a whole, 90% of ALS cases are sporadic in nature (referred to as “SALS”), as patients present with no family history of the disease. The remaining 10% of cases are familial in nature (referred to as “FALS”) and present with Mendelian genetic inheritance. Currently, an identifiable genetic cause has been identified for 20% of SALS cases and 60% of FALS cases. Mutations in over 32 genes and genetic loci are now implicated in ALS pathogenesis (**Figure I.1**) (Sreedharan and Brown, 2013).

The first gene identified as causative in FALS was *SOD1* in 1993 (Rosen et al., 1993). Mutations in *SOD1* account for ~20% of FALS cases. The mechanism of SOD1-mediated motor neuron death is not yet understood, but current understanding links the mutations to a toxic gain of function of the SOD1 enzyme rather than a loss of function. Patients with *SOD1* mutations exhibit increased free radical levels. Further, *SOD1* mutations destabilize the SOD1 protein, resulting in intracellular aggregate formation that inhibits proteasomal function, disrupts axonal transport, and activates microglia (Bruijn et al., 1997; Bruijn et al., 1998; Rotunno and Bosco, 2013; Rotunno et al., 2014; Williamson and Cleveland, 1999; Zetterström et al., 2007).

Following the SOD1 discovery, genetic association studies and candidate gene screening identified rare ALS-related mutations in the *alsin*, senataxin (*SETX*), dynactin (*DCTN1*), and *VAPB* genes (Chance et al., 1998; Hadano et al., 2001; Nishimura et al., 2004; Puls et al., 2003; Yang et al., 2001).

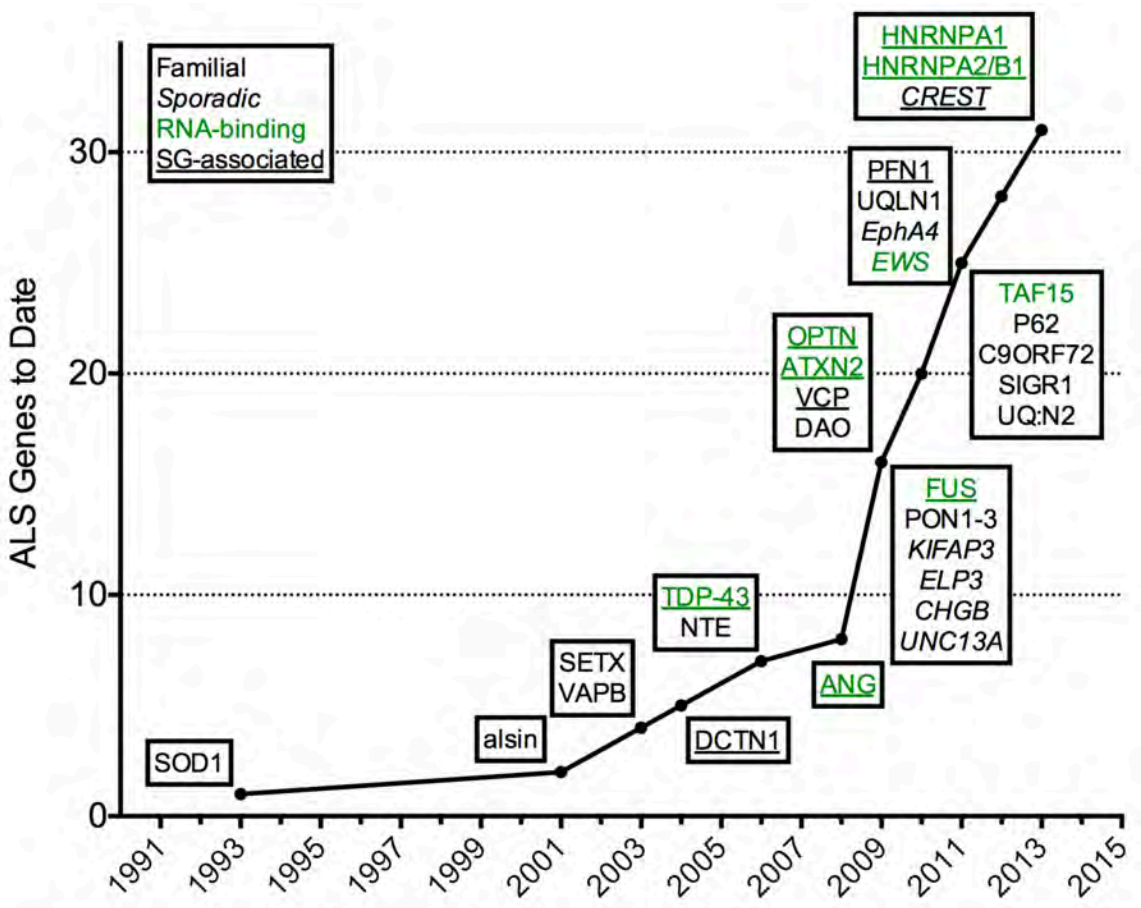

Figure I.1: Mutations in ALS genes to date. The rate of discovery of genes with mutations that cause amyotrophic lateral sclerosis is depicted on the y-axis versus year of discovery on the x-axis. Italics indicate that the gene is found in sporadic cases (SALS), whereas otherwise genes are familial in nature (FALS). Green indicates RNA-binding proteins, and Underline indicates stress granule-associated proteins. This figure was generated with inspiration from Sreedharan and Brown, 2013.

In 2006, a major milestone came with the identification of the RNA-binding protein, tar-DNA binding protein 43 (TDP-43), as the major component of the cytoplasmic protein inclusions in most ALS and FTLD cases (Arai et al., 2006; Neumann et al., 2006). Mutations in the TDP-43 gene (*TARDBP*) were reported two years later to cause ~4% of FALS (Kabashi et al., 2008; Sreedharan et al., 2008). Based on the homology between the *TARDBP* and the gene encoding the RNA-binding protein Fused In Sarcoma (FUS*)*, mutations in the *FUS* gene were subsequently identified in FALS patients in 2009. The FUS protein, also RNA-binding, was found in cytoplasmic inclusions in ALS patients with FUS mutations (Kwiatkowski et al., 2009; Vance et al., 2009) as well as in rare cases of TDP-43-negative FTLD (Munoz et al., 2009; Neumann et al., 2009a; 2009b). FUS is discussed in detail in a subsequent section.

TDP-43 and FUS were the first of several additional RNA-binding proteins discovered to cause ALS and other degenerative diseases (King et al., 2012). For example, wild-type TAF15 and EWSR1 are now associated with SALS, as they are aberrantly translocated and present as aggregate components in the cytoplasm of degenerating neurons (Couthouis et al., 2011; Couthouis et al., 2012; Neumann et al., 2011; Ticozzi et al., 2011).

Expanding on the RNA-focused class of FALS proteins, an abnormal intronic expansion of a hexanucleotide repeat (GGGGCC) in the *C9ORF72* gene was identified as a common genetic cause of both FTLD and ALS (DeJesus-Hernandez et al., 2011b; Gijselinck et al., 2012; Renton et al., 2011). These

intronic repeats are intriguingly translated into dipeptide repeat (DPR) proteins, leading to widespread neuronal aggregates of DPR proteins in C9orf72 mutations carriers (Mori et al. 2013 and Ash et al. 2013). In addition, the intronic DNA repeat forms G-quadruplexes, a strong binding motif for many RNA-binding proteins (Darnell, 2013).

Mutations in sequences encoding the prion-like domain of *hnRNPA1* and *hnRNPA2*/*B1* were further discovered to be connected with both FALS and SALS (Kim et al., 2013). These prion mutations introduce a steric zipper, which promotes self-complementary amyloid fibril formation (Sawaya et al., 2007) and accelerates hnRNPA1 and hnRNPA2/B1 misfolding (Kim et al., 2013). Finally, hnRNPA3 is mislocalized and forms cytoplasmic inclusions in ALS and FTLD cases harboring *C9ORF72* repeat expansions (Mori et al., 2013). Collectively, these findings implicate RNA-binding proteins as major players in neurodegenerative disorders.

Similarities to Frontotemporal Lobar Dementia

ALS and Frontotemporal Lobar Dementia (FTLD) are related disorders with overlapping clinical symptoms, pathology and genetics. FTLD is the second most common cause of dementia in people under the age of 65 and is marked by cortical degeneration in the frontal and temporal lobes of the brain. Clinically, this syndrome is distinguished from Alzheimer’s disease in its initial preservation of

memory. FTLD symptoms include progressive alterations in behavior, language and personality (Rademakers et al., 2012).

Intriguingly, 15% of patients initially diagnosed with ALS also meet the clinical criteria of FTLD, and 30–50% of the remaining ALS pool present with milder cognitive decline during disease progression. Conversely, 15% of initial FTLD patients also meet ALS clinical criteria, with ~30% of remaining FTLD cases exhibiting minor motor neuron dysfunction. It is thus highly likely that ALS and FTLD lie on the same disease continuum (Lomen Hoerth et al., 2002).

Clinical overlap between ALS and FTLD is explained by common genetic factors. Non-mutated TDP-43 is a major component of the cytoplasmic inclusions in most ALS and FTLD cases (Arai et al., 2006; Neumann et al., 2006), while inclusions staining positively for endogenous FUS protein are found in rare cases of TDP-43-negative FTLD (Munoz et al., 2009) (Neumann et al., 2009b) (Neumann et al., 2009a). Moreover, in 2011, hexanucleotide repeat (GGGGCC) expansions in an intron of the *C9ORF72* gene was identified as a common genetic cause of both FTLD and ALS (DeJesus-Hernandez et al., 2011a; Gijselinck et al., 2012; Renton et al., 2011), leading to widespread neuronal aggregates of dipeptide repeat proteins (Mori et al., 2013; Ash et al., 2013).

Genetic overlap between ALS and FTLD is not complete, however, as some genetic mutations and protein deposits are unique to either FTLD or ALS. Progranulin (*PGRN*) and tau (*MAPT*) mutations, for instance, cause a purely FTLD phenotype. Conversely, mutations in *SOD1*, *TARDBP* (TDP-43) or *FUS*

cause a purely ALS phenotype (Seelaar et al., 2010). Interestingly, protein inclusions between patients with mutated, ALS-associated FUS and those with wild-type, FTLD-associated FUS both contain FUS but have an otherwise distinct protein composition (Neumann et al., 2011). This data suggests separate disease mechanisms with some common themes.

RNA-BINDING PROTEINS IN ALS: LINK TO STRESS GRANULES

Introduction to Stress Granules

Eukaryotic cells have evolved sophisticated strategies to combat cellular stresses, which include heat shock, chemical toxicity, oxidative stress, and the protein misfolding accumulated during aging (Morimoto, 2011). During stress, cells must conserve energy to concentrate cellular resources toward restoring homeostasis. Under oxidative stress, for example, certain mRNAs, including mRNAs encoding stress protective molecules, increase in association with ribosomes, while others are blocked from translation (Bozaykut et al., 2014; Shenton et al., 2006). Eukaryotes organize mRNA resources and regulate protein synthesis, in part, through rapid assembly of cytoplasmic, non-membrane-bound complexes called stress granules (SGs) (Buchan and Parker, 2009; Kedersha and Anderson, 2002). Stress granules are aggregate-like structures selectively composed of transiently stored proteins and stalled mRNA translational complexes that form in response to translational arrest following a stress stimulus (e.g. oxidative insult, DNA damage, temperature shifts, ER

dysfunction, and viral infection) (Anderson and Kedersha, 2008). When stress granule formation is inhibited during stress, either by agents that inhibit translation termination or by disruption of cytoskeletal tracks upon which they form, cells die more readily (Loschi et al., 2009). Therefore, stress granule integrity is important for the cellular survival mechanisms in stress response.

Stress granule composition includes mRNA-bound, translationally stalled 48S pre-initiation complexes (e.g. eIF3, eIF4E and eIF4G) as well as proteins involved in mRNA stabilization, processing and transport, such as polyA-binding protein 1 (PABP1), T cell internal antigen-1 (TIA-1), and Ras-GTPase-activating protein SH3-domain-binding protein (G3BP) (Kedersha et al., 1999; 2005; Kimball et al., 2003). These proteins are essential to stress granule assembly and serve as specific stress granule “nucleators” (Anderson and Kedersha, 2008). Stress granules also sequester signaling proteins, facilitating cell survival during stress (Arimoto et al., 2008).

Importantly, RNA and RNA-binding proteins localize to stress granules in a differentially regulated manner, resulting in a different composition depending on the source of stress (Shah et al 2013). For instance, storage of mRNA in stress granules blocks their degradation and allows cells to efficiently and rapidly restore synthesis of vital proteins following recovery from cell stress (Lavut and Raveh, 2012). Stress granules also regulate mRNA degradation through exchange with another RNA granule type called P-bodies, which contain RNA degradation machinery like the RNA-induced silencing complex (RISC) and

p54/RCK (DDX6). P-bodies physically interact with stress granules to receive specific sets of mRNA for their temporally regulated degradation (Jain and Parker, 2013). Therefore, stress granule formation appears to be critical to reprogram mRNA translation under adverse conditions to facilitate adaptive stress responses (Anderson and Kedersha, 2008).

Conversely, mRNAs encoding for proteins necessary for stress response escape sequestration in stress granules and P-bodies and instead enter translation via ribosome docking on internal ribosome entry sites (IRES) in a limited set of mRNA (Spriggs et al., 2010; Stöhr et al., 2006; Thakor and Holcik, 2012). While stress conditions stall cap-dependent translation (Clemens et al., 2000), this cap-independent mechanism allows a group of mRNAs to be actively translated despite overall suppression of translation initiation. A limited, specialized set of mammalian mRNAs contain cellular IRES elements and utilize IRES-dependent translation during stress conditions such as oxidative stress and apoptosis (Bushell et al., 2006; Nevins et al., 2003). The balance between protein signaling, mRNA translation, mRNA silencing, and mRNA decay facilitated by stress granules result in nuanced translational regulation that allows cells to overcome stress.

Stress Granule Assembly and Disassembly

Stress granules assemble under conditions of acute stress when actively-translating polysomes disassemble. Experimental stressors that induce stress

granule formation include oxidative stress induced by arsenite or hydrogen peroxide, disruption of the ubiquitin-proteasome system (UPS), thermal stress, endoplasmic reticulum stress induced by thapsigargin or tunicamycin, mitochondrial stress induced by clotrimazole, DNA damage, viral infection, and osmotic shock induced by exposure to sorbitol (Hofmann et al., 2012; Kedersha and Anderson, 2007; Lloyd, 2012; Mazroui et al., 2007; Sama et al., 2013). Small molecules that inhibit translation initiation also induce stress granules (Kedersha et al., 1999). Collectively, these stimuli impair translation initiation via eIF2a-dependent or eIF2a-independent pathways, ultimately leading to translational arrest.

eIF2a-dependent stress granule assembly occurs when stress stimuli activate specific serine/threonine kinases (i.e. heme-regulated initiation factor 2α kinase (HRI), protein kinase R (PKR), PKR- like endoplasmic reticulum kinase (PERK), general control non-derepressible 2 (GCN)) (Anderson and Kedersha, 2008). These kinases phosphorylate and inactivate the α-subunit of eIF2 (Kedersha et al., 1999), which inhibits translation initiation by impairing production of the ternary complex (eIF2-GTP-Met-tRNAiMet). The ternary complex binds to the 40S small ribosomal subunit to initiate mRNA scanning (Aitken and Lorsch, 2012). As a result of the decreased availability of eIFs and ternary complexes, translation cannot be initiated. eIF2a-independent stress granule assembly occurs when chemicals (e.g. hippuristanol, pateamine A) inhibit eIF4A helicase, which is required for ribosome recruitment during

translation initiation. Thus, when the eIF4A helicase is impaired, translation initiation is stalled regardless of eIF2a inhibition (Bordeleau et al., 2005; 2006; Low et al., 2005; Mazroui et al., 2006; Mokas et al., 2009). The result of both pathways is ribosome run-off from the transcript, a failure to reload new ribosomes, and a stalled 48S pre-initiation complex bound to the 5′ UTR of mRNA (Anderson and Kedersha, 2008).

The next step in stress granule assembly, termed nucleation, is not fully understood. However, studies revealed that aggregation-prone RNA-binding proteins, such as G3BP, TIA-1 contain prion-like domains and polyglycine-rich domains, which confer the ability to reversibly aggregate (Gilks et al., 2004). The primary aggregation of these proteins with stalled mRNA transcripts promotes protein-protein and protein-mRNA interactions by proteins such as poly-A-binding protein (PABP1), YB-1 (YBOX1), and fragile X mental retardation proteins (FMRP/FXR1). From here, additional secondary protein–protein and protein-RNA interactions accelerate clustering into microscopically visible stress granules (Anderson and Kedersha, 2008; Kim, 2006; Tourrière et al., 2003). Once formed, stress granules are reversible and do not have all the properties of aggregates typically associated with neurodegenerative diseases, as they lack insoluble β-sheets (Gilks et al., 2004).

Additional post-translational modifications may play an important role in regulating stress granule assembly or the recruitment of RNA-binding proteins to stress granules. One post-translational modification linked to stress granules is

arginine methylation by peptidylarginine methyltransferases (PRMTs). The stress granule proteins FMRP, Cold Inducible RNA Binding Protein (CIRP) and even FUS have RGG motifs that can be methylated, and all have been shown to be methylated in stress granules (De Leeuw et al., 2007; Dolzhanskaya et al., 2006; Dormann et al., 2012). In addition to arginine methylation, proteins modified with poly(ADP)-ribose accumulate in stress granules. Interestingly, the depletion of key poly(ADP)-ribose phosphatases (PARPs) or overexpression of poly(ADP)-ribose glycohydrolases (PARGs) impairs stress granule formation, suggesting that poly(ADP)-ribose modifications are important for proper stress granule formation (Leung et al., 2011; Shi, 2012). Possible functional explanations are that these molecules act as a molecular scaffold in the coalescence and stability of stress granule structure.

Eventually, stress conditions either resolve or the cell enters into cell death pathways. Upon recovery from sub-lethal stress conditions, stress granules rapidly disassemble and translation recommences (Kedersha et al., 1999). The restoration of polysomes from 48S pre-initiation complexes in stress granules requires chaperones and can be promoted by staufen overexpression (Thomas et al., 2009). Further, disassembly is regulated by the dual specificity tyrosine-phosphorylation-regulated kinase 3 (DYRK3). In its inhibited state, DYRK3 remains associated with stress granules and prevents their dissolution through retention of sequestered mTORC1. Upon activation after stress is relieved, the kinase activity of DYRK3 reactivates mTORC1 signaling and

subsequent stress granule disassembly (Wippich et al., 2013). The drugs cycloheximide and emetine can also dissolve pre-formed stress granules without the resolution of stress by stalling ribosomes on translating mRNA during elongation, inhibiting ribosome run-off and pushing the dynamic equilibrium of stress granules toward disassembly (Kedersha et al., 2000; Kozak et al. 2006).

Stress Granules in Neurodegeneration

Stress granules occur not only in cultured cells, but also *in vivo*, as seen in *Drosophila* muscles under osmotic stress (van der Laan et al., 2012) and in mouse neurons under oxidative stress (Jamison et al., 2008; Kayali et al., 2005). Stress granules also form in the brain tissues of rats after experimentally-induced acute traumatic brain injury (Kim et al., 2006). Further, chronic stress-inducing states exacerbate stress granule formation, such as the lasting physical damage associated with traumatic encephalopathy (Goldstein et al., 2012) or oxidative stress associated with aging (Ghezzi and Bonetto, 2003), creating the conditions for pathological stress granule dysfunction. Traumatic brain injury, vascular damage, oxidative stress, and chronic viral infections are risk factors for ALS and FTLD (Barber and Shaw, 2010; De Chiara et al., 2012; Garbuzova-Davis et al., 2011; Gavett et al., 2011; Piazza et al., 2004). Thus, in circumstances where the brain is vulnerable, the potential importance of proper stress granule function becomes apparent.

Importantly, most RNA binding proteins linked to neurodegenerative diseases associate with stress granules *in vitro*. ALS-causing FUS (**Figure I.2**), ataxin-2, TDP-43, optineurin and angiogenin variants all co-localize with stress granules in stressed cells, among others (see **Figure I.1**) (Bosco et al., 2010; Colombrita et al., 2009; Hart and Gitler, 2012; Liu-Yesucevitz et al., 2010a). Mutations in genes encoding for stress granule proteins are found not only in ALS, but in several degenerative disorders including Alzheimer's disease (AD), Huntington's disease and inclusion body myopathy (Goggin et al., 2008; Li et al., 2013; Vanderweyde et al., 2013).

Potential stress granule pathology from neurodegeneration-causing RNA-binding proteins may lie in their propensity to aggregate, as biochemical fractionation of cellular lysates reveals a gradient in the solubility potential of stress granule-associated proteins. For example, stress granule nucleating RNA-binding proteins such as TIA-1, TTP and G3BP form semi-soluble aggregates (Vanderweyde et al., 2012). In contrast, pathological aggregates of tau, β-amyloid, TDP-43 and FUS are highly insoluble in inclusions within the brain tissue of subjects with AD and FUS-ALS (Bosco et al., 2010; Huang et al., 2010; Liu-Yesucevitz et al., 2010a; Vanderweyde et al., 2012). Strikingly, stress granule proteins, such as TIA-1, eIF3 and PABP1, co-localize with these neuronal inclusion in FUS-ALS and AD (Vanderweyde et al., 2012; Woulfe et al., 2010), suggesting a common pathway between neurodegeneration and stress granule biology.

FUSED IN SARCOMA

Discovery of FUS

Fused in Sarcoma (FUS), also known as Translocated in Liposarcoma (TLS), was discovered in 1993 as the N-terminal portion of an aberrantly fused gene pair in human myxoid liposarcomas. In these deep soft tissue cancers, a chromosomal translocation in the DNA code results in the fusion of the N-terminus of the FUS protein to the DNA-binding domain of other transcription factor proteins, such as (CHOP) (Crozat et al., 1993; Rabbitts et al., 1993) and (ERG) (Ichikawa et al., 1994), resulting in cancer-causing “oncogenes”. Until its discovery as a causative gene in ALS, FUS research was centered on its role in these cancers and on the mechanisms by which its N-terminus promotes oncogenic transformation (Kovar, 2010).

In 2009, two groups concurrently discovered that mutations in the *FUS* gene cause a subset of FALS, the pathogenesis of which included FUS protein depositions in pathological brain and spinal cord tissue inclusions (Kwiatkowski et al., 2009; Vance et al., 2009). Endogenous, or non-mutated, FUS deposits were also found in the brain inclusions of a subset of FTLD patients (Munoz et al., 2009; Neumann et al., 2009a; 2009b)**.**

Family Characteristics of FUS

FUS is a member of the “FET” protein family, named after its three core members, Fused in Sarcoma (FUS), Ewing sarcoma protein (EWS) and TATA

binding protein-associated factor 15 (TAF15). Each protein member, while not yet exhaustively characterized, has apparently similar roles in transcription and splicing (Tan and Manley, 2009). EWS and TAF15 exhibit the same domain structure organization as FUS, including a PY-NLS nuclear localizing signal (Lee et al., 2006; Marko et al., 2012; Zakaryan and Gehring, 2006), and each also forms fusion oncogenes in a several cancers (Tan and Manley, 2009). TAF15 and EWSR1 have recently been linked with ALS and FTLD, as they are found translocated and aggregated in the cytoplasm of degenerating neurons (Couthouis et al., 2011; Couthouis et al., 2012; Neumann et al., 2011; Ticozzi et al., 2011). Though TAF15 and EWS co-accumulate with FUS in neuronal cytoplasmic inclusions of FTLD patients (Davidson et al., 2012), this co-deposition does not occur in ALS. Hence, FTLD may involve dysfunction of the entire FET family, while ALS caused by mutant FUS appears specific to FUS dysfunction.

Domains and Structure of FUS

The *FUS* gene encodes a 526 amino acid protein marked by transcription activation and RNA/DNA binding domains (**Figure I.2**). The N-terminal, prion-like transcriptional activation domain is rich in QGSY residues (“QGSY”) and is a potent transcriptional activator when fused to the DNA binding domain of other transcription factors (Zinszner et al., 1994; Prasad et al. 1994), such as CHOP in myxoid liposarcoma (Crozat et al., 1993; Rabbitts et al., 1993). Moreover, the

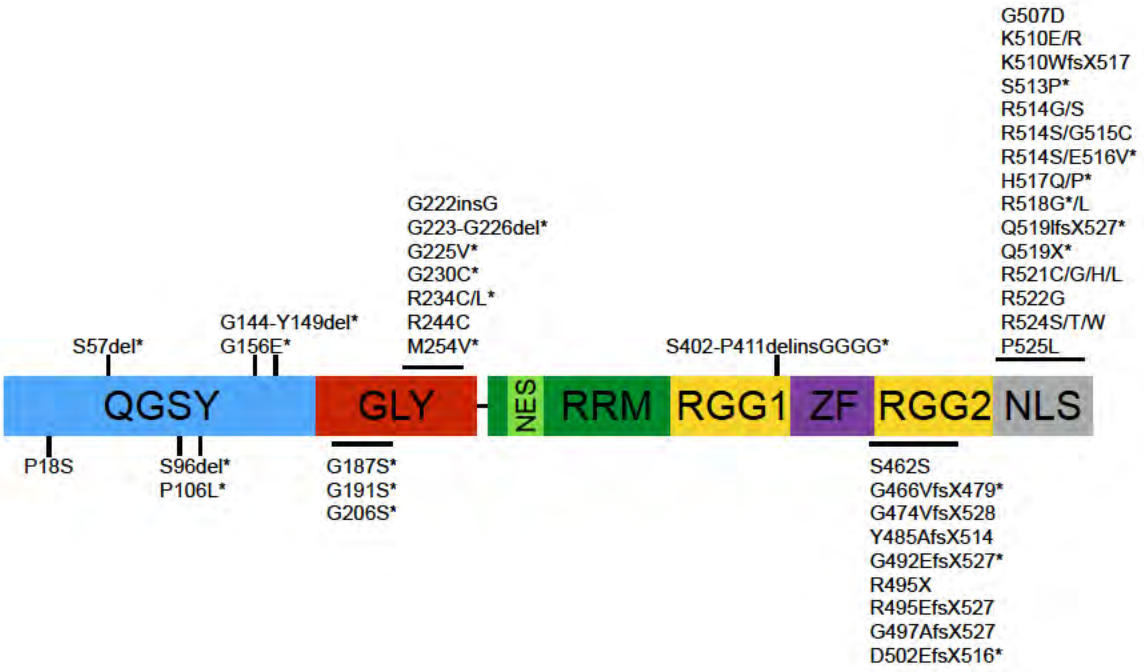

Figure I.2: The functional domains of FUS and ALS-linked mutations. FUS domains (www.uniprot.org) include a Gln-Gly-Ser-Tyr (QGSY)-rich region (blue), a Gly-rich domain (red), an RNA recognition motif (RRM; green), two Arg-Gly (RG)-rich regions (yellow), a RanBP2-type zinc finger domain (ZF; purple) and a putative NLS (gray). Labeled are fALS-linked mutants. *Asterisk indicates that the mutation was reported in a single patient. del = deletion; ins = insertion; fs = frameshift, X = stop.

QGSY domain was predicted to contain prion-like patterns via bioinformatics approaches. QGSY is also required for *in vitro* aggregation of FUS into filamentous structures (Kato et al., 2012; Sun et al., 2011).

In addition to transcriptional activation domains, FUS contains multiple domains with nucleic acid binding motifs: A glycine-rich domain (Gly), an RNA recognition motif (RRM), two arginine–glycine–glycine (RGG) motifs, and a zinc finger (ZnF) (Burd and Dreyfuss, 1994) (**Figure I.2**). Different *in vitro* studies suggested that the RGG1-ZnF-RGG2 region of FUS is most likely the major RNA binding domain that binds GU-rich sequences and G-quadruplexes (Bentmann et al., 2012; Iko et al., 2004; Lerga et al., 2001). Both the RRM and RGG domains are involved in binding RNA, but less is known about the respective roles of these domains *in vivo* (Bentmann et al., 2012; Daigle et al., 2012; Iko et al., 2004; Lerga et al., 2001).

Finally, at its very C-terminus FUS features a non-classical nuclear localization signal (NLS), composed of a proline–tyrosine NLS (PY-NLS) (Dormann et al., 2010; Zhang and Chook, 2012). Although nuclear pore complexes are freely permeable to proteins smaller than ~40 kDa, larger proteins like FUS require an active mechanism that includes nuclear transport factors such as karyopherins and the small GTPase Ran to control the directionality of the transport. Kaps recognize NLS motifs that guide their cargo into the nucleus (Strambio-De-Castillia et al., 2010). The FUS NLS is recognized by the nuclear import receptor Karyopherin β2 (Transportin), which shuttles PY-NLS-containing

proteins from the cytoplasm into the cell nucleus in a RanGTP-dependent manner (Lee et al., 2006). Dominant mutations that cause FALS are located within the NLS and destroy the effectiveness of this signal, disrupting Transportin binding and nuclear import of FUS (Bosco et al., 2010; Dormann et al., 2010; Gal et al., 2011; Ito et al., 2011; Kino et al., 2010; Niu et al., 2012; Zhang and Chook, 2012). The cytoplasmic retention of mutant FUS is a key event in ALS pathogenesis because severely mislocalized variants (e.g. P525L and R495X) cause an unusually early disease onset and rapid disease progression (Bosco, et al., 2010; Dormann and Haass, 2011; Dormann et al., 2010; Niu et al., 2012; Zhang and Chook, 2012).

Localized Functions and Interactions of FUS

FUS functions across several gene expression avenues at the DNA, RNA, and protein level. In particular, FUS is associated with key cellular functions such as DNA damage repair, RNA processing and local translation, and these functions depend on the sub-cellular localization of FUS (Sama et al., 2014).

At the DNA level, nuclear endogenous FUS binds both single- and double-stranded DNA, associates with higher order DNA structures such as D-loops and G-quadruplexes, and participates in homologous DNA pairing (Akhmedov et al., 1995; Baechtold et al., 1999; Bertrand et al., 1999; Takahama et al., 2013). FUS is a transcriptional factor and regulates the expression of several genes (Yang et al., 2014). FUS is also located at telomeres, where it regulates telomere length

(Takahama et al., 2009; 2013). Another important nuclear role of FUS is DNA damage repair, as it rapidly localizes to sites of laser-induced DNA damage (Dutertre et al., 2014; Mastrocola et al., 2013; Rulten et al., 2013; Wang et al., 2013).

At the RNA level, FUS is a heteronuclear ribonuclear protein (hnRNP), also known as hnRNP P2 (Calvio et al., 1995). Early studies using EMSA (electrophoretic mobility shift assays) analyses showed a preference for FUS to bind GGUG motifs in RNA (Lerga et al., 2001), though that notion was put into question by recent deep-sequencing studies of mRNAs bound by FUS *in vivo*, which have generated mixed findings on RNA motif preference (Colombrita et al., 2012; Hoell et al., 2012; Ishigaki et al., 2012; Lagier-Tourenne et al., 2012; Nakaya et al., 2013; Rogelj et al., 2012). Despite the disparity in binding motif, these studies show that FUS binds long mRNA introns.

An important nuclear-based role FUS plays is the regulation of pre-mRNA splicing. FUS associates with members of the spliceosome (Meissner et al., 2003; Yang et al., 1998) and regulates 5'-splicing of E1A pre-mRNA (Hallier et al., 1998; Lerga et al., 2001). Indeed, FUS binds hundreds of mRNA introns including its own mRNA, thus implicating it in self-regulation (Lagier-Tourenne et al., 2012; Ling et al., 2013; Nakaya et al., 2013).

Roles for FUS that center on RNA continue into the cytoplasm, as FUS is capable of shuttling (Zinszner et al., 1997) via Transportin (Dormann et al., 2010) and an export mechanism shown to be consistent with that of Exportin-1 (Kino et

al., 2011). FUS transports RNA from the nucleus to the cytoplasm and distant regions of the cell (Zinszner et al., 1997) via several motor proteins, including the ATP-dependent actin binding myosin motors Myo5A (Yoshimura et al., 2006) and Myo6 (Takarada et al., 2009), and the microtubule-dependent kinesin motor protein KIF5B (Kanai et al., 2004). The association of FUS with such transport machinery may be important for FUS mediated local translation at distal regions of the cell, such as dendrites (Fujii et al., 2005; Fujii and Takumi, 2005; Yasuda et al., 2013). At dendrites, FUS is believed to facilitate local translation of actin-associated proteins necessary for spine plasticity, such as Nd1-L (Fujii and Takumi, 2005). FUS knockout mice support this notion, as they exhibit abnormal spine morphology and attenuated spine density in hippocampal pyramidal neurons (Fujii et al., 2005). Moreover, translation of kank-2 (KN motif and ankyrin repeat domains 2), a component of actin remodeling, is dependent upon FUS expression (Yasuda et al., 2013). Thus, local and temporal FUS localization may have a significant impact on cell fate through its roles involved with RNA-binding and processing.

Cytoplasmic Mutant FUS Localizes to Stress Granules and Alters Their Morphology, Formation and Dynamics

ALS-associated mutations in the NLS of FUS causes cytoplasmic mislocalization and sequestration of FUS into stress granules under conditions of

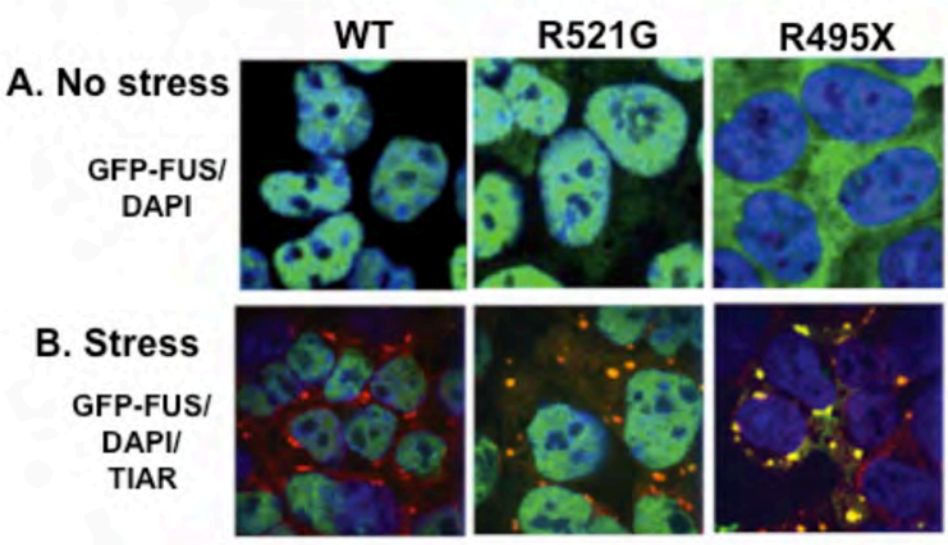

Figure I.3: Mutant FUS localizes to stress granules. (A) In the absence of stress, GFP-FUS WT is localized to the nucleus, whereas GFP-FUS R521G and R495X (green) mislocalize to the cytoplasm. **(B)** GFP-FUS R521G and R495X co-localize with the stress granule marker TIAR (red), formed in response to arsenite stress. This figure was adapted from Bosco et al., 2010.

acute stress (**Figure I.3**) (Bentmann et al., 2012; Bosco et al., 2010; Dormann et al., 2010; Ito et al., 2011; Kato et al., 2012). FUS expression is not required for stress granule formation (Aulas et al., 2012; Blechingberg et al., 2012). Under almost all stressors tested, endogenous or ectopically expressed WT FUS remains predominantly nuclear and is thus largely excluded from cytoplasmic stress granules, though modest association of WT FUS has been reported under over-expression conditions (Andersson et al., 2008; Blechingberg et al., 2012; Goodier et al., 2007). To date, only osmotic stress is known to cause translocation of endogenous FUS from the nucleus to cytoplasmic stress granules (Sama et al., 2013). Mutant FUS expression at endogenous levels does not induce spontaneous stress granule formation; rather, additional stress is required for stress granule formation and subsequent FUS localization. Overexpression of FUS mutants by transient transfection induces stress granule formation *a priori* of additional stress, though the physiological relevance of this phenomenon is under debate (Baron et al., 2013; Gal et al., 2011; Ito et al., 2011; Kino et al., 2011). All ALS-causing FUS mutations that disrupt the NLS that have been tested to date localize to stress granules, though to degrees that correlate with the extent of mislocalization. In fact, the P525L and R495X mutations in FUS, which abolish Transportin binding, cause nearly complete FUS localization to the cytoplasm, are associated with a relatively early onset of ALS, and localize most robustly to stress granules (Bosco et al., 2010; Dormann et al., 2010; Zhang and Chook, 2012).

Our group recently discovered that mutant FUS association with stress granules promotes several morphological and kinetic abnormalities, part of the published work that encompasses my study in Chapter II (Baron et al., 2013). Namely, under conditions of arsenite stress, we show that mutant FUS delays stress granule formation in mammalian cell culture (**Appendix IV, Figures 1 and 2**). Once sodium arsenite-induced stress granules are formed, however, those containing mutant FUS are more dynamic, larger and more abundant compared to stress granules lacking FUS (**Appendix IV, Figures 3 and 4**). Finally, upon removal of stress, stress granules disassemble more rapidly in cells expressing cytoplasmic mutant FUS (**Appendix IV, Figure I**). The consequent alterations in stress granule functional output caused by the cytoplasmic mislocalization of mutant FUS likely promotes conditions that favor neurodegeneration in ALS (Bosco et al., 2010; Sun et al., 2011), a hypothesis that is therefore the foundation of my dissertation.

4. PROJECT SUMMARY

The fatal motor neuron disease Amyotrophic Lateral Sclerosis (ALS) develops in an age-related manner and is marked by progressive neuronal death, with cytoplasmic protein aggregation and increased oxidative stress as major hallmarks. Fused in Sarcoma/Translocated in Liposarcoma (FUS) is an RNA-binding protein mutated in ALS that aberrantly localizes in the cytoplasm due to a disruption in the nuclear localization sequence. Pathological inclusions

in human FUS-ALS cases contain aggregated FUS as well as several stress granule-associated proteins (Woulfe et al., 2010)**.** Further, cytoplasmic mutant FUS incorporates into stress granules, which increases their volume and number, delays their assembly, accelerates their disassembly, and alters their dynamics (Baron et al., 2013).

I posit in this work that mutant FUS association with stress granules is a toxic gain-of-function in ALS that alters the function of stress granules by interaction with stress granule components. Here, I show that mutant FUS incorporates in to stress granules via its C-terminal RGG motifs, the methylation of which is not required for this localization (**Appendix IV**). Further, I identify protein interactions specific to full-length mutant FUS under stress conditions that are potentially capable of interacting with FUS in stress granules. I also identify proteins that differentially associate with mutant FUS over WT FUS in stressed and unstressed conditions, providing groundwork for an expanded set of biological questions. Finally, I demonstrate a potential change in the protein composition of stress granules upon incorporation of mutant FUS (**Chapter II**). These findings advance the understanding of pathogenic mechanisms in ALS as well as the knowledgebase within the field of stress granule biology.

PREFACE TO CHAPTER II

Laura Kaushansky (LK) planned and performed the majority of experiments. Dr. John Leszyk (JL) and Dr. Kristin Boggio (KB) performed mass spectrometry runs; Dr. Daryl Bosco (DB), Dr. Melissa Rotunno (MR), and Maeve Tischbein (MT) contributed to the design and data interpretation for experiments.

In addition to the work discussed in Chapter II, the following related proteomics data is presented in **Appendix I**:

Table A1.1 – Enriched proteins identified in full-length FLAGHA-FUS FUS-P525L-FL IPs over FLAG control IPs under stress conditions.

CHAPTER II:

ASSESSING MUTANT FUS INTERACTIONS IN STRESS GRANULES AND THE SUBSEQUENT EFFECTS ON STRESS GRANULE COMPOSITION

INTRODUCTION

Mutations in the gene encoding fused in sarcoma/ translocated in liposarcoma (FUS) cause inherited cases of amyotrophic lateral sclerosis (ALS) (Kwiatkowski et al., 2009; Vance et al., 2009). ALS is a fatal neurodegenerative disease marked by motor neuron death, progressive muscle weakening and paralysis (Bosco and Landers, 2010; Kiernan et al., 2011). Most ALS-linked FUS mutations are located within the C-terminal nuclear localization signal (NLS) that binds the import factor Transportin, leading to an impairment of FUS import from the cytoplasm to the nucleus (Dormann et al., 2010; 2012). FUS is mainly nuclear in most cell types (Andersson et al., 2008) but also has nucleo-cytoplasmic shuttling activity important for mRNA transport (Zinszner et al., 1997), where it is thought to play a role in local translation at neuronal dendrites (Fujii et al., 2005; Fujii and Takumi, 2005; Lagier-Tourenne et al., 2012). Disruption of Transportin binding to FUS leads to cytoplasmic accumulation of FUS in cultured mammalian cells and *in vivo* (Dormann et al., 2010; Lanson and Pandey, 2012).

Cytoplasmic mutant FUS, including R521G, R495X and P525L, localizes to stress granules upon stress induction (Bentmann et al., 2012; Bosco et al.,

2010; Daigle et al., 2012; Dormann et al., 2010; 2012; Gal et al., 2011; Ito et al., 2011; Vance et al., 2013). Stress granules are non-membrane-bound structures assembled along the microtubule cytoskeleton and are composed of stalled mRNA-protein translational complexes. Formed transiently as a normal response to environmental and physiological stress, such as oxidation, heat-shock, viral infection and hypoxia, these structures are nucleated by key stress granule marker proteins, such as G3BP1 and TIA-1, among other scaffolding networks (Anderson and Kedersha, 2008; Ivanov et al., 2011). Stress granules are thought to regulate mRNA translation during stress by acting as mRNA storage and transfer centers. Indeed, stress granules exchange mRNA with degradation machinery in P-bodies (Jain and Parker, 2013). Stress granule also participate in cell signaling during stress by controlling kinase activity (Wippich et al., 2013). The result is a dynamic balance of mRNA expression, storage and degradation driven by stress granules that changes with the surrounding environment and facilitates homeostasis (Kedersha and Anderson, 2002).

Our group recently showed that under conditions of oxidative stress induced by sodium arsenite, mutant FUS delays stress granule formation and accelerates their disassembly in mammalian cell culture. Further, expression of mutant FUS also impairs stress granule abundance, volume and dynamics (**Appendix IV**) (Baron et al., 2013). Finally, we identified the C-terminal RGG domains as the main structural features in mutant FUS that direct its assembly into stress granules (**Figure II.1; adapted from Appendix IV**), a discovery that

serves as a useful tool and is utilized by us later in this report. Importantly, stress granule marker proteins are found within the pathological aggregates of ALS-FUS and other neurodegenerative disease tissues (Dormann et al., 2010; Fujita et al., 2008; Halliday et al., 2012; Kwiatkowski et al., 2009; Liu-Yesucevitz et al., 2010a; Vance et al., 2013). Thus, we hypothesize that mutant FUS incorporation into stress granules impairs stress response and contributes to disease progression by disrupting one or more stress granule functions, a notion gaining considerable attention in the field (Wolozin, 2012).

In this study, we aim to identify protein interactions of mutant FUS in stress granules as well as changes in the stress granule interactome induced by mutant FUS incorporation. Here, we report that full-length mutant FUS P525L (heretofore called FUS-P525L-FL) associates with 52 proteins during stress that have potential to direct its localization to stress granules. These hits, discovered using mass spectrometry proteomics of stable mammalian cell line immunoprecipitation experiments, bind neither wild-type FUS (FUS-WT) nor a truncation of mutant FUS that lacks the RGG domains (FUS-ΔRGG), which are required for FUS localization to stress granules. Further, all but six of these hits are RNA-mediated, and more than half are influenced by the integrity of a stress granule scaffolding component, poly(ADP)-ribose (PAR). Finally, we show that the presence of FUS during stress alters the G3BP1 interactome during stress, a finding that supports a broad disruption in stress granule composition caused by mutant FUS incorporation. The results shown in this study provides important

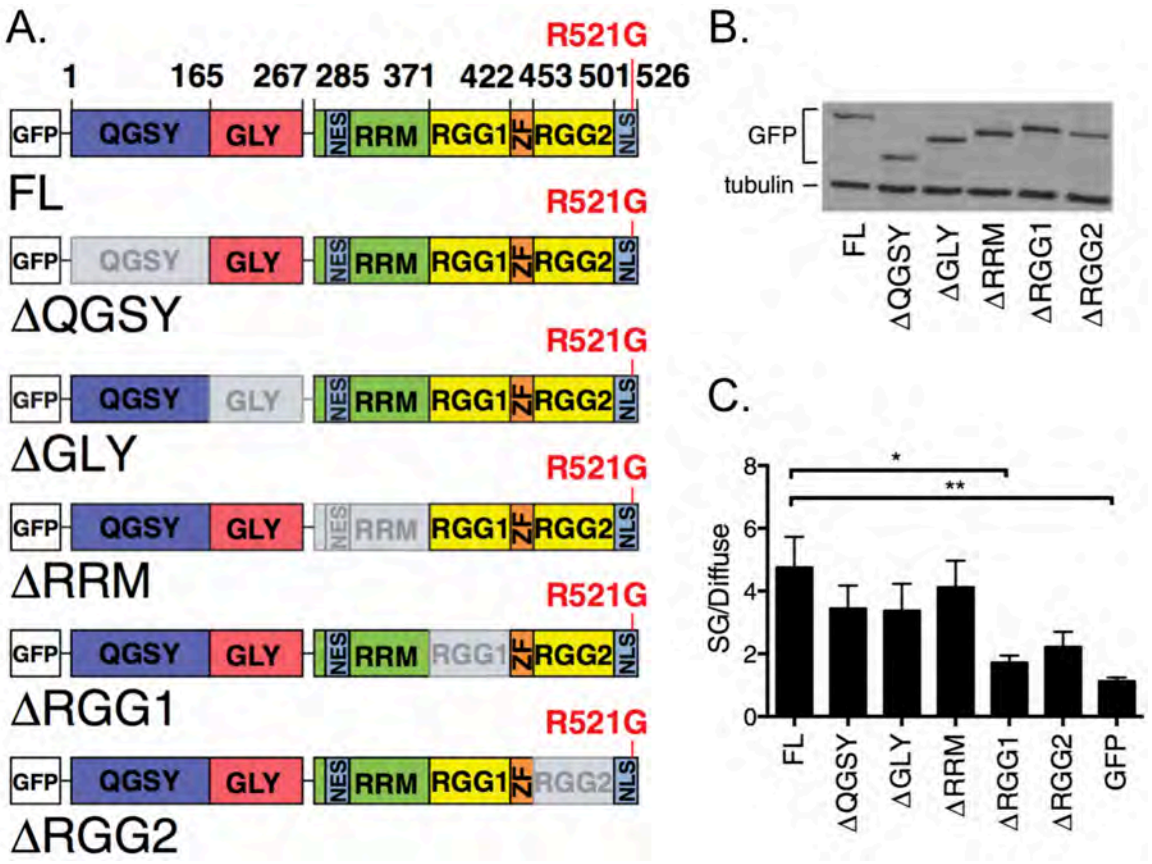

Figure II.1: The RGG domains modulate the incorporation of FUS into arsenite-induced stress granules. (A) Illustration of full length (FL) GFP-FUS R521G and constructs lacking the following sequences: Gln-Gly-Ser-Tyr-rich (ΔQGSY), Gly-rich (ΔGLY), RNA recognition motif (ΔRRM), and Arg-Gly-Gly- rich (RGG) regions (ΔRGG1 and ΔRGG2). **(B)** Western blot analysis of HeLa cells in (B) demonstrates equivalent expression levels for all GFP-FUS R521G constructs. **(C)** Quantitative analysis (see Materials and methods) of (D) reveals that constructs lacking RGG domains (ΔRGG1 and ΔRGG2) exhibit impaired localization to stress granules. Statistically significant comparisons include FL and ΔRGG1 (*$P < 0.05$), FL and GFP (**$P < 0.01$), and ΔQGSY and GFP (*$P < 0.05$; not shown on graph for clarity) by one-way ANOVA followed by a Dunnett's post-hoc test on n=3 independent experiments. All error bars represent SEMs. (**continued on the next page**)

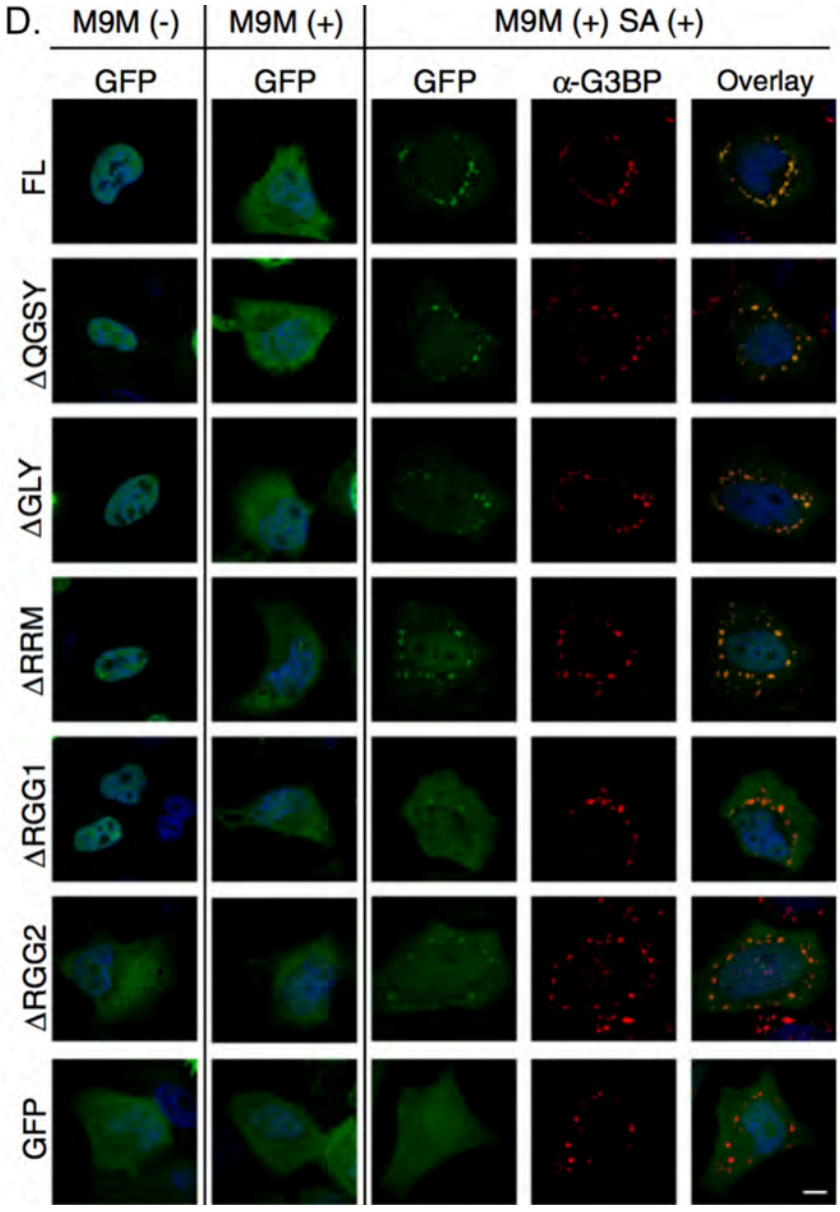

Figure II.1 continued: (D) Confocal images of HeLa cells transfected with GFP-FUS R521G constructs (green) alone (−) or co- transfected (+) with MBP-M9M, a transportin-1 inhibitor. Note the increased cytoplasmic GFP-FUS in M9M(+) cells (compare columns 1 and 2). Confocal fluorescence images of arsenite-stressed co-transfected cells were used to assess the ability of GFP-FUS R521G constructs (green; column 3) to associate with stress granules (G3BP; red; column 4). The greatest degree of GFP and G3BP co-localization occurred for GFP-FUS R521G-FL compared to GFP control cells. This figure was adapted from Baron et al., 2013 (For Materials and Methods for this figure, please see **Appendix IV**).

groundwork toward uncovering pathways likely disrupted by ALS-causing FUS mutants.

MATERIALS AND METHODS

FLAGHA-FUS construct design and generation

FLAGHA-FUS expression cassette vectors were generated as follows: pFRT-TO-DEST-FLAGHA-FUS-WT was obtained from Addgene (#26737) and converted to FUS-P525L-FL using the following site-directed mutagenesis primers: P525L_fwd: CGCAGGGAGAGGCTGTATTAAGCGGCC ; P525L_rev: GGCCGCTTAATACAGCCTCTCCCTGCG. To generate deletion constructs, the following primers were designed by joining the up-stream and downstream sequences flanking the domain that was deleted in the FUS-P525L-FL background: ΔRGG1_fwd: CATTTGCTACTCGCGCTGGTGACTGGAAG; ΔRGG1_rev: CTTCCAGTCACCAGCGCGAGTAGCAAATG; ΔRGG2_fwd: CCCCTAAACCAGATAAGATGGATTCCAG; ΔRGG2_rev: CTGGAATCCATCTTATCTGGTTTAGGGG. The ΔRGG1/2 deletion construct was made from the product of the ΔRGG1 reaction using the ΔRGG2 primers. The FLAGHA_control construct was made using pFRT-TO-DEST-FLAGHA-FUS-WT as a template and the following primers to introduce a stop codon adjacent to FLAGHA: FLAGHA_fwd: CCGATTACGCTTAGAACCAGATATC; FLAGHA_rev: GATATCTGGTTCTAAGCGTAATCGG. All experiments were conducted with the

QuikChange II Mutagenesis kit (Stratagene; 200523) according to the manufacturer's instructions.

Cell line generation

Isogenic cell lines expressing FLAGHA-FUS variants inducible under doxycyline expression were generated using the Flp-In T-REx system (Invitrogen R780-07). This system contains a single stably integrated, isogenic FRT site that facilitates expression of each FLAGHA-FUS expression cassette at the same genomic locus among all lines. Flp-In T-REx 293 cells were co-transfected with the Flp recombinase vector (pOG44) and the desired expression vector (pFRT-TO-DEST containing FLAGHA-FUS) using the Lipofectamine 2000 transfection reagent (Invitrogen 11668). Selection for stable integration began 48 h post-transfection using media supplemented with 100 mg/mL Hygromycin B (Invitrogen 10687-010) and 15 mg/mL blasticidin, which yielded isogenic cell populations that could induce FLAGHA-FUS at approximately one to two times that of endogenous FUS upon doxycycline induction.

Drug treatments

The following drug treatment stocks were prepared and stored at freezing temperatures: 7.5 mg/mL blasticidin (Invitrogen R210-01) in water (−20°C); 50 mg/mL doxycycline (Sigma D9891) in water (−80°C), 100 mM sodium arsenite (Sigma 71287) in water (−20°C), and 1 mM ADP-HPD (EMD Millipore 118415)

(−80˚C). FUS expression in the FlpIn HEK-293 lines was induced with the addition of 1 µg/mL doxycycline for 24 h unless otherwise noted.

Immunofluorescence

Standard immunofluorescence protocols were employed as described previously (Bosco et al., 2010). Briefly, cells were fixed with 4% paraformaldehyde for 10 minutes then blocked with PBSAT (1X PBS/1% BSA/0.5% Triton-X 100) for 30–60 minutes at ambient temperature. Primary antibodies described in each experiment were diluted in PBSAT and applied to cells at ambient temperature for 1 h. Primary antibody dilutions were as follows: 1:2000 for mouse anti-G3BP (BD Transduction Labs, 611126), 1:1000 for rabbit anti-G3BP (Proteintech; 130-57-2AP), 1:1000 for mouse anti-FLAG (Sigma F1804) and 1:375 rabbit anti-FUS. Rabbit anti-FUS antibodies were generated by GenScript against a C-terminal epitope, using the peptide CKFGGPRDQGSRHDSEQDNSD. Cells were then incubated with secondary antibodies diluted 1:1000–1:2500 in PBSAT for 45 minutes at ambient temperature. Secondary antibodies included Dylight 549 conjugated anti-mouse IgG (Jackson ImmunoResearch Labs; 715-505-151), Cy3 conjugated anti-mouse IgG (Jackson ImmunoResearch Labs; 715-165-151), Cy3 conjugated anti-rabbit IgG (Jackson ImmunoResearch Labs; 711-165-152), and Cy5 conjugated anti-mouse IgG (Jackson ImmunoResearch Labs; 715-175-151). Cells were stained with 34 ng/mL DAPI in water, and coverslips were mounted with ProLong Gold anti-fade reagent (Invitrogen; P36930).

Western blot

Standard western blotting protocols were employed as described previously (Bosco et al., 2010). Primary antibodies described in each experiment were diluted as follows: 1:1000 for mouse anti-FLAG (Living Colors; Clontech 632380), 1:1000 for rabbit anti-G3BP (Proteintech), 1:1000 for mouse anti-TIAR (Proteintech), 1:1000 rabbit anti-SMN (Sigma) and 1:1000 for rabbit anti-FUS. Rabbit anti-FUS antibodies were generated by GenScript against a C-terminal epitope, using the peptide CKFGGPRDQGSRHDSEQDNSD. Blots were incubated with primary antibodies overnight at 4°C. Secondary antibodies, including anti-mouse IRDye 680 (Licor 926–32220) or IRDye 800 (LiCor 926–32210) and anti-rabbit IRDye 680 (LiCor 926–32220) or IRDye 800 (Licor 926–32211), were diluted 1:10000 and incubated with blots for 1–2h at ambient temperature. Bands were visualized with an Odyssey Infrared Imager (LiCor Model 9120), and densitometry measurements performed with the Odyssey Software (LiCor V3.0).

FLAG formaldehyde-crosslinked immunoprecipitation

HEK cells were induced to express FLAGHA alone, FLAGHA-tagged FUS-P525L-FL, FUS-WT, or FUS-P525L-ΔRGG for 24h, followed by stress with 0.5 mM sodium arsenite for 1h in duplicate plates for all conditions (for a total of 8 samples). After stress, cells were lysed with IP buffer (25 mM HEPES (Sigma H3375), 25 mM KCl (Sigma P9541), 5 mM EDTA (Fisher; E478-500), 1% NP-40 (MP Biomedicals; 198596), and 10% v/v glycerol ((Acros; 15982–0010) in water;

pH 7.0) supplemented with protease inhibitors (Roche 11836170001). Protein content was measured using a standard BCA Assay (Thermo Scientific) and lysates were treated according to manufacturer's instructions.

For FLAG immunoprecipitation (IP) reactions, cells were plated at a density of 4 x 10^5 cells/mL in 15 cm plates and induced with doxycycline 24h to induce FLAGHA-FUS expression. Prior to IP, cells were washed once in DPBS, then crosslinked in the plate with 5 mL 0.5% formaldehyde for 10 minutes at ambient temperature. Crosslinking was quenched with 500 µL quenching buffer (2.5M glycine in DPBS, pH 7.0) for 5 minutes at ambient temperature. Cells were lysed for 15 minutes in 3 mL IP buffer (25 mM HEPES, 25 mM KCl, 5 mM EDTA (Fisher; E478-500), 1% NP-40 (MP Biomedicals; 198596), and 10% v/v glycerol ((Acros; 15982–0010) in water; pH 7.0), then sonicated using a Branson Sonifier® cell disrupter equipped with a 3 mm microtip (VWR 33996-163) for 45 s at 40% amplitude in 2 s bursts with 10 s intervals. Lysates were cleared by centrifugation at 13000 rpm for 15 minutes at 4°C, and total protein concentration was determined using a BCA assay (Invitrogen). Anti-FLAG agarose beads (Sigma A2220) were prepared by washing them 3 times in 10X v/v IP buffer. The cleared lysate supernatant was added to anti-FLAG agarose beads at a concentration of 50 µg total protein per µL bead slurry, and IP reactions were performed at 4°C for 2h. Following IP incubation, anti-FLAG beads were washed three times with 10x v/v IP buffer supplemented with KCl to a final concentration of 250 mM. For experiments testing RNA mediation, beads were treated at this

point with 250 µg/mL RNase A (Qiagen 19101) for 1h at 4˚C, then washed as before.

Protein elution *under crosslinked conditions* was accomplished via boiling the beads with 50 µL 1X SDS loading buffer (Boston Bioproducts; BP11R) for 5 minutes at 95°C. Following boil elution, 10 µL of sample was subjected to western blot analysis as described above, and the remaining 40 µL was subjected to proteomics analysis as described below.

FLAG poly(ADP)-ribose-mediated immunoprecipitation (no crosslinking)

For immunoprecipitation (IP) reactions, cells were plated at a density of 4 x 10^5 cells/mL in 15 cm plates and induced with doxycycline for 24h to induce FUS expression. Prior to IP, cells were washed once in DPBS (Cellgro 21-030-CV), then cells were lysed for 15 minutes in 3 mL IP buffer (25 mM HEPES (Sigma H3375), 25 mM KCl (Sigma P9541), 5 mM EDTA (Fisher; E478-500), 1% NP-40 (MP Biomedicals; 198596), and 10% v/v glycerol ((Acros; 15982–0010) in water; pH 7.0) supplemented with 1 mM ADP-HPD (EMD Millipore 118415). Cells were sonicated using a Branson Sonifier® cell disrupter equipped with a 3 mm microtip (VWR 33996-163) for 15 s at 40% amplitude in 2 s bursts with 10 s intervals. Lysates were cleared by centrifugation at 13000 rpm for 15 minutes at 4°C, and total protein concentration was determined using a BCA assay (Thermo Scientific Pierce 23227).

For FLAG IPs, anti-FLAG agarose beads (Sigma A2220) were prepared by washing them 3 times in 10X v/v IP buffer. The cleared lysate supernatant

was added to anti-FLAG agarose beads at a concentration of 50 µg total protein per µL bead slurry, and IP reactions were performed at 4°C for 2 h. FLAG IP protein elution under *uncrosslinked conditions only* was accomplished with one bed volume of 250 µg/mL 3X FLAG peptide (Sigma-Aldrich F4799) three times sequentially for 30 minutes each at ambient temperature and pooled. Gel samples were then prepared to a total volume of 50 µL with 6X SDS loading buffer (Boston Bioproducts; BP11R) for 5 minutes at 95°C, and 10 µL of sample was subjected to western blot analysis as described above. The remaining 40 µL was subjected to proteomics analysis, as described below.

G3BP1 immunoprecipitation:

For G3BP1 IPs, polyclonal anti-G3BP (Rabbit, Anova H00010146-D01) was added to Dynabeads Protein G (Invitrogen 10004D) for 10 minutes at 25˚C according to the manufacturer's instructions. The cleared lysate supernatant was added to the anti-G3BP1 beads at a concentration of 50 µg total protein per µL beads, and IP reactions were performed at 4°C for 2h. G3BP1 IP protein elution was accomplished via boiling the samples with 50 µL 1X SDS loading buffer (Boston Bioproducts; BP11R) for 5 minutes at 95°C. Following boil elution, 10 µL of sample was subjected to western blot analysis as described above, and the remaining 40 µL was subjected to proteomics analysis in n=2 technical replicates, as described below.

Mass spectrometry sample preparation:

All samples, regardless of IP source, were processed for mass spectrometry using an in-gel digestion method (Schevchenko et al., 2007). Briefly, samples were run on a 5% SDS-PAGE gel to 2 cm below the loading well, then stained with Coomassie for 1h at room temperature and destained overnight in water. Gels were soaked in water for 1h, and bands were cut into 1 mm cubes and dehydrated in acetonitrile for 10 minutes before reconstitution in 100 mM ammonium bicarbonate. Disulfide bonds were reduced with 10 mM dithiothreitol (DTT) for 1h at 55°C, and cysteine residues were alkylated with 55 mM iodoacetamide (IAA) for 30 minutes at ambient temperature, protected from light. Samples were then digested overnight at 37°C with 150 µL of 13 ng/µL Trypsin (Promega (Madison, WI, USA), sequencing grade), followed by extraction with 150 µL of 1:2 (vol/vol) 5% formic acid/acetonitrile for 15 minutes at 37˚C. Finally, samples were lyophilized, and reconstituted for mass spectrometry analysis.

Liquid chromatography tandem mass spectrometry (LC/MS/MS) run information:

Samples were dissolved in 25 µl of 5% Acetonitrile in 0.1% trifluroacetic acid prior to injection on LC/MS/MS. A 4.0 µl aliquot was directly injected onto a custom packed 2cm x 100µm C18 Magic 5µ particle trap column. Peptides were then eluted and sprayed from a custom packed emitter (75µm x 25cm C18 Magic 3µm particle) with a linear gradient from 95% solvent A (0.1% formic acid in

water) to 35% solvent B (0.1% formic acid in Acetonitrile) in 90 minutes at a flow rate of 300 nL/minute on a Waters Nano Acquity UPLC system. Data dependent acquisitions were performed on a Q Exactive mass spectrometer (Thermo Scientific) according to an experiment where full MS scans from 300-1750 m/z were acquired at a resolution of 70,000 followed by 10 MS/MS scans acquired under higher-energy collisional dissociation (HCD) fragmentation at a resolution of 17,500 with an isolation width of 1.6 Da. Two independent experiments (biological replicates) were tested.

Proteomics data analysis parameters:

Database searching: All MS/MS samples were analyzed using Mascot (Matrix Science, London, UK; version 1.4.1.14). Mascot was set up to search Mascot5_Uniprot_Human_All entries (unknown version, 77417 entries) assuming the digestion enzyme entry “StrictTrypsin”. Mascot was searched with a fragment ion mass tolerance of 0.050 Da and a parent ion tolerance of 10.0 parts per million (ppm). Carbamidomethyl of cysteine was specified in Mascot as a fixed modification. Gln->pyro-Glu of the N-terminus, oxidation of methionine and acetyl of the N-terminus were specified in Mascot as variable modifications.

Criteria for protein identification: Scaffold (version Scaffold_4.4.3, Proteome Software Inc., Portland, OR) was used to validate MS/MS based peptide and protein identifications. Peptide identifications were accepted if they could be established at greater than 70% probability by the Peptide Prophet algorithm (Keller et al., 2002) with Scaffold delta-mass correction. Protein

identifications were accepted if they could be established at greater than 90% probability and contained at least 2 identified peptides. Protein probabilities were assigned by the Protein Prophet algorithm (Nesvizhskii et al., 2003). Proteins that contained similar peptides and could not be differentiated based on MS/MS analysis alone were grouped to satisfy the principles of parsimony. Proteins sharing significant peptide evidence were grouped into clusters. Absolute protein amounts were calculated and compared between samples as the sum of all peptide peak intensities divided by the number of theoretically observable tryptic peptides (intensity based absolute quantification, or “iBAQ”) (Schwanhausser et al., 2011).

RESULTS

1. Inducible cell lines stably express FLAGHA-FUS

To determine protein interactions of mutant FUS in stress granules, we engineered stable HEK-293 cell lines that express doxycycline-inducible FLAGHA-tagged FUS constructs, including FUS-WT, cytoplasmic mutant FUS-P525L-FL, a truncation construct (FUS-P525L-ΔRGG), and a FLAGHA control construct. FUS-P525L-FL represents the aforementioned stress granule-localizing FALS mutant (**Figure II.2a**). All FLAGHA-FUS proteins were expressed in these cells lines within 1-to-2 fold relative to one other upon induction with doxycycline for 24h, as western blot analysis using an antibody to FLAG confirmed. An anti-FUS antibody (see Materials and Methods) also showed that induced FLAGHA-FUS proteins were expressed at near-endogenous levels, and

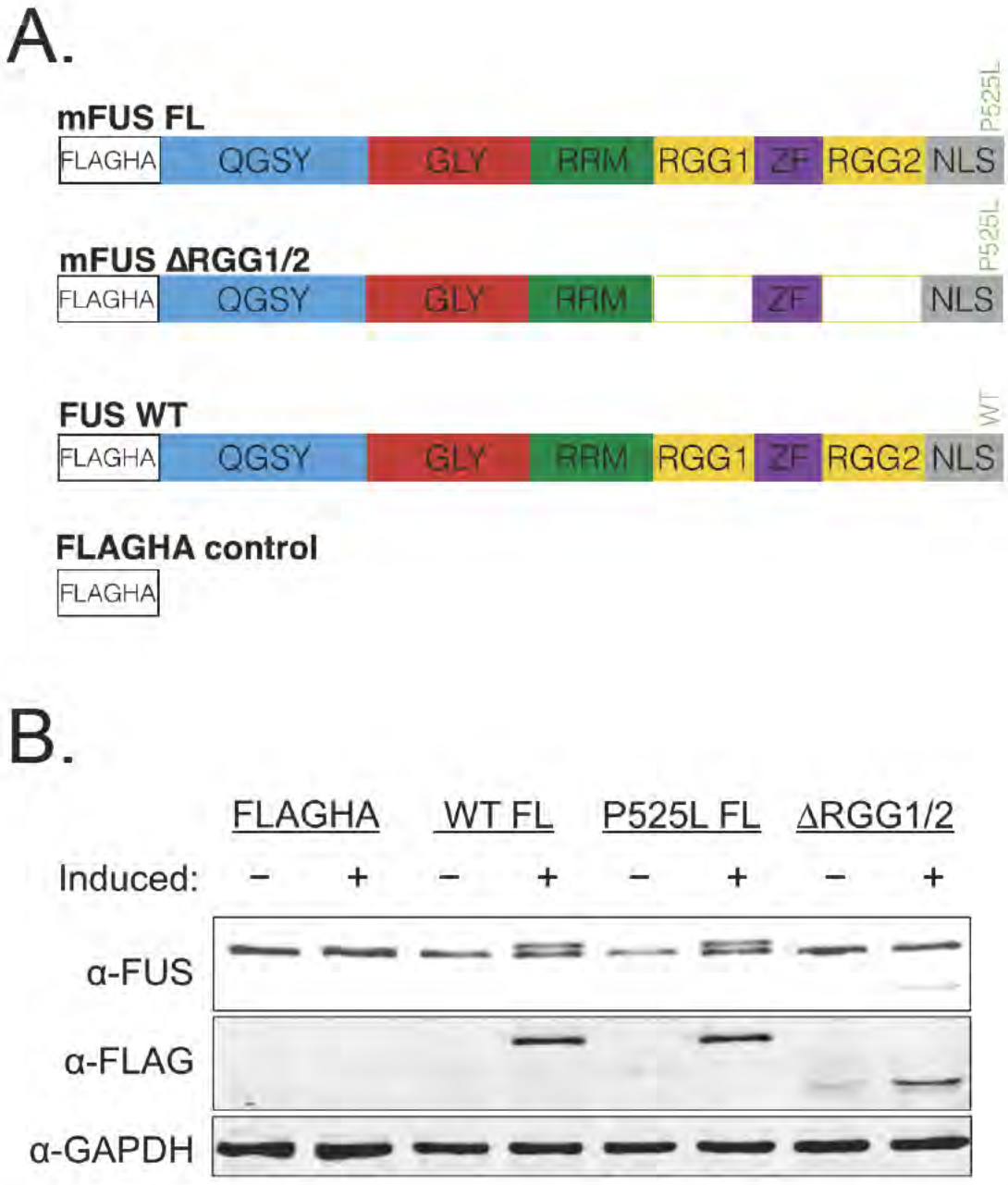

Figure II.2: Stable cell lines used for mass spectrometry proteomics show expected localization of FLAGHA-FUS variants to stress granules. (A) Domain structure of gene expression cassettes used to construct FlpIn TRex HEK293 cells. **(B)** Cell lines express FLAGHA-FUS at levels similar to endogenous FUS, as seen by western blot using antibodies against FLAG and FUS. (**continued on the next page**)

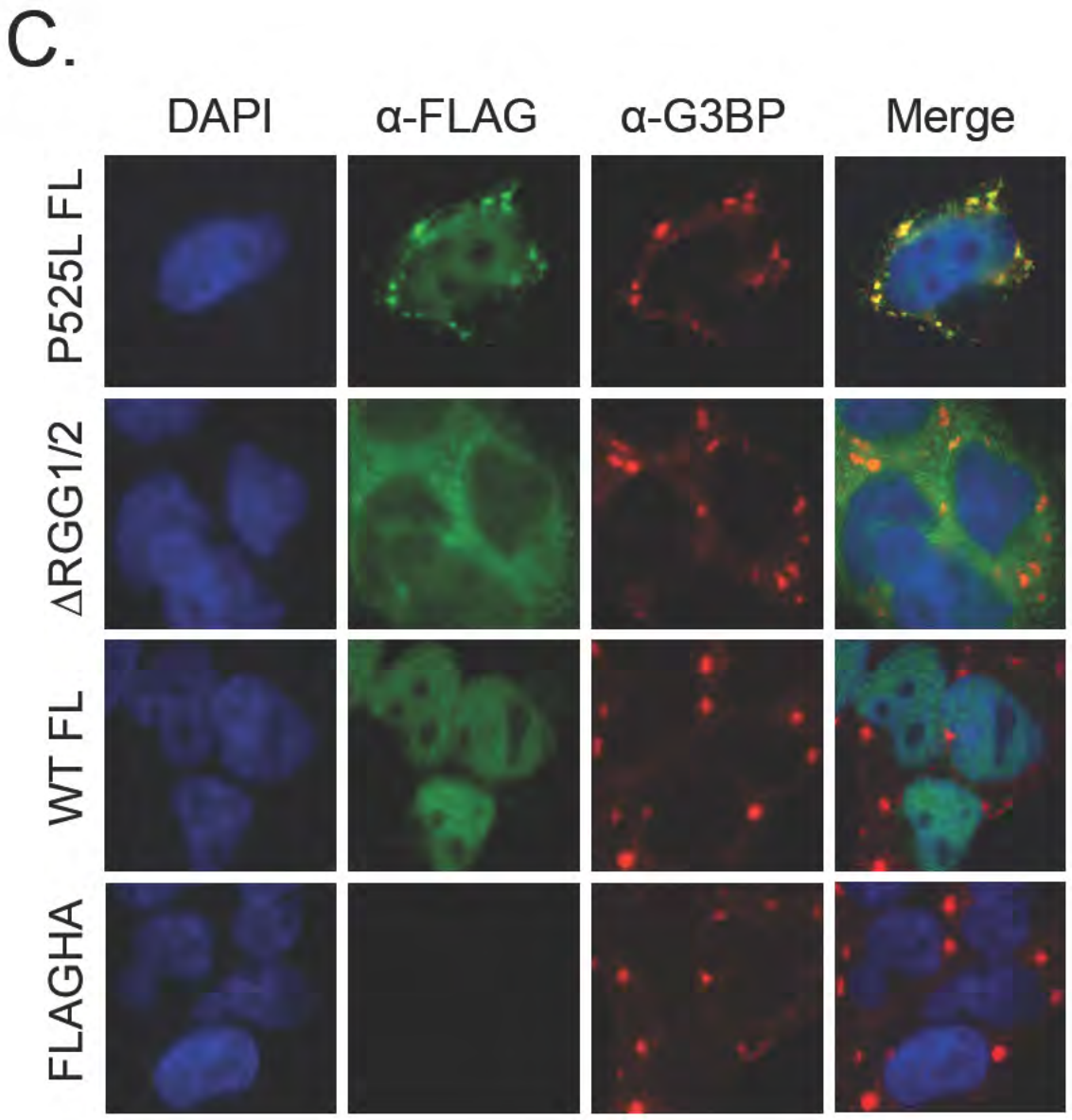

Figure II.2 continued: (C) Immunofluorescence showing FLAGHA-FUS cell lines stressed with sodium arsenite. P525L-FL (top; green) localizes robustly to G3BP(+) stress granules (red), whereas ΔRGG1/2, WT and FLAGHA control lines do not localize to stress granules.

the expression of these exogenous proteins did not greatly alter endogenous FUS expression levels (**Figure II.2b**).

Immunofluorescence of these HEK-293 cells revealed an intense nuclear FLAGHA-FUS expression for FUS-WT and contrasting shift to cytoplasmic localization for FUS-P525L-FL and FUS-P525L-ΔRGG constructs. Additionally, FUS-P525L-FL cell lines show robust localization of FLAGHA-FUS to arsenite-induced stress granules, while FUS-WT and FUS-P525L-ΔRGG lines remain excluded (**Figure II.2c**). FLAGHA-FUS expression throughout continuous exposure to doxycycline was not associated with any overt change in cellular morphology or proliferation for up to 4 days compared to uninduced cells [data not shown].

2. Crosslinking stabilizes stress granule interactions of mutant FUS

Next, we optimized formaldehyde crosslinking conditions to stabilize and preserve transient FLAGHA-FUS protein interactions under stress in a manner compatible with mass spectrometry analysis (Sutherland et al., 2008). FLAGHA-tagged FUS-P525L-FL cells were stressed with sodium arsenite and treated with varying concentrations of formaldehyde before quenching, lysis and western analysis (**Figure II.3a** and Materials and Methods). FLAGHA-FUS diminished from the soluble fraction of lysates starting with minor precipitation at 0.25% formaldehyde and nearly complete precipitation into the insoluble fraction at 1% formaldehyde. We therefore chose 0.5% formaldehyde as the best condition to preserve relevant protein interactions.

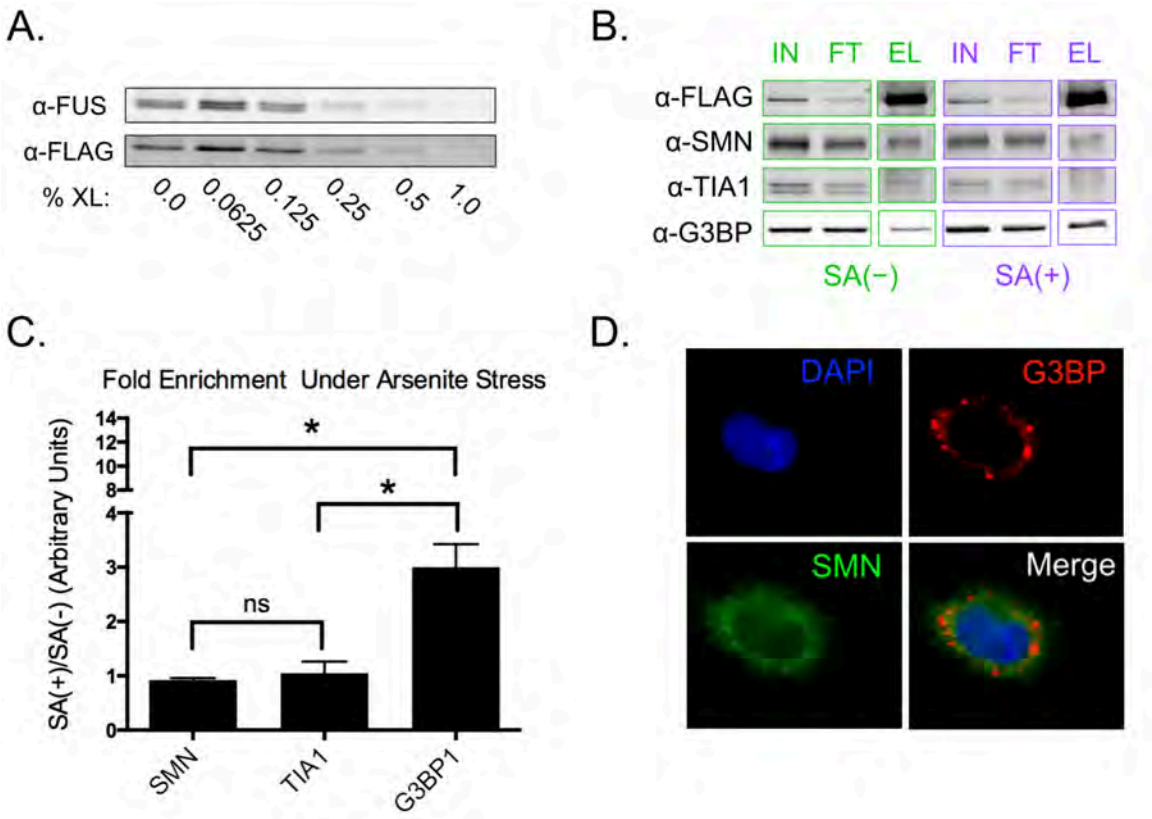

Figure II.3: Under stress, crosslinked FLAGHA-FUS P525L is effectively immunoprecipitated, shows enhanced binding under stress to G3BP1, but does not increase in TIA1 or SMN binding. (A) FLAGHA-FUS-P525L-FL begins to be removed from the soluble fraction during crosslinking starting at 0.25% formaldehyde, as shown via western of soluble lysate fractions with anti-FLAG and anti-FUS antibodies. **(B)** Anti-FLAG immunoprecipitation of arsenite-stressed FlpIn HEK cells expressing FLAGHA-FUS-P525L-FLwith (SA(+)) and without (SA(-)) arsenite stress. Note enriched G3BP1 association under stress conditions (bottom row left vs. right). **(C)** Fold enrichment under arsenite stress of indicated proteins with FLAGHA-FUS-P525L-FL, as quantified by western blot densitometry measurements from two biological replicate IPs and compared by unpaired t-test (*p= <0.05). **(D)** Immunofluorescence of FLAGHA-FUS-P525L-FL expressing cells under arsenite stress do not show anti-SMN (green) localization to stress granules, as visualized by anti-G3BP1 (red).

Cross-linked lysates were then subjected to anti-FLAG immunoprecipitation to isolate FLAGHA-FUS protein interactions (see Materials and Methods). The majority of FLAGHA-FUS was immunoprecipitated from the input sample (**Figure II.3b, top row**). Because we were not able to elute the FLAGHA-FUS from the anti-FLAG beads using a FLAG peptide elution, possibly due to crosslinking epitope obstruction (data not shown), we boiled the samples to elute the protein interactions under crosslinked conditions (**Figure II.3b, rightmost columns**).

To validate that our methods preserved transient stress granule interactions, we subjected FLAGHA-tagged FUS-P525L-FL immunoprecipitation products to western analysis of several stress granule marker proteins (**Figure II.3b, bottom rows**). Under stress conditions, FUS-P525L-FL pulled down ~3X more G3BP1 than in unstressed conditions, a result consistent with the preservation of mutant FUS stress granule interactions. Conversely, FUS-P525L-FL did not show enhanced binding to a known binding partner, SMN, under stress granule-inducing conditions (**Figure II.3c**). This result is in line with the observation that SMN does not localize to stress granules in our system (**Figure II.3d**). Finally, FUS-P525L-FL did not exhibit enriched binding under stress with another stress granule maker protein, TIA-1 (**Figure II.3b, third row, and Figure II.3c**), compared to that of G3BP1 (**Figure II.3b, fourth row, and Figure II.3d**). This observation supports the notion that crosslinking conditions were not overly

promiscuous, but rather likely preserved nearby stress granule interactions of FUS-P525L-FL.

3. Proteomics reveal binding partners enriched in full-length mutant FUS IPs under stress

With IPs established, we next sought to identify FUS-P525L-FL stress granule interactions. To assess the full complement of proteins associated with FUS-P525L-FL in stress granules, we performed comprehensive mass spectrometry analyses of FLAGHA-tagged samples subjected to formaldehyde crosslinking and FLAG IP from cells expressing FUS-P525L-FL, FUS-P525L-ΔRGG, FUS-WT, and FLAGHA control (to control for nonspecific interactions).

Of the 223 proteins identified that were enriched 4-fold over FLAGHA control IPs under stress conditions (**Appendix I**), 146 proteins were enriched in the FUS-P525L-FL IPs at least 4-fold over FUS-WT IPs. These proteins represent the population of interactions available to cytoplasmic FUS-P525L-FL for possible localization to stress granules. Remarkably, 52 of these FUS-P525L-FL-enriched proteins were also at least 4-fold enriched compared to FUS-P525L-ΔRGG IPs and present in biological replicate experiments (**Table II.1**). Since mutant FUS lacking RGG domains fails to localize to stress granules (**Figure II.1**), and since WT FUS does not localize to stress granules under arsenite stress (**Figure I.3**) (Bosco et al., 2010), these enriched proteins represent possible stress granule-associated protein interactions for mutant FUS.

Table II.1: Associations of full-length mutant FUS under stress conditions. For each protein hit, binding bias under stress (SA), RNA and PAR conditions are shown (middle columns). Hits fall into seven distinct categories based on DAVID and GeneCard literature searches, as shown in the “Pathway” column. Finally, literature information on FUS binding and stress granule involvement is shown (left columns).

Table II.1 is displayed across the next four pages for visual clarity.

Gene[1]	Protein Name	Binding Bias			Pathway[5]	Published Literature				
		SA[2]	RNA[3]	PAR[4]		FUS Binder?[6]	SG Binder?[7]	KD Effect on SGs[8]	OE Effect on SGs[8]	Refs.
AGO2	Argonaute-2	–	–	+	mRNA Degradation	-	yes (nucleator)	-	-	Leung et al., 2006
ATX2L	Ataxin-2-like protein	+	+	–	RNA Oligomerization	yes	yes	-	-	Kaehler et al., 2012; Wang et al., 2014
ATXN2	Ataxin-2	+	–	–	RNA Oligomerization	-	yes (nucleator)	↓assembly	-	Ralser et al., 2005; Nonhoff et al., 2007
CAPR1	Caprin-1	+	+	–	RNA Oligomerization	-	yes (nucleator)	-	↑assembly	Solomon et al., 2007
DCTN2	Dynactin subunit 2	+	+	–	Motor/Cytoskeleton	-	-	-	-	
DDX19A	RNA helicase DDX19A	=	+	–	mRNA Translation/Transport	-	-	-	-	
DDX6	RNA helicase DDX6 (P54/Rck)	=	+	–	mRNA Degradation	-	yes (nucleator)	↓assembly	↑assembly	Ernoult-Lange et al., 2012
DHX36	RNA helicase DHX36	+	+++	+	mRNA Stability	-	yes (nucleator)	↓assembly	↑assembly	Chalupnikova et al., 2008
DHX57	RNA helicase DHX57	+	+++	+	mRNA Stability	-	-	-	-	
EIF4H	Eukaryotic translation initiation factor 4H	+	+	–	mRNA Translation/Transport	-	yes	↑assembly	-	Mokas et al., 2009
ERF3A	Eukaryotic peptide chain release factor	=	–	–	mRNA Degradation	-	-	-	-	
F120A	Constitutive coactivator of PPAR-gamma-like protein 1	=	+	+	Signaling	-	-	-	-	
FA98A	Family with sequence similarity 98 (FAM98A)	+	+	+	mRNA Translation/Transport	yes	-	-	-	Wang et al., 20014
FAKD5	FAST kinase domain-containing protein 5	+	+	–	Signaling	-	yes (nucleator)	-	-	Kedersha et al., 2005
FMR1	Fragile X mental retardation protein 1	=	–	–	RNA Oligomerization	-	yes (nucleator)	-	-	Mazroui et al., 2002

Gene[1]	Protein Name	Binding Bias			Pathway[5]	Published Literature				
		SA[2]	RNA[3]	PAR[4]		FUS Binder?[6]	SG Binder?[7]	KD Effect on SGs[8]	OE Effect on SGs[8]	Refs.
FXR1	Fragile X mental retardation-related protein 1	=	+	–	RNA Oligomerization	-	yes (nucleator)	↓assembly	↑assembly	Antar et al., 2005
FXR2	Fragile X mental retardation-related protein 2	=	+	–	RNA Oligomerization	-	yes (nucleator)	-	-	Antar et al., 2005
G3BP1	Ras GTPase-activating protein-binding protein 1	+	+	–	RNA Oligomerization	-	yes (nucleator)	↓assembly	↑assembly	Tourriere et al., 2003
G3BP2	Ras GTPase-activating protein-binding protein 2	+	+++	+	RNA Oligomerization	-	yes (nucleator)	↓assembly	↑assembly	Matsuki et al., 2013
HDAC1	Histone deacetylase 1	=	+	–	Signaling	-	-	-	-	
HNRPQ	Heterogeneous nuclear ribonucleoprotein Q	=	+	–	mRNA Stability	-	yes	-	-	Quaresmae et al., 2009
IF2B1	Insulin-like growth factor 2 mRNA-binding protein 1	=	+	–	mRNA Stability	-	yes	-	-	Deigendesch, et al., 2006
IF2B2	Insulin-like growth factor 2 mRNA-binding protein 2	=	+	+	mRNA Stability	-	yes	-	-	Deigendesch, et al., 2006
IF2B3	Insulin-like growth factor 2 mRNA-binding protein 3	=	+	–	mRNA Stability	-	yes	-	-	Deigendesch, et al., 2006
LAR4B	La-related protein 4B	+	+++	+	Signaling	-	yes	-	-	Schäffler et al., 2010
LARP1	La-related protein 1	+	+	+	Signaling	-	yes	-	-	Kedersha et al., 2008
LARP4	La-related protein 4	=	–	+	Signaling	-	yes	-	-	Yang et al., 2011
MCTS1	Malignant T-cell-amplified sequence 1	=	+++	–	mRNA Translation/Transport	-	-	-	-	
MOV10	Putative helicase MOV-10	=	+	+	mRNA Degradation	-	yes	-	-	Meister et al., 2005
MSI1H	RNA-binding protein Musashi homolog 1	=	+++	–	mRNA Degradation	-	yes	↑assembly	-	ErLin et al., 2015

Gene[1]	Protein Name	Binding Bias			Pathway[5]	Published Literature				
		SA[2]	RNA[3]	PAR[4]		FUS Binder?[6]	SG Binder?[7]	KD Effect on SGs[8]	OE Effect on SGs[8]	Refs.
MSI2H	RNA-binding protein Musashi homolog 2	+	+++	+	mRNA Degradation	-	yes	↑assembly	-	ErLin et al., 2015
NAPA	Alpha-soluble NSF attachment protein	–	+++	–	Signaling	-	-	-	-	
NMT1	Glycylpeptide N-tetradecanoyltransferase 1	+	+++	–	mRNA Stability	-	-	-	-	
NUFP2	Nuclear fragile X mental retardation-interacting protein 2	+	+	+	Motor/Cytoskeleton	-	-	-	-	
NUP62	Nuclear pore glycoprotein p62	=	+++	–	mRNA Translation/Transport	-	-	-	-	
PABP4	Polyadenylate-binding protein 4	=	+	+	mRNA Translation/Transport	-	yes	-	-	Burgess et al., 2011
PRC2A	Proline-Rich Coiled-Coil 2A	=	+++	–	mRNA Stability	-	-	-	-	
PSA	Puromycin-sensitive aminopeptidase	=	+	–	RNA Oligomerization	-	-	-	-	
PSMF1	Proteasome inhibitor PI31 subunit	=	–	–	Proteasome	-	-	-	-	
PUM1	Pumilio homolog 1	+	+++	+	mRNA Degradation	-	yes (nucleator)	↓assembly	↑assembly	Vessey et al., 2006
PURA	Transcriptional activator protein Pur-alpha	+	+++	–	mRNA Translation/Transport	-	yes	-	-	Donnelly et al., 2010
PURB	Transcriptional activator protein Pur-beta	=	+++	+	mRNA Translation/Transport	-	yes	-	-	Donnelly et al., 2010
RENT1	Regulator of nonsense transcripts 1	–	+	+	mRNA Degradation	yes	yes	-	-	Barmada, et al., 2015; Gardner et al., 2008
RIR2	Ribonucleoside-diphosphate reductase subunit M2	–	+	–	Signaling	-	-	-	-	
STAU2	Staufen 2	–	+++	+	Motor/Cytoskeleton	-	yes	↑assembly	↓assembly	Thomas et al., 2009

Gene[1]	Protein Name	Binding Bias			Pathway[5]	Published Literature				
		SA[2]	RNA[3]	PAR[4]		FUS Binder?[6]	SG Binder?[7]	KD Effect on SGs[8]	OE Effect on SGs[8]	Refs.
USP10	Ubiquitin carboxyl-terminal hydrolase 10	+	+	–	Proteasome	-	yes (nucleator)	↓assembly	-	Takahashi et al., 2013
UBP2L	Ubiquitin-associated protein 2-like	+	+	–	Proteasome	yes	-	-	-	Wang et al., 2014
UFD1	Ubiquitin fusion degradation protein 1 homolog	+	+	–	Proteasome	-	-	-	-	
YBOX1	Nuclease-sensitive element-binding protein 1	=	+++	–	mRNA Stability	yes	yes	↓assembly	-	Onishi et al., 2008; Somasekharan et al., 2015; Wang et al., 2014
YTHD3	YTH domain-containing family protein 3	+	+	+	mRNA Degradation	-	yes	-	-	
ZCHC3	Zinc finger CCHC domain-containing protein 3	+	+	+	mRNA Translation/Transport	-	-	-	-	
ZN598	Zinc finger protein 598	+	+	–	mRNA Translation/Transport	-	-	-	-	

[1]Gene name according to UniProt. For UniProt accession numbers for each gene, please see **Appendix I**.

[2]Hits categorized based on their enrichment under arsenite stress conditions (SA) vs. unstressed. Color coding matches **Figure II.4.** ("+" is enriched ≥2-fold; "–" is enriched <0.5-fold' "=" is enriched 0.5-2-fold)

[3]Hits categorized based on their % retention after RNase A treatment vs. untreated. Color coding matches **Figure II.4.** ("+" is retained 10-49% ; "+++" is retained 50-100%; "–" is retained <10%)

[4]Hits categorized based on % retention under poly(ADP)-ribose (PAR) preservation conditions (ADP-HPD treatment) vs. untreated. Also see **Table II.2.** ("+" is enriched ≥5-fold; "–" is enriched <5-fold)

[5]Hits are divided into distinct categories based on DAVID and GeneCard searches.

[6]Evidence for binding to FUS based on published literature.

[7]Evidence for localization to stress granules (SG) based on published literature.

[8]Effect of knock-down (KD) or over-expression (OE) of each hit on stress granule assembly based on published literature.

Among the most abundant stress granule-relevant hits, enriched exclusively in FUS-P525L-FL IPs, were proteins known to localize to stress granules: YBOX1, PABP4, G3BP1/2, ATXN2L/ATXN2, FMP1/FXR1/FXR2. Of the 27 known stress granule proteins found within the hits, several are essential for stress granule formation and are known as stress granule “nucleators” (e.g., G3BP1/G3BP2, ATXN2/ATXN2L, YBOX1) (Aulas et al., 2015; Kaehler et al., 2012; Somasekharan et al., 2015; Tourrière et al., 2003). Notably absent are the stress granule nucleators TIA-1 and HuR. The most highly enriched known stress granule component was G3BP1, though a set of known peripheral G3BP1 complexes (such as Caprin1 and USP10) were also detected at lower abundance than G3BP1 (**see Appendix I Table AI.1**). Additionally, 39% of FUS-P525L-FL associated proteins were not significantly enriched between stressed compared to unstressed conditions (**Figure II.4a, right**), implying that mutant FUS binds them regardless of stress. A similar percentage of FUS-P525L-FL hits (38%) are enriched at least 2-fold in arsenite stress compared to unstressed conditions. These proteins include G3BP1/G3BP2, helicase DDX1, translation initiation factor EIF4E, YTH domain-containing protein, and transcriptional activator Pur-alpha (PURA), all known stress granule proteins. In addition to known stress granule proteins, 17 proteins bound to FUS-P525L-FL have not yet been identified in stress granules and therefore represent a potentially novel set of stress granule-associated proteins. These include the RNA helicases DDX19A

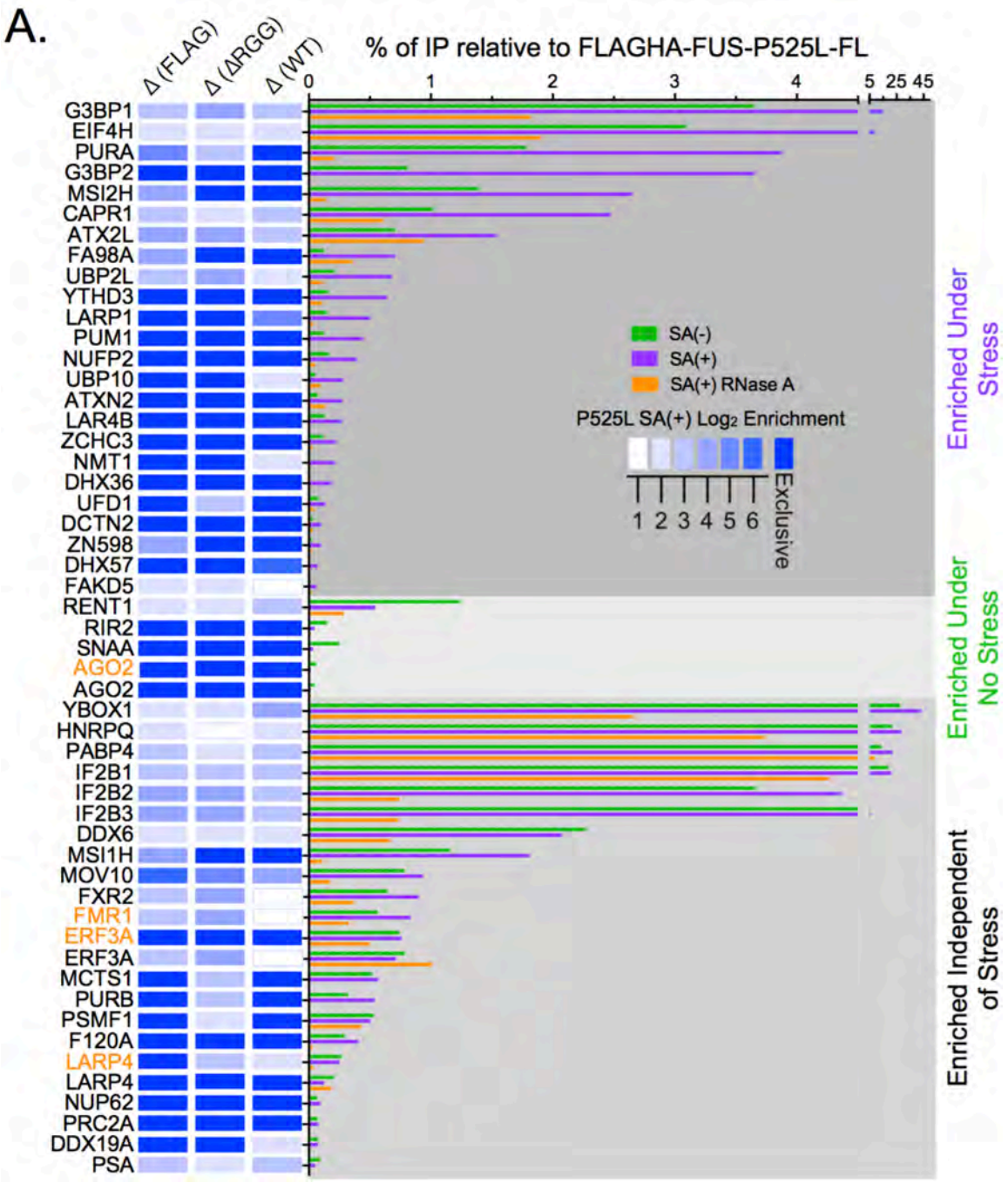
A.
Δ (FLAG)
Δ (ΔRGG)
Δ (WT)
% of IP relative to FLAGHA-FUS-P525L-FL
0
1
2
3
4
5
25
45
G3BP1
EIF4H
PURA
G3BP2
MSI2H
CAPR1
ATX2L
FA98A
UBP2L
YTHD3
LARP1
PUM1
NUFP2
UBP10
ATXN2
LAR4B
ZCHC3
NMT1
DHX36
UFD1
DCTN2
ZN598
DHX57
FAKD5
RENT1
RIR2
SNAA
AGO2
AGO2
YBOX1
HNRPQ
PABP4
IF2B1
IF2B2
IF2B3
DDX6
MSI1H
MOV10
FXR2
FMR1
ERF3A
ERF3A
MCTS1
PURB
PSMF1
F120A
LARP4
LARP4
NUP62
PRC2A
DDX19A
PSA
SA(-)
SA(+)
SA(+) RNase A
P525L SA(+) Log2 Enrichment
1 2 3 4 5 6
Exclusive
Enriched Under Stress
Enriched Under No Stress
Enriched Independent of Stress

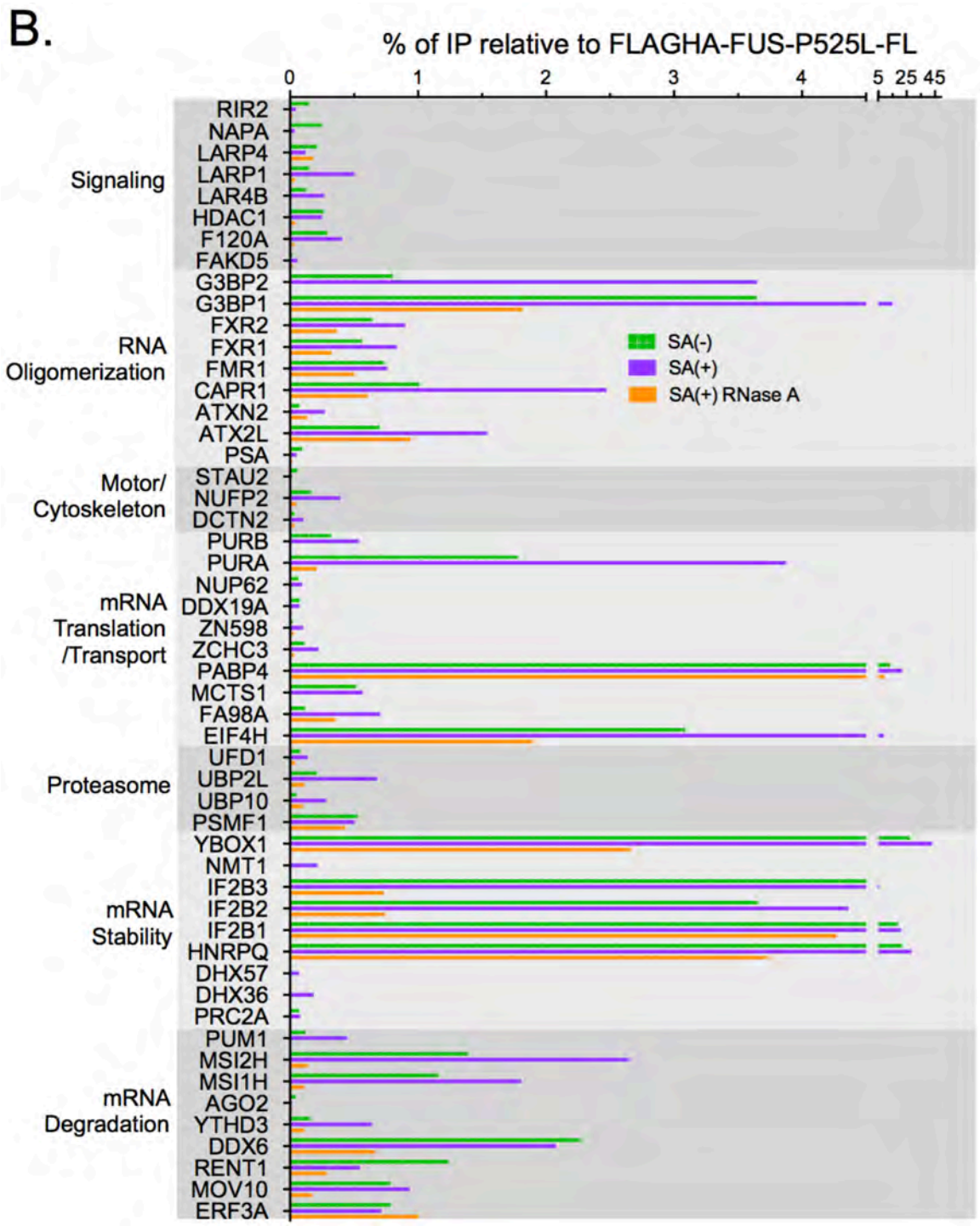
B.
% of IP relative to FLAGHA-FUS-P525L-FL
0
1
2
3
4
5
25
45
SA(-)
SA(+)
SA(+) RNase A
Signaling
RIR2
NAPA
LARP4
LARP1
LAR4B
HDAC1
F120A
FAKD5
RNA Oligomerization
G3BP2
G3BP1
FXR2
FXR1
FMR1
CAPR1
ATXN2
ATX2L
PSA
Motor/ Cytoskeleton
STAU2
NUFP2
DCTN2
mRNA Translation /Transport
PURB
PURA
NUP62
DDX19A
ZN598
ZCHC3
PABP4
MCTS1
FA98A
EIF4H
Proteasome
UFD1
UBP2L
UBP10
PSMF1
mRNA Stability
YBOX1
NMT1
IF2B3
IF2B2
IF2B1
HNRPQ
DHX57
DHX36
PRC2A
mRNA Degradation
PUM1
MSI2H
MSI1H
AGO2
YTHD3
DDX6
RENT1
MOV10
ERF3A

Figure II.4: The FLAGHA-FUS-P525L-FL interactome with and without arsenite stress. (A) (Left) Heatmap showing fold enrichment of each indicated protein in stressed FLAGHA-FUS P525L-FL IPs relative to its level in a FLAGHA peptide control IP (Δ (FLAG)), FLAGHA-FUS-P525L-ΔRGG1/2 IP (Δ (ΔRGG)), and FLAGHA-FUS-WT IP (Δ (WT)). Heatmap log2 color scale is shown on the right. All proteins shown were at least 4-fold enriched in FLAGHA-FUS IPs compared to FLAGHA control IPs, which translates into a log2 value of 2. Many hits are completely absent from FLAG control IPs, are shown as "Exclusive" in the heatmap; ATXN2 is an example of this case. (Center) Bar graph showing % iBAQ abundance of each protein in FLAGHA-FUS-P525L-FL IPs in unstressed (SA(-); green), arsenite-stressed (SA(+); purple), or arsenite-stressed and RNase A-treated (orange) conditions. % abundance for each hit is calculated relative to iBAQ values of the FLAGHA-FUS protein within the same IP. Note that FLAGHA-FUS iBAQ values encompass not only the exogenously-expressed FLAGHA-FUS peptides identified in mass spec, but also endogenous FUS-specific peptides. Therefore, the FLAGHA-FUS iBAQ could also contain endogenous FUS detection. For all iBAQ values, please see **Appendix I**. (Right) Enriched proteins are divided into sections based on their relative enrichment during each condition. **(B)** Protein hits in A divided into distinct categories based on DAVID and GeneCards literature information, also listed in **Table II.1**.

and DHX57, Ubiquitin-associated protein 2-like (UBP2L), FAM98, and dynactin subunit 2 (DCTN2).

Associations of FUS-P525L-FL could be organized into 7 readily definable categories (**Table II.1 and Figure II.4b**). Intriguingly, the most populated categories include mRNA degradation and stress granule dynamics, each with 9 hits. Of the mRNA degradation proteins, two are proteins that are thought to be specific for P-bodies (YTHD3, DDX6) (Richter, 2007), three are key members of the nonsense-mediated decay (NMD) pathway (RENT1, MOV10 and ERF3A) (Gardner, 2010), and four are members of the RNA-induced silencing complex (RISC), including two Mushashi homologues (MSI1/MSI2), Argonaut-2 (AGO2) and Pumilio-1 (PUM1) (Jain and Parker, 2013). Of the remaining hits, the most highly enriched fall into categories associated with mRNA stability, such as nuclease-sensitive element binding protein 1 (YBOX1) and insulin-like growth factors IF2B1/2/3, and mRNA translation, such as poly(A)-binding protein 4 (PABP4) and eukaryotic initiation factor 4H (EIF4H). These interactions represent diverse areas of cellular function potentially impacted by mutant FUS localization to stress granules.

4. Indirect interactions of mutant FUS under stress reveal a role for RNA and poly(ADP)-ribose on FUS stress granule interactions.

FUS is a RNA-binding protein that binds over 900 mRNA transcripts in the cytoplasm (Hoell et al., 2011). Hence, we assessed the requirement for RNA on mutant FUS interactions under stress. Cells expressing FLAGHA-tagged FUS-

P525L-FL under stress conditions were crosslinked, precipitated with anti-FLAG, and subsequently treated with RNase A prior to elution and mass spec analysis. **Figure II.4a** and **Table II.1** reveals that all but six interactions of full-length mutant FUS hits are at least partially RNA-mediated, with 16 out of the 52 hits completely disappearing under RNase conditions. The remaining 30 hits are partially RNA-mediated in that they remain associated with FUS within 10-40% of RNase(-) conditions. The six interactions that remain under RNase(+) conditions within 50% of RNase(-) conditions include the ND-associated proteins Ataxin2 and FMRP. Also present in direct FUS interactions are the proteasome inhibitor PSMF1, NMD component eukaryotic release factor 3 (ERF3A), and RISC factor Ago2, all implicated in important degradation pathways (Gardner, 2010; Li et al., 2014; Rand et al., 2005). These results implicate RNA binding as a major factor in mutant FUS localization to stress granules and identify potentially important RNA-independent interactions of mutant FUS during stress.

Next, we examined the role of poly(ADP)-ribose (PAR) in mutant FUS interactions during stress. Proteins modified with PAR accumulate in stress granules, and the depletion of key PAR phosphatases (PARPs), which polymerize PAR structures, or overexpression of PAR glycohydrolases (PARGs), which hydrolyze the glycosidic bond between ADP-ribose units, impairs stress granule formation (Leung et al., 2011; Schreiber et al., 2006; Shi, 2012). These findings suggest that PAR modifications are important for proper stress granule formation. A functional theory on the role of PAR in stress granules is that these

molecules act as molecular scaffolds in the coalescence and stability of stress granule structure, not unlike RNA oligomerization (Ivanov et al., 2011). In order to assess the dependence of mutant FUS stress granule interactions on PAR, FlpIn HEK cells expressing full-length FLAGHA-FUS P525L were stressed and lysed under uncrosslinked conditions in the presence of a PARG inhibitor, ADP-HPD (Leung et al., 2011), then subjected to uncrosslinked anti-FLAG immunoprecipitation and mass spectrometry proteomics. ADP-HPD inhibits PARG activity, thereby preventing PAR de-polymerization and preserving PAR structures. We therefore expect to preserve stress granule structures using this inhibitor. **Figure II.5a** confirms the success of 3X FLAG peptide elution under uncrosslinked conditions, though a reduced amount of G3BP1 was pulled down by FUS-P525L-FL compared to crosslinked conditions. Nonetheless, **Table II.1** and **Table II.2** reveal that 28 out of 53 full-length mutant FUS interactions (52%) are at least 5-fold enriched under ADP-HPD(+) conditions, where PAR is theoretically preserved. Stress granule nucleators, such as G3BP2 and PABP4, are included in this list, as are 6 out of the 9 proteins that fall under the category of mRNA degradation, such as MOV10 and RENT1. Further, two out of the five hits that were RNA-mediated, LARP4 and AGO2, are also mediated by PAR. The remaining three RNA-independent hits, ERF3A, PSMF1 and FMRP, were not enriched under ADP-HPD(+) conditions, suggesting that they are not mediated by PAR. These data suggest a role for PAR in stabilizing mutant FUS interactions under stress, possibly through stress granule preservation.

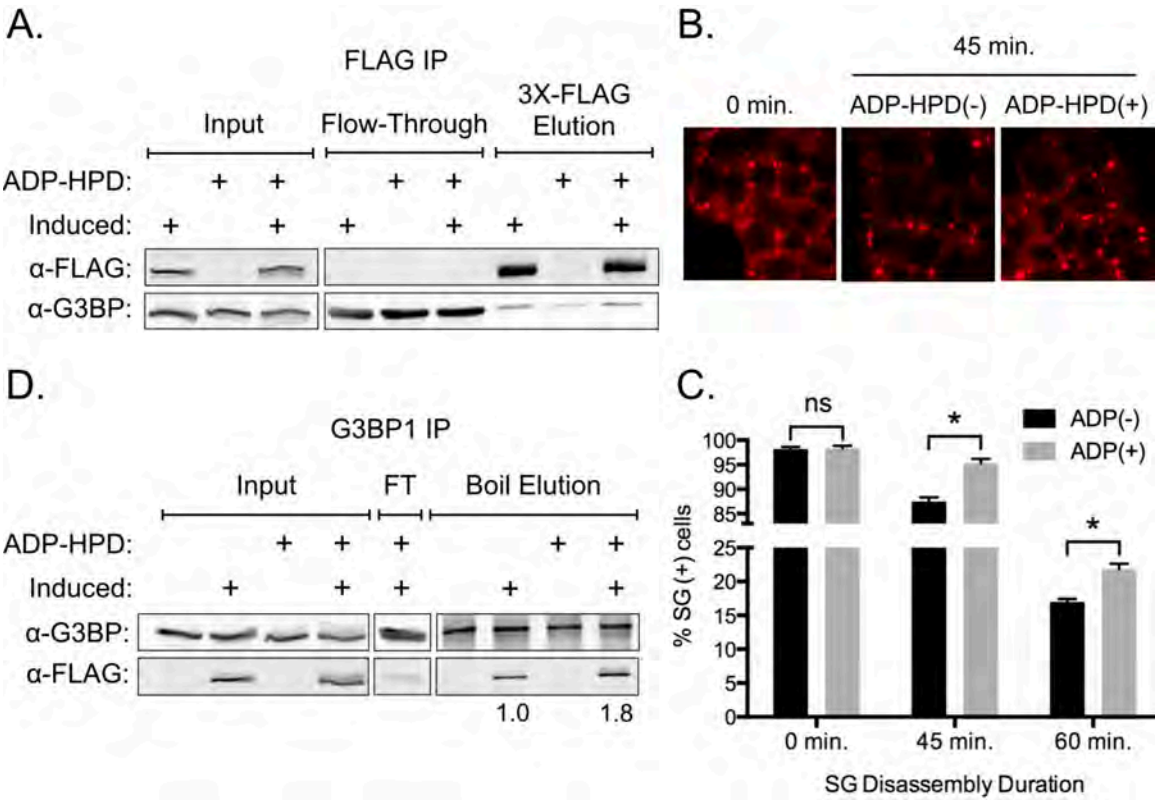

Figure II.5: PARG inhibition does not enhance G3BP1 binding via FLAGHA-FUS P525L IP, but does enhance FLAGHA-FUS binding via G3BP1 IP and mildly delays stress granule disassembly following arsenite stress. (A) Immunoprecipitation of arsenite-stressed FlpIn HEK cells with (+) and without FLAG-FUS P525L induction and ADP-HPD treatment reveals complete FLAG IP and efficient peptide elution. **(B)** FlpIn HEK cells treated with ADP-HPD were stressed for 1h prior to disassembly, after which cells were removed from arsenite conditions for 45-60 minutes, then processed for anti-G3BP immunofluorescence (red). **(C)** Quantification for B reveals significantly increased SG(+) cells via unpaired t-test (n=2, 300 cells each; * = p< 0.05). **(D)** Immunoprecipitation of G3BP under conditions of ADP-HPD treatment displays enhanced binding to FLAGHA-FUS P525L. Westerns in A and D were each detected with anti-G3BP and anti-FLAG antibodies.

Table II.2: PAR-mediated FLAGHA-FUS-P525L-FL interactions enriched under uncrosslinked conditions. iBAQ values for each protein are indicated (see Materials and Methods). Fold change values of ADP-HPD(+) IP (PARG inhibitor present) relative to the ADP-HPD(-) IP (PARG inhibitor absent) are shown, with infinity symbols (∞) indicating exclusive detection in the ADP-HPD(+) IP. Results reflect n=1 biological replicate.

Table II.2 is displayed across the next two pages for visual clarity.

Gene	Protein	ADP (+) (iBAQ ×10^5)	ADP (–) (iBAQ ×10^5)	Δ (+/–)
ABC3C	DNA dC->dU-editing enzyme APOBEC-3C	96.4	-	∞
AGO1	Protein argonaute-1	3.2	-	∞
AGO2	Protein argonaute-2	6.2	-	∞
ASCC2	Activating signal cointegrator 1 complex subunit 2	14.0	1.0	13.6
ATXN2	Ataxin-2	13.8	-	∞
C17ORF75	Protein Njmu-R1	6.4	-	∞
C2D1A	Coiled-coil and C2 domain-containing protein 1A	0.5	-	∞
CDC27	Cell division cycle protein 27 homolog	1.5	-	∞
CHD1L	Chromodomain-helicase-DNA-binding protein 1-like	60.5	2.2	28.1
CLPB	Caseinolytic peptidase B protein homolog	9.6	-	∞
DDX28	Probable ATP-dependent RNA helicase DDX28	7.6	-	∞
DHX29	ATP-dependent RNA helicase DHX29	11.2	2.2	5.0
DHX36	ATP-dependent RNA helicase DHX36	26.6	-	∞
DHX37	Probable ATP-dependent RNA helicase DHX37	3.1	-	∞
DHX40	Probable ATP-dependent RNA helicase DHX40	1.4	-	∞
DHX57	Putative ATP-dependent RNA helicase DHX57	7.0	-	∞
DJC10	DnaJ homolog subfamily C member 10	19.6	1.5	13.2
DPCD	Protein DPCD	6.0	-	∞
DPYL3	Dihydropyrimidinase-related protein 3	13.3	-	∞
ECI2	Enoyl-CoA delta isomerase 2, mitochondrial	1.4	-	∞
EI2BA	Translation initiation factor eIF-2B subunit alpha	24.3	-	∞
EI2BD	Translation initiation factor eIF-2B subunit delta	185.5	36.3	5.1
EIF1	Eukaryotic translation initiation factor 1	140.6	27.9	5.0
ELAV2	ELAV-like protein 2	198.7	-	∞
EMD	Emerin	15.5	-	∞
ERI1	3'-5' exoribonuclease 1	8.4	-	∞
F120A	Constitutive coactivator of PPAR-gamma-like protein 1	68.8	-	∞
F91A1	Protein FAM91A1	9.9	-	∞
FA98A	Protein FAM98A	96.0	-	∞
FETA	Alpha-fetoprotein	37.8	-	∞
FOCAD	Focadhesin	2.3	-	∞
G3BP2	Ras GTPase-activating protein-binding protein 2	55.9	-	∞
GEMI8	Gem-associated protein 8	13.3	-	∞
GYS1	Glycogen [starch] synthase, muscle	30.3	-	∞
HELZ	Probable helicase with zinc finger domain	0.8	-	∞
IF2B2	Insulin-like growth factor 2 mRNA-binding protein 2	273.4	38.9	7.0
IF4E2	Eukaryotic translation initiation factor 4E type 2	7.0	-	∞
IMA7	Importin subunit alpha-7	9.7	-	∞
KAPCA	cAMP-dependent protein kinase catalytic subunit alpha	16.7	-	∞
LAR4B	La-related protein 4B	78.8	10.4	7.6
LARP1	La-related protein 1	244.2	45.4	5.4
LARP4	La-related protein 4	6.4	-	∞
LN28B	Protein lin-28 homolog B	19.9	-	∞
LORF1	LINE-1 retrotransposable element ORF1 protein	13.7	-	∞

Gene	Protein	ADP (+) (iBAQ ×10⁵)	ADP (–) (iBAQ ×10⁵)	Δ (+/–)
MKRN2	Probable E3 ubiquitin-protein ligase makorin-2	17.9	-	∞
MOV10	Putative helicase MOV-10	125.6	8.2	15.4
MRE11	Double-strand break repair protein MRE11A	1.5	-	∞
MSI2H	RNA-binding protein Musashi homolog 2	7.0	-	∞
NEP1	Ribosomal RNA small subunit methyltransferase NEP1	10.2	-	∞
NEUA	N-acylneuraminate cytidylyltransferase	31.2	4.9	6.4
NHP2	H/ACA ribonucleoprotein complex subunit 2	24.9	-	∞
NSUN5	Putative methyltransferase NSUN5	1.2	-	∞
NUFP2	Nuclear fragile X mental retardation-interacting protein 2	29.6	-	∞
P5CR1	Pyrroline-5-carboxylate reductase 1, mitochondrial	31.6	-	∞
PABP4	Polyadenylate-binding protein 4	2764.6	558.0	5.0
PAIP1	Polyadenylate-binding protein-interacting protein 1	16.5	-	∞
PHAX	Phosphorylated adapter RNA export protein	27.2	-	∞
PHF6	PHD finger protein 6	9.4	-	∞
PPM1G	Protein phosphatase 1G	17.4	-	∞
PRC2B	Protein PRRC2B	1.0	-	∞
PRC2C	Protein PRRC2C	5.0	-	∞
PTRH2	Peptidyl-tRNA hydrolase 2, mitochondrial	14.9	-	∞
PUM1	Pumilio homolog 1	12.7	-	∞
PURB	Transcriptional activator protein Pur-beta	47.3	-	∞
PWP1	Periodic tryptophan protein 1 homolog	19.2	-	∞
RENT1	Regulator of nonsense transcripts 1	58.4	10.3	5.7
RFA3	Replication protein A 14 kDa subunit	55.0	-	∞
RFC5	Replication factor C subunit 5	11.1	-	∞
RLA1	60S acidic ribosomal protein P1	2537.9	470.3	5.4
RRP12	RRP12-like protein	1.3	-	∞
RU1C	U1 small nuclear ribonucleoprotein C	274.7	-	∞
RUXGL	Putative small nuclear ribonucleoprotein G-like protein 15	132.7	-	∞
SNP29	Synaptosomal-associated protein 29	6.5	-	∞
SRP14	Signal recognition particle 14 kDa protein	214.3	38.0	5.6
SRP72	Signal recognition particle subunit SRP72	15.4	-	∞
SRPR	Signal recognition particle receptor subunit alpha	1.1	-	∞
STAU2	Double-stranded RNA-binding protein Staufen	10.2	-	∞
TNPO3	Transportin-3	0.6	-	∞
TOE1	Target of EGR1 protein 1	1.9	-	∞
TRI25	E3 ubiquitin/ISG15 ligase TRIM25	64.1	11.6	5.5
U2AF1	Splicing factor U2AF 35 kDa subunit	51.2	-	∞
VP33A	Vacuolar protein sorting-associated protein 33A	6.9	-	∞
VRK3	Inactive serine/threonine-protein kinase VRK3	1.5	-	∞
YTHD3	YTH domain-containing family protein 3	10.5	-	∞
ZCCHV	Zinc finger CCCH-type antiviral protein 1	20.5	1.4	14.3
ZCHC3	Zinc finger CCHC domain-containing protein 3	90.5	1.0	93.1
ZN622	Zinc finger protein 622	8.1	-	∞

5. Mutant FUS alters the G3BP1 interactome under stress.

Next, we investigated the effect of mutant FUS incorporation into stress granules on the G3BP1 interactome during stress. We noted that under PARG-inhibiting conditions, FlpIn HEK cells show significantly delayed stress granule disassembly (**Figure II.5b**). Thus, after many unsuccessful attempts at G3BP1 IP under crosslinked conditions (data not shown), we utilized the PARG inhibitor ADP-HPD based on the notion that PAR mediates stress granule stability (Leung et al., 2011). Arsenite-stressed FlpIn HEK cells, induced and uninduced for full-length P525L expression, were stressed with arsenite and subjected to uncrosslinked G3BP1 IP in the presence of the PARG inhibitor, ADP-HPD. **Figure II.5c** confirms the success of G3BP1 IP under uncrosslinked conditions. Interestingly, we noted a 1.8-fold increase in FLAGHA-FUS present in the G3BP elution under ADP-HPD(+) conditions compared to ADP-HPD(-) conditions (**Figure II.5c**; representative of two experiments). This data is in agreement with crosslinked FLAGHA-FUS experiments that show G3BP enrichment under stress and suggests that stress granules are at least partially stabilized under PARG inhibiting conditions.

Table II.3 shows the proteins identified by mass spec analysis that were enriched at least 10-fold in induced conditions expressing FUS-P525L-FL over uninduced conditions (i.e. lacking FUS-P525L0-FL expression) for the ADP-HPD(+) G3BP1 IP. These hits are also at least 10-fold enriched over those found

Table II.3: G3BP1 IP interactions that are at least 3-fold enriched upon FLAGHA-FUS-P525L-FL expression. (Data reflects interactions found from a *G3BP1 IP*.) iBAQ values for each protein are indicated. Fold change values of G3BP1 interactions from FLAGHA-FUS FlpIn HEK cells in the induced presence (P525L(+)) or uninduced absence (P525L(-))are shown, with infinity symbols (∞) indicating exclusive detection in the P525L(+) IP. None of these proteins was found in FLAGHA-FUS-WT IPs (**Appendix I**), ruling out non-specific nuclear FUS-mediated interactions during lysis.

Gene	Protein	P525L (+) (iBAQ × 10^5)	P525L (–) (iBAQ × 10^5)	Δ (+/–)	Present in FUS-WT IP?
A2MG	Alpha-2-macroglobulin	38.6	4.3	9.0	no
AL9A1	4-trimethylaminobutyraldehyde dehydrogenase	1.9		∞	no
ANC2	Anaphase-promoting complex subunit 2	51.9	13.3	3.9	no
CALR	Calreticulin	7.4		∞	no
CNDD3	Condensin-2 complex subunit D3	9.6	0.9	10.5	no
COPE	Coatomer subunit epsilon	1.2		∞	no
CUL4B	Cullin-4B	2.5	0.6	4.2	no
DC1I2	Cytoplasmic dynein 1 intermediate chain 2	37.0		∞	no
DCTN3	Dynactin subunit 3	9.7	2.6	3.7	no
DDX28	Probable ATP-dependent RNA helicase DDX28	2.6		∞	no
DLRB2	Dynein light chain roadblock-type 2	75.2		∞	no
DOCK7	Dedicator of cytokinesis protein 7	0.4		∞	no
E9PPU0	Epiplakin	4.7	0.4	10.6	no
EI2BE	Translation initiation factor eIF-2B subunit epsilon	8.4		∞	no
ELOB	Transcription elongation factor B polypeptide 2	86.4	13.1	6.6	no
F5H456	RRP12-like protein	6.3	1.3	5.0	no
FKB1A	Peptidyl-prolyl cis-trans isomerase FKBP1A	115.2		∞	no
FLII	Protein flightless-1 homolog	0.6		∞	no
FRYL	Protein furry homolog-like	0.3		∞	no
GT251	Procollagen galactosyltransferase 1	76.9	8.1	9.5	no
HBA	Hemoglobin subunit alpha	222.1	27.8	8.0	no
HCFC1	Host cell factor 1	4.2		∞	no
IMA7	Importin subunit alpha-7	10.2		∞	no
NP1L4	Nucleosome assembly protein 1-like 4	31.2		∞	no
NPM3	Nucleoplasmin-3	88.1		∞	no
NUDC	Nuclear migration protein nudC	6.3		∞	no
PARP9	Poly [ADP-ribose] polymerase 9	10.5	2.8	3.7	no
PNO1	RNA-binding protein PNO1	45.6		∞	no
PPM1G	Protein phosphatase 1G	2.5		∞	no
PRPS2	Ribose-phosphate pyrophosphokinase 2	75.9		∞	no
SAE2	SUMO-activating enzyme subunit 2	2.4		∞	no
SMC5	Structural maintenance of chromosomes protein 5	7.6	1.7	4.4	no
SMCA4	Transcription activator BRG1	0.4	0.1	6.5	no
SMRC1	SWI/SNF complex subunit SMARCC1	2.8		∞	no
UBC9	SUMO-conjugating enzyme UBC9	5.9		∞	no
UFD1	Ubiquitin fusion degradation protein 1	4.5		∞	no
VPS53	Vacuolar protein sorting-associated protein 53	6.3	1.3	4.8	no
XRCC1	DNA repair protein XRCC1	14.1		∞	no
ZRAB2	Zinc finger Ran-binding domain-containing protein 2	31.9	5.2	6.2	no

in FUS-WT IPs (**Appendix I**), suggesting that they are not non-specific hits, nor are they contaminated by potential endogenous FUS interactions.

Interesting proteins enriched in G3BP1 IP under FUS-P525L-FL(+) conditions include several cytoskeletal motor-associated proteins, such as dynein intermediate chain 2 (DC1I2), dynein light chain roadblock type2 (DLRB2), and dynactin subunit 3 (DCTN3). These hits may explain our previous findings that mutant FUS expression delays stress granule assembly and accelerates disassembly (Appendix IV; Baron et al., 2013). Also present is PARP9, a PAR-polymerizing protein, a hit that may contribute to the larger stress granule volume found in mutant FUS-expressing cells by way of increased PAR production (Baron et al., 2013). In addition to proteins that are enriched in G3BP1 binding in the presence of FUS-P525L-FL, 30 proteins are at least 4-fold diminished in association under FUS-P525L-FL(+) conditions and are absent from FUS-P525L-FL IPs (**Table II.4**). These include the kinesin-like proteins KIF14 and KIFC1, once again pointing to a possible loss of important stress granule assembly and disassembly interactions for stress granules in the presence of mutant FUS. Together, these data reveal the disruption of G3BP1 interactions due to mutant FUS expression, likely resulting in an altered stress granule composition.

Table II.4: G3BP1 IP interactions that are at least 3-fold diminished upon FLAGHA-FUS-P525L-FL expression. (Data reflects interactions found from a *G3BP1 IP*.) iBAQ values for each protein are indicated. Fold change values of G3BP1 interactions from FLAGHA-FUS FlpIn HEK cells in the induced presence (P525L(+)) or uninduced absence (P525L(-))are shown, with infinity symbols (∞) indicating exclusive detection in the P525L(+) IP. None of these proteins was found in FLAGHA-FUS-WT or P525L-FL IPs (**Appendix I**), ruling out non-specific FUS-mediated interactions during lysis.

Table II.4 is displayed on the next page for visual clarity.

Gene	Protein	P525L (–) (iBAQ × 10^5)	P525L (+) (iBAQ × 10^5)	Δ (–/+)	Present in FUS-WT IP?	Present in FUS-P525L-FL IP?
APC4	Anaphase-promoting complex subunit 4	14.7	3.7	4.0	no	no
CNOT6L	CCR4-NOT transcription complex subunit 6-like	7.7	-	∞	no	no
COEA1	Collagen alpha-1(XIV) chain	3.2	-	∞	no	no
TF3C2	General transcription factor 3C polypeptide 2	4.3	-	∞	no	no
HAUS6	HAUS augmin-like complex subunit 6	8.2	1.7	4.9	no	no
IKKA	Inhibitor of nuclear factor kappa-B kinase subunit alpha	2.6	-	∞	no	no
AQR	Intron-binding protein aquarius	0.2	-	∞	no	no
XRN1	5'-3' exoribonuclease 1	1.2	-	∞	no	no
NIP7	60S ribosome subunit biogenesis protein NIP7	83.9	17.1	4.9	no	no
CNDG2	Condensin-2 complex subunit G2	1.5	-	∞	no	no
GTPB2	GTP-binding protein 2	19.0	-	∞	no	no
IF172	Intraflagellar transport protein 172 homolog	2.0	-	∞	no	no
NAA30	N-alpha-acetyltransferase 30	28.7	-	∞	no	no
SGT1	Protein SGT1	3.3	0.2	13.5	no	no
SMG8	Protein SMG8	14.5	1.6	9.1	no	no
SPS2L	SPATS2-like protein	56.6	0.8	66.7	no	no
Z3H7B	Zinc finger CCCH domain-containing protein 7B	15.3	-	∞	no	no
PATL1	Protein PAT1 homolog 1	4.4	1.0	4.3	no	no
MMS19	MMS19 nucleotide excision repair protein	5.6	1.0	5.6	no	no
TNR6A	Trinucleotide repeat-containing gene 6A protein	2.6	0.6	4.4	no	no
KIF14	Kinesin-like protein KIF14	0.8	-	∞	no	no
KIFC1	Kinesin-like protein KIFC1	4.0	-	∞	no	no
NDUA9	NADH dehydrogenase 1 alpha subcomplex subunit 9	9.6	1.8	5.4	no	no
GPX4	Phospholipid hydroperoxide glutathione peroxidase	7.6	-	∞	no	no
HECTD4	Probable E3 ubiquitin-protein ligase HECTD4	0.8	0.2	4.2	no	no
SACS	Sacsin	0.1	-	∞	no	no
SAM50	Sorting and assembly machinery component 50	8.5	-	∞	no	no
WDR3	WD repeat-containing protein 3	48.0	5.5	8.8	no	no
WDR59	WD repeat-containing protein 59	12.1	2.9	4.1	no	no
ZC11A	Zinc finger CCCH domain-containing protein 11A	3.0	-	∞	no	no

DISCUSSION

Characterization of the ALS-linked mutant FUS interactome in stressed human cells was a starting point to explore the hypothesis that mutant FUS-induced changes in stress granule dynamics, morphology and function. In this study, I investigated this gain of function theory for mutant FUS in ALS pathogenesis by utilizing the knowledge that the RGG domain recruit FUS to stress granules (**Figure II.1**) and developing several stable FLAGHA-tagged FUS mammalian cell culture models (**Figure II.2**) to assess the interactions of mutant FUS under stress. Upon characterization of these cell lines under arsenite stress using stringent crosslinked immunoprecipitation conditions (**Figure II.3**) and mass spectrometry, I identified 52 proteins capable of recruiting FUS-P525L-FL to stress granules (**Figure II.4**), most of which are RNA-mediated and rely on the apparent integrity of poly(ADP)-ribose (**Table II.1 and Table II.3**). These proteins are associated with multiple processes, such as mRNA degradation, mRNA stability, and cytoskeletal motor function. Further, FUS binding events were accompanied by interactome changes in a key stress granule nucleating protein, G3BP1 (**Figure II.5** and **Table II.4**). These data suggest a broader alteration in stress granule composition not limited to FUS binders. Together, this work narrows down an array of cellular pathways that may be negatively influenced by the incorporation of FUS into stress granules.

How might the interactions of mutant FUS impact stress response? Our results show that mutant FUS interacts with proteins in several functional

categories. I will focus the discussion below on three categories that contain highly enriched proteins to provide a basis for future investigations.

mRNA degradation:

One important class of proteins enriched in our results is mRNA degradation. The RNA interference (RNAi) pathway is a major pathway that controls mRNA translation and stability by a mechanism involving the microRNA (miRNA)-associated RISC complex, which is enriched in P-bodies along with the helicase DDX6 (Jain and Parker, 2013). DDX6 interacts with proteins of the RISC complex, including AGO2, another mRNA degradation hit in our study, and participates in the miRNA pathway (Chu and Rana, 2006). Although a mild association of DDX6 and stress granules has been demonstrated recently (Wilczynska et al., 2005), this association occurs at low levels compared to P-bodies. In fact, DDX6 has often been used as a P-body marker (Kedersha and Anderson, 2007). Importantly, the accumulation of P-body structures is impaired in the absence of DDX6, showing that DDX6 is an essential component for P-body function (Andrei et al., 2005). Mutant FUS does not localize to P-bodies (Bosco et al., 2010), thus making its strong interaction with DDX6 a potentially interesting case of inappropriate sequestration of stress response factors by mutant FUS are normally not enriched in stress granules. This notion awaits further investigation, including, but not limited to, immunofluorescence interrogation of DDX6 localization in the presence of mutant FUS.

Another regulator in mRNA decay, the helicase MOV10 (Liu *et al.*, 2012), was also among the most enriched hits for mutant FUS (**Table II.1**). MOV10 displays widespread binding to 3′ untranslated regions (3′ UTRs) of mRNAs and interacts with RENT1 (a.k.a. UPF1), the key factor in nonsense-mediated decay (NMD) (REF). Importantly, several NMD-targeted transcripts promote cellular adaptation in response to environmental stress, and NMD also degrades oxidatively-damaged RNA (Gardner, 2010). Knockdown of MOV10 results in increased mRNA half-lives of MOV10-bound as well as RENT1-regulated transcripts, revealing an important role for MOV10 in nonsense-mediated decay (Gregersen et al., 2014). Mutant FUS binds MOV10 regardless of stress in our study, but in an RNA-dependent manner. That mutant FUS binds a large set of 3'UTRs in the cytoplasm (Colombrita et al., 2012; Farg et al., 2012) begs the question of whether it disrupts the close interaction necessary between RENT1 and MOV10 in regulating these important stress-specific transcripts and warrants future study. This association may not only prevent important mRNA degradation, but these mRNAs being aberrantly sequestered into stress granule by mutant FUS may factor into the larger volume of stress granules seen in our studies (Baron et al., 2013).

Mutant FUS could not only disrupt the 3'UTR-centered MOV10-RENT1 NMD pathway, but it may also alter the regulation of NMD at exon junctions. This is made clear with the evidence gathered in this study that mutant FUS binds the eukaryotic release factor ERF3A without RNA or poly(ADP)-ribose (PAR)

mediation. In fact, ERF3A is the most “direct” interaction of all the hits and is present regardless of stress (**Table II.1** and **Table II.2**). When the translation complex pauses at a premature termination codon in mRNA that is upstream of an exon junction complex, ERF3 physically binds to and recruits RENT1 (Czaplinski et al., 1998; Gehring et al., 2003; Lykke-Andersen et al., 2000). Subsequently, SMG-1 is recruited to complete the formation of the SURF complex, which then binds to related RENT proteins in the exon junction complex to facilitate the NMD pathway (Gardner, 2010). A disproportionate percentage of reported NMD-regulated transcripts are involved in stress response pathways, a phenomenon that is conserved (Gardner, 2008; Mendell et al., 2004; Rodríguez-Gabriel et al., 2006). For example, stress-induced phosphorylation of eIF2α leads to a stimulation in the translation of the transcription factor ATF-4, a strong NMD target (Gardner, 2008). ATF-4 manages oxidative and ER stress through transcriptional up-regulation of protein chaperones and other stress response genes (Gardner, 2008; Genestra, 2007; Harding et al., 2002; Liu et al., 2008). Although necessary for survival to stress, ATF-4 is harmful to cellular survival when highly expressed in unstressed cells (Gardner, 2008), emphasizing the need to tightly regulate its expression through rapid degradation by NMD. Thus, the NMD pathway is a particularly interesting avenue to pursue regarding the role of mutant FUS in stress impairment in ALS, with a particular focus on ERF3A, as it has the potential to result in inappropriate stress response via NMD (Gardner, 2010).

mRNA stability:

While mRNA degradation plays a key role in post-transcriptional gene regulation during stress, mRNA stability is also required to strike a balance for homeostasis recovery. As shown in our results, mutant FUS binds nine proteins involved in mRNA stability during stress. Indeed, the highest enriched in our study are members of the insulin growth factor binding protein (IF2B1/2/3). A major function of IGF2B1 is the control of target mRNA translation, where it hinders translation of β-actin mRNA via binding to the Zipcode in the 3'-UTR, a function that is abolished by IFG2B phosphorylation by Src signaling (Hüttelmaier et al., 2005). IGF2BP1 also promotes mRNA stabilization of master regulating proteins, preventing their degradation by binding within a complex to a sequence in the open reading frame, termed the coding region determinant (CRD). Under stress conditions, IG2B1 knockdown induces a selective destabilization of target mRNAs, whereas over-expression increased mRNA stability (Stöhr et al., 2006). Members of the CRD complex, nuclease sensitive element binding protein 1 ("YB-1" or YBOX1), and hnRNP Q (SYNCRIP) (Weidensdorfer et al., 2008), are among the most enriched hits for mutant FUS under stressed and unstressed conditions (**Figure II.3**). These findings indicate that the stabilization of mRNAs during cellular stress requires specific protein-mRNA interactions. This, in addition to the fact that FUS is capable of the strong association of mutant FUS with IG2B1 and its binding partners, provides evidence for the notion that mutant FUS may interfere with the stability of mRNAs important to stress response.

Cytoskeletal motor function:

Recently, several publications have described the importance of molecular motors in stress granule dynamics. A report by Loschi et al. identified the subunits of two molecular microtubule motors, dynein and kinesin, that localize to stress granules and function cooperatively in both stress granule assembly and disassembly (Loschi et al., 2009). Kinesins are the main molecular motors that drive cargoes along the microtubules in the anterograde direction and cooperate with dynein complexes, understood to drive retrograde microtubule-based transport (Bartoli et al., 2011; Tsai and Tsui, 2009). As seen in the published work related to Chapter II (see **Appendix IV**), mutant FUS association with stress granules delays stress granule assembly and hastens its disassembly. Therefore, it is likely that FUS physically interferes with the motors necessary for stress granule formation and disassembly. Several proteins with the potential to impair stress granule assembly and disassembly bind to full-length mutant FUS according to our data (**Table II.1**).

Relating to cytoskeletal motors, our work shows that expression of mutant FUS in the cytoplasm during stress alters the protein interaction network of the stress granule nucleator, G3BP1 (**Table II.4**). Of particular interest is the marked increase in association with three retrograde transport motor proteins, dynein light chain roadblock protein 2 (DLRB2), dynactin subunit 3 (DCTN3), and the dynein 1 intermediate chain 2 (DC1I2), a motor known to impact stress granule

dynamics (Bartoli et al., 2011; Lo et al., 2007; Wanschers et al., 2008). The binding of cargo to intermediate and light dynein chains is modulated by the multiprotein dynactin complex, where DCTN3 usually works in concert with DCTN2 (Bartoli et al., 2011). Importantly, mutant FUS IPs are enriched in DCTN2 just as G3BP1 IPs are enriched in DCTN3 in presence of mutant FUS. This pairing suggesting a possible association G3BP1 and mutant FUS mediated by dynactin that may alter stress granule assembly and disassembly.

We also noted in our results that mutant FUS did not show an enrichment in binding to the stress granule marker proteins TIA-1 and HuR. These results are intriguing, as Tsai, et al. show showed that in arsenite-stressed culture, TIA-1 is biochemically co-localized with DLC2A in stress granules of mouse neurites. These results, in concert with ours, suggests a possible loss of G3BP association to TIA-1, interrupted by mutant FUS binding (Tsai et al., 2009), which may lead to the impaired stress granule assembly, disassembly and altered dynamics.

Cytoskeletal motor defects by mutant FUS may be broadly applicable to ALS pathogenesis. In fact, deceleration in dynein-mediated retrograde axonal transport occurs before all other pathology in mouse models of ALS, as visualization of a fluorescent tetanus toxin in SOD1G93A mice showed compared to WT mice (Bilsland et al., 2010). In addition, a 2003 study detected mutations in the gene encoding the dynactin subunit DCTN1 that cause lower motor neuron disease (Puls et al., 2003). Postnatal transgenic overexpression of DCTN2 in mouse motor neurons also causes neurodegeneration that is due to the selective

impairment of retrograde transport (LaMonte et al., 2002). These findings strongly support the view that dysfunction of dynein-mediated axonal transport can cause neurodegeneration, emphasizing the need for future work regarding the role of mutant FUS in this system.

Regardless of stress, mutant FUS expression in the cytoplasm may tip the motor-based balance of other neurodegeneration-related proteins it interacts with. A final important example lies in motor-associated mRNA granules in neurons. A 2004 report revealed that mouse neuronal dendrites contain a large mRNP granule, transported by kinesin and bidirectionally directed with an unidentified opposite motor (Kanai et al., 2004). This granule contains 42 proteins, and after stringent RNase conditions authors could still detect an insoluble, stabilized 'core' containing the purine-rich single stranded DNA-binding proteins α and β (PURA and PURB), Staufen, FMRP, FXR1, FXR2, SYNCRIP, and kinesin 5 (KIF5). Nearly all of these proteins are present in high abundance in our full-length mutant FUS IPs (**Table II.1**). They also detected mRNA encoding for α-calcium/calmodulin-dependent protein kinase II (α-CaMKII) and activity-regulated cytoskeletal-associated protein (ARC) in these stabilized granules, suggesting a role for them in local translation of motor proteins. Importantly, the authors also discovered endogenous FUS within these granules, though in a soluble fashion and at such low levels that they were unable to detect it in granules via immunofluorescence; instead, endogenous FUS was grossly nuclear (Kanai et al., 2004). These results suggest that while endogenous FUS

plays an important transport-associated role in the cytoplasm, it does so with nuanced, attenuated levels. The vast presence of mutant FUS in the cytoplasm, unable to retreat to the nucleus, therefore likely interferes with the balance of the remaining mRNP granule proteins as they function along in dendritic microtubules (Ling et al., 2004). This impediment of mutant FUS localization may also recruit its binding partner DCTN2, disrupting a balanced bidirectional transport. These imbalanced interactions persist under stress conditions, as we show (**Table II.1**), thus providing a potential transport-based mechanism for mutant FUS toxicity in stress granules.

In conclusion, the interactions we have identified that are able to interact with mutant FUS in stress granules fall into distinct categories applicable to stress-related ALS pathogenesis. Future work is necessary to elucidate the most important factors involved.

CHAPTER 4:

CONCLUSION

Amyotrophic lateral sclerosis is a vicious neurodegenerative disease that will manifest itself in 500,000 people living today in the USA at some point in their lives. The disease is debilitating and costly for patients and families, and there is only one barely effective FDA approved treatment that exists, Riluzole. Despite the urgent need for an effective treatment and the public support for ALS research, there is still no known mechanism for ALS. Nonetheless, there has been significant progress in our understanding of ALS pathogenesis thanks to the advances in deep sequencing and genetic exploration of the 10% of ALS cases inherited in families. In only twenty years, well over half of familial ALS (FALS) cases have been linked to specific genetic mutations (Sreedharan and Brown, 2013).

Fused in sarcoma (FUS) is a key gene mutated in FALS and explains 5% of these cases. Since 2009, investigation into the normal functions of FUS and its pathogenesis in ALS has grown rapidly. FUS is being discovered as a multifunctional protein involved in an array of key cellular functions such as transcriptional regulation, DNA damage repair, RNA processing, translation and stress response (Dormann and Haass, 2013; Ling *et al.*, 2013). Because most FUS mutations cause its mislocalization from the nucleus to the cytoplasm, it remains unclear if its loss of function or gain-of-toxic function in the nucleus or

cytoplasm drives ALS pathogenesis. Perplexingly, several reports exist that show a defect in both cellular compartments. For instance, ALS-linked mutant FUS variants fail to effectively function in DNA damage response, a finding that supports a loss of function mechanism (Mastrocola *et al.*, 2013; Rulten *et al.*, 2013; Wang *et al.*, 2013). Conversely, mislocalized mutant FUS binds a distinct set of ~900 mRNA compared to endogenous FUS (Hoell et al., 2011). More so, mutant FUS preferentially binds the 3'UTR of its targets in the cytoplasm, while WT FUS instead binds intronic regions in the nucleus (Hoell et al., 2011), implicating irregular splicing in hundreds of genes. These results implicate mutant FUS in a broad range of cellular pathways.

FUS is also a ubiquitously expressed protein (Åman et al., 1996). Why, therefore, does it exclusively cause disease in the central nervous system? The answer may lie in the fact that neurons cannot divide and must be preserved for a lifetime, whereas other cell types can be replaced as damage occurs. ALS also occurs later in life, which implicates a time-dependent factor involved in disease development. An intriguing idea regarding vulnerable cell populations like neurons is that FUS may require a "two-hit" mode of disease progression, with another insult necessary to drive toxicity in the brain (Dormann and Haass, 2011). With this in mind, the relevance of stress granules in ALS pathogenesis becomes clear. The discovery that ALS-linked mutant FUS associates with stress granules (Bosco et al., 2010) has been reproduced several times over (Bentmann et al., 2012; Daigle et al., 2012; Dormann et al., 2010; 2012; Gal et

al., 2011; Ito et al., 2011; Vance et al., 2013) and is made even more interesting by the fact that stress granule marker proteins are present within the pathological brain tissue aggregates of neurodegenerative disease tissues (Wolozin, 2012). The effects of mutant FUS on stress granule function are in the early stages of investigation, but our lab has made the discovery that mutant FUS incorporation in stress granules alters several of their characteristics, such as size, number, and assembly rate (**Appendix V** and Baron et al., 2013).

Here, I have investigated a gain of function hypothesis for mutant FUS in ALS pathogenesis that centers on stress granules. To this end, I contributed to the work by Baron, et al. discussed above (Baron et al., 2013) and determined the structural requirements of mutant FUS localization to stress granules (**Appendix IV**). I also developed several stable epitope-tagged mutant FUS mammalian cell culture models to assess the interactions of mutant FUS under stress (**Chapter II**). The structure-function results reveal the C-terminal RGG motifs as the key regions directing FUS to stress granules, a process that does not depend on post-translational arginine methylation (**Appendix IV**). Upon further characterization using the stable cell lines model, I identified several proteins capable of bringing FUS to stress granules (**Figure II.3**), most of which are RNA-mediated and rely on the apparent integrity of poly(ADP)-ribose (**Table II.1**). These proteins are associated with multiple processes, such as mRNA degradation, mRNA stability, and cytoskeletal motor function. These binding events were accompanied by interactome changes in a key stress granule

nucleating protein, G3BP1, suggesting a broader alteration in stress granule composition not limited to FUS binders. Together, this work narrows down an array of cellular pathways and therapeutic targets that may be useful in the treatment of ALS.

APPENDIX I: CHAPTER II PROTEOMICS DATASET

The following table contains the proteomics hits that were enriched at least 4X above controls in FLAGHA-FUS immunoprecipitation experiments from Chapter II.

Table AI.1 is presented across the next 8 pages for visual clarity. It is recommended to view this table at 200% zoom if viewing on a computer.

Table AI.1 –Proteins identified in FLAGHA-FUS IPs that are 4-fold enriched over FLAGHA control IPs under stress conditions. Shown are iBAQ values for replicate proteomics analysis experiments from IPs of FLAGHA-tagged FUS-P525L-FL (P525L), FUS-P525L-ΔRGG (ΔRGG), FUS-WT (WT), and FLAGHA control (FLAG) lysates under arsenite stress (SA(+)) or unstressed (SA(-)) conditions. iBAQ values for FLAGHA-FUS from each IP is shown in the first row (see **Figure II.4a**, **center**).

UniProt Acc. #	Gene Name	Protein Name	P525L SA(-) (iBAQ × 10^5)		P525L SA(+) (iBAQ × 10^5)		P525L SA(+) RNase(+) (iBAQ × 10^5)		ΔRGG SA(+) (iBAQ × 10^5)		WT SA(-) (iBAQ × 10^5)		WT SA(+) (iBAQ × 10^5)		FLAG SA(+) (iBAQ × 10^5)		P525L_SA(+) /FLAG_SA(+)	Replicate Hit?
			N1	N2	N1	N2	N1	N2	N1	N2	N1	N2	N1	N2	N1	N2		
–	–	**FLAGHA-FUS**	**9947.7**	**9534.9**	**6678.8**	**9988.7**	**5580.4**	**7887.0**	**10713.0**	**13403.0**	**17205.0**	**14106.0**	**6348.9**	**858.3**	**48.7**	**68.3**	–	–
Q8IZ83	A16A1	Aldehyde dehydrogenase family 16 member A1	3.3	1.6	0.9					1.4	1.9	2.4					*	
A4D212	A4D212	DKFZP586J0619 protein			0.6	0.6			0.5				1.3				*	N2 Hit
Q9NRG9	AAAS	Aladin	40.8	2.2		9.3			7.1	19.3	15.5	26.8	37.9	10.1			*	
Q8IUX4	ABC3F	DNA dC->dU-editing enzyme APOBEC-3F			34.5												*	
Q13085	ACACA	Acetyl-CoA carboxylase 1	3.6	3.2	1.9	1.5	1.7		1.2		3.4						*	N2 Hit
P49748	ACADV	Very long-chain specific acyl-CoA dehydrogenase, mitochondrial	7.2		14.3												*	
Q13015	AF1Q	Protein AF1q		149.1		145.3		51.9		232.2	148.8			68.9		25.8	5.6	
Q53H12	AGK	Acylglycerol kinase, mitochondrial	4.3		4.8								7.4				*	
Q9UKV8	AGO2	Protein argonaute-2	5.7	2.9	2.3			2.4									*	
P51648	AL3A2	Fatty aldehyde dehydrogenase	16.7		5.3		3.4		10.5			8.7	7.7				*	
Q9H4A4	AMPB	Aminopeptidase B	12.7	4.5	18.0	7.6			9.7	14.8		8.9	10.9			5.0	5.1	N2 Hit
P08133	ANXA6	Annexin A6	9.2		2.9							1.6	2.3	6.7			*	
P20073	ANXA7	Annexin A7	8.1	9.2	6.7				4.4	33.0		29.9	6.5			0.6	10.7	
O95782	AP2A1	AP-2 complex subunit alpha-1			7.1		6.1	0.7	4.4	6.6	5.4		5.3				*	
O94973	AP2A2	AP-2 complex subunit alpha-2	2.6		7.3		2.1	0.7	2.9	5.8	5.5		3.3				*	
Q9Y2T2	AP3M1	AP-3 complex subunit mu-1	33.0	20.0	17.0				11.4	51.3	49.9	44.1	34.0				*	
Q92747	ARC1A	Actin-related protein 2/3 complex subunit 1A	37.2			19.1				26.8		18.2					*	
Q9Y4X5	ARI1	E3 ubiquitin-protein ligase ARIH1	8.5		3.6	5.1				7.1							*	N2 Hit
O15145	ARPC3	Actin-related protein 2/3 complex subunit 3	123.1		9.0							18.4			1.4		6.5	
Q9NWX5	ASB6	Ankyrin repeat and SOCS box protein 6			0.7				3.7					1.2			*	
Q8WWM7	ATX2L	Ataxin-2-like protein	100.9	35.7	156.2	100.4	99.9	27.2	19.6			22.2	28.4		8.6	3.9	20.4	N2 Hit
B3KS98	B3KS98	Eukaryotic translation initiation factor 3 subunit H	67.1	22.5	43.6	82.4	20.5	18.0		45.3	47.8			32.9	3.9		32.6	N2 Hit
B4DXZ6	B4DXZ6	Fragile X mental retardation syndrome-related protein 1	43.1	66.7	53.2	85.8	12.0	32.0	11.5		42.8	22.0	11.9	54.7	18.9		7.3	N2 Hit
B4DZI8	B4DZI8	Coatomer protein complex, subunit beta 2 (Beta prime)	14.2	16.0	23.3	16.7	9.9	9.5	10.9	42.1	40.4	5.1	13.1	16.6		5.7	7.0	N2 Hit
O95817	BAG3	BAG family molecular chaperone regulator 3	2.5		1.2					2.7		0.7					*	
P35613	BASI	Basigin		277.2		211.8		98.2		412.3	199.8			447.1			*	
Q9H3K6	BOLA2	BolA-like protein 2			22.9		65.4					193.9					*	
Q13112	CAF1B	Chromatin assembly factor 1 subunit B	7.6	4.2		3.2				11.8				5.5			*	
Q14444	CAPR1	Caprin-1	98.6	98.8	160.8	251.4	15.8	66.3	52.6	56.6	80.7	57.5	48.1			38.1	10.8	N2 Hit
Q9Y5K6	CD2AP	CD2-associated protein	6.4		2.1		2.2						1.8				*	

UniProt Acc. #	Gene Name	Protein Name	P525L SA(-) (iBAQ × 10^5)		P525L SA(+) (iBAQ × 10^5)		P525L SA(+) RNase(+) (iBAQ × 10^5)		ΔRGG SA(+) (iBAQ × 10^5)		WT SA(-) (iBAQ × 10^5)		WT SA(+) (iBAQ × 10^5)		FLAG SA(+) (iBAQ × 10^5)		P525L_SA(+) /FLAG_SA(+)	Replicate Hit?
			N1	N2	N1	N2	N1	N2	N1	N2	N1	N2	N1	N2	N1	N2		
Q7Z7K6	CENPV	Centromere protein V	8.8			8.5			4.0		15.9	7.8		77.7			*	
P61604	CH10	10 kDa heat shock protein, mitochondrial		135.0	139.3	103.3			33.5	103.8	117.7	73.0	26.9				*	N2 Hit
Q96JM3	CHAP1	Chromosome alignment-maintaining phosphoprotein 1	0.5		1.7				1.3	4.6		1.5		1.6			*	
Q8N999	CL029	Uncharacterized protein C12orf29	7.1		16.6		4.2		5.4			5.0					*	
Q9UJS0	CMC2	Calcium-binding mitochondrial carrier protein Aralar2	20.1	26.4	21.4		5.0		4.2	12.9	34.3	31.9	8.4	16.3	1.5		14.8	
Q9BPX3	CND3	Condensin complex subunit 3	2.3		2.2				3.8		0.9			4.0		0.4	5.2	
P38432	COIL	Coilin	3.2		0.9				1.0			2.9		33.7			*	
Q9Y678	COPG1	Coatomer subunit gamma-1	11.9	7.0	16.4	5.1		3.1	3.7	20.4	9.1	0.7		0.8	0.9	0.6	15.1	N2 Hit
Q9UBF2	COPG2	Coatomer subunit gamma-2	3.0	7.4	9.3	6.1		3.3	2.7	8.2	6.3	0.8		6.1		1.1	14.3	N2 Hit
P61923	COPZ1	Coatomer subunit zeta-1	8.8		8.9					94.4	11.1			61.6			*	
Q9UKF6	CPSF3	Cleavage and polyadenylation specificity factor subunit 3			2.2				2.2			11.3					*	
Q8WYA6	CTBL1	Beta-catenin-like protein 1	2.2		3.2				2.0	17.3		8.5	4.6				*	
Q13616	CUL1	Cullin-1	15.7	1.3	1.9	3.4	2.8	4.3	0.7	6.6	3.2	6.5		16.0			*	N2 Hit
Q13618	CUL3	Cullin-3	21.0	15.1	3.3	10.1				15.0	2.7			6.1	1.2	1.8	4.5	N2 Hit
P99999	CYC	Cytochrome c			94.2												*	
D6REP8	D6REP8	Histidine triad nucleotide-binding protein 1			355.9					166.7							*	
Q9NV06	DCA13	DDB1- and CUL4-associated factor 13				1.5								317.2			*	
Q13561	DCTN2	Dynactin subunit 2	6.4		17.2		4.2				5.3						*	
Q9H773	DCTP1	dCTP pyrophosphatase 1	26.1		14.4							44.2					*	
Q16531	DDB1	DNA damage-binding protein 1	16.3	2.1	9.5		3.4		3.3	33.6	10.3	13.2	9.8	17.0			*	
Q8TDD1	DDX54	ATP-dependent RNA helicase DDX54				4.0								1174.5			*	
P26196	DDX6	Probable ATP-dependent RNA helicase DDX6	269.1	172.8	189.8	156.2	39.9	49.7	32.8	37.7	74.7	105.2	35.5	75.9	30.3	48.5	4.4	N2 Hit
Q9BUN8	DERL1	Derlin-1	16.9	8.4	9.1	11.3			16.6			18.3	8.9	12.8			*	N2 Hit
Q9H2U1	DHX36	ATP-dependent RNA helicase DHX36	2.0		14.4	16.5											*	N2 Hit
Q6P158	DHX57	Putative ATP-dependent RNA helicase DHX57		0.5	5.0	6.5					4.0			0.3			*	N2 Hit
P25685	DNJB1	DnaJ homolog subfamily B member 1	15.1		4.1				5.7			11.0					*	
Q8WXX5	DNJC9	DnaJ homolog subfamily C member 9				3.3			2.6	8.7		4.8		34.9			*	
E7EVD1	E7EVD1	U4/U6 small nuclear ribonucleoprotein Prp3	17.3	10.1		8.9			4.1	22.1	11.6			8.0			*	
Q15125	EBP	3-beta-hydroxysteroid-Delta(8),Delta(7)-isomerase	148.5		101.2						122.9		127.4	224.0			*	
Q6P2E9	EDC4	Enhancer of mRNA-decapping protein 4	15.9	11.7	9.4	3.9	6.6			234.0	5.5	5.3		1.8		1.7	7.8	N2 Hit
O75822	EIF3J	Eukaryotic translation initiation factor 3 subunit J	49.8		62.6				24.0			9.6					*	

UniProt Acc. #	Gene Name	Protein Name	P525L SA(-) (iBAQ × 10^5)		P525L SA(+) (iBAQ × 10^5)		P525L SA(+) RNase(+) (iBAQ × 10^5)		ΔRGG SA(+) (iBAQ × 10^5)		WT SA(-) (iBAQ × 10^5)		WT SA(+) (iBAQ × 10^5)		FLAG SA(+) (iBAQ × 10^5)		P525L_SA(+) /FLAG_SA(+)	Replicate Hit?
			N1	N2	N1	N2	N1	N2	N1	N2	N1	N2	N1	N2	N1	N2		
Q7L2H7	EIF3M	Eukaryotic translation initiation factor 3 subunit M		1.6		2.4				2.2		9.8					*	
Q12926	ELAV2	ELAV-like protein 2	183.8	247.5	167.3	236.7	28.9	104.8		311.3							*	N2 Hit
Q92556	ELMO1	Engulfment and cell motility protein 1	1.7		0.7		2.2										*	
P15170	ERF3A	Eukaryotic peptide chain release factor GTP-binding subunit ERF3A	36.8	116.2	33.6	85.3	82.3	53.2	5.4	4.7	40.5	22.8	9.4	39.7	12.2	2.4	8.1	N2 Hit
O00471	EXOC5	Exocyst complex component 5	6.5		22.0		1.3		2.2	6.2	0.7	2.9					*	
Q9NZB2	F120A	Constitutive coactivator of PPAR-gamma-like protein 1	35.2	21.8	40.9	26.9	3.9										*	N2 Hit
F5GXM1	F5GXM1	Histone deacetylase 1	51.4		31.7	9.9	5.2		5.2				10.3				*	N2 Hit
F5H8J4	F5H8J4	Eukaryotic translation initiation factor 4 gamma 3	12.2	12.7	14.0	13.3	0.3		0.4	10.7	11.9	5.8		9.6	5.6	0.9	4.2	N2 Hit
F8VQP2	F8VQP2	Ataxin-2	3.7	10.2	28.0	17.2	4.3	13.5			10.3	1.6					*	N2 Hit
Q8NCA5	FA98A	Protein FAM98A	6.8	16.3	41.1	76.3	6.7	41.5			29.1					6.0	19.5	N2 Hit
Q52LJ0	FA98B	Protein FAM98B	9.9		155.2	6.6	2.0		265.3	21.4		23.7	6.9	7.1		3.5	46.4	N2 Hit
Q7L8L6	FAKD5	FAST kinase domain-containing protein 5	1.4	1.8	5.0	4.6		2.9	2.1		6.3		3.5	0.7	0.9	1.2	4.6	N2 Hit
Q14192	FHL2	Four and a half LIM domains protein 2	26.8	18.3	14.6	16.4	4.5			27.2		18.1					*	N2 Hit
Q13045	FLII	Protein flightless-1 homolog	2.7		2.1												*	
Q06787	FMR1	Fragile X mental retardation protein 1	57.0	86.9		126.8	16.5	50.7									*	
Q96I24	FUBP3	Far upstream element-binding protein 3	520.6	452.4	260.2	578.6	55.5	238.8	38.1	312.0	132.8	563.3	68.6	43.0		184.8	4.5	N2 Hit
P51116	FXR2	Fragile X mental retardation syndrome-related protein 2	48.3	77.0	51.6	98.1	10.8	38.3	9.9		36.7	18.8	10.2	60.2	16.2	7.3	6.4	N2 Hit
Q13283	G3BP1	Ras GTPase-activating protein-binding protein 1	403.9	306.7	877.7	1619.5	75.0	170.1	65.6	106.2	430.2	61.2	88.5	144.1	177.1	216.9	6.3	N2 Hit
Q9UN86	G3BP2	Ras GTPase-activating protein-binding protein 2	129.7	26.8	220.2	388.3											*	N2 Hit
Q9H3P7	GCP60	Golgi resident protein GCP60	4.2	17.8	7.8	14.7		5.8	1.9	25.1		6.6				2.9	7.7	N2 Hit
Q92990	GLMN	Glomulin			2.8				3.3	6.3		2.8	2.2	4.3	0.7		4.2	
Q9BVP2	GNL3	Guanine nucleotide-binding protein-like 3	7.4	1.7		1.7		4.0				12.5	12.3	3062.2			*	
Q9NVN8	GNL3L	Guanine nucleotide-binding protein-like 3-like protein				3.7						1.2		268.4			*	
Q9BRR8	GPTC1	G patch domain-containing protein 1				2.8		6.8		4.3	2.5	4.0	2.8				*	
Q12849	GRSF1	G-rich sequence factor 1	0.3			9.3	3.5										*	
H3BND8	H3BND8	Ubiquitin carboxyl-terminal hydrolase (Fragment)	6.0	12.4	9.1	5.0	3.5	2.2	5.8	24.0		5.1	3.0	1.8		1.7	8.1	N2 Hit
H3BPE1	H3BPE1	Microtubule-actin cross-linking factor 1, isoforms 1/2/3/5	2.4		0.5		0.0			54.4		0.3					*	
O75146	HIP1R	Huntingtin-interacting protein 1-related protein			1.4				0.9								*	
Q8WVV9	HNRLL	Heterogeneous nuclear ribonucleoprotein L-like	73.1	5.4	119.2	28.6			166.2	58.1		64.9	6.1			37.3	4.0	N2 Hit
O60506	HNRPQ	Heterogeneous nuclear ribonucleoprotein Q	2087.6	2162.0	1881.7	2868.0	167.5	335.8	237.6	1474.7	1005.4	1417.8	576.9	358.9	177.6	944.9	4.2	N2 Hit
Q3SXM5	HSDL1	Inactive hydroxysteroid dehydrogenase-like protein 1	7.2		1.1	6.8	0.9		0.9	6.4		2.5					*	N2 Hit

UniProt Acc. #	Gene Name	Protein Name	P525L SA(-) (iBAQ × 10^5)		P525L SA(+) (iBAQ × 10^5)		P525L SA(+) RNase(+) (iBAQ × 10^5)		ΔRGG SA(+) (iBAQ × 10^5)		WT SA(-) (iBAQ × 10^5)		WT SA(+) (iBAQ × 10^5)		FLAG SA(+) (iBAQ × 10^5)		P525L_SA(+) /FLAG_SA(+)	Replicate Hit?
			N1	N2	N1	N2	N1	N2	N1	N2	N1	N2	N1	N2	N1	N2		
I3L0H8	I3L0H8	ATP-dependent RNA helicase DDX19A	8.0	6.2	5.7	6.6	1.4					4.9	2.3				*	N2 Hit
Q9NZI8	IF2B1	Insulin-like growth factor 2 mRNA-binding protein 1	2246.4	1451.5	2026.1	1472.8	212.4	361.8	175.4	177.5	353.0	342.4	173.0	262.3	234.1	116.8	10.0	N2 Hit
Q9Y6M1	IF2B2	Insulin-like growth factor 2 mRNA-binding protein 2	418.8	294.0	340.0	387.0	11.1	88.9	17.4	44.5	77.7	47.8	22.3	76.6	33.9	14.0	15.2	N2 Hit
O00425	IF2B3	Insulin-like growth factor 2 mRNA-binding protein 3	623.7	378.1	403.0	581.8	9.2	89.8	23.3	43.2	82.9	46.6	40.2	71.9	68.3	10.7	12.5	N2 Hit
Q15056	IF4H	Eukaryotic translation initiation factor 4H	318.5	283.0	685.3	790.6	106.8	148.8	217.5	150.7	214.5	314.7	211.4	127.3	191.3	140.2	4.5	N2 Hit
Q5TA45	INT11	Integrator complex subunit 11				11.0			8.8								*	
P46940	IQGA1	Ras GTPase-activating-like protein IQGAP1	5.9	1.6	3.6	1.0	1.4		0.8	17.6			0.6	1.8	1.0		4.6	N2 Hit
Q14012	KCC1A	Calcium/calmodulin-dependent protein kinase type 1	25.2		16.5		3.0		2.7			24.0					*	
P12532	KCRU	Creatine kinase U-type, mitochondrial	56.6		46.1		1.6		16.2	15.4		104.7	153.0	46.3			*	
P30085	KCY	UMP-CMP kinase	33.9		13.4				5.0			64.4					*	
P52732	KIF11	Kinesin-like protein KIF11	40.5	1.8	25.5		9.3	1.9	15.6		2.6	18.6	7.6		5.8		4.4	
H7BYN4	KIF23	Kinesin-like protein KIF23	3.5			1.1			0.2		1.0			63.7			*	
P46020	KPB1	Phosphorylase b kinase regulatory subunit alpha		2.0	0.8				0.2					1.7			*	
Q92615	LAR4B	La-related protein 4B	13.1	11.7	23.7	20.7											*	N2 Hit
Q6PKG0	LARP1	La-related protein 1	15.9	12.9	46.3	37.3	4.8				11.2			3.2			*	N2 Hit
Q71RC2	LARP4	La-related protein 4	14.6	25.7		20.4	11.0	13.6			25.5						*	
P43034	LIS1	Platelet-activating factor acetylhydrolase IB subunit alpha	33.3	20.8	5.7	6.4	14.6		4.6		9.0			13.4			*	N2 Hit
P49257	LMAN1	Protein ERGIC-53	14.4	32.0	18.4			9.8	7.5		25.4	23.2	12.5				*	
Q6ZN17	LN28B	Protein lin-28 homolog B	20.0		31.6	11.4								48.0			*	N2 Hit
Q9H9A6	LRC40	Leucine-rich repeat-containing protein 40	14.5			3.0	3.4		3.5		4.6	11.2	4.3	4.8			*	
O94822	LTN1	E3 ubiquitin-protein ligase listerin	3.9	0.3		2.6	1.0	0.2	0.6		2.0			1.4			*	
Q7L5Y9	MAEA	Macrophage erythroblast attacher	4.9		1.1			1.9	0.5	7.3							*	
Q9H0U3	MAGT1	Magnesium transporter protein 1	21.4	34.3	22.6				12.7				4.4				*	
Q9ULC4	MCTS1	Malignant T-cell-amplified sequence 1	100.7		92.2	2.3			6.0	5.2		9.1					*	N2 Hit
O95140	MFN2	Mitofusin-2				4.5											*	
Q9Y6X9	MORC2	MORC family CW-type zinc finger protein 2	2.5		1.1								1.4				*	
P53985	MOT1	Monocarboxylate transporter 1	82.4	128.6	37.2	80.1	12.7	53.0	21.4	80.2	122.6	48.9	12.9	73.7		28.7	4.1	N2 Hit
Q9HCE1	MOV10	Putative helicase MOV-10	105.6	47.0	76.7	79.0	12.1	11.1	5.1	1.6	11.3	9.8	1.4	5.8		1.9	82.0	N2 Hit
Q02750	MP2K1	Dual specificity mitogen-activated protein kinase kinase 1	44.2		38.2		18.8		14.2			33.1					*	
P43246	MSH2	DNA mismatch repair protein Msh2	4.2	8.0	6.8	10.5		5.5	3.1	23.3	24.6	2.9	8.3	9.9		2.9	5.9	N2 Hit
O43347	MSI1H	RNA-binding protein Musashi homolog 1	109.4	115.8	110.7	190.2		14.9			38.6					23.5	12.8	N2 Hit

UniProt Acc. #	Gene Name	Protein Name	P525L SA(-) (iBAQ × 10^5)		P525L SA(+) (iBAQ × 10^5)		P525L SA(+) RNase(+) (iBAQ × 10^5)		ΔRGG SA(+) (iBAQ × 10^5)		WT SA(-) (iBAQ × 10^5)		WT SA(+) (iBAQ × 10^5)		FLAG SA(+) (iBAQ × 10^5)		P525L_SA(+) /FLAG_SA(+)	Replicate Hit?
			N1	N2	N1	N2	N1	N2	N1	N2	N1	N2	N1	N2	N1	N2		
Q96DH6	MSI2H	RNA-binding protein Musashi homolog 2	115.5	155.9	183.8	257.9		18.3			47.6					29.0	15.2	N2 Hit
Q96E29	MTER1	mTERF domain-containing protein 1, mitochondrial			2.0												*	
Q13613	MTMR1	Myotubularin-related protein 1	7.2		3.4		2.9		4.4			4.6					*	
O94832	MYO1D	Unconventional myosin-Id	2.7	1.6	0.5	2.3			0.9		3.6	0.6		1.7			*	N2 Hit
Q9UM54	MYO6	Unconventional myosin-VI	12.5	4.5	4.0	18.8	3.6	3.1	3.2	213.0	4.2	8.5	6.1	2.7	3.4	1.9	4.3	N2 Hit
E9PAV3	NACAM	Nascent polypeptide-associated complex subunit alpha	40.2	19.4	371.9	27.8			122.2		32.5	43.5	50.7	19.1	62.2	28.7	4.4	N2 Hit
P43490	NAMPT	Nicotinamide phosphoribosyltransferase	178.6	37.6	220.4	22.0	93.8		58.6	98.3	77.9	77.2	184.2	39.1	39.0	12.3	4.7	N2 Hit
Q09161	NCBP1	Nuclear cap-binding protein subunit 1	4.5	5.0		4.9			2.6	8.6	82.6	14.6	6.1	0.9			*	
O60524	NEMF	Nuclear export mediator factor NEMF	1.8		1.5				1.2			4.1	3.2				*	
P30419	NMT1	Glycylpeptide N-tetradecanoyltransferase 1			25.7	9.8					10.6			7.6			*	N2 Hit
P46087	NOP2	Putative ribosomal RNA methyltransferase NOP2				8.8					6.6		6.5	4995.7			*	
O43847	NRDC	Nardilysin			1.1				0.9								*	
Q9NXE4	NSMA3	Sphingomyelin phosphodiesterase 4	3.5		2.8				1.9			8.0					*	
P61970	NTF2	Nuclear transport factor 2			78.4				39.7			82.8					*	
Q7Z417	NUFP2	Nuclear fragile X mental retardation-interacting protein 2	31.7		41.9	23.5	1.8	5.0			4.4						*	N2 Hit
P37198	NUP62	Nuclear pore glycoprotein p62		12.5	10.1	5.7					12.9						*	N2 Hit
P08559	ODPA	Pyruvate dehydrogenase E1 component subunit alpha			23.6	14.9	216.8		4.8		4.0	44.7	9.6	31.1	9.5		4.1	N2 Hit
Q9NTK5	OLA1	Obg-like ATPase 1	41.6	41.3	31.3	21.1	0.2	3.4	8.8	33.3	22.6	15.8	1.0	34.8		9.1	5.8	N2 Hit
Q96C36	P5CR2	Pyrroline-5-carboxylate reductase 2	6.4	16.4	2.6	10.8	17.4	8.0	7.6	13.6	3.6	2.3		5.5			*	N2 Hit
P68402	PA1B2	Platelet-activating factor acetylhydrolase IB subunit beta	13.8		104.9		17.4		33.2			13.2					*	
Q13310	PABP4	Polyadenylate-binding protein 4	1197.9	1446.6	1816.0	1829.1	433.5	793.8	312.5	351.4	653.9	377.9	349.2	260.5	284.8	242.2	6.9	N2 Hit
Q5JVF3	PCID2	PCI domain-containing protein 2	25.1	10.7	6.1	24.9	1.8	9.0	5.9	10.7	9.2	30.4	12.3	26.6		6.1	5.1	N2 Hit
O14737	PDCD5	Programmed cell death protein 5	57.5	270.3	82.6	21.8	20.3	20.3	62.2	166.8	115.2	186.4	37.6	106.2			*	N2 Hit
Q9BY77	PDIP3	Polymerase delta-interacting protein 3	27.2	33.1		28.5		16.6	7.7	33.4	48.6	68.0	29.8				*	
Q6Y7W6	PERQ2	PERQ amino acid-rich with GYF domain-containing protein 2		2.2		8.3	0.7	2.0			10.1			5.6		1.9	4.4	
Q7RTV0	PHF5A	PHD finger-like domain-containing protein 5A			42.6	6.1	18.5	31.5	34.4	64.3		140.5	73.7			6.8	7.1	N2 Hit
P61457	PHS	Pterin-4-alpha-carbinolamine dehydratase			104.1		30.8					89.3					*	
Q99943	PLCA	1-acyl-sn-glycerol-3-phosphate acyltransferase alpha				7.5				6.9	6.7						*	
O15305	PMM2	Phosphomannomutase 2	8.5		3.8												*	
P48634	PRC2A	Protein PRRC2A	11.1	2.5	3.8	9.2	0.2					0.5					*	N2 Hit
P49642	PRI1	DNA primase small subunit	5.5		2.3		6.1		1.8			2.1					*	

UniProt Acc. #	Gene Name	Protein Name	P525L SA(-) (iBAQ × 10^5)		P525L SA(+) (iBAQ × 10^5)		P525L SA(+) RNase(+) (iBAQ × 10^5)		ΔRGG SA(+) (iBAQ × 10^5)		WT SA(-) (iBAQ × 10^5)		WT SA(+) (iBAQ × 10^5)		FLAG SA(+) (iBAQ × 10^5)		P525L_SA(+) /FLAG_SA(+)	Replicate Hit?
			N1	N2	N1	N2	N1	N2	N1	N2	N1	N2	N1	N2	N1	N2		
P35080	PROF2	Profilin-2			154.4		102.5			189.4	154.3	217.2	161.1				*	
P62195	PRS8	26S protease regulatory subunit 8	65.7	56.6	51.6	45.2			28.0	77.8	51.4	45.6	36.4		16.7		5.8	N2 Hit
P55786	PSA	Puromycin-sensitive aminopeptidase	13.2	5.2	5.6	2.9	2.0		1.7		5.3		1.0		0.8		10.3	N2 Hit
O00232	PSD12	26S proteasome non-ATPase regulatory subunit 12	15.7	35.2	19.1	12.1	2.8		5.1	25.0	22.7	7.2	5.0	12.1	5.1	2.3	4.2	N2 Hit
Q9UNM6	PSD13	26S proteasome non-ATPase regulatory subunit 13	14.3	29.8		16.4				54.2			13.3	12.5			*	
O75475	PSIP1	PC4 and SFRS1-interacting protein	34.7	49.0	2.9					50.4	51.7	26.0		23.7			*	
P51665	PSMD7	26S proteasome non-ATPase regulatory subunit 7	34.7		22.3												*	
Q92530	PSMF1	Proteasome inhibitor PI31 subunit	103.5		70.4	13.5	45.3	12.5	14.3	9.9		87.3					*	N2 Hit
Q06124	PTN11	Tyrosine-protein phosphatase non-receptor type 11	28.2	7.8	2.5		8.5	1.9				7.1	4.7				*	
Q14671	PUM1	Pumilio homolog 1	23.5		24.1	50.2											*	N2 Hit
Q00577	PURA	Transcriptional activator protein Pur-alpha	224.6	122.4	372.8	273.4		27.9	35.9	38.6	40.2	46.5				27.2	23.8	N2 Hit
P30520	PURA2	Adenylosuccinate synthetase isozyme 2		16.2	2.6	9.5			1.1	34.7		14.4	9.2	10.6		2.1	5.7	N2 Hit
Q96QR8	PURB	Transcriptional activator protein Pur-beta	49.8	12.9	28.4	61.5			12.7			10.5					*	N2 Hit
R4GNH3	R4GNH3	26S protease regulatory subunit 6A	15.8		20.2	9.6			10.3	30.6	27.9	13.2	11.0	9.1			*	N2 Hit
Q15276	RABE1	Rab GTPase-binding effector protein 1	2.4		0.8	1.5		1.0	0.5	2.4	2.4	1.0					*	N2 Hit
P29373	RABP2	Cellular retinoic acid-binding protein 2	5.5		48.4		22.6					13.4			7.1		6.8	
P63000	RAC1	Ras-related C3 botulinum toxin substrate 1	69.6	171.1	111.1			54.7				92.7	85.0				*	
Q15907	RB11B	Ras-related protein Rab-11B	61.4	39.3	70.1	71.0	77.5	22.1	25.3	12.4	11.9	62.3	45.5		14.5	6.5	6.7	N2 Hit
Q92900	RENT1	Regulator of nonsense transcripts 1	165.2	76.4	69.3	21.4	26.4	12.4	17.3		2.6	19.8	13.7		15.9	6.3	4.1	N2 Hit
P35249	RFC4	Replication factor C subunit 4				4.5				4.9				9.8			*	
P61586	RHOA	Transforming protein RhoA				71.1											*	
P23921	RIR1	Ribonucleoside-diphosphate reductase large subunit		21.4	20.7	20.1	2.9	9.3		78.2	24.6	35.4	15.7	63.6		9.1	4.5	N2 Hit
P31350	RIR2	Ribonucleoside-diphosphate reductase subunit M2	20.5	8.8	7.4			2.3			5.6	6.6					*	
P30876	RPB2	DNA-directed RNA polymerase II subunit RPB2	21.8	7.6	6.4	4.0	2.3		5.0	8.0	5.6	7.7	5.8			2.3	4.5	N2 Hit
Q8N122	RPTOR	Regulatory-associated protein of mTOR	1.2		0.7												*	
Q15050	RRS1	Ribosome biogenesis regulatory protein homolog				22.2								995.5			*	
O95487	SC24B	Protein transport protein Sec24B	6.3	2.8	5.3			2.1	2.6			2.2	1.5				*	
O94979	SC31A	Protein transport protein Sec31A	7.7	4.2	0.7	99.0	4.0			108.7	2.8		0.3				*	N2 Hit
Q9UHD8	SEPT9	Septin-9	6.5	7.6	3.0	4.0			3.6	16.5	13.8	16.6		6.8			*	N2 Hit
P42285	SK2L2	Superkiller viralicidic activity 2-like 2	6.9	7.9		1.4	1.9			2.7	13.8	7.8	3.9	182.5			*	
Q8IX90	SKA3	Spindle and kinetochore-associated protein 3	6.7	6.5	6.5	4.3	1.4		2.8		5.5	10.4					*	N2 Hit

UniProt Acc. #	Gene Name	Protein Name	P525L SA(-) (iBAQ × 10^5)		P525L SA(+) (iBAQ × 10^5)		P525L SA(+) RNase(+) (iBAQ × 10^5)		ΔRGG SA(+) (iBAQ × 10^5)		WT SA(-) (iBAQ × 10^5)		WT SA(+) (iBAQ × 10^5)		FLAG SA(+) (iBAQ × 10^5)		P525L_SA(+) /FLAG_SA(+)	Replicate Hit?
			N1	N2	N1	N2	N1	N2	N1	N2	N1	N2	N1	N2	N1	N2		
O95391	SLU7	Pre-mRNA-splicing factor SLU7				2.0						5.7					*	
P54920	SNAA	Alpha-soluble NSF attachment protein	38.9	9.9	5.9						13.1	15.9					*	
Q15005	SPCS2	Signal peptidase complex subunit 2	22.8		8.6				6.1	12.6		43.4	26.4				*	
O75934	SPF27	Pre-mRNA-splicing factor SPF27		22.4	8.2						4.6	4.1		33.8			*	
Q96SB4	SRPK1	SRSF protein kinase 1	21.4		6.6	8.0						4.5	3.6	40.2	0.9		15.7	N2 Hit
P50225	ST1A1	Sulfotransferase 1A1	7.9		22.5		16.1			3.9							*	
Q9NUL3	STAU2	Double-stranded RNA-binding protein Staufen homolog 2	11.4		2.4												*	
Q8TCJ2	STT3B	Dolichyl-diphosphooligosaccharide-protein glycosyltransferase	3.3			21.8				5.0	20.9					1.7	12.8	
Q15833	STXB2	Syntaxin-binding protein 2			7.3				2.1		7.3	5.4	2.7				*	
P49588	SYAC	Alanine--tRNA ligase, cytoplasmic	13.2		233.4				1.7	7.2	2.7	3.1				3.0	78.9	
P12081	SYHC	Histidine--tRNA ligase, cytoplasmic	18.6		27.2	143.5			7.9	191.1	187.0		16.6		10.6	12.0	7.5	N2 Hit
Q9NSE4	SYIM	Isoleucine--tRNA ligase, mitochondrial	14.2	14.5	14.6	9.9	2.2	7.8	4.1	13.2	6.9	14.3	10.0	5.4			*	N2 Hit
P49591	SYSC	Serine--tRNA ligase, cytoplasmic			48.9		1.1		13.2	6.8		4.7			5.9		8.3	
Q9Y6A5	TACC3	Transforming acidic coiled-coil-containing protein 3	3.8	1.2	6.7		2.5										*	
P37837	TALDO	Transaldolase			5.9												*	
Q99426	TBCB	Tubulin-folding cofactor B		91.6	57.9	43.6	27.2			84.8	79.9	49.7		3.3	25.5		4.0	N2 Hit
Q9BTW9	TBCD	Tubulin-specific chaperone D	0.6	3.4	4.0		0.8	1.5	0.6	5.2			0.8	0.8	0.4		10.4	
Q15813	TBCE	Tubulin-specific chaperone E	14.3	2.7	14.2		7.4		8.9			16.5	12.5		2.9		4.8	
O43615	TIM44	Mitochondrial import inner membrane translocase subunit TIM44	2.9		1.6				0.4	5.0							*	
P49755	TMEDA	Transmembrane emp24 domain-containing protein 10	25.1		12.2												*	
Q9UKE5	TNIK	TRAF2 and NCK-interacting protein kinase	2.4		1.5												*	
Q15631	TSN	Translin	36.4		41.2											5.7	7.3	
Q6PGP7	TTC37	Tetratricopeptide repeat protein 37	7.5	2.7	8.0	2.3	2.6		5.8	1.3	3.5	1.8	1.6			1.1	9.0	N2 Hit
Q14694	UBP10	Ubiquitin carboxyl-terminal hydrolase 10		10.0	21.7	25.3	5.2	8.0					1.8	11.0			*	N2 Hit
Q14157	UBP2L	Ubiquitin-associated protein 2-like	20.3	19.4	58.6	54.7	14.8		8.4		34.0	16.0	7.5	12.9	3.7	11.5	7.5	N2 Hit
Q92890	UFD1	Ubiquitin fusion degradation protein 1 homolog	15.2		17.4	5.6	5.1		2.3			20.2					*	N2 Hit
Q00341	VIGLN	Vigilin	29.1	9.8	24.3	4.2	12.2	2.7	9.8	6.3	7.3		7.4			4.3	6.6	N2 Hit
O75436	VP26A	Vacuolar protein sorting-associated protein 26A	31.1		11.6				8.1	29.6		20.5	29.7				*	
Q4G0F5	VP26B	Vacuolar protein sorting-associated protein 26B	3.5		6.2				4.3		3.0		2.8				*	
Q8NI36	WDR36	WD repeat-containing protein 36				0.9						0.8		1003.1			*	
P67809	YBOX1	Nuclease-sensitive element-binding protein 1	2590.6	2742.7	3375.1	3803.1	204.2	153.9	578.9	735.2	895.1	635.6	230.5	371.3	686.5	810.2	4.8	N2 Hit

UniProt Acc. #	Gene Name	Protein Name	P525L SA(-) (iBAQ × 10^5)		P525L SA(+) (iBAQ × 10^5)		P525L SA(+) RNase(+) (iBAQ × 10^5)		ΔRGG SA(+) (iBAQ × 10^5)		WT SA(-) (iBAQ × 10^5)		WT SA(+) (iBAQ × 10^5)		FLAG SA(+) (iBAQ × 10^5)		P525L_SA(+) /FLAG_SA(+)	Replicate Hit?
			N1	N2	N1	N2	N1	N2	N1	N2	N1	N2	N1	N2	N1	N2		
Q9H6S0	YTDC2	Probable ATP-dependent RNA helicase YTHDC2				4.1			1.6								*	
Q7Z739	YTHD3	YTH domain-containing family protein 3	31.1		45.8	60.7		14.6			17.3						*	N2 Hit
Q9NUD5	ZCHC3	Zinc finger CCHC domain-containing protein 3	9.1	13.0	14.5	22.3	4.0										*	N2 Hit
Q86UK7	ZN598	Zinc finger protein 598	4.2		12.9	4.0	1.8	1.6							0.3	1.1	11.6	N2 Hit
Q15942	ZYX	Zyxin	55.1		21.9												*	

APPENDIX II:

NEURONAL PROTEOMICS METHODS

PREFACE

In an effort to identify FUS interactions during stress in primary cortical neurons (PCNs), I designed and generated several entry and lentiviral plasmids for the transduction of V5-FUS and FLAGHA-FUS constructs. I was able to express mutant FUS in PCNs starting on day in vitro (DIV) 4 at an efficiency of 40% of the total population (data not shown). Within each transduced cell, expression of exogenous FUS was ~2X that of endogenous FUS based on immunofluorescence microscopy quantitation (data not shown).

Unfortunately, high background from the immunoprecipitation and a failure of peptide elution approaches caused the mass spectrometry data to be largely uninterpretable (data not shown). Nonetheless, the success of the neuronal transductions will serve as a useful protocol for future research in the Bosco lab. Therefore, I have detailed the protocol for lentivirus design and generation as well as transduction steps in PCNs.

MATERIALS AND METHODS

Primary cortical neuron harvesting and maintenance:

Primary cortical neurons were harvested on embryonic day 14 (E14) at a density of 1.8 x 10^5 cells/mL on 10 cm plates coated with 15 µg/mL poly-L-ornithine with 12 mm coverslips. Media was Neurobasal (Invitrogen 21103049) supplemented with 5% Glutamax (Invitrogen 35050-061), penicillin/streptomycin (Invitrogen 15140122), and B27 supplement (Invitrogen 17504044). Neurons were maintained every three days by exchanging half the media with fresh media and supplement.

Lentivirus design and generation:

Entry vectors with V5-FUS expression vectors were generated as follows: Expression cassettes of V5-FUS were cloned into pLenti-CMV-TO-DEST lentiviral expression vector (Addgene 670-1) using the Gateway LR Clonase II reaction as per manufacturer's instructions (Invitrogen 11791020). Lentivirus was generated via calcium phosphate co-transfection of the following vectors into HEK-293T cells: CMVrh.8, VSV-G (both courtesy of Dr. Miguel Esteves), and the pLenti-CMV-TO-DEST vector containing the V5-FUS expression cassette of interest. Media was changed to Opti-MEM (Invitrogen 31985070) 16h post-transfection, and media was collected, filtered in a 0.45 µM syringe filter (Fisher 09-754-21), and concentrated via ultracentrifugation at 28,000 RPM for 2 h. The pellet from centrifugation was resuspended in 75 µL Opti-MEM and stored at -80˚C until transduction.

Lentiviral transduction:

DIV4 primary cortical neurons, plated at a density of 1.8 x 10^5 cells/mL on 10 cm plates, were treated with 10 µL concentrated lentivirus and left on the cells for 24h, after which media was diluted one-fold with fresh Neurobasal media +B27 supplement. Cells transduced for ten days, after which they were processed for IF and IP on DIV14.

Immunofluorescence:

Coverslips were processed as previous IF methods in Chapter II using the following antibody dilutions: 1:1000 mouse anti-V5 (Invitrogen R96025), 1:200 mouse anti-NeuN (Millipore MAB377), 1:1000 rabbit anti-G3BP (Proteintech 13057-2-AP), 1:1000 rabbit anti-FUS (Bethyl Laboratories A300-293A).

APPENDIX III:

SAMA, ET AL. 2013

The following chapter is a manuscript published in the Journal of Cellular Physiology (Publisher: John Wiley and Sons; License #3397800087634).

My contributions to this manuscript included execution, analysis and manuscript preparation of Figure 6, intellectual input, and experimental design strategies used herein.

ORIGINAL RESEARCH ARTICLE

Journal of Cellular Physiology

2222

FUS/TLS Assembles Into Stress Granules and Is a Prosurvival Factor During Hyperosmolar Stress

REDDY RANJITH K. SAMA,[1] CATHERINE L. WARD,[1] LAURA J. KAUSHANSKY,[1] NATHAN LEMAY,[1] SHINSUKE ISHIGAKI,[2] FUMIHIKO URANO,[3] AND DARYL A. BOSCO[1,4]*

[1]*Department of Neurology, University of Massachusetts Medical School, Worcester, Massachusetts*

[2]*Department of Neurology, Center for Neurological Diseases and Cancer, Nagoya University Graduate School of Medicine, Nagoya, Japan*

[3]*Division of Endocrinology, Metabolism and Lipid Research, Department of Medicine and Department of Pathology and Immunology, Washington University School of Medicine, St. Louis, Missouri*

[4]*Department of Biochemistry and Molecular Pharmacology, University of Massachusetts Medical School, Worcester, Massachusetts*

FUsed in Sarcoma/Translocated in LipoSarcoma (FUS/TLS or FUS) has been linked to several biological processes involving DNA and RNA processing, and has been associated with multiple diseases, including myxoid liposarcoma and amyotrophic lateral sclerosis (ALS). ALS-associated mutations cause FUS to associate with stalled translational complexes called stress granules under conditions of stress. However, little is known regarding the normal role of endogenous (non-disease linked) FUS in cellular stress response. Here, we demonstrate that endogenous FUS exerts a robust response to hyperosmolar stress induced by sorbitol. Hyperosmolar stress causes an immediate re-distribution of nuclear FUS to the cytoplasm, where it incorporates into stress granules. The redistribution of FUS to the cytoplasm is modulated by methyltransferase activity, whereas the inhibition of methyltransferase activity does not affect the incorporation of FUS into stress granules. The response to hyperosmolar stress is specific, since endogenous FUS does not redistribute to the cytoplasm in response to sodium arsenite, hydrogen peroxide, thapsigargin, or heat shock, all of which induce stress granule assembly. Intriguingly, cells with reduced expression of FUS exhibit a loss of cell viability in response to sorbitol, indicating a prosurvival role for endogenous FUS in the cellular response to hyperosmolar stress.

J. Cell. Physiol. 228: 2222–2231, 2013.

Fused in sarcoma/translocated in liposarcoma (FUS/TLS or FUS) is an RNA/DNA-binding protein that is implicated in a diverse array of cellular processes. FUS, also known as heterogeneous ribonuclear protein hnRNP P2 (Calvio et al., 1995), is a member of the TET family of proteins that also includes EWS (Ewing's sarcoma) and TAF15 (TATA-binding protein-associated factor 15) (Tan and Manley, 2009). FUS was originally discovered in the context of a fusion oncoprotein in myxoid liposarcoma cells (Crozat et al., 1993). Since then, this multifunctional protein has been linked to various aspects of RNA and DNA-processing, including mRNA splicing (Ishigaki et al., 2012), transcription (Wang et al., 2008), and DNA repair (Kuroda et al., 2000). Recently, mutations in FUS have been linked to the fatal neurodegenerative disease amyotrophic lateral sclerosis (ALS; Kwiatkowski et al., 2009; Vance et al., 2009).

FUS is predominately expressed in the nucleus of most cells (Andersson et al., 2008), although it shuttles between the nucleus and cytoplasm during mRNA transport (Zinszner et al., 1997; Fujii and Takumi, 2005). Several reports have shown that ALS-linked FUS mutants associate with cytoplasmic stress granules under conditions of oxidative stress and heat shock (Bosco et al., 2010; Dormann et al., 2010; Gal et al., 2010). Stress granules are stalled translational complexes comprised of mRNA, ribosomes, and RNA-binding proteins that form in response to induced stress, such as hyperosmolar stress, oxidative stress, heat shock, ultraviolet irradiation and viral infection (Anderson and Kedersha, 2009). These dynamic complexes are thought to play a role in sorting mRNAs for expression, storage or degradation (Kedersha and Anderson, 2002). More recently, stress granules have also been shown to directly regulate protein activity in the context of

Author contributions: R.R.K.S., C.L.W., L.J.K., and D.A.B. designed the experiments and analyzed the data; R.R.K.S., C.L.W., L.J.K., and N.L. performed the experiments; S.I. and F.U. constructed the inducible FUS knock-down NSC-34 cells; R.R.K.S. and D.A.B. wrote the manuscript. All authors approved the manuscript.

Contract grant sponsor: Worcester Foundation (DAB).
Contract grant sponsor: US National Institutes of Health/National Institute on Neurological Disorders and Stroke;
Contract grant number: R01NS078145-01.

*Correspondence to: Daryl Bosco, Department of Neurology, Albert Sherman Center, AS6-1057, 368 Plantation Dr., Worcester, MA 01605. E-mail: daryl.bosco@umassmed.edu

Manuscript Received 13 April 2013
Manuscript Accepted 17 April 2013

Accepted manuscript online in Wiley Online Library (wileyonlinelibrary.com): 27 April 2013.
DOI: 10.1002/jcp.24395

cellular signaling (Wippich et al., 2013). In contrast to the aforementioned mutant FUS, much less is known about the association of endogenous FUS with stress granules and the role of endogenous FUS in stress response.

Herein, we sought to examine the response of endogenous FUS to various cellular stressors. We found that inducers of stress granule assembly shown to direct mutant-FUS to stress granules, such as sodium arsenite, thapsigargin, hydrogen peroxide, and heat shock, had no effect on the subcellular distribution of endogenous FUS. In striking contrast, endogenous FUS exhibited a robust redistribution from the nucleus to the cytoplasm and assembled into stress granules under conditions of hyperosmolar stress induced by sorbitol and sucrose. Not only was the response of FUS stress-specific, it was also regulated by methyltransferase activity. Cells with reduced FUS expression were more susceptible to sorbitol-induced toxicity, suggesting that FUS plays protective role with regard to cellular homeostasis. These data establish a novel role for the multifunctional FUS protein in cellular stress response.

Materials and Methods

Cell culture and induced stress

HeLa cells and HEK293 cells were cultured in minimal essential medium (MEM, Gibco, Grand Island, NY) supplemented with 10% fetal bovine serum (FBS, Sigma, St. Louis, MO) and 1% penicillin and streptomycin (P/S, Gibco) under standard culture conditions (37° C, 5% CO_2/95% air). NSC-34 cells and mouse embryonic fibroblasts (MEFs) were cultured in Dulbecco's MEM (DMEM, Gibco) supplemented with 10% FBS and 1% P/S under standard culture conditions. FlpIn HEK293 cells with stably integrated GFP-FUS G515X were cultured as described previously (Bosco et al., 2010). Sorbitol (Sigma) was dissolved directly into the media to obtain a concentration of 0.4 M and added to the cells (Kedersha and Anderson, 2007). Sucrose (Electron Microscopy Sciences, Fort Washington, PA) was dissolved into media to obtain a final concentration of 600 osmol/L and added to the cells (Bevilacqua et al., 2010). Stock solutions of 100 mM sodium arsenite (Sigma) in DMSO (Sigma), 10 mM thapsigargin (Sigma) in DMSO, 1 M hydrogen peroxide (Sigma) in media, 30 mM emetine (Sigma) in water and 20 mM Adenosine-2′,3′-dialdehyde (AdOx, Sigma) in water were prepared and added to the media to obtain the final concentrations of 0.5 mM, 50 μM, 1.5 mM, 50 μg/ml, and 50 μM, respectively. Doxycycline (Sigma) was used at a final concentration of 1 μg/ml from a stock of 50 mg/ml prepared in water. Cells were exposed to heat shock by adding media, pre-warmed to 43°C, followed by immediate transfer to an incubator set to 43°C. ON-TARGETplus SMARTpool (Dharmacon, Waltham, MA) consisting of a pool of siRNAs against FUS (Cat # L-009497-00-0005) and ON-TARGETplus non-targeting pool siRNA (Cat # D-001810-10-05) as control were transfected using Lipofectamine-2000 (Invitrogen, Grand Island, NY) according to the manufacturer's instructions.

NSC-34 cell lines were a kind gift from Dr. Neil Cashman (University of British Columbia). Stable NSC-34 cell lines expressing short hairpin (sh) RNA against mouse FUS (shFUS) or non-targeting scrambled RNA (shSC) were prepared by first transducing with the Tet repressor. A single clone that demonstrated good induction without any leaky expression was then selected. NSC34-TetR cells were then transduced with inducible lentivirus-Tet-on/shFUS or Tet-on/shSC (Ishigaki et al., 2012). Cells were treated with 1 μg/ml doxycycline to induce the expression of the shRNAs.

Immunofluorescence

Immunofluorescence was performed as described in (Bosco et al., 2010). Primary antibody incubation conditions were as follows: 1:500–1,000 rabbit anti-FUS (A300-293A, Bethyl Labs, Montgomery, TX); 1:2,500 mouse anti-TIAR (610352, BD Transduction Labs, San Jose, CA); 1:1,500 rabbit ant-ASYM24 (07-414, Millipore, Billerica, MA); 1:2,500 mouse anti-G3BP (611126, BD Transduction Labs) for 1 h at room temperature; and 1:250 mouse anti-GE-1/hedls/p70 S6 kinase (sc-8418, Santa Cruz Biotechnology, Santa Cruz, CA) for 12 h at 4°C. Secondary anti-mouse IgG antibody conjugated to Dylight 549 (715-505-151, Jackson ImmunoResearch Labs, West Grove, PA) was used at 1:1,500–1:3,000. Secondary anti-rabbit IgG antibody conjugated to Dylight 488 (711-485-152, Jackson ImmunoResearch Labs) and secondary anti-rabbit IgG antibody conjugated to Cy5 (711-175-152, Jackson ImmunoResearch Labs) were used at 1:1,500–1:3,000. GFP signal was enhanced using 1:2,000 Alexa Fluor 488-conjugated rabbit anti-GFP (A21311, Invitrogen). Nuclei were stained with 50 nM 4′,6′-diamidine-2-phenylindole dihydrochloride (DAPI; D1306, Invitrogen) for 5 min at room temperature. Coverslips were mounted with ProLong Gold Antifade Reagent (P36930, Invitrogen).

Image acquisition and quantification

Fixed cell images were acquired using a Solamere Technology Group CSU10B (Salt Lake City, UT) spinning disk confocal system as described (Bosco et al., 2010) or using a Leica DMI6000B microscope (Leica Microsystems, Buffalo grove, IL). For images acquired with the Leica microscope, a 100× objective was used with LAS AF One Software (Leica Microsystems) and the Leica DFC365FX camera. Maximum projection images were created from acquired image stacks ($z = 0.2–0.25$ μm, $n = 6–44$ planes) and analyzed using NIH Image J software.

For quantifying the percentage (%) of nuclear FUS, image stacks ($z = 0.2$ μm, $n = 13$ planes) of 60 cells were collected from $n = 3$ experiments with the spinning disk confocal system above. Images were analyzed using MetaMorph software (Molecular Devices, Sunnyvale, CA). Sum projections of each image stack were created after subtracting the background signal as described (Bosco et al., 2010). The integrated morphometry analysis tool was used to calculate the percent (%) nuclear FUS. Statistical significance between conditions was determined by an ANOVA and Tukey's post hoc pairwise test.

Western blots

Western blots were performed essentially as described in (Bosco et al., 2010). Briefly, blots were incubated at 4°C with shaking overnight in the presence of primary antibodies as per the following dilutions: 1:500 anti-tubulin (Sigma), 1:500 anti-FUS (in house antibody created against 264–284 peptide sequence of FUS, Genscript, Piscataway, NJ), 1:500 anti-FUS (47711, Santacruz, Santa Cruz, CA) and 1:1,000 anti-ASYM24 (07–414, Millipore). Densitometry was performed using the Odyssey infrared imaging systems software (Licor Biosciences, Lincoln, NE).

Immunoprecipitation

Cells resuspended in 50 mM Tris–HCl (pH 7.5) supplemented with 1% NP-40, 150 mM NaCl, 5 mM EDTA, 10% glycerol and complete protease inhibitor (lysis buffer) were briefly sonicated and incubated at 4°C with shaking for 30 min. The lysates were centrifuged for 15 min at 13,000 rpm and 4°C. Pre-clearing of the supernatants was achieved by incubation with 100 μl of Biomag Protein G beads (Invitrogen) at 4°C with shaking for 2 h. The beads were removed with a magnet and the protein concentration of the supernatant was determined using a bicinchoninic assay (ThermoScientific, Billerica, MA). Anti-FUS (Genscript) or anti-GFP antibody (ab290, Abcam, Cambridge, MA) was bound to fresh beads with shaking for 2 h at 4°C. A total of 1 mg of the pre-cleared supernatant was then added to 100 μl of antibody-bound beads

and incubated overnight with shaking at 4°C. The lysate was removed and beads were washed three times with lysis buffer. Proteins bound to the beads were eluted with 1X SDS sample buffer at 95°C for 5 min, and probed by western as described above.

Cell toxicity assays

NSC-34 cell lines shSC and shFUS were plated in 24 well dishes. 48 h after induction with doxycyline, cells were treated with 0.4 M sorbitol or 0.25 mM sodium arsenite for 8 h. For the MTT (3-[4,5-dimethylthiazol-2-yl]-2,5-diphenyl tetrazolium bromide) assay 100 μl of 5 mg/ml MTT (Invitrogen) was added to the wells for 35 min followed by cell lysis overnight with 300 μl lysis buffer (10% SDS in 1:1 *N,N*-dimethylformamide:water/2% acetic acid/2.5% HCl 1 M) and absorbance measurement at 550 nm using the VICTOR V plate reader (Perkin Elmer, Waltham, MA). Cell viability for each sample was calculated using the formula: % viability = $100 \times (OD_{sample} - OD_{blank})/(OD_{untreated} - OD_{blank})$. Lactate dehyrodenase (LDH) assay was performed as per manufacturer's protocol (CytoTox 96 Non-radioactive Cytotoxicity Assay, Promega, Madison, WI). After the 8 h treatment, 50 μl of media from each well was transferred to wells of 96 well plate. 50 μl of substrate mix was then added to each well and the plates were covered and incubated at ambient temperature, protected from light for 30 min. After the incubation, 50 μl stop solution was added to each well and absorbance was recorded at 490 nm using the above plate reader. Percentage (%) cytotoxicity was determined for each experimental condition (Expt) using the formula: % cytotoxicity = $100 \times (OD_{expt} - OD_{untreated})/(OD_{max} - OD_{untreated})$, where OD_{max} represents the absorbance of the media from a well with complete lysis of cells releasing maximum LDH. All assays were performed at least three independent times. Statistical significance was determined by a two-tailed Student's *t*-test.

Results

Endogenous FUS redistributes to the cytoplasm and assembles into stress granules in response to hyperosmolar stress

In order to investigate the role of FUS in stress response, we examined the nucleo-cytoplasmic distribution of FUS in response to various cellular stressors. Hyperosmolar stress induced by the administration of 0.4 M sorbitol to HeLa cells for 1 h resulted in a striking redistribution of FUS from the nucleus to the cytoplasm, where FUS assembled into numerous puncta. A majority of FUS-positive puncta co-localized with the stress granule marker proteins, G3BP (Fig. 1A; supplementary material Movie M1) and TIAR (Fig. 1B; supplementary material Movie M2; Kedersha and Anderson, 2007). The redistribution and incorporation of FUS into stress granules in response to sorbitol is reminiscent of other nuclear hnRNPs, such as hnRNP A1 (Guil et al., 2006) and TDP-43 (Dewey et al., 2011). However, not all hnRNP proteins redistribute to stress granules in response to sorbitol (van der Houven van Oordt et al., 2000), suggesting a functional role in stress response for those hnRNPs that do localize to these structures. In addition to sorbitol, hyperosmolar stress induced by sucrose also caused FUS to redistribute to the cytoplasm and incorporate into stress granules (supplementary Fig. S1).

Since stress granules are functionally related to processing bodies (P-bodies), which are cellular sites of mRNA degradation (Moore, 2005), we also probed for the co-localization of endogenous FUS with GE-1/hedls, a constituent of P-bodies but not stress granules (Kedersha and Anderson, 2007). The majority of P-bodies did not co-localize with FUS-positive granules. However, some P-bodies appeared to associate with and/or dock onto FUS-positive granules (Fig. 1C; supplementary material Movie M3), consistent with the physical association between P-bodies and stress granules that has been previously described (Kedersha et al., 2005; Bosco et al., 2010).

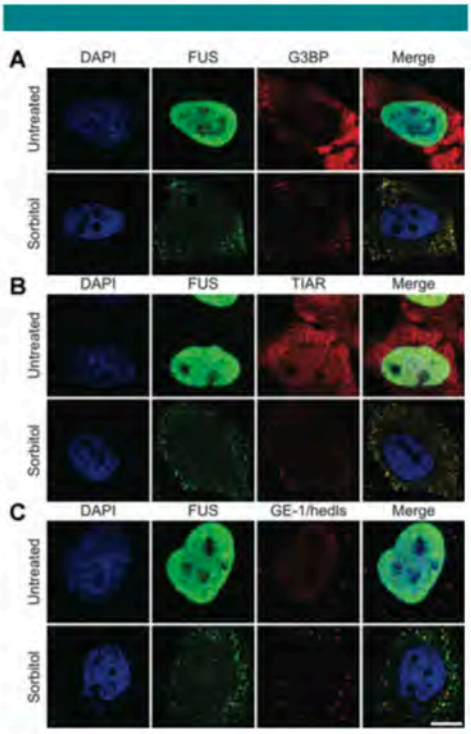

Fig. 1. Endogenous FUS redistributes to the cytoplasm and localizes to cytoplasmic stress granules in response to sorbitol. Confocal images of untreated HeLa cells (top row in each panel) as compared to cells treated with 0.4 M sorbitol for 1 h (bottom row in each panel; A–C) are shown. Cells probed with an anti-FUS antibody (green) and either the stress granule marker anti-G3BP (A) or anti-TIAR (B) revealed that FUS co-localizes with stress granules in response to sorbitol (see also supplementary material Movies M1 and M2). C: P-bodies were detected by anti-GE-1/hedls antibody in both untreated and treated conditions; however, the majority of P-bodies did not exhibit co-localization with FUS (see also supplementary material Movie M3). Cells were counter stained with the nuclear marker DAPI (blue; A–C). Images are representative of at least n = 3 experiments. Scale bar represents 10 μm.

Next, we investigated the effect of sorbitol in other cell lines. Administration of sorbitol to HEK (human embryonic kidney)-293T, MEFs, and NSC-34 (neuroblastoma × spinal cord hybrid; Cashman et al., 1992) cell lines recapitulated the results from HeLa cells; FUS redistributed from the nucleus to the cytoplasm, where it assembled into G3BP- and TIAR-positive stress granules (supplementary material Fig. S2). Therefore, the response of FUS to hyperosmolar stress is not a cell type-specific phenomenon, but rather is detected in several different mammalian cell lines.

In contrast to sorbitol and sucrose, FUS did not redistribute to the cytoplasm when HeLa cells were exposed to inducers of oxidative stress (e.g., sodium arsenite and hydrogen peroxide), endoplasmic reticulum (ER) stress (e.g., thapsigargin) or heat shock, all of which induce the formation of stress granules in a majority of cells (Fig. 2; Kedersha and Anderson, 2007; Emara et al., 2012). Endogenous FUS was not detected in any of the G3BP-positive stress granules that formed under these conditions; we did not detect any cells with elevated cytoplasmic FUS or FUS-positive stress granules under these conditions. Similarly, exogenously expressed wild-type FUS did not redistribute nor assemble into stress granules under the aforementioned conditions (Bosco et al., 2010; Dormann et al., 2010; Bentmann et al., 2012; Daigle et al., 2013), although the effect of sorbitol on endogenous or exogenous FUS has not been reported. Thus our results demonstrate that the formation of stress granules by various stressors is not sufficient to cause a redistribution of FUS to the cytoplasm, indicating that there are specific factors associated with hyperosmolar stress that elicit this response for endogenous FUS.

The assembly of FUS into stress granules is rapid and reversible

The formation of stress granules represents a fast, almost immediate, response of cells to induced stress. To determine the time frame in which FUS responds to sorbitol, we monitored the cellular redistribution of FUS by immunofluorescence microscopy over a 1 h time course of sorbitol exposure. G3BP is an effector of stress granule assembly (Tourriere et al., 2003; Aulas et al., 2012) and was therefore used as a marker to monitor the assembly process. The cytoplasmic redistribution of FUS was detected within 10 min of sorbitol treatment, a time point that preceded the appearance of discreet G3BP-positive cytoplasmic foci, demonstrating that FUS starts to accumulate in the cytoplasm before stress granules are fully formed (Fig. 3A). Within 20 min of sorbitol treatment, discreet G3BP-positive stress granules containing FUS were detected. Therefore FUS appears to incorporate into stress granules on the same time scale that

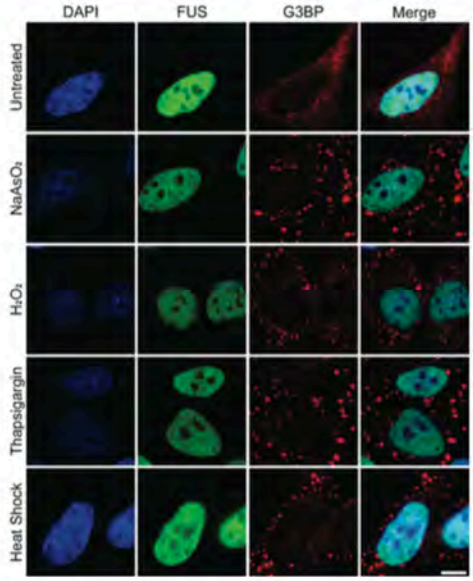

Fig. 2. The recruitment of FUS to cytoplasmic stress granules is stress-specific. HeLa cells were treated with either 0.5 mM sodium arsenite ($NaAsO_2$) for 1 h, 1.5 mM hydrogen peroxide (H_2O_2) for 2 h, 50 μM thapsigargin for 30 min, or heat shock at 43° C for 30 min. Immunofluorescence revealed that G3BP-positive stress granules (red) formed under all stress conditions. FUS (green) remained nuclear and absent from stress granules under these stress conditions, similar to the unstressed condition (top part). Nuclei were stained with DAPI (blue). All images are representative of n = 3 independent experiments. Scale bar represents 10 μm.

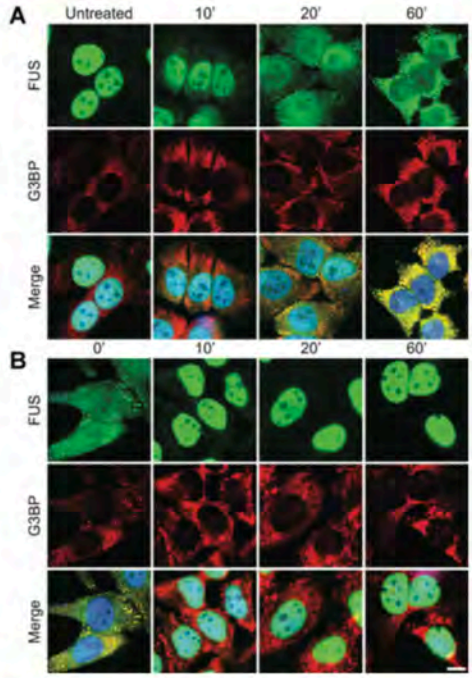

Fig. 3. The response of FUS to sorbitol is rapid and reversible. A: A representative time-course for the cytoplasmic redistribution of FUS into stress granules upon exposure to hyperosmolar stress. HeLa cells were treated with 0.4 M sorbitol for the indicated time points, fixed, and assessed by immunofluorescence with anti-FUS (green) and anti-G3BP (red) antibodies, and the nuclear marker DAPI (blue). Elevated levels of cytoplasmic FUS were detected as early as 10 min. FUS accumulated into discreet stress granules by 20 min. The nucleo-cytoplasmic distribution of FUS continued to shift towards the cytoplasm over the remaining time course. B: A representative time-course for the return of FUS to the nucleus and the concomitant disassembly of stress granules upon withdrawal of sorbitol. HeLa cells were treated with 0.4 M sorbitol for 1 h, after which the sorbitol was replaced with fresh media and the cells were processed as described in (A). A majority of FUS re-localized to the nucleus within 10 min. Some G3BP positive stress granules persisted for up to 1 h. Images are representative of at least n = 3 experiments. Scale bar represents 10 μm.

these foci are being formed. G3BP- and FUS-positive stress granules appear fully formed by 60 min, at which time a substantial fraction of FUS was redistributed to the cytoplasm.

The formation of stress granules is a reversible process (Anderson and Kedersha, 2008). After the induced stress is removed, stress granules disassemble as the cell re-establishes homeostasis. We monitored the disassembly of stress granules in HeLa cells pre-treated with sorbitol to determine the subcellular fate of FUS as cells re-established homeostasis. The disassembly of stress granules was initiated by replacing media containing sorbitol with fresh media lacking sorbitol, and cells were monitored for 60 min by immunofluorescence microscopy as described above. Within 10 min of removing sorbitol from the media, FUS dissociated from stress granules and redistributed to the nucleus in virtually all (~90%) cells. However, G3BP-positive, FUS-negative foci persisted in approximately one third of cells at this time point (Fig. 3B). For the remainder of the time course, FUS was localized to the nucleus while G3BP-positive stress granules gradually continued to disassemble until the 60 min time point, when ~20% of cells contained G3BP-positive stress granules. These data show that FUS exhibits a rapid response not only to the administration of sorbitol (Fig. 3A), but also to the removal of this stressor (Fig. 3B).

Stress granule assembly is required for robust cytoplasmic redistribution of FUS

FUS is a nucleo-cytoplasmic shuttling protein. Therefore, the accumulation of FUS in the cytoplasm can result from increased export of the protein from the nucleus and/or decreased import to the nucleus from the cytoplasm. The nucleo-cytoplasmic equilibrium of FUS may be shifted towards the cytoplasm through FUS binding interactions. For example, injection of anti-FUS antibodies into cells trapped the majority of FUS in the cytoplasm within 2 h (Zinszner et al., 1997). Since the timescale of FUS redistribution from the nucleus to the cytoplasm under conditions of hyperosmolar stress (1 h, Fig. 3) is similar to that in aforementioned antibody study (2 h, Zinszner et al., 1997), we asked whether or not stress granules serve as a "cytoplasmic sink" that effectively traps FUS in the cytoplasm through mass action. Stress granule assembly was inhibited by the addition of 50 μg/ml emetine, which stabilizes polysomes and blocks translation elongation (Kedersha et al., 2000), for 1 h prior to the administration of hyperosmolar stress. As expected, only diffuse G3BP signal (i.e., no G3BP-positive stress granules) was observed under these conditions (Fig. 4A). Interestingly, emetine treatment also markedly attenuated the cytoplasmic redistribution of FUS

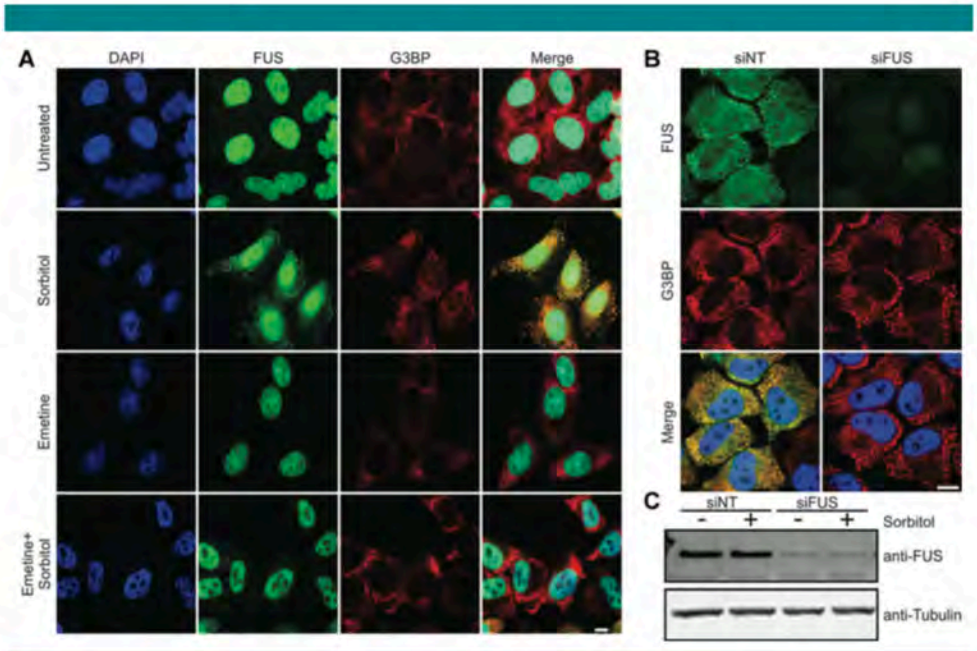

Fig. 4. An inhibitor of stress granule assembly prevents the cytoplasmic redistribution of FUS, though stress granules still assemble in the absence of FUS. A: HeLa cells were treated with 0.4 M sorbitol for 1 h, 50 μg/ml emetine for 1 h or pre-treated with emetine followed by sorbitol treatment. Cells were then fixed and probed by immunofluorescence for DAPI (blue), FUS (green), and G3BP (red). Emetine pre-treatment inhibited both stress granule assembly, as evidenced by the diffuse G3BP signal, and the cytoplasmic redistribution of FUS in the presence of sorbitol. B: HeLa cells were transfected with non-targeting siRNA (siNT) or siRNA against FUS (siFUS) for 48 h, subsequently treated with 0.4 M sorbitol for 1 h, and then processed for immunofluorescence as described above. Cells treated with either siFUS or siNT exhibited normal stress granule formation (B, red) in response to sorbitol, despite a significant reduction in FUS protein levels in siFUS treated cells as evidenced by immunofluorescence (green; B) and Western blot (C). All images are representative of at least n = 3 independent experiments. Scale bar represents 10 μm.

(Fig. 4A) in the presence of sorbitol. These data implicate stress granule formation as a requisite for the cytoplasmic redistribution of FUS, and suggest that the full response of FUS to hyperosmolar stress includes its assembly into stress granules.

Next we investigated the role of FUS in stress granule assembly under conditions of hyperosmolar stress. HeLa cells were first treated with either siRNA specific for FUS or non-targeting siRNA as a control for 48 h, and were then exposed to 0.4 M sorbitol for 30 min to induce the formation of stress granules (Fig. 4B). Although cells treated with FUS siRNA exhibited a ~90% reduction in FUS protein levels (Fig. 4C), these cells produced G3BP-positive stress granules in response to sorbitol that were indistinguishable from control cells (Fig. 4B). While the physical response of FUS to hyperosmolar stress depends on the stress granule assembly pathway (Fig. 4A), FUS does not appear to dictate the ability of stress granules to form.

Methylation regulates the nucleo-cytoplasmic distribution of FUS under hyperosmolar stress

Next we investigated the mechanisms by which FUS relocalizes to the cytoplasm and incorporates into stress granules in response to hyperosmolar stress. Methylation of arginine residues is a post-translational modification that modulates the nucleo-cytoplasmic distribution of hnRNP proteins, such as the cold-inducible RNA-binding protein (CIRP; De Leeuw et al., 2007). Some reports implicate a link between the arginine methylation status of ALS-linked FUS and its subcellular localization (Tradewell et al., 2012; Yamaguchi and Kitajo, 2012). In fact, mass spectrometry analyses demonstrate that up to 20 arginine residues are asymmetrically dimethylated in FUS (Rappsilber et al., 2003). That protein arginine *N*-methyltransferase-1 (PRMT1), which accounts for ~85% of arginine methylation in the cell (Bedford and Clarke, 2009), and FUS interact suggests that the methylation of FUS is catalyzed by PRMT1 (Du et al., 2011; Tradewell et al., 2012; Yamaguchi and Kitajo, 2012). Interestingly, stress granules contain arginine methylated hnRNP proteins, raising the possibility that this post-translational modification influences stress granule dynamics (Xie and Denman, 2011). This notion is supported by an attenuation of fragile X mental retardation protein (FMRP) in stress granules upon exposure to adenosine-2′, 3′-dialdehyde (AdOx) (Dolzhanskaya et al., 2006), a general inhibitor of methyltransferases (O'Dea et al., 1987).

To determine whether or not the methylation status of FUS regulates its subcellular localization under conditions of hyperosmolar stress, we examined the nucleo-cytoplasmic distribution of FUS after treatment of HeLa cells with AdOx. FUS remained predominately nuclear in the presence of AdOx alone (data not shown). However, when cells were pre-treated with AdOx prior to sorbitol exposure, there was a significant effect on the nucleo-cytoplasmic partitioning of FUS compared to cells treated with sorbitol alone (Fig. 5A,B). While sorbitol treatment resulted in a ~50% reduction of nuclear FUS compared to control cells, pre-treatment with AdOx restored ~30% of FUS to the nucleus (Fig. 5B). To quantify the methylation status of the FUS protein itself, FUS was immunoprecipitated from untreated cells or from cells treated with AdOx in combination with sorbitol and probed for asymmetrically dimethylated arginine residues with the ASYM24 antibody (Tradewell et al., 2012). Arginine methylation of FUS in untreated cells was detected by ASYM24 (Fig. 5C), which is expected since FUS is reportedly arginine methylated under homeostatic conditions (Rappsilber et al., 2003). The level of methylated FUS was not significantly altered by the addition of sorbitol (data not shown). However, the arginine methylation status of FUS decreased by more than 50% in cells pre-treated with AdOx (data not shown) or AdOx in combination with sorbitol (Fig. 5C,D). Since AdOx is a general methyltransferase inhibitor, we cannot exclude the possibility that other methylation events influence the subcellular distribution of FUS in these experiments. Nonetheless, these data suggest that the methylation status of FUS must be maintained in order for it to redistribute to the cytoplasm under conditions of hyperosmolar stress, and are consistent with the notion that hypomethylated forms of FUS fail to shuttle out of the nucleus (Tradewell et al., 2012; Yamaguchi and Kitajo, 2012).

Next, we sought to determine if hypomethylated FUS could still assemble into stress granules. Since the assembly of FUS into stress granules occurs concomitantly with cytoplasmic accumulation (Fig. 3), it was necessary to first dissect these two processes. To this end, we transiently transfected HeLa cells with the GFP-tagged FUS 515X truncation construct, which lacks the nuclear localization signal (NLS) and is therefore retained in the cytoplasm under homeostatic conditions (Bosco et al., 2010). GFP-FUS 515X assembled into stress granules in response to 0.4 M sorbitol, and the extent of this association was the same whether cells were pre-treated with AdOx or not (Fig. 6A,B). The same outcome was observed in HEK-293 cells stably expressing GFP-FUS 515X (data not shown). In contrast to the GFP-FUS signal, there was a dramatic decrease in the ASYM24 signal in cells pre-treated with AdOx (Fig. 6A,B), indicating that pre-treatment with AdOx effectively inhibited methyltransferase activity within these cells. Immunoprecipitation with anti-GFP followed by western blot analysis with the ASYM24 antibody confirmed that GFP-FUS 515X was indeed hypomethylated due to AdOx pre-treatment (Fig. 6C). Thus, despite a large reduction in the methylation status of FUS in AdOx pre-treated cells (Figs. 5 and 6), FUS still robustly associated with stress granules. We note that a small fraction of FUS remained dimethylated in the AdOx condition (Fig. 6C), presumably FUS protein that was methylated prior to AdOx exposure but had not turned over during the course of the experiment (Xie and Denman, 2011). In the absence of commercially available antibodies that are specific for dimethylated FUS, we cannot exclude the possibility that stress granules contain some dimethylated FUS in these experiments. However, the dramatic decrease in ASYM24 signal is consistent with a reduced load of methylated proteins within stress granules, and therefore it is unlikely that all of the residual methylated FUS is sequestered into these structures. Together, these studies argue against a role for arginine methylation in regulating the incorporation of FUS in stress granules.

Cells are susceptible to sorbitol toxicity and death when FUS expression is reduced

Given that the full response of FUS to hyperosmolar stress includes its assembly into stress granules (Fig. 4), and that the role of stress granules is to overcome stress and re-establish cellular homeostasis, we investigated whether the expression of FUS is important for cellular viability under conditions of hyperosmolar stress. The normal cellular response to hyperosmolar stress includes cell cycle arrest, during which time cells may adapt to stress and resume proliferation (Burg et al., 2007). However, severe hyperosmolar stress induces apoptosis and cell death (Burg et al., 2007; Bevilacqua et al., 2010). To address the susceptibility of cells to hyperosmolar toxicity in the absence of FUS, we employed inducible NSC-34 cell lines that stably express either shRNA specific for FUS (shFUS) or a scrambled control shRNA (shSC) sequence. These cell lines are advantageous for cell viability measurements since cell death resulting from chemical transfection protocols is eliminated. NSC-34 cells were induced with doxycycline for 48 h, resulting in ~70% knock

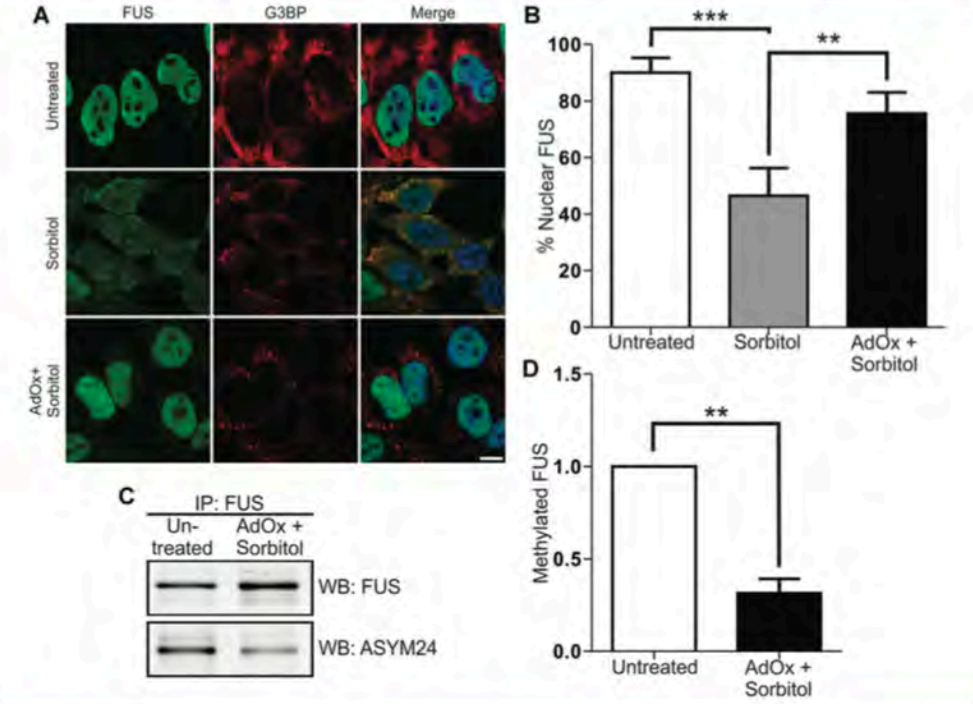

Fig. 5. Methylation regulates the nucleo-cytoplasmic distribution of FUS. A,B: HeLa cells were treated with 0.4 M sorbitol for 1 h, or pre-treated with 50 μM AdOx for 24 h prior to sorbitol treatment (AdOx + sorbitol) and subjected to confocal immunofluorescence imaging with anti-FUS (green) and anti-G3BP (red) antibodies. Sorbitol decreased the percentage of cellular FUS in the nucleus from 90 ± 5.1% in untreated cells to 46.5 ± 9.8%. Pre-treatment of cells with AdOx prior to sorbitol increased the percentage of cellular FUS in the nucleus to 75.6 ± 7.4%. Data shown are the average of three independent experiments ± standard deviation. Statistical significance was determined by ANOVA and Tukey's post hoc pairwise test ($P < 0.005$, *** $P < 0.0005$). No other comparisons were statistically significant. Scale bar represents 10 μm. C: FUS was immunoprecipitated from untreated HeLa cells or from AdOx + sorbitol cells and probed with the ASYM24 antibody by Western blot. FUS was used as a loading control. D: Densitometry analysis of (C) revealed a 68.6 ± 7.8% decrease in the amount of FUS that is arginine dimethylated when cells were pre-treated with AdOx compared to untreated cells. Data shown are the average of three independent experiments ± standard deviation. Statistical significance was determined by Student's t-test (** $P < 0.005$).**

down of FUS in the shFUS line (Fig. 7A) but not a loss of cell viability in either shFUS or shSC cells (data not shown). Cells were then treated for 8 h with either 0.4 M sorbitol or 0.25 mM sodium arsenite as a negative control. Sodium arsenite induces stress granule assembly, however endogenous FUS does not associate with stress granules under this condition (Fig. 2). Moreover, others have reported that mammalian cells with knocked-down FUS expression are not susceptible to sodium arsenite (Aulas et al., 2012). In agreement with this report, we did not detect a difference in percentage cell viability (Fig. 7B) or cell death (Fig. 7C) between shFUS and shSC cells in response to sodium arsenite using the MTT and LDH assays, respectively. In contrast, the percentage of viable cells was approximately twofold lower in the shFUS cells compared to shSC cells after sorbitol treatment (Fig. 7B). That shFUS cells are more susceptible to sorbitol-induced toxicity was confirmed by the LDH cell death assay, which revealed threefold greater cell death in shFUS cells treated with sorbitol compared to shSC cells under the same conditions. Therefore, while the expression of FUS is not required for the assembly of stress granules (Fig. 4B), cellular homeostasis and survival during hyperosmolar stress is mediated by the expression of FUS.

Discussion

Although FUS is predominately expressed in the nucleus of most cell types (Andersson et al., 2008), it can shuttle between the nucleus and the cytoplasm during mRNA transport (Zinszner et al., 1997; Fujii and Takumi, 2005). The equilibrium of FUS expression can be shifted towards the cytoplasm using inhibitors against RNA polymerase II (Pol II; Zinszner et al., 1994) or against the nuclear import receptor Transportin-1 (Trp), also known as Karyopherin β2 (Dormann et al., 2010). Genetic perturbations of its NLS also increase the cytoplasmic expression of FUS in the neurodegenerative disease ALS (Kwiatkowski et al., 2009; Vance et al., 2009). Herein we demonstrate a novel and

robust response of endogenous FUS to hyperosmolar stress, whereby FUS redistributes from the nucleus to the cytoplasm within minutes of exposure to sorbitol (Figs. 1–3) or sucrose (Fig. S1).

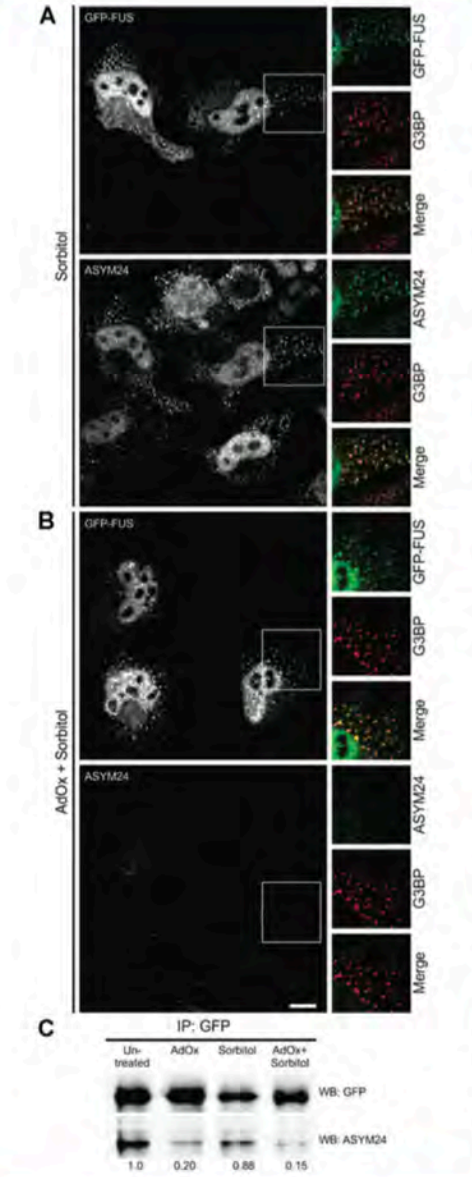

A role for FUS in hyperosmolar stress response is further supported by its association with stress granules under this condition. Stress granules are stalled translational complexes; as such, they are thought to regulate mRNAs processing during stress (Anderson and Kedersha, 2008). Recently, the activity of mTORC1 was shown to correlate with its sequestration inside stress granules, suggesting that these complexes can also regulate cell signaling at the protein level (Wippich et al., 2013). Importantly, no other chemical or environmental stressor has been shown to cause endogenous FUS to redistribute from the nucleus into the cytoplasm and enter into stress granules. While different stressors, such as oxidative stress and heat shock, have been shown to influence the association of ALS-linked mutant forms of FUS with stress granules, the nature of the NLS mutations causes FUS to accumulate in the cytoplasm a priori of stress (Bosco et al., 2010; Dormann et al., 2010). In contrast, hyperosmolar stress triggers both the cytoplasmic redistribution of FUS and its assembly into stress granules. Therefore, the response of endogenous FUS to hyperosmolar stress represents an altogether different mechanism compared to the previously described mutant forms of FUS. Further, our data support a normal and important role for endogenous FUS in stress response (discussed further below), whereas the association of ALS-linked FUS with stress granules is thought to represent a pathogenic mechanism in disease (Wolozin, 2012).

In order to dissect the processes governing the cytoplasmic redistribution of FUS from its incorporation into stress granules, we employed the GFP-FUS G515X construct, which lacks the nuclear localization domain. This allowed us to investigate the role of methylation as a post-translational modification in both events. Inhibition of methyltransferases with AdOx significantly reduced the cytoplasmic redistribution of FUS during hyperosmolar stress (Fig. 5). Moreover, analysis with the ASYM24 antibody revealed that FUS is asymmetrically dimethylated at arginine residues under homeostatic conditions but is hypomethylated in the presence of AdOx (Figs. 5 and 6). These observations, together with a mass spectrometry study demonstrating that ~20 arginine residues within FUS are asymmetrically dimethylated (Rappsilber et al., 2003), supports the possibility that methylation of the FUS protein itself dictates its subcellular localization during hyperosmolar stress. Conversely, the methylation status of FUS, or other cellular factors for that matter, does not appear to regulate the association of FUS with stress granules (Fig. 6). A remaining possibility is that

Fig. 6. Methylation does not regulate the incorporation of FUS into stress granules. HeLa cells were transiently transfected to express GFP-FUS G515X. Cells were exposed to 0.4 M sorbitol for 1 h either (A) in the absence of AdOx or (B) after cells had been pre-treated with 25 μM AdOx for 8 h. A: Confocal imaging showed that GFP-FUS G515X (green) assembles into G3BP-positive stress granules (red) upon sorbitol treatment (top panel). Co-staining with the ASYM24 antibody (a far-red fluorescence probe was employed; green is used in the images for clarity) revealed that these same stress granules contained asymmetrically dimethylated proteins (bottom panel). B: While the ASYM24 signal is dramatically decreased within stress granules and cells pre-treated with AdOx (bottom panel), there is still a robust association of GFP-FUS with stress granules under the same conditions (top panel). Scale bar represents 10 μm. C: Immunoprecipitation of GFP-FUS G515X with an anti-GFP antibody and a subsequent Western blot analysis with ASYM24 revealed that FUS is hypomethylated due to AdOx pretreatment. The ratio of the ASYM24 signal intensity to that of GFP was determined by densitometry and normalized to the untreated condition. Ratios are shown below the blot for each condition. All data are representative of n = 3 independent experiments.

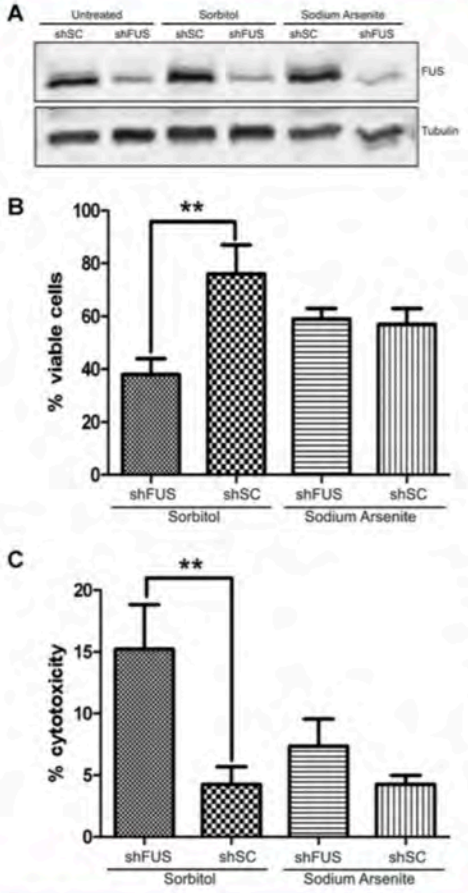

Fig. 7. Reduced FUS expression causes cells to become susceptible to sorbitol induced toxicity. A: Expression of either a non-targeting scrambled shRNA (shSC) or shRNA against FUS (shFUS) was induced by doxycycline for 48 h in NSC-34 cell lines, resulting in ~70% knock-down of the FUS protein as determined by Western blot. Tubulin was used as a loading control. Cells were then treated with 0.4 M sorbitol or 0.25 mM sodium arsenite for 8 h and subjected to the (B) MTT cell viability assay or (C) LDH cell toxicity assay. B: A significant decrease in cell viability was detected in shFUS cells (38 ± 6%) compared to shSC cells (76 ± 11%) when treated with sorbitol, whereas shFUS cells did not exhibit an analogous susceptibility to sodium arsenite (59 ± 4% for shFUS vs. 57 ± 6% for shSC). C: A higher percentage of cell death was detected in shFUS cells (15.2 ± 3.6%) compared to shSC cells (4.2 ± 1.4%) in response to sorbitol, whereas no difference in cell death was detected when these lines were stressed with sodium arsenite (7.4 ± 2.2% for shFUS vs. 4.3 ± 0.7% for shSC). B,C: Data shown are an average from n = 3 independent experiments ± standard deviation. Statistical significance was determined by Student's t-test ($P < 0.005$).**

other post-translational modifications of FUS influence its association with stress granules.

What are the biological implications of FUS in hyperosmolar stress response? Hyperosmolar stress is implicated in a myriad of disease conditions in humans, including renal failure, diabetes, neurodegeneration and inflammation, as well as disorders of the eye, heart, and liver (Brocker et al., 2012). Moreover, the cell shrinkage caused by hyperosmolar stress triggers many adverse subcellular events, such as mitochondrial depolarization, inhibition of DNA replication and transcription, damage to DNA and proteins, and cell cycle arrest, all of which can ultimately lead to cell death (Alfieri and Petronini, 2007; Burg et al., 2007; Brocker et al., 2012).

Our results are consistent with a prosurvival mechanism for endogenous FUS in human conditions that involve hyperosmolar stress. First, the response to hyperosmolar stress is specific, since alternative stressors that induce stress granule assembly such as oxidative stress and heat shock fail to elicit a similar response from endogenous FUS (Figs. 1–3). This data suggests a potentially distinct cellular response to hyperosmolar conditions compared to other stressors. Second, cells are more susceptible to hyperosmolar toxicity when FUS expression is reduced (Fig. 7), supporting a prosurvival role for FUS in this type of stress response.

Other nuclear hnRNPs, such as hnRNP A1, also respond to hyperosmolar stress by redistributing to the cytoplasm and assembling into stress granules. When localized to stress granules, hnRNP A1 is thought to specifically suppress the translation of anti-apoptotic factors and in turn initiate apoptosis under conditions of severe hyperosmolar stress (Bevilacqua et al., 2010). An intriguing possibility is that FUS sequesters specific mRNAs and proteins into stress granules, thereby altering their expression and/or function in response to the hyperosmolar stress. Indeed, recent PAR-CLIP (Hoell et al., 2011) and RIP-Chip (Colombrita et al., 2012) analyses have identified thousands and hundreds, respectively, of mRNA transcripts that are bound by FUS in the cell under homeostatic conditions. Interestingly, FUS binds mRNAs that encode genes involved in DNA damage repair and cell cycle regulation (Colombrita et al., 2012), two pathways that are altered during hyperosmolar stress (Burg et al., 2007).

In summary, our results support a prosurvival function for endogenous FUS during hyperosmolar stress. These findings have implications for human disorders with an etiology that involves hyperosmolar stress. Identifying the factors that regulate the response of FUS to hyperosmolar stress, as well as the pathways affected by FUS under this stress condition, will be critical to further our understanding of this prosurvival role of FUS.

Acknowledgments

We acknowledge the assistance from Dr. Paul Furcinitti of the UMass Medical School Core Digital Imaging Facility. We would like to thank Maeve Tischbein for her assistance with the immunofluorescence experiments, and Dr. Neil Cashman from University of British Columbia for naïve NSC-34 cell lines. We acknowledge financial support from the Worcester Foundation (D.A.B.) and the US National Institutes of Health/National Institute of Neurological Disorders and Stroke (R01NS078145-01 to D.A.B.) for this work.

Literature Cited

Alfieri RR, Petronini PG. 2007. Hyperosmotic stress response: Comparison with other cellular stresses. Pflugers Arch 454:173–185.
Anderson P, Kedersha N. 2008. Stress granules: The Tao of RNA triage. Trends Biochem Sci 33:141–150.
Anderson P, Kedersha N. 2009. Stress granules. Curr Biol 19:R397–R398.

Andersson MK, Stahlberg A, Arvidsson Y, Olofsson A, Semb H, Stenman G, Nilsson O, Aman P. 2008. The multifunctional FUS, EWS and TAF15 proto-oncoproteins show cell type-specific expression patterns and involvement in cell spreading and stress response. BMC Cell Biol 9:37.
Aulas A, Stabile S, Vande Velde C. 2012. Endogenous TDP-43, but not FUS, contributes to stress granule assembly via G3BP. Mol Neurodegener 7:54.
Bedford MT, Clarke SG. 2009. Protein arginine methylation in mammals: Who, what, and why. Mol Cell 33:1–13.
Bentmann E, Neumann M, Tahirovic S, Rodde R, Dormann D, Haass C. 2012. Requirements for stress granule recruitment of fused in sarcoma (FUS) and TAR DNA-binding protein of 43 kDa (TDP-43). J Biol Chem 287:23079–23094.
Bevilacqua E, Wang X, Majumder M, Gaccioli F, Yuan CL, Wang C, Zhu X, Jordan LE, Scheuner D, Kaufman RJ, Koromilas AE, Snider MD, Holcik M, Hatzoglou M. 2010. eIF2alpha phosphorylation tips the balance to apoptosis during osmotic stress. J Biol Chem 285:17098–17111.
Bosco DA, Lemay N, Ko HK, Zhou H, Burke C, Kwiatkowski TJ, Jr., Sapp P, McKenna-Yasek D, Brown RH, Jr., Hayward LJ. 2010. Mutant FUS proteins that cause amyotrophic lateral sclerosis incorporate into stress granules. Hum Mol Genet 19:4160–4175.
Brocker C, Thompson DC, Vasiliou V. 2012. The role of hyperosmotic stress in inflammation and disease. Biomol Concepts 3:345–364.
Burg MB, Ferraris JD, Dmitrieva NI. 2007. Cellular response to hyperosmotic stresses. Physiol Rev 87:1441–1474.
Calvio C, Neubauer G, Mann M, Lamond AI. 1995. Identification of hnRNP P2 as TLS/FUS using electrospray mass spectrometry. RNA 1:724–733.
Cashman NR, Durham HD, Blusztajn JK, Oda K, Tabira T, Shaw IT, Dahrouge S, Antel JP. 1992. Neuroblastoma × spinal cord (NSC) hybrid cell lines resemble developing motor neurons. Dev Dyn 194:209–221.
Colombrita C, Onesto E, Megiorni F, Pizzuti A, Baralle FE, Buratti E, Silani V, Ratti A. 2012. TDP-43 and FUS RNA-binding proteins bind distinct sets of cytoplasmic messenger RNAs and differently regulate their post-transcriptional fate in motoneuron-like cells. J Biol Chem 287:15635–15647.
Crozat A, Aman P, Mandahl N, Ron D. 1993. Fusion of CHOP to a novel RNA-binding protein in human myxoid liposarcoma. Nature 363:640–644.
Daigle JG, Lanson NA, Jr., Smith RB, Casci I, Maltare A, Monaghan J, Nichols CD, Kryndushkin D, Shewmaker F, Pandey UB. 2013. RNA-binding ability of FUS regulates neurodegeneration, cytoplasmic mislocalization and incorporation into stress granules associated with FUS carrying ALS-linked mutations. Hum Mol Genet 22:1193–1205.
De Leeuw F, Zhang T, Wauquier C, Huez G, Kruys V, Gueydan C. 2007. The cold-inducible RNA-binding protein migrates from the nucleus to cytoplasmic stress granules by a methylation-dependent mechanism and acts as a translational repressor. Exp Cell Res 313:4130–4144.
Dewey CM, Cenik B, Sephton CF, Dries DR, Mayer P, III, Good SK, Johnson BA, Herz J, Yu G. 2011. TDP-43 is directed to stress granules by sorbitol, a novel physiological osmotic and oxidative stressor. Mol Cell Biol 31:1098–1108.
Dolzhanskaya N, Merz G, Aletta JM, Denman RB. 2006. Methylation regulates the intracellular protein-protein and protein-RNA interactions of FMRP. J Cell Sci 119:1933–1946.
Dormann D, Rodde R, Edbauer D, Bentmann E, Fischer I, Hruscha A, Than ME, Mackenzie IR, Capell A, Schmid B, Neumann M, Haass C. 2010. ALS-associated fused in sarcoma (FUS) mutations disrupt Transportin-mediated nuclear import. Embo J 29:2841–2857.
Du K, Arai S, Kawamura T, Matsushita A, Kurokawa R. 2011. TLS and PRMT1 synergistically coactivate transcription at the survivin promoter through TLS arginine methylation. Biochem Biophys Res Commun 404:991–996.
Emara MM, Fujimura K, Sciaranghella D, Ivanova V, Ivanov P, Anderson P. 2012. Hydrogen peroxide induces stress granule formation independent of eIF2alpha phosphorylation. Biochem Biophys Res Commun 423:763–769.
Fujii R, Takumi T. 2005. TLS facilitates transport of mRNA encoding an actin-stabilizing protein to dendritic spines. J Cell Sci 118:5755–5765.
Gal J, Zhang J, Kwinter DM, Zhai J, Jia H, Jia J, Zhu H. 2011. Nuclear localization sequence of FUS and induction of stress granules by ALS mutants. Neurobiol Aging 32:2323.e27–2323.e40.
Guil S, Long JC, Caceres JF. 2006. hnRNP A1 relocalization to the stress granules reflects a role in the stress response. Mol Cell Biol 26:5744–5758.
Hoell JI, Larsson E, Runge S, Nusbaum JD, Duggimpudi S, Farazi TA, Hafner M, Borkhardt A, Sander C, Tuschl T. 2011. RNA targets of wild-type and mutant FET family proteins. Nat Struct Mol Biol 18:1428–1431.
Ishigaki S, Masuda A, Fujioka Y, Iguchi Y, Katsuno M, Shibata A, Urano F, Sobue G, Ohno K. 2012. Position-dependent FUS-RNA interactions regulate alternative splicing events and transcriptions. Sci Rep 2:529.
Kedersha N, Anderson P. 2002. Stress granules: Sites of mRNA triage that regulate mRNA stability and translatability. Biochem Soc Trans 30:963–969.
Kedersha N, Anderson P. 2007. Mammalian stress granules and processing bodies. Methods Enzymol 431:61–81.
Kedersha N, Cho MR, Li W, Yacono PW, Chen S, Gilks N, Golan DE, Anderson P. 2000. Dynamic shuttling of TIA-1 accompanies the recruitment of mRNA to mammalian stress granules. J Cell Biol 151:1257–1268.
Kedersha N, Stoecklin G, Ayodele M, Yacono P, Lykke-Andersen J, Fritzler MJ, Scheuner D, Kaufman RJ, Golan DE, Anderson P. 2005. Stress granules and processing bodies are dynamically linked sites of mRNP remodeling. J Cell Biol 169:871–884.
Kuroda M, Sok J, Webb L, Baechtold H, Urano F, Yin Y, Chung P, de Rooij DG, Akhmedov A, Ashley T, Ron D. 2000. Male sterility and enhanced radiation sensitivity in TLS(−/−) mice. Embo J 19:453–462.
Kwiatkowski TJ, Jr., Bosco DA, Leclerc AL, Tamrazian E, Vanderburg CR, Russ C, Davis A, Gilchrist J, Kasarskis EJ, Munsat T, Valdmanis P, Rouleau GA, Hosler BA, Cortelli P, de Jong PJ, Yoshinaga Y, Haines JL, Pericak-Vance MA, Yan J, Ticozzi N, Siddique T, McKenna-Yasek D, Sapp PC, Horvitz HR, Landers JE, Brown RH, Jr. 2009. Mutations in the FUS/TLS gene on chromosome 16 cause familial amyotrophic lateral sclerosis. Science 323:1205–1208.
Moore MJ. 2005. From birth to death: The complex lives of eukaryotic mRNAs. Science 309:1514–1518.
O'Dea RF, Mirkin BL, Hogenkamp HP, Barten DM. 1987. Effect of adenosine analogues on protein carboxylmethyltransferase, S-adenosylhomocysteine hydrolase, and ribonucleotide reductase activity in murine neuroblastoma cells. Cancer Res 47:3656–3661.
Rappsilber J, Friesen WJ, Paushkin S, Dreyfuss G, Mann M. 2003. Detection of arginine dimethylated peptides by parallel precursor ion scanning mass spectrometry in positive ion mode. Anal Chem 75:3107–3114.
Tan AY, Manley JL. 2009. The TET family of proteins: Functions and roles in disease. J Mol Cell Biol 1:82–92.
Tourriere H, Chebli K, Zekri L, Courselaud B, Blanchard JM, Bertrand E, Tazi J. 2003. The RasGAP-associated endoribonuclease G3BP assembles stress granules. J Cell Biol 160:823–831.
Tradewell ML, Yu Z, Tibshirani M, Boulanger MC, Durham HD, Richard S. 2012. Arginine methylation by PRMT1 regulates nuclear-cytoplasmic localization and toxicity of FUS/TLS harbouring ALS-linked mutations. Hum Mol Genet 21:136–149.
van der Houven van Oordt W, Diaz-Meco MT, Lozano J, Krainer AR, Moscat J, Caceres JF. 2000. The MKK(3/6)-p38-signaling cascade alters the subcellular distribution of hnRNP A1 and modulates alternative splicing regulation. J Cell Biol 149:307–316.
Vance C, Rogelj B, Hortobagyi T, De Vos KJ, Nishimura AL, Sreedharan J, Hu X, Smith B, Ruddy D, Wright P, Ganesalingam J, Williams KL, Tripathi V, Al-Saraj S, Al-Chalabi A, Leigh PN, Blair IP, Nicholson G, de Belleroche J, Gallo JM, Miller CC, Shaw CE. 2009. Mutations in FUS, an RNA processing protein, cause familial amyotrophic lateral sclerosis type 6. Science 323:1208–1211.
Wang X, Arai S, Song X, Reichart D, Du K, Pascual G, Tempst P, Rosenfeld MG, Glass CK, Kurokawa R. 2008. Induced ncRNAs allosterically modify RNA-binding proteins in cis to inhibit transcription. Nature 454:126–130.
Wippich F, Bodenmiller B, Trajkovska MG, Wanka S, Aebersold R, Pelkmans L. 2013. Dual specificity kinase DYRK3 couples stress granule condensation/dissolution to mTORC1 signaling. Cell 152:791–805.
Wolozin B. 2012. Regulated protein aggregation: Stress granules and neurodegeneration. Mol Neurodegener 7:56.
Xie W, Denman RB. 2011. Protein methylation and stress granules: Posttranslational remodeler or innocent bystander? Mol Biol Int 2011:137459.
Yamaguchi A, Kitajo K. 2012. The effect of PRMT1-mediated arginine methylation on the subcellular localization, stress granules, and detergent-insoluble aggregates of FUS/TLS. PLoS ONE 7:e49267.
Zinszner H, Albalat R, Ron D. 1994. A novel effector domain from the RNA-binding protein TLS or EWS is required for oncogenic transformation by CHOP. Genes Dev 8:2513–2526.
Zinszner H, Sok J, Immanuel D, Yin Y, Ron D. 1997. TLS (FUS) binds RNA in vivo and engages in nucleo-cytoplasmic shuttling. J Cell Sci 110:1741–1750.

Supporting Information

Additional supporting information may be found in the online version of this article at the publisher's web-site.

Fig. S1. FUS redistributes to the cytoplasm and localizes to cytoplasmic stress granules in response to sucrose. HeLa cells untreated (top row) or treated with 300 mM sucrose for 1 h (bottom row) were fixed and imaged. Cells probed with the anti-FUS (green) and anti-G3BP antibodies revealed that FUS co-localized with stress granules in response to sucrose. Cells were counter stained with the nuclear marker DAPI (blue). Images are representative of at least n = 3 experiments. Scale bar represents 10 μm.

Fig. S2. The response of FUS to sorbitol is recapitulated in several mammalian cell lines. HEK-293 (A), MEF (B), and NSC-34 (C) cells were either untreated (top row in each part) or treated (bottom row in each part) with 0.4 M sorbitol for 1 h. Immunofluorescence with the anti-FUS (green) and anti-G3BP (A) or anti-TIAR (B,C) antibodies showed that FUS localized to stress granules in response to sorbitol in all three cell lines. Cells were counter-stained with the nuclear marker DAPI (blue; A–C). All images are representative of n = 3 independent experiments. Scale bar represents 10 μm.

APPENDIX IV: BARON, ET AL. 2013

The following chapter is a manuscript published in Molecular Neurodegeneration (Publisher: John Wiley and Sons; License #3397800087634). Laura Kaushansky (LK) planned and performed experiments for **Figure 5**, which appears as **Figure II.1** in Chapter II**,** and **Figure 6.**

Desiree Baron (DB) and Catherine Ward (CW) planned and performed the remainder of experiments. DB, Alexandre Quaresma (AJQ) and Jeffrey Nickerson (JAN) planned, performed and analyzed data for FRAP; Ru-ju Chian (RJC) cloned deletion constructs for structure-function analyses; Reddy Sama (RS) and Kristin Boggio (KB) contributed to the design and data interpretation for experiments; DB, LK and Daryl A. Bosco (DAB) wrote the paper. All authors read and approved the final manuscript.

Baron et al. Molecular Neurodegeneration 2013, 8:30
http://www.molecularneurodegeneration.com/content/8/1/30

MOLECULAR NEURODEGENERATION

RESEARCH ARTICLE Open Access

Amyotrophic lateral sclerosis-linked FUS/TLS alters stress granule assembly and dynamics

Desiree M Baron[1], Laura J Kaushansky[1], Catherine L Ward[1], Reddy Ranjith K Sama[1], Ru-Ju Chian[1], Kristin J Boggio[1], Alexandre J C Quaresma[2], Jeffrey A Nickerson[2] and Daryl A Bosco[1,3*]

Abstract

Background: Amyotrophic lateral sclerosis (ALS)-linked fused in sarcoma/translocated in liposarcoma (FUS/TLS or FUS) is concentrated within cytoplasmic stress granules under conditions of induced stress. Since only the mutants, but not the endogenous wild-type FUS, are associated with stress granules under most of the stress conditions reported to date, the relationship between FUS and stress granules represents a mutant-specific phenotype and thus may be of significance in mutant-induced pathogenesis. While the association of mutant-FUS with stress granules is well established, the effect of the mutant protein on stress granules has not been examined. Here we investigated the effect of mutant-FUS on stress granule formation and dynamics under conditions of oxidative stress.

Results: We found that expression of mutant-FUS delays the assembly of stress granules. However, once stress granules containing mutant-FUS are formed, they are more dynamic, larger and more abundant compared to stress granules lacking FUS. Once stress is removed, stress granules disassemble more rapidly in cells expressing mutant-FUS. These effects directly correlate with the degree of mutant-FUS cytoplasmic localization, which is induced by mutations in the nuclear localization signal of the protein. We also determine that the RGG domains within FUS play a key role in its association to stress granules. While there has been speculation that arginine methylation within these RGG domains modulates the incorporation of FUS into stress granules, our results demonstrate that this post-translational modification is not involved.

Conclusions: Our results indicate that mutant-FUS alters the dynamic properties of stress granules, which is consistent with a gain-of-toxic mechanism for mutant-FUS in stress granule assembly and cellular stress response.

Keywords: Stress granule, Amyotrophic lateral sclerosis, Frontotemporal lobar degeneration, FUS/TLS, Oxidative stress

Background

Mutations in the gene encoding fused in sarcoma/translocated in liposarcoma (FUS/TLS or FUS), also known as the heterogeneous nuclear ribonucleoprotein (hnRNP) P2 [1], are linked to inherited cases of amyotrophic lateral sclerosis (ALS) [2,3]. ALS is a fatal neurodegenerative disease characterized by motor neuron loss, progressive muscle weakening and paralysis [4]. Most ALS-linked FUS mutations are located within the C-terminal nuclear localization signal (NLS) that binds transportin, the nuclear importer that translocates FUS from the cytoplasm into the nucleus [5,6]. Although FUS is predominately localized to the nucleus in most cell types [7], it has nucleo-cytoplasmic shuttling capabilities that may be important for mRNA transport [8]. In fact, FUS is thought to play a role in local translation at the dendrites of neuronal cells [9-11]. Disruption of the FUS/transportin interaction leads to nuclear depletion with concomitant cytoplasmic accumulation of FUS in cultured mammalian cells [6]. The potential relevance of this interaction is underscored by the cytoplasmic accumulation of FUS in both ALS [2,3] and frontotemporal lobar degeneration (FTLD) [12] post-mortem central nervous system (CNS) tissues.

The extent to which FUS mutants redistribute to the cytoplasm correlates with ALS disease severity [6,13].

* Correspondence: Daryl.Bosco@umassmed.edu
[1]Department of Neurology, University of Massachusetts Medical School, Worcester, MA, USA
[3]Department of Biochemistry and Molecular Pharmacology, University of Massachusetts Medical School, Worcester, MA, USA
Full list of author information is available at the end of the article

For example, individuals with the FUS R495X mutation, which leads to truncation of the NLS and significant cytoplasmic retention of FUS, exhibit early disease onset and a relatively severe disease course [13]. Nuclear depletion of FUS may impair putative nuclear functions involving mRNA [14,15] and DNA [16,17] processing. An alternative, though not mutually exclusive, possibility is that mutant-FUS exerts a gain-of-toxic function in the cytoplasm [18].

Recently, a two-hit model has been proposed to account for cytoplasmic FUS toxicity in ALS and FTLD [19]. Cytoplasmic mislocalization of FUS, either through genetic mutations or other unidentified factors, represents the first hit. The first hit alone may not be sufficient to cause disease. However, a second hit stemming from cellular stress directs cytoplasmic FUS into stress granules. Stress granules are stalled translational complexes that form as a normal response to induced stressors such as oxidation, heat-shock, viral infection or hypoxia [20]. The function of stress granules is thought to be in the triage of mRNAs that are destined for expression, storage or degradation, which in turn restores cellular homeostasis [21]. Stress granule function may not be limited to mRNA processing, as the activity of certain proteins can also be controlled by their sequestration into stress granules [22]. It follows that the association of mutant-FUS with stress granules may impair stress response and ultimately cause disease [23]. This notion is supported by evidence of stress granule marker proteins within the pathological aggregates of neurodegenerative disease tissues [6,24,25].

While we and others have firmly established a mutant-specific phenotype with respect to FUS in stress granules [5,6,13,26-30], there is little evidence that mutant-FUS actually alters the properties of stress granules. Although there is no functional assay per se for stress granules, the properties of stress granules that are thought to be relevant to their function include assembly kinetics, dynamics, morphology and abundance [21,31]. Under conditions of oxidative stress, we show that mutant-FUS delays stress granule formation in mammalian cell culture. Once sodium arsenite-induced stress granules are formed, however, those containing mutant-FUS are more dynamic, larger and more abundant compared to stress granules lacking FUS. Upon removal of stress, stress granules disassemble more rapidly in cells expressing cytoplasmic mutant-FUS. Further, we identified the RGG domains within FUS as playing a key role in the assembly of mutant-FUS into stress granules, although the methylation of arginine residues within these RGG domains does not play a significant role. The evidence presented here supports the hypothesis that the association of mutant-FUS with stress granules represents a gain-of-toxic interaction in ALS pathogenesis.

Results

The expression of cytoplasmic mutant FUS influences stress granule assembly and disassembly

We and others previously demonstrated that ALS-linked FUS mutants assemble into stress granules to an extent that directly correlates with their cytoplasmic mislocalization [6,13]. These experiments were performed under conditions of acute stress such that stress granules assembled rapidly and did not address whether mutant-FUS affects the processes of stress granule assembly and disassembly. First, we employed our previously characterized, doxycycline-inducible HEK-293 cell lines expressing GFP-tagged wild-type FUS and ALS-linked FUS mutants (R495X and H517Q) [13] to examine the effect of mutant-FUS on stress granule assembly under conditions of oxidative stress. The R495X mutation truncates the nuclear localization signal (NLS), causing FUS to significantly redistribute from the nucleus to the cytoplasm (Figure 1A and [13]). On the opposite end of the mislocalization spectrum is H517Q, an autosomal recessive mutation in the NLS that induces a mild mislocalization phenotype (Figure 1A and [2,13]).

Stress granule assembly was initiated in GFP-FUS (WT, R495X, and H517Q) cell lines with 0.25 mM sodium arsenite, an inducer of oxidative stress [32] and an environmental toxicant that can cause neural defects [33,34]. Sodium arsenite has been shown to induce the incorporation of cytoplasmic FUS-mutants into stress granules, but does not influence endogenous FUS or exogenously expressed GFP-FUS WT proteins [13,35]. In fact there is no difference in cellular response to sodium arsenite with respect to stress granule formation or cell viability when FUS expression is reduced [31,35]. Therefore, sodium arsenite induces a mutant-specific phenotype with respect to FUS localization to stress granules. The concentration of sodium arsenite employed here was reduced from the 0.5 mM concentration that is typically used [13,36] in order to lengthen the timescale of stress granule assembly and resolve differences in this process between cell lines. Ras GTPase-activating protein-binding protein 1 (G3BP), a stress granule specific marker [36], was used to probe for stress granules by immunofluorescence (IF) over a 90 min time course of sodium arsenite exposure. At 0 min, there were no stress granules; G3BP remained diffusely cytoplasmic and no cytoplasmic GFP-FUS puncta were detected in any cell line (Figure 1A). By 90 min, all cell lines contained stress granules in virtually every cell. As expected, GFP-FUS R495X co-localized with G3BP in stress granules, as did GFP-FUS H517Q albeit to a far lesser degree. In contrast, GFP-FUS WT remained entirely nuclear and was not detected within these structures (Figure 1A and Additional file 1). Strikingly, fewer GFP-FUS R495X expressing cells contained G3BP-positive stress granules compared to GFP-FUS (WT

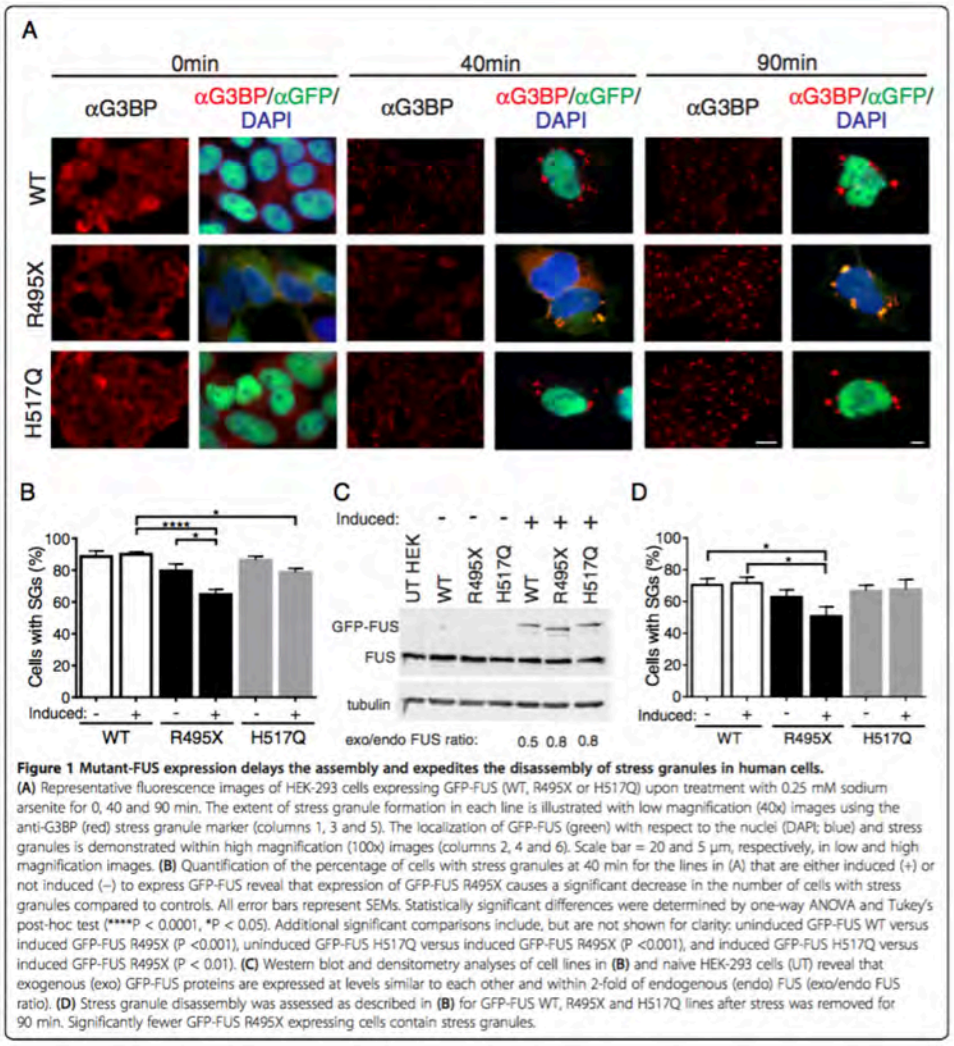

Figure 1 Mutant-FUS expression delays the assembly and expedites the disassembly of stress granules in human cells. **(A)** Representative fluorescence images of HEK-293 cells expressing GFP-FUS (WT, R495X or H517Q) upon treatment with 0.25 mM sodium arsenite for 0, 40 and 90 min. The extent of stress granule formation in each line is illustrated with low magnification (40x) images using the anti-G3BP (red) stress granule marker (columns 1, 3 and 5). The localization of GFP-FUS (green) with respect to the nuclei (DAPI; blue) and stress granules is demonstrated within high magnification (100x) images (columns 2, 4 and 6). Scale bar = 20 and 5 μm, respectively, in low and high magnification images. **(B)** Quantification of the percentage of cells with stress granules at 40 min for the lines in (A) that are either induced (+) or not induced (–) to express GFP-FUS reveal that expression of GFP-FUS R495X causes a significant decrease in the number of cells with stress granules compared to controls. All error bars represent SEMs. Statistically significant differences were determined by one-way ANOVA and Tukey's post-hoc test (****$P < 0.0001$, *$P < 0.05$). Additional significant comparisons include, but are not shown for clarity: uninduced GFP-FUS WT versus induced GFP-FUS R495X ($P < 0.001$), uninduced GFP-FUS H517Q versus induced GFP-FUS R495X ($P < 0.001$), and induced GFP-FUS H517Q versus induced GFP-FUS R495X ($P < 0.01$). **(C)** Western blot and densitometry analyses of cell lines in **(B)** and naïve HEK-293 cells (UT) reveal that exogenous (exo) GFP-FUS proteins are expressed at levels similar to each other and within 2-fold of endogenous (endo) FUS (exo/endo FUS ratio). **(D)** Stress granule disassembly was assessed as described in **(B)** for GFP-FUS WT, R495X and H517Q lines after stress was removed for 90 min. Significantly fewer GFP-FUS R495X expressing cells contain stress granules.

and H517Q) lines after approximately 40 min of sodium arsenite exposure (Figure 1A).

Quantification of these results revealed that the greatest difference in cells containing stress granules occurred between the GFP-FUS R495X (65 ± 3.3%) and GFP-FUS WT (90 ± 1.5%) lines after 40 min of sodium arsenite exposure (Figure 1B). Stress granules were also assembled in GFP-FUS H517Q cells (79 ± 2.5%), though to a lesser extent than WT cells. Therefore, the expression of mutant-FUS is not sufficient to cause a delay in stress granule assembly, but rather, the delay in assembly depends on the extent that FUS is redistributed to the cytoplasm (WT<H517Q<R495X). Artifacts from FUS over-expression are not expected to influence these results since the expression levels of all exogenous GFP-FUS proteins were similar to each other and within two-

fold of endogenous FUS (Figure 1C). To rule out an inherent difference between cell lines irrespective of GFP-FUS expression, identical experiments were performed in uninduced cells (i.e., without doxycycline). Uninduced GFP-FUS (WT and H517Q) lines did not express detectable GFP-FUS and behaved similarly to induced GFP-FUS WT cells, confirming that GFP-FUS WT expression has no effect on stress granule assembly. There was a small yet insignificant difference between uninduced GFP-FUS (WT and R495X) lines (Figure 1B). We suspect this may be due to low levels, below the limit of detection via western analysis (Figure 1C), of GFP-FUS R495X expression in the absence of doxycycline. Nonetheless, induced expression of GFP-FUS R495X in these cells significantly attenuated the assembly of stress granules compared to the uninduced condition in the same line (Figure 1B).

The reversible nature of stress granules is an important functional feature of these structures; upon removal of stress, stress granules disassemble as the cell re-establishes homeostasis. Since mutant-FUS delays the assembly of stress granules, we sought to determine whether mutant FUS also influences the reverse process of disassembly. Cells were treated with 0.25 mM sodium arsenite for 1 h, at which point ~100% of cells in all cell lines contained stress granules. The disassembly process was initiated by replacing sodium arsenite with fresh media, and the percentage of cells with stress granules was quantified after 90 min. At this time point, fewer GFP-FUS R495X expressing cells (51 ± 6.0%) contained stress granules compared to GFP-FUS WT (72 ± 3.7%) and GFP-FUS H517Q (68 ± 6.0%). Therefore, expression of GFP-FUS (WT and H517Q) had virtually no effect, while expression of the cytoplasmic GFP-FUS R495X exerted the most pronounced effect on the kinetics of stress granule disassembly (Figure 1D). Interestingly, a similar effect on stress granule assembly and disassembly was observed upon depletion of endogenous TAR DNA-binding protein 43 (TDP-43) [37], which, unlike FUS, is thought to play a normal role in arsenite-induced stress response [31]. Thus, both a loss of TDP-43 function and a potential toxic gain of mutant-FUS function manifests in delayed stress granule assembly and more rapid stress granule disassembly under conditions of oxidative stress.

While HEK-293 GFP-FUS lines are ideal for microscopic measurements of stress granule properties, owing to the GFP tag on FUS and the relatively flat nature of these cells, we wanted to both confirm these stress granule assembly trends in neuronal cells and rule out a potential "tag effect" from GFP. To this end, motor neuron-like NSC-34 [38] cell lines were engineered to constitutively express untagged human FUS WT or FUS R495X using a lentiviral transduction expression system. FUS protein expression in these cells was accomplished with an IRES-containing bicistronic vector (CSCW2-IRES-GFP), which allowed for the simultaneous expression of both FUS and GFP separately (i.e., not as a fusion protein) but from the same RNA transcript. Therefore, GFP served as a reporter for cells transduced to express either untagged FUS WT or R495X. The expression levels of FUS (WT and R495X) proteins were similar to each other and within two-fold of endogenous FUS (Figure 2A and Additional file 2). In the absence of stress, elevated levels of cytoplasmic FUS were observed in NSC-34 cells expressing FUS R495X, and diffuse cytoplasmic G3BP signal was observed in both FUS R495X and WT cells. Upon exposure to 0.25 mM sodium arsenite for 1 hr, FUS was detected within G3BP-positive stress granules only in cells expressing FUS R495X. Although sodium arsenite exposure lead to fewer NSC-34 cells with stress granules overall compared to HEK-293 cells, the same phenotype was observed in that fewer cells formed stress granules in FUS R495X expressing cells compared to those expressing FUS WT (Figure 2B). Quantification of this phenotype revealed a 2.4-fold lower percentage of stress granule-containing NSC-34 cells for FUS R495X (23 ± 1.6%) compared to FUS WT (55 ± 2.8%) lines (Figure 2C). To assess whether the expression of exogenous human FUS proteins had any effect on stress response in these cells, the percentage of cells with stress granules was also quantified in the parent, or non-transduced, NSC-34 cell line after 1 h of sodium arsenite exposure. While FUS WT and R495X lines exhibited the most significant difference, there were also more FUS WT cells with stress granules relative to the parent (37 ± 3.6%) line (Figure 2C). Possible explanations for why an effect of exogenous FUS WT is observed in NSC-34 but not HEK-293 (Figure 1B) cells is that the expression of exogenous human FUS WT exerts an additional stress due to i) higher relative protein levels (compare exogenous to endogenous FUS in Figures 1C and 2A), and/or ii) different species of cells (expression of human FUS in mouse versus human cells), either of which could heighten the stress response of these cells to sodium arsenite. In fact, expression of FUS WT is sufficient to induce stress and toxicity in different model organisms [39-41]. Nonetheless, the efficiency of stress granule assembly in the parent NSC-34 line is more similar to that of FUS WT than FUS R495X (Figure 2C). Moreover, one would expect FUS R495X to also impose an additional stress, and yet stress granule assembly is attenuated in these cells, providing further evidence that expression of mutant-FUS interferes with the assembly of stress granules under conditions of stress.

Unlike HEK-293 cells (Figure 1), the percentage of NSC-34 cells containing stress granules never reached 100% in any line, and the FUS WT line always contained double the percentage of cells with stress granules compared to FUS R495X. This behavior precluded our ability to perform a similar disassembly analysis as described

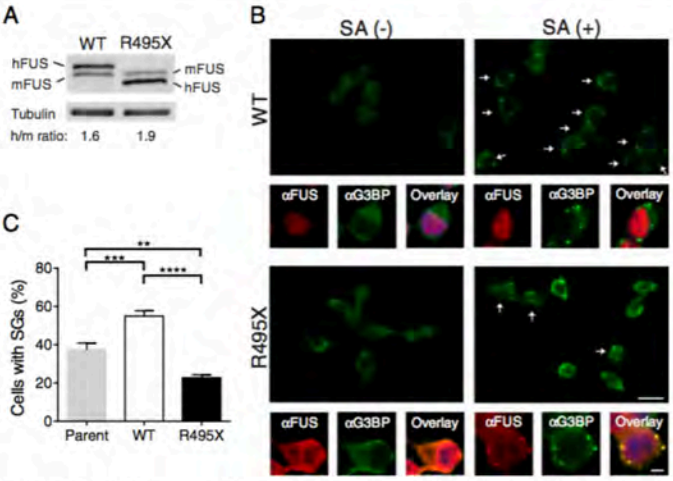

Figure 2 Expression of the FUS R495X mutant interferes with stress granule assembly in neuronal cells. (A) Exogenous human (h) FUS proteins are similar to each other and within 2-fold of endogenous mouse (m) FUS as determined by western blot and densitometry analyses. The ratio of hFUS/mFUS proteins is indicated for each cell line. **(B)** Immunofluorescence images of NSC-34 cells expressing untagged FUS (WT and R495X) either in the absence (–) or presence (+) of 0.25 mM sodium arsenite (SA) for 1 hr. Low magnification (40x) images of SA (+) treated cells using the anti-G3BP stress granule marker (green) show a greater number of stress granule-positive cells (denoted by arrows) in the FUS WT line compared to the FUS R495X line. High magnification (100X) images showing a single cell reveal the localization of FUS (red) and G3BP (note: the far red channel was used for detection of G3BP and the images are shown in green for clarity) under all conditions. DAPI (nuclei) is included in the overlay images. Note that in cells with stress granules, cytoplasmic R495X co-localizes to these structures as expected (see overlay image in bottom right). Scale bar = 20 and 5 μm, respectively, in low and high magnification images. **(C)** Quantitative analysis (as described in Figure 1B) of the percentage of NSC-34 cells with stress granules after 1 hr of sodium arsenite treatment revealed that expression of FUS R495X inhibited stress granule assembly compared to cells expressing FUS WT and the parent line. All error bars represent SEMs. Statistically significant differences were determined by one-way ANOVA and Tukey's post-hoc test (****$P < 0.0001$, ***$P < 0.001$, **$P < 0.01$).

above for HEK-293 cells (Figure 1D), which compared the absolute percentage of cells with stress granules at different time points.

The expression of cytoplasmic mutant-FUS alters the dynamic binding properties of stress granule-associated proteins

Stress granules are highly dynamic structures [32,42,43]. Proteins and mRNA continuously shuttle in and out of stress granules, reversibly binding to other stress granule components in a manner that is thought to regulate both protein signaling activity [22] and mRNA fates towards translational arrest, expression or decay [20]. To study the effect of stress granule-associated mutant-FUS on the dynamic properties of stress granules, we employed fluorescence recovery after photobleaching (FRAP). FRAP measures the relative kinetics and affinities of protein binding within complexes, such as stress granules, over the time course of the experiment [44,45]. Because FRAP reports on binding events in live cells, fluorescently tagged-proteins were employed for these experiments [32,42,43,46]. We transiently expressed monomeric RFP (mRFP)-tagged proteins T-cell-restricted intracellular antigen-1 (TIA-1) or G3BP, two established stress granule-associated proteins, to mark stress granules for FRAP within HEK-293 GFP-FUS (WT and R495X) cells. Overexpression of G3BP is sufficient to form inclusions that resemble stress granules in the absence of stress [31,47]. Since it is not clear whether these G3BP overexpression-induced stress granules have different properties than sodium arsenite-induced stress granules, conditions were optimized for transfection of mRFP-G3BP that minimized the formation of G3BP-positive inclusions *a priori* of sodium arsenite treatment (Figure 3A; see Materials and methods).

During a FRAP experiment on stress granules, the fluorescence from a tagged species (GFP-FUS R495X, mRFP-TIA-1 or mRFP-G3BP in our case) is bleached. The fluorescence signal recovers as bleached molecules unbind from sites in the stress granules, un-bleached fluorescent molecules exchange back into the photobleached area and then bind. The fluorescence recovery time is limited by

Baron et al. Molecular Neurodegeneration 2013, 8:30
http://www.molecularneurodegeneration.com/content/8/1/30

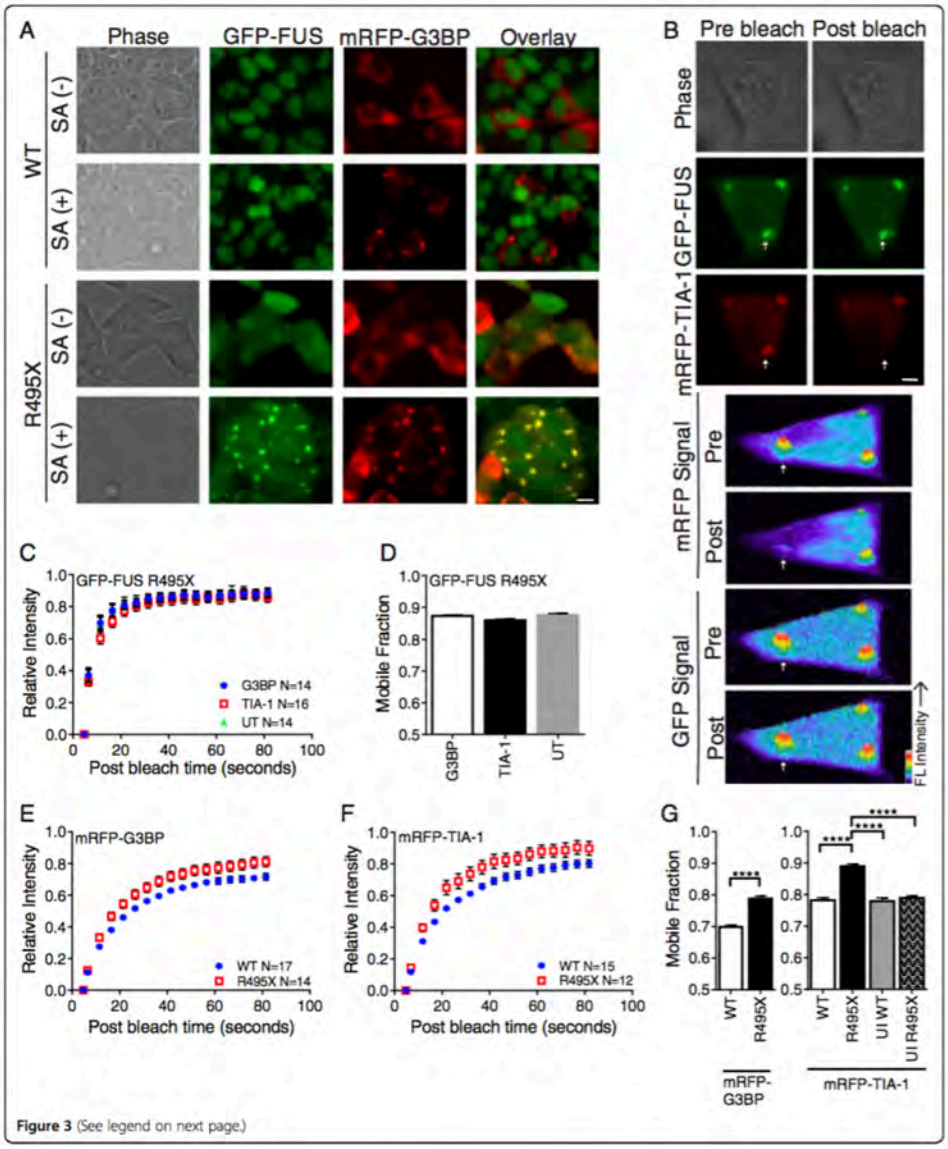

Figure 3 (See legend on next page.)

(See figure on previous page.)
Figure 3 GFP-FUS R495X is weakly bound to stress granules and alters binding of stress granule-associated proteins. (A) Live cell images of GFP-FUS (WT and R495X) expressing HEK-293 cells transfected with mRFP-G3BP. Images are shown before (–) and after (+) treatment with 0.2 mM sodium arsenite (SA) for 1 hr. Scale bar = 10 μm. **(B)** Top three panels: exemplar GFP and mRFP images of a SA treated cell for a mRFP-TIA-1 FRAP experiment before and after photobleaching. The mRFP signal, but not GFP signal, is lost from the stress granule (indicated by arrow). Scale bar = 5 μm. Bottom four panels: fluorescence intensity profiles corresponding to the above panels (rotated 90° clockwise). **(C)** The recovery curve for GFP-FUS R495X in untransfected (UT; green triangle) cells are indicative of fast fluorescence recovery. The GFP-FUS R495X profile does not change upon transfection with either mRFP-G3BP (blue circle) or mRFP-TIA-1 (red square). **(D)** Nearly identical mobile fractions support the conclusions in **(C)**. **(E & F)** Recovery curves for mRFP-G3BP **(E)** and mRFP-TIA-1 **(F)** differ for GFP-FUS WT (blue circle) and R495X (red square) expressing cells. **(G)** Mobile fractions for the curves in **(E & F)** are significantly higher for GFP-FUS R495X (black bars) relative to GFP-FUS WT (white bars) cells. Mobile fractions for mRFP-TIA-1 are the same for the following control experiments: GFP-FUS WT expressing cells (white bars), uninduced (UI) GFP-FUS WT cells (grey bar) and uninduced GFP-FUS R495X cells (hatched bar). Asterisks indicate statistically significant differences between cell lines as determined by two-way ANOVA and Tukey's post-hoc test (****$P < 0.0001$) on data from at least n=2 independent experiments. All error bars represent SEMs. The total number (N) of stress granule analyzed is indicated on the recovery panels.

either diffusion, which is faster than the rates we report here, or by binding kinetics; thus, proteins that are tightly bound to other proteins or cellular structures exhibit relatively long half times of fluorescence recovery ($t_{1/2}$) [44]. The population of fluorescent molecules that exchange with their bleached counterparts over the time course of the experiment comprise the "mobile fraction" [44]. The "immobile fraction" is the population that is tightly bound and does not exchange over the time course of the experiment. Here, each experiment was carried out such that the photobleaching occurred in only a single channel and fluorescence was diminished evenly over the entire stress granule (Figure 3B). Initially, the dynamics of GFP-FUS R495X within stress granules were investigated since the dynamic binding properties of this protein under stress conditions have not been reported. GFP-FUS R495X cells alone or transfected with either mRFP-G3BP (Figure 3A) or mRFP-TIA-1 (Figure 3B) were exposed to 0.20 mM sodium arsenite for 1 hr, at which point the majority of cells contained fully formed stress granules. The fast recovery ($t_{1/2}$ of 3.6 ± 2.1s; Figure 3C) of GFP-FUS R495X by FRAP shows that this protein re-binds within stress granules relatively quickly compared to other stress granule-associated proteins (see below). Moreover, ~87% of GFP-FUS R495X molecules constituted the mobile fraction, indicating that GFP-FUS R495X is weakly bound within stress granules (Figure 3D). Neither the $t_{1/2}$ nor the mobile fraction of GFP-FUS R495X changed significantly upon transient transfection of either mRFP-G3BP or mRFP-TIA-1 (Figure 3C and D). Therefore, neither the process of transient transfection itself, nor the over-expression of stress-granule associated proteins, influenced the dynamic properties of mutant-FUS.

Next we performed FRAP on mRFP-G3BP or mRFP-TIA-1 to determine the effect of mutant-FUS on the dynamic properties of proteins within stress granules. Fluorescence recovery for mRFP-G3BP ($t_{1/2}$ 12 ± 4.4s; 70 ± 2% mobile) and mRFP-TIA-1 ($t_{1/2}$ 12 ± 3.9s; 78 ± 2% mobile) within GFP-FUS WT expressing cells was observed (Figure 3E and F). Our measurements of mRFP-TIA-1 in control HEK-293 cells were similar to those reported for GFP-TIA-1 COS7 cells [32]. In cells expressing GFP-FUS R495X, the fluorescence recovery half times were nearly the same for mRFP-G3BP ($t_{1/2}$ 11 ± 2.8s) and mRFP-TIA-1 ($t_{1/2}$ 10 ± 2.8s). However, the mobile fraction for both mRFP-G3BP and mRFP-TIA-1 increased significantly in GFP-FUS R495X cells to 79 ± 3% and 89 ± 4%, respectively, compared to GFP-FUS WT cells (Figure 3E-G). Control experiments in GFP-FUS WT (induced and uninduced) and GFP-FUS R495X (uninduced) cells confirmed that an increase in mRFP-TIA-1 mobile fraction required the expression of mutant-FUS (Figure 3G). The increased mobile fraction for mRFP-G3BP and mRFP-TIA-1 indicates that these proteins bind more weakly to factors within GFP-FUS R495X positive stress granules compared to stress granules lacking mutant-FUS. As a result, there is increased exchange of mRFP-G3BP and mRFP-TIA-1 between the area that is photobleached and the area that is not photobleached, resulting in fluorescence recovery. Together, these data demonstrate that the incorporation of mutant-FUS into sodium arsenite-induced stress granules decreases the binding of other stress granule-associated proteins within these structures.

Because we and others observed that stress granules form as a result of G3BP overexpression [31,47], we examined whether their dynamic properties were different compared to those stress granules induced by sodium arsenite. mRFP-G3BP exhibited significantly weaker binding (i.e., larger mobile fraction, $P < 0.05$) within stress granules in GFP-FUS WT cells under conditions of G3BP over-expression compared to sodium arsenite stress, indicating that the dynamic properties of these stress granules are inherently different (Additional file 3). The most striking difference was the effect of mutant-FUS: GFP-FUS R495X significantly *increased* mRFP-G3BP binding within stress granules (i.e., smaller mobile fraction) under conditions of G3BP over-expression compared to all other conditions, which is the opposite trend in sodium arsenite-induced stress granules (Figure 3). Therefore, the effect of GFP-FUS R495X on the dynamic properties of stress granules

depends on the stressor and is consistent with observations that the source of stress influences the constituents within stress granules [48]. Irrespective of the stress, our results show that the incorporation of GFP-FUS R495X into stress granules alters the dynamic binding interactions of other well-characterized stress granule-associated proteins within in these structures.

Expression of mutant-FUS increases the size and abundance of stress granules

In addition to dynamics, stress granule size and abundance could also be altered by the presence of mutant-FUS. As such, both stress granule size and abundance were quantified in HEK-293 cell lines expressing either GFP-FUS (WT or R495X) after exposure to 0.5 mM sodium arsenite for 1 hr, at which point stress granules were fully formed (>95% of cells contain stress granules). In contrast to previous methods that measure the area of stress granules, which does not take into account the three-dimensional aspect of these structures, we developed a method to quantify the volume of stress granules based on fluorescence intensity measurements (see Materials and methods). Briefly, fixed cells were labeled with an anti-G3BP antibody and then optically sectioned by confocal microscopy. Three-dimensional reconstruction of these sections allowed us to quantify the volume of selected stress granules (Figure 4A). This analysis revealed that GFP-FUS R495X expressing cells produced significantly larger stress granules (3.8 ± 0.1 μm^3) compared to GFP-FUS WT cells (2.7 ± 0.2 μm^3; Figure 4B and C). This trend is consistent with ALS-linked TDP-43 mutants, which also show an increased stress granule size under conditions of hyperosmolar stress [49], suggesting that this may be a common disease-related characteristic.

Our quantitative analysis also revealed that mutant-FUS expressing cells contained 27% more stress granules per cell (8.8 ± 0.3) compared to WT-FUS (6.9 ± 0.4; Figure 4B and D). This result is consistent with a recent report demonstrating a greater abundance of stress granules within patient FUS (R521C and R514G) fibroblast lines under conditions of sodium arsenite relative to control lines [30]. Moreover, cells expressing ALS-linked TDP-43 also produce more stress granules compared to control cells under stress [25]. Therefore, disease-causing FUS and TDP-43 proteins appear to alter stress granules morphology by increasing their size and abundance.

The RGG domains play a key role in modulating the association of mutant-FUS with stress granules

In order to understand the factors modulating the incorporation of mutant FUS into stress granules, we engineered GFP-tagged FUS constructs lacking the functional domains of FUS and tested their ability to incorporate into stress granules. The functional domains of FUS are as follows: the prion-like QGSY-rich region (QGSY), a glycine-rich region (GLY), an RNA recognition motif (RRM), and two arginine-glycine-glycine-rich domains (RGG1 and RGG2) separated by a C2-C2 zinc finger motif (ZF) (Figure 5A). All of these domains have been shown to play a role in modulating the incorporation of other RNA binding proteins into stress granules [26,50-52] and thus each have the potential to influence the association of mutant-FUS with stress granules. The extent with which FUS mutants localize to arsenite-induced SGs correlates with their level of cytoplasmic expression (Figures 1, 2 and [13]). However, since transient transfection of highly cytoplasmic FUS mutants (e.g., R495X) has the potential to produce cytoplasmic protein aggregates that could confound our stress granule analysis [13], domain deletion constructs were engineered within the background of the less aggregation-prone R521G mutant.

Transient transfection of GFP-FUS R521G deletion constructs in HeLa cells resulted in varying degrees of GFP-FUS cytoplasmic expression: FL, ΔQGSY, ΔRGG1, ΔGLY and ΔRRM were predominately expressed in the nucleus, whereas relatively high cytoplasmic expression was observed for ΔRGG2, which lacks part of the signal used for nuclear import of FUS [5] (Figure 5B). Deletion of the zinc finger motif resulted in a construct that failed to express in mammalian cells (data not shown), possibly because this construct is unstable and/or structurally altered [53]. Although GFP-FUS R521G exhibits cytoplasmic expression upon transient transfection [2], the levels here were not sufficient for an accurate stress granule analysis. It was therefore necessary to increase the cytoplasmic expression of FUS-deletion constructs by co-transfection with maltose binding protein (MBP)-tagged M9M. M9M is a transportin/Kapβ2-specific nuclear import inhibitor that blocks the nuclear import of FUS [6,54]. Co-transfection with MBP-M9M increased cytoplasmic retention of GFP-FUS for all constructs, ensuring that each construct had equal potential to assemble into stress granules (Figure 5B).

Administration of 0.5 mM sodium arsenite for 1 hr induced stress granule formation (Figure 5B) in ~75% of cells for all constructs. A ratio of the GFP signal within stress granules relative to the diffuse GFP-FUS signal in the cytoplasm (stress granule/diffuse FUS signal) was used to quantify the incorporation of each construct within stress granules. Full length GFP-FUS R521G exhibited a robust localization to stress granules with a stress granule/diffuse FUS ratio of 4.75 +/− 0.97 (Figure 5B and C). As expected for a protein that does not associate with stress granules, analysis with free GFP as a negative control produced the lowest ratio of 1.13 +/− 0.11. GFP-FUS R521G ΔQGSY, ΔGLY, and ΔRRM were not significantly different from FL GFP-FUS R521G. In contrast, deletion of the RGG1

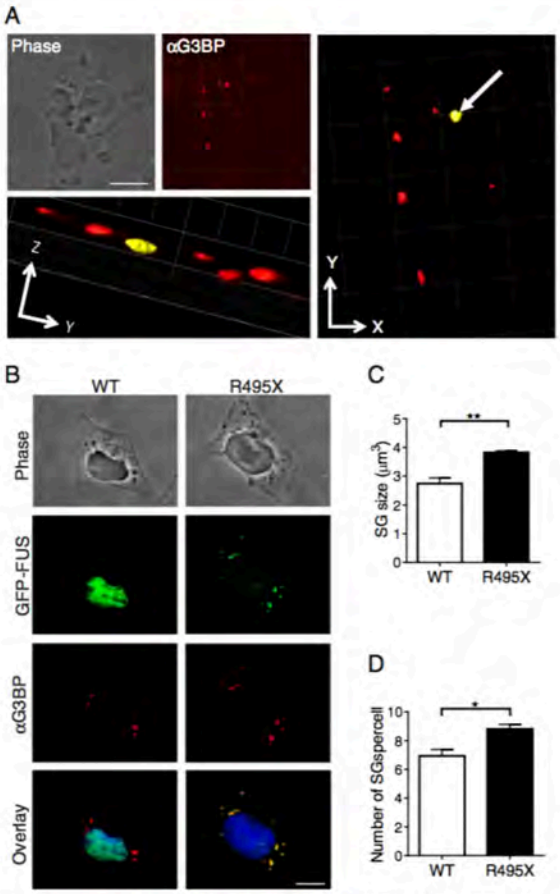

Figure 4 Stress granule size and number are increased in GFP-FUS R495X expressing cells. (A) Clockwise order: representative single-plane phase (top left) and anti-G3BP (stress granule marker; red) immunofluorescence (top middle) confocal images of an HEK-293 cell expressing GFP-FUS WT treated with 0.5 mM sodium arsenite for 1 hr. Three-dimensional (3D) reconstruction was used to quantify stress granule volume (see Materials and methods, and C within this figure). The *xy* (right) and *yz* (bottom; view along arrow in xy image) planes for this 3D reconstructed image are shown; the stress granule highlighted in yellow is marked for volume analysis. Scale bar = 10 μm. **(B)** Representative maximum projection confocal images of GFP-FUS WT and GFP-FUS R495X expressing cells treated as in **(A)** exemplify the size and number of stress granules for each line. Scale bar = 10 μm. **(C and D)** GFP-FUS R495X expressing cells contain stress granules with larger volume **(C)** and in greater abundance **(D)** relative to cells expressing GFP-FUS WT. Asterisks indicate statistically significant differences between cell lines as determined by the Student's t-test (**$P < 0.01$, *$P < 0.05$) on data from n=3 independent experiments. All error bars represent SEMs.

domain (ΔRGG1) significantly impaired the localization of FUS into stress granules (1.72 +/− 0.22), and deletion of the RGG2 domain (ΔRGG2) exhibited a similar impairment trend (2.23 +/− 0.48). We note that while distinct FUS-positive stress granules are observed for ΔRGG2, a comparatively high level of GFP-FUS signal remains diffuse, yielding a low stress granule/diffuse FUS ratio. All constructs were expressed at comparable levels (Figure 5D)

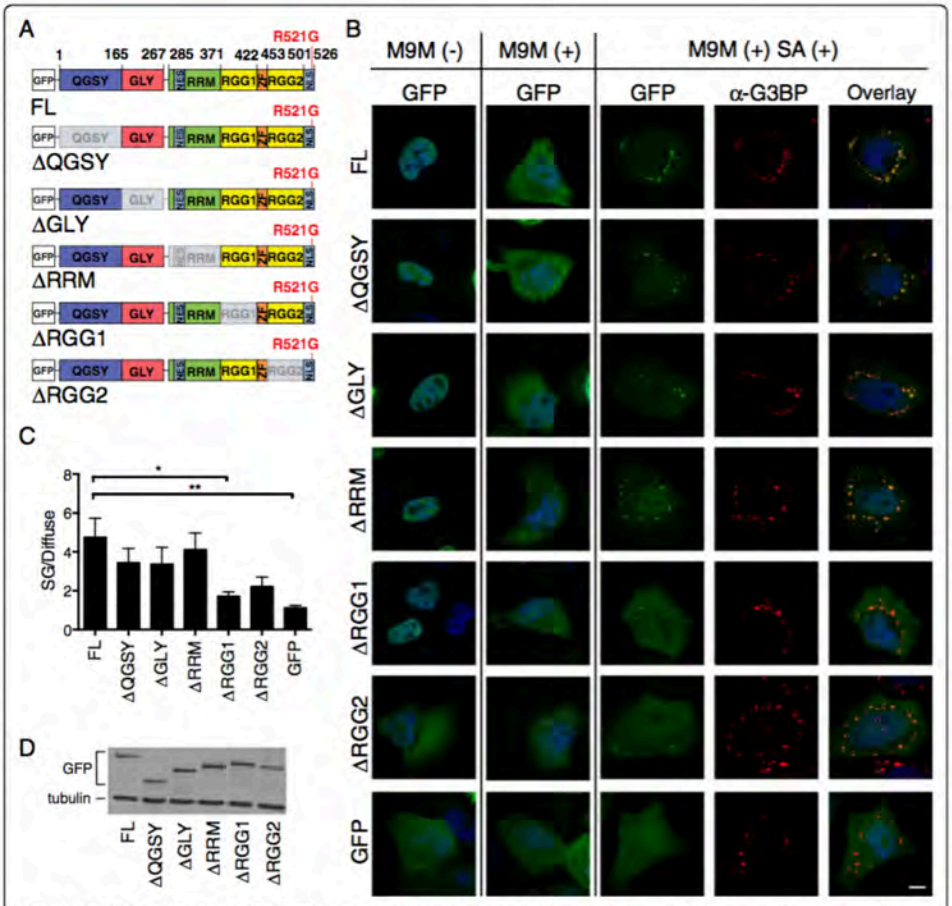

Figure 5 The RGG domains modulate the incorporation of FUS into arsenite-induced stress granules. (A) Illustration of full length (FL) GFP-FUS R521G and constructs lacking the following sequences: Gln-Gly-Ser-Tyr-rich (ΔQGSY), Gly-rich (ΔGLY), RNA recognition motif (ΔRRM), and Arg-Gly-Gly-rich (RGG) regions (ΔRGG1 and ΔRGG2). **(B)** Confocal images of HeLa cells transfected with GFP-FUS R521G constructs (green) alone (–) or co-transfected (+) with MBP-M9M, the transportin-1 inhibitor. Note the increased levels of cytoplasmic GFP-FUS in co-transfected cells (compare columns 1 and 2). Confocal fluorescence images of co-transfected cells treated with 0.5 mM sodium arsenite for 1 hr were used to assess the ability of GFP-FUS R521G constructs (green; column 3) to associate with stress granules (G3BP; red; column 4). The greatest degree of GFP and G3BP co-localization was observed in cells expressing FL GFP-FUS R521G, whereas there was minimal co-localization in control cells expressing free GFP (compare panels in column 5). **(C)** Quantitative analysis (see Materials and methods) of **(B)** reveals that constructs lacking RGG domains (ΔRGG1 and ΔRGG2) exhibit impaired localization to stress granules. Statistically significant comparisons include FL and ΔRGG1 (*$P < 0.05$), FL and GFP (**$P < 0.01$), and ΔQGSY and GFP (*$P < 0.05$; not shown on graph for clarity) by one-way ANOVA followed by a Dunnett's post-hoc test on n=3 independent experiments. All error bars represent SEMs. **(D)** Western blot analysis of HeLa cells in **(B)** demonstrates equivalent expression levels for all GFP-FUS R521G constructs.

and a threshold was applied (see Materials and methods) such that all cells included in this analysis expressed similar levels of FUS. Together, these data demonstrate that the RGG domains in FUS are the most important for mutant-FUS localization to stress granules.

Methylation of mutant-FUS is not required for its assembly into stress

In light of the 20 dimethylated arginine residues within the RGG domains of FUS [55], and the fact that arginine dimethylation dictates protein and RNA interactions as

well as protein subcellular localization [56], we explored the possibility that arginine dimethylation of mutant-FUS regulates its association with stress granules. While methylated FUS has been detected within stress granules in cell culture and pathological CNS inclusions from individuals harboring FUS mutations [5], it is not clear whether methylation is actually required for FUS incorporation into these structures. To investigate this question, HeLa cells were pre-treated with the global methyltransferase inhibitor adenosine 2,3-dialdehyde (AdOx) [57] prior to expression of the highly cytoplasmic GFP-FUS R495X mutant and sodium arsenite exposure. We note that conditions (see Materials and methods) were used to minimize GFP-FUS R495X aggregation in these experiments. Immunoprecipitation of GFP-FUS R495X using an anti-GFP antibody, followed by western analysis with the dimethyl-specific ASYM24 antibody, confirmed that GFP-FUS R495X is hypomethylated in the presence of AdOx (Figure 6A). Despite the significant degree of hypomethylation, GFP-FUS R495X maintains a robust association with stress granules under these conditions (Figure 6B and C). Conversely, the overall ASYM24 signal, including the signal within stress granules, is significantly attenuated. Similar results were seen in our stable HEK-293 GFP-FUS R495X line (data not shown). While the small population of methylated GFP-FUS R495X that remains after AdOx treatment (Figure 6A) could be sequestered into stress granules, the significant decrease in ASYM24 signal (i.e., the decrease in signal for methylated proteins) with no decrease in GFP-FUS signal argues against this possibility. Therefore, while methylated mutant-FUS can assemble into stress granules, this post-translational modification is not a prerequisite for its incorporation.

Discussion

The association of cytoplasmically mislocalized ALS-linked FUS mutants with stress granules is well established [5,6,13,26-30], but what affect does mutant-FUS have on the properties of stress granules? We sought to examine the effect of mutant-FUS on the physical properties of stress granules that are potentially linked to function. While there is no functional assay per se for stress granules, they are believed to represent sites of mRNA triage, which influences whether particular mRNA transcripts are retained within stress granules, translated on ribosomes or degraded within P-bodies [20]. There is also evidence that the signaling activity of proteins can be controlled by their sequestration and/or release from stress granules during stress [22]. Thus, the cellular response to stress is modulated, at least in part, by stress granules. Since mutant-FUS, but not WT-FUS, is incorporated into stress granules under various induced stressors, the mutant protein has the potential to disturb stress granules and impair cellular stress response in ways that could contribute to ALS pathogenesis [19].

Stress granules assemble in response to induced stress. Our results show that ALS-linked, cytoplasmic FUS R495X delays the assembly of stress granules in both HEK-293 (Figure 1) and neuronal NSC-34 (Figure 2) cells under conditions of acute oxidative stress. The predominantly nuclear FUS H517Q mutant also delays stress granule assembly, but to a lesser degree than FUS R495X (Figure 1). Therefore, the delay in stress granule assembly correlates with cytoplasmic levels of mutant-FUS, probably because the protein is poised to enter stress granules once stress is induced. Since over-expression of some ALS-FUS mutants reportedly induce the spontaneous formation of cytoplasmic inclusions that stain positively for stress granule markers [28,29], one might expect the expression of mutant-FUS to correlate with a faster rate of stress granule assembly. However, the properties of stress granules are influenced by the nature of the induced stressor [48], and we show that stress granules induced by protein over-expression exhibit different dynamic properties than those induced by sodium arsenite (Additional file 3). We also demonstrate that mutant-FUS accelerates the disassembly of stress granules (Figure 1D). Therefore, expression of mutant-FUS appears to disfavor the formation of and/or destabilizes stress granules, possibly by interfering with protein interactions within these structures (Figure 3). The effects of mutant-FUS on stress granule assembly and disassembly are reminiscent of effects seen during TDP-43 knock-down [37]. Considering that stress granule assembly is a regulated process [20], factors that either delay or accelerate stress granule assembly/disassembly may adversely affect cellular homeostasis.

Interestingly, once stress granules are formed, mutant-FUS exerts an effect on both stress granule morphology and abundance that may appear counterintuitive based on the effect of FUS during the processes of assembly and disassembly. While the expression of GFP-FUS R495X both disfavors stress granule assembly and weakens stress granule associated interactions, under conditions of persistent stress the size and abundance of stress granules is augmented by the expression of mutant-FUS (Figure 4). This increased size and abundance of stress granules does not necessarily mean these structures are held together more tightly, but rather is a likely consequence of the additional protein load associated with these structures from the GFP-FUS R495X protein itself. This rationale may also be relevant to the increased size of stress granules in ALS-linked TDP-43 mutants under conditions of hyperosmolar stress [49] and suggests that this phenotype may be part of a common disease pathway. An intriguing, but not mutually exclusive, possibility is that mutant-FUS and TDP-43 recruit additional protein partners and mRNA substrates into stress granules, thereby further increasing their size

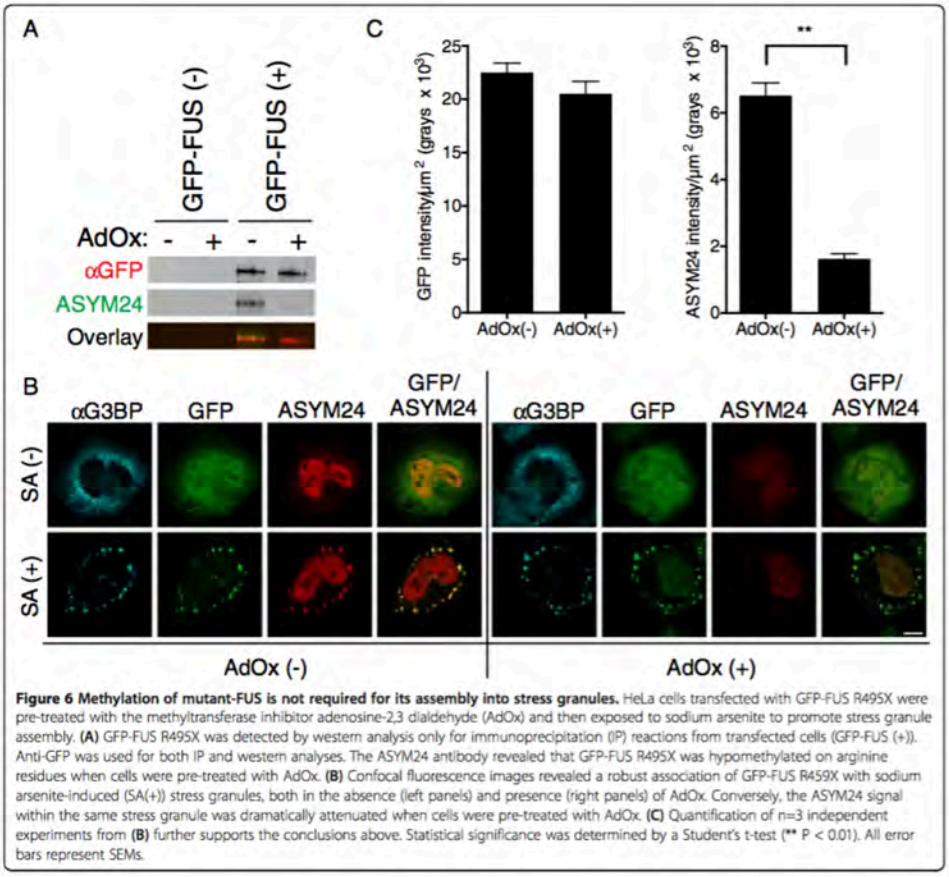

Figure 6 Methylation of mutant-FUS is not required for its assembly into stress granules. HeLa cells transfected with GFP-FUS R495X were pre-treated with the methyltransferase inhibitor adenosine-2,3 dialdehyde (AdOx) and then exposed to sodium arsenite to promote stress granule assembly. **(A)** GFP-FUS R495X was detected by western analysis only for immunoprecipitation (IP) reactions from transfected cells (GFP-FUS (+)). Anti-GFP was used for both IP and western analyses. The ASYM24 antibody revealed that GFP-FUS R495X was hypomethylated on arginine residues when cells were pre-treated with AdOx. **(B)** Confocal fluorescence images revealed a robust association of GFP-FUS R459X with sodium arsenite-induced (SA(+)) stress granules, both in the absence (left panels) and presence (right panels) of AdOx. Conversely, the ASYM24 signal within the same stress granule was dramatically attenuated when cells were pre-treated with AdOx. **(C)** Quantification of n=3 independent experiments from **(B)** further supports the conclusions above. Statistical significance was determined by a Student's t-test (** $P < 0.01$). All error bars represent SEMs.

and abundance (Figure 4 and [25,30]). Indeed, thousands of mRNA transcripts are bound by FUS [58,59] with many distinct mRNAs bound by cytoplasmic mutant-FUS but not WT FUS [59]. Therefore, mutant-FUS may inappropriately process mRNAs and/or facilitate aberrant cytoplasmic protein interactions during stress. The latter possibility is supported by our FRAP analyses, which showed that both mRFP-G3BP and mRFP-TIA-1 exhibit weaker binding and heightened dynamics within sodium arsenite-induced stress granules containing mutant-FUS (Figure 3). In fact, GFP-FUS R495X altered the dynamic properties of stress granules in all of our FRAP experiments, raising the possibility that mutant-FUS interferes with the sorting mechanisms [21,22] associated with these structures under stress.

If the association of mutant-FUS with stress granules does indeed represent a gain of toxic interaction, it will be important to identify factors that modulate this association. Although FUS contains multiple domains that contribute to FUS aggregation [60] and/or are homologous to sequences that direct other proteins into stress granules [26,50-52], our results show that the RGG domains are largely responsible for directing FUS into stress granules (Figure 5). Our results are in general agreement with a recent report by Bentmann et al., which also demonstrated a key role for the RGG domains in assembling FUS into stress granules [26]. However, our results do not support a role for the Gly-rich and RRM domains in this process, whereas the former study did. This discrepancy may be due to the difference in FUS constructs, stressor (sodium

arsenite versus heat shock [26]) and/or the FUS mutation (R521G versus P525L [26]) that were employed in these studies. Whether the RNA-binding ability of FUS is required for its localization to stress granules is not altogether clear [26,27]. Several domains within FUS exhibit RNA-binding capabilities, including the RMM, RGG, and zinc finger domains. Bentmann et al. demonstrated a correlation between cytoplasmic FUS constructs that bound RNA and were incorporated into stress granules, consistent with a role for RNA-binding in the assembly of mutant-FUS into stress granules [26].

That the RGG domains direct mutant-FUS to stress granules raises the possibly that this process is controlled by arginine dimethylation of RGG motifs [61]. Emerging evidence indicates that the RGG motifs within FUS are methylated by protein arginine N-methyltransferase-1 (PRMT1) [55,62,63], and that this post-translational modification can influence the subcellular localization of mutant-FUS [62,63]. While stress granules contain methylated proteins (Figure 6B), and methylated forms of mutant-FUS have been detected in both stress granules and diseased-tissues [5], our data suggests that methylation of FUS is not a prerequisite for its incorporation into stress granules (Figure 6).

How might the incorporation of mutant-FUS into stress granules alter cellular homeostasis under conditions of induced stress, and what are the implications for neurodegenerative disease? We show that mutant-FUS delays stress granule assembly (Figures 1 and 2), decreases the binding of stress granule-associated proteins within stress granules (Figure 3), and increases both size and abundance of stress granules (Figure 4). These physical and dynamic properties of stress granules are thought to be linked to stress granule function, and thus the effects of mutant-FUS may culminate in impaired stress response and, eventually, in neurodegeneration. Although there have been no reports of overt cytotoxicity in mutant-FUS cellular models exposed to sodium arsenite or other stressors, the effects of impaired stress response may appear more distinctly as a function of age, disease progression and/or chronic stress in the human disease [19]. In fact, stress granule marker proteins have been detected within the pathological inclusions of CNS tissues from patients with ALS and FTLD [6,25], supporting the notion that stress response factors are altered during the course of disease. Moreover, these observations raise the possibility that stress granules are precursors to the end-stage aggregates that are characteristic of these diseases [23]. Although our data show that mutant-FUS accelerates stress granule disassembly, under conditions of persistent stress these granules containing mutant-FUS are larger and more numerous and thus have the potential to coalesce into larger aggregates. Extending analyses of stress granules to other models systems, such as human iPS cells from individuals with ALS or ALS rodent models, may allow us to better address whether altered stress granule assembly plays a role in disease onset and/or progression, and whether the association of ALS-linked proteins with stress granules does in fact impact disease.

Conclusions

ALS-linked FUS mutants that mislocalize to the cytoplasm not only incorporate into stress granules under conditions of oxidative stress, but the presence of mutant-FUS in stress granules alters the properties of these structures. Expression of mutant-FUS delays the assembly and expedites the disassembly of stress granules. Furthermore, the morphology and dynamics of these structures is influenced by the presence of mutant-FUS. Therefore, our data are consistent with a gain of toxic function for mutant-FUS with respect to stress granule assembly and dynamics.

Materials and methods

Cell culture and drug treatments

Inducible GFP-FUS expressing FlpIn HEK-293 cells were maintained as described previously [13]. Human cervical carcinoma cells (HeLa) were maintained in Modified Eagle's medium (MEM, Gibco 10370) supplemented with 10% (v/v) heat inactivated fetal bovine serum (Sigma, F4135), 2 mM L-glutamine (Gibco, 25030), and 1% (v/v) penicillin and streptomycin solution (Gibco, 15140). Mouse motor neuron–like hybrid cell lines (NSC-34) [38] constitutively expressing untagged human FUS were maintained in Dulbecco's modified Eagle's medium (Invitrogen, 11965118) supplemented with 10% (v/v) tetracycline-tested fetal bovine serum (Sigma, F6178), and 2 μg/mL puromycin (Invitrogen, A11138-03).

NSC-34 cells constitutively expressing untagged human FUS constructs were generated by lentiviral transduction of the CSCW2-IRES-GFP lentivector (a generous gift from Dr. Miguel Esteves, University of Massachusetts Medical School) containing FUS (WT or mutant R495X). Flow cytometry was used to enrich for expression of the GFP reporter in each line. Cells with equivalent levels of exogenous FUS proteins were employed.

For drug treatments, the following stocks were prepared and stored at freezing temperatures: 50 mg/mL doxycycline (Sigma, D9891) in water (−80°C), 100 mM sodium arsenite (Sigma, 71287) in water (−20°C) and 20 mM adenosine-2,3 dialdehyde ("AdOx"; Sigma, A7154) in water (−20°C). FUS expression in the FlpIn HEK-293 lines was induced with the addition of 1 μg/mL doxycycline for 24 hrs unless otherwise noted. Cells were then exposed to sodium arsenite and/or AdOx as described below.

Plasmids and cloning

The pEmRFP-G3BP and mRFP-TIA-1 plasmids for FRAP analyses were generously provided by Drs. Nancy Kedersha and Paul Anderson (Brigham and Women's Hospital, Harvard Medical School). The mRFP-TIA-1 was subcloned into the low expression lentivirus vector CShPW2 (a gift from Miguel Estevez, UMMS) with NheI and Knp1 restriction sites using BP Clonase II (Invitrogen, 11789–020), thereby creating CShPW2-RFP-TIA-1. MBP-M9M was a kind gift from Dr. Yuh Min Chook (University of Texas Southwestern Medical Center).

GFP-FUS R521G deletion constructs were constructed as follows: PCR amplified full length GFP-FUS R521G, flanked by attB homologous sequences, was cloned into pDONR221 vector (Invitrogen, 12536–017) with BP Clonase II (Invitrogen, 11789–020) to generate the starting plasmid pDONR221:GFP-FUS R521G. To facilitate substitution of the full length gene with deletion/truncation variants, restriction sites for KpnI and XbaI were introduced upstream of the ATG start codon and downstream the TAA stop codon, respectively, using the following primers: **fwd**: GGGGACAAGTTTGTACAAAAAAGCAGGCTGG TACC**ATG**GCCTCAAACGATTATACCC, **rev**: GGGGA CCACTTTGTACAAGAAAGCTGGGTTCTAGA**TTA**AT ACGGCCTCTCCCTGC. To generate deletion constructs, the following primers were designed by joining the upstream and downstream sequences flanking the domain that was deleted: **ΔGLY_fwd**: AGAACCAGTACAACAG CAGCAGTACCATCTTTGTGCAAGGCC; **ΔGLY_rev**: ACTCAATTGTAACATTCTCACCCAGACTGCCAGA CAACAACACCCGGGCAGACTTTAATCGGG; **ΔRR M_rev**: CCACGACCATTGCCACCACCGTTGTTGTC TGAATTATCCTGTTCG; **ΔRGG1_fwd**: CAAGGTCT CATTTGCTACTCGCGCTGGTGACTGGAAGTGTCC; **ΔRGG1_rev**: CATATTCTCACAGGTGGGATTAGGCC GATTAAAGTCTGCCCGGC; **ΔRGG2_fwd**: CCAGTGT AAGGCCCCTAAACCAGATAAGATGGATTCCAGGGG TGAGCAC; **ΔRGG2_rev**: GTGCTCACCCCTGGAATC CATCTTATCTGGTTTAGGGGCCTTACACTGG; **Δ422-526_fwd**: GGGGACAAGTTTGTACAAAAAAGCAGGC TGGTACC**ATG**GCCTCAAACGATTATACCC; **Δ422-526_rev**: GGGGACCACTTTGTACAAGAAAGCTGG GTTCTAGA**TTA**TCGCTGCTGTCCTCCACC. The deletion reactions were performed using the pDONR221: FUS R521G plasmid as template and the QuikChange II Mutagenesis kit (Stratagene; 200523) according to the manufacturer's instructions. For the ΔQGSY truncation construct, PCR was performed using a reverse primer for the full-length R521G gene paired with a forward primer containing the 5'-end sequences of ΔGLY flanked by the restriction enzyme KpnI recognition sequence: **ΔQGSY_fwd**: CAGGCTGGTACCGGTGGTGGAGGTGGAGGT. All constructs were then sub-cloned into the expression vector pDEST-53 (Invitrogen) using Gateway cloning method with LR Clonase II (Invitrogen, 11791–100) according to the manufacturer's instructions.

Immunofluorescence

Standard immunofluorescence protocols were employed as described previously [13]. Briefly, cells were fixed with 4% paraformaldehyde for 10–15 min then blocked with PBSAT (1X PBS/1% BSA/0.5% Triton-X 100) for 30–60 min at ambient temperature. Primary antibodies described in each experiment were diluted in PBSAT and applied to cells at ambient temperature for 1 hr. Primary antibody dilutions were as follows: 1:2000 for mouse anti-G3BP (BD Transduction Labs, 611126), 1:1000 for rabbit anti-G3BP (Proteintech, 130-57-2AP), 1:1500 for rabbit anti-dimethyl arginine ("ASYM24"; Millipore, 07–414) and 1:200 mouse anti-FUS (Santa Cruz, SC-4771). Cells were then incubated with secondary antibodies diluted 1:1000–1:2500 in PBSAT for 45 min at ambient temperature. Secondary antibodies included Dylight 549 conjugated anti-mouse IgG (Jackson ImmunoResearch Labs, 715-505-151), Cy3 conjugated anti-mouse IgG (Jackson ImmunoResearch Labs, 715-165-151), Cy3 conjugated anti-rabbit IgG (Jackson ImmunoResearch Labs, 711-165-152), and Cy5 conjugated anti-mouse IgG (Jackson ImmunoResearch Labs, 715-175-151). GFP signal was enhanced by 1:1000 dilution of Alexa Fluor 488-conjugated rabbit anti-GFP (Invitrogen, A21311). Cells were stained with 34 ng/mL DAPI in dH_2O, and coverslips were mounted with ProLong Gold anti-fade reagent (Invitrogen, P36930).

Western blotting

Standard western blotting protocols were employed as described previously [13]. Primary antibodies described in each experiment were diluted as follows: 1:1000 for mouse anti-GFP (Living Colors; Clontech, 632380), 1:1000 for rabbit anti-dimethyl-arginine ("ASYM24"; Millipore, 07–414), 1:1000 for mouse anti-tubulin (Sigma, T9026), and 1:1000 for rabbit anti-FUS. Rabbit anti-FUS antibodies were generated by GenScript against a C-terminal epitope, using the peptide CKFGGPRDQGSRHDSEQDNSD. Blots were incubated with primary antibodies for 1 hr at ambient temperature or overnight at 4°C. Secondary antibodies, including anti-mouse IRDye 680 (Licor, 926–32220) or IRDye 800 (LiCor, 926–32210) and anti-rabbit IRDye 680 (LiCor, 926–32220) or IRDye 800 (Licor, 926–32211), were diluted 1:10000 and incubated with blots for 1–2 hrs at ambient temperature. Bands were visualized with an Odyssey Infrared Imager (LiCor, Model 9120), and densitometry measurements performed with the Odyssey Software (LiCor, V3.0).

Stress granule assembly and disassembly kinetics

Inducible GFP-FUS (WT, R495X and H517Q) HEK-293 cells were plated on coverslips at a density of 5×10^4

cells/coverslip. The next day, GFP-FUS expression was induced as described above. For stress granule assembly measurements, cells were treated with 0.25 mM sodium arsenite for 40 or 90 min. Coverslips were then fixed and processed for immunofluorescence (IF) with the mouse anti-G3BP and rabbit anti-GFP antibodies listed above. For stress granule disassembly measurements, cells were treated with 0.25 mM sodium arsenite for 60 min, at which time the media containing sodium arsenite was replaced with fresh media. After 90 min in fresh media, cells were processed for IF as described above. The percentage of cells with stress granules was determined as [(the number of cells containing at least one stress granule / total number of cells) × 100]. More than 2000 healthy, interphase, non-crowded cells were counted in multiple (between n=4 and n=11, depending on cell line and condition) independent experiments for both assembly and disassembly conditions. A one-way ANOVA with Tukey's multiple comparisons post-test was used to compare the induced and uninduced groups. Similar parameters were used for assembly kinetics in NSC-34 parent cells and cells expressing untagged human FUS proteins with the following changes: cells were treated with sodium arsenite for 1 hr, and immunofluorescence was performed with the rabbit anti-G3BP and mouse anti-FUS antibodies listed above. More than 2000 cells were counted in at least n=11 independent experiments per condition. Statistical significance was determined by one-way ANOVA with Tukey's multiple comparisons post-test.

Fluorescence recovery after photobleaching

GFP-FUS WT and GFP-FUS R495X HEK-293 cells were plated at a density of 8×10^4 cells/plate in 35 mm glass bottom dishes (MatTek Corp, P35GC-1.5-14-C), allowed to adhere for 48 hrs, then transfected with either CShPW2-RFP-TIA-1 or pEmRFP-G3BP expression plasmids using Lipofectamine 2000 (Invitrogen, 11668–019) according to the manufacturer's instructions with a 1.6 μl Lipo: 3.2 μg DNA ratio. Approximately 23 hr post-transfection, phenol red(−) growth media without (overexpression experiments) or containing 0.2 mM sodium arsenite (stress granule experiments) was applied to the cells for 1 hr prior to FRAP.

FRAP experiments were performed at 37°C as previously described [45]. Multiple cells were analyzed in each experiment over a 30 min period starting at 60 min of sodium arsenite exposure. Experiments were carried out on a Leica SP5 AOBS laser scanning confocal microscope using a 40× 1.3NA water immersion objective or a Leica SP1 system using a 40×, 1.25NA oil immersion objective. No more than two stress granules, from opposite sides of a cell, were individually bleached using a 1-3s laser pulse delivered by a 488 nm or 561 nm laser. A pre-bleach, immediate post-bleach and 16 additional post-bleach images spaced at 5 sec intervals were captured. Leica Confocal Software (Leica Microsystems, Exton, PA) was used to measure fluorescence intensity in the bleached region of interest (ROI), the whole cell, and in a background control area lacking cells at each time point. The data was analyzed and background fluorescence subtracted using Excel. The relative fluorescence intensity (I_{rel}) in the bleached area was calculated as previously shown [45]. Briefly, the following equation was used: $I_{rel,\ t} = (I_t \times (C_0/C_t))-(I_{pbl} \times (C_0/C_{bl}))/(I_0-(I_{pbl} \times (C_0/C_{pbl}))$, where C_0 is the total cellular fluorescence before bleaching, C_{pbl} is the total cellular fluorescence in the post-bleach image, C_t is the total cellular fluorescence at time t, I_0 is the pre-bleach ROI fluorescence intensity, I_t is the ROI fluorescence intensity at time t, and I_{pbl} is the post-bleach ROI fluorescence intensity. The data was normalized using this equation such that the post-bleach ROI fluorescence intensity was set to 0 and the pre-bleach ROI fluorescence intensity to 1. I_t was calculated as the percentage difference between the relative fluorescence asymptote of the recovery curve and a relative recovery of 1, a value that would reflect complete recovery without an immobile fraction. Recovery curves were drawn using Graphpad Prism 6 (Graphpad Software), with individual time points presented as means ± SEMs. Fluorescence recovery half times were calculated from exponential one-phase association curves best fit for the recovery graphs: $F(t) = F_{max}\ (1- e^{-kt})$. Mobile fractions were calculated from the plateau region from each curve, which was identified as the series of data points with < 2% change in slope over time.

At least two independent experiments were performed for all conditions. The total number of stress granules analyzed for each condition is shown in Figure 3. A two-way ANOVA was used to determine statistical significance between the mobile fractions for each of the experiments.

Morphology experiments

Stable GFP-FUS HEK-293 cells were plated and processed for immunofluorescence as described under 'stress granule assembly and disassembly kinetics' above, except that cells were treated with 0.5 mM sodium arsenite for 1 hr. Confocal stacked images (0.2 μm stack step, 4 μm range) were acquired using a Zeiss Axiovert 200 microscope with a PerkinElmer UltraView LAS spinning disc equipped with a 100× phase objective. Imaris analytical software (Bitplane Scientific Software) was used to construct 3D projections of image stacks. Volume measurements were taken of each stress granule with a G3BP fluorescence signal that was at least 2-fold above background. Because P-bodies had an average volume of 0.5 μm^3 (data not shown) by the same analysis, only stress granules with a volume > 0.5 μm^3 were included in the analysis. Data is averaged from three independent experiments per line, using approximately 30 stress granules per condition. Statistical significance was determined using the Student's t-test.

Analysis of FUS deletion constructs in stress granule assembly

HeLa cells were plated on coverslips at a density of 2.5 × 10^4 cells/coverslip and adhered at 37°C for 24 hrs, after which GFP-FUS R521G truncation constructs and MBP-M9M were transiently transfected into cells using Lipofectamine-2000 (Invitrogen, 11668) according to the manufacturer's instructions. Twenty-four hours post transfection, cells were subjected to media containing 0.5 mM sodium arsenite for 1 hr. Cells were processed immunofluorescence with mouse anti-G3BP as described above.

Confocal microscopy was performed using a Solamere Technology Group CSU10B spinning disk confocal system equipped with a Yokogawa CSU10 spinning disk confocal scan head. Image stacks (0.2 μm stack step; 13 stack range) were acquired using a 100× oil objective, a Roper Cool-snap HQ2 camera and MetaMorph V7.6.3 software. Background signal was subtracted by removing fluorescence from a dark-current image (acquired with the laser off) from each raw image. For the GFP images, variations in illumination and detection efficiencies at each pixel were corrected by dividing the dark-adjusted intensities by a normalized flat-field image of a uniformly green fluorescent slide (Chroma Technology, Rockingham, VT, USA) acquired using the same 525/50 nm band-pass filter. Four channels were imaged per cell: FITC for GFP-FUS, Cy3 for G3BP, DAPI for nuclei and phase for cell borders.

The extent of GFP-FUS incorporation into stress granules was analyzed with MetaMorph V7.6.3 software using the Integrated Morphometry Analysis tool. Since cells with a GFP signal brighter than 1.5 × 10^6 grays/μm^2 tended to form cytoplasmic aggregates *a priori* of arsenite treatment (data not shown), only transfected cells with GFP-FUS expression levels < 1.5 × 10^6 grays/μm^2 were selected for analysis. Stress granules were selected using the Cy3 (G3BP) channel as a reference. The slice corresponding to the center of the stress granule was selected from each image stack. Stress granules with an area of at least 0.5 μm^2 were selected. An outline was drawn around each G3BP granule, and this outline was then transferred to the corresponding FITC (GFP-FUS) image, such that the GFP-FUS signal intensity ("stress granules intensity") within that granule could be measured. GFP signal intensity measurements were also acquired in the region proximal to the stress granule, and was referred to as the "Diffuse intensity". The ratio of stress granule intensity (i.e., GFP-FUS inside the stress granule) to diffuse intensity (i.e., GFP-FUS outside the stress granule) was determined for a total of 75–150 stress granules per construct over three independent experiments. Statistical significance was determined by a one-way ANOVA followed by a Dunnett's post hoc test in Graphpad Prism 6 (Graphpad software).

Methyltransferase inhibition studies

HeLa cells were plated at a density of 2.5 × 10^4 cells/coverslip and adhered for 24 hrs, after which GFP-FUS R495X expression constructs were transiently transfected with Lipofectamine-2000 either with or without 25 μM AdOx for 24 hr. Cells were then exposed to 0.5 mM sodium arsenite for 1 hr, and coverslips were processed for immunofluorescence using the mouse anti-G3BP rabbit and ASYM24 antibodies as described above. For quantification, confocal images of 30 cells per condition across three independent experiments were taken, and the intensity of GFP-FUS and ASYM24 signal within stress granules was determined between AdOx-treated and untreated conditions using MetaMorph as described above. Statistical significance was determined using a Student's t-test.

For GFP immunoprecipitation (IP) reactions, cells were lysed for 15 min in IP buffer (400 μL 1% NP-40 (MP Biomedicals, 198596)/50 mM Tris–HCl (Sigma T3253-500G)/5 mM EDTA (Fisher E478-500)/150 mM NaCl and 10% v/v glycerol (Acros 15982–0010) in water; pH 7.5), and centrifuged at 13000 rpm for 15 min at 4°C. The supernatant was pre-cleared with 50 μL Biomag Protein G beads (Qiagen, 311812) for 2 hrs at 4°C. Anti-GFP-coated beads for each sample were prepared by incubating 0.5 μL of anti-GFP (Abcam, ab290) in 400 μL of IP buffer with 50 μL Biomag Protein G beads for 2 hrs at 4°C. IP reactions were performed at 4°C overnight with 100 μg of pre-cleared lysate. Protein elution was accomplished with 50 μL 1X SDS loading buffer (Boston Bioproducts BP11R) for 5 min at 95°C, and 20 μL of sample was subjected to western blot analysis with mouse anti-GFP, mouse anti-tubulin and ASYM24 as described above.

Additional files

Additional file 1: A minor fraction of GFP-FUS H517Q incorporates into stress granules in response to sodium arsenite. Images for the indicated GFP-FUS cell line (top 3 rows) were collected as described in Figure 1A. Antibody markers used for immunofluorescence are indicated on the left. Images overexposed for GFP detection (bottom row) reveal that a minor fraction of GFP-FUS H517Q (green) co-localizes with G3BP-positive stress granules (red). FUS H517Q containing stress granules are denoted by arrows. Conversely, GFP-FUS WT is not detected in stress granule (i.e., there is no GFP-positive signal that co-localized with G3BP), even with high exposure. Scale bar = 5 μm.

Additional file 2: NSC-34 cells expressing untagged human FUS WT and R495X exhibit similar transduction efficiencies. Fluorescent images of the GFP reporter (green) in NSC-34 cells transduced with lentivirus containing untagged human FUS WT or R495X. Transduction efficiencies of approximately 100% were determined for both lines. Cellular nuclei are stained with DAPI (blue). Scale bar = 20 μm.

Additional file 3: Sodium arsenite induced stressed granules display different dynamics compared to those induced by mRFP-G3BP over-expression. (A) Transfection of mRFP-G3BP was sufficient to induce G3BP positive stress granules in a subset of both GFP-FUS WT and GFP-FUS R495X cells as determined by live cell imaging. Scale bar = 20 μm. **(B)** The FRAP recovery curve for mRFP-G3BP inside the stress granule

27. Daigle JG, Lanson NA Jr, Smith RB, Casci I, Maltare A, Monaghan J, Nichols CD, Kryndushkin D, Shewmaker F, Pandey UB: **RNA-binding ability of FUS regulates neurodegeneration, cytoplasmic mislocalization and incorporation into stress granules associated with FUS carrying ALS-linked mutations.** *Human Mol Genet* 2013.
28. Gal J, Zhang J, Kwinter DM, Zhai J, Jia H, Jia J, Zhu H: **Nuclear localization sequence of FUS and induction of stress granules by ALS mutants.** *Neurobiol Aging* 2010, **32**:2323.e27-40.
29. Ito D, Seki M, Tsunoda Y, Uchiyama H, Suzuki N: **Nuclear transport impairment of amyotrophic lateral sclerosis-linked mutations in FUS/TLS.** *Ann Neurol* 2011, **69**:152–162.
30. Vance C, Scotter EL, Nishimura AL, Troakes C, Mitchell JC, Kathe C, Urwin H, Manser C, Miller CC, Hortobagyi T, *et al*: **ALS mutant FUS disrupts nuclear localisation and sequesters wild-type FUS within cytoplasmic stress granules.** *Human Mol Genet* 2013, **22**:2676–2688.
31. Aulas A, Stabile S, Vande Velde C: **Endogenous TDP-43, but not FUS, contributes to stress granule assembly via G3BP.** *Mol Neurodegener* 2012, **7**:54.
32. Kedersha N, Cho MR, Li W, Yacono PW, Chen S, Gilks N, Golan DE, Anderson P: **Dynamic shuttling of TIA-1 accompanies the recruitment of mRNA to mammalian stress granules.** *J Cell Biol* 2000, **151**:1257–1268.
33. Rodriguez VM, Carrizales L, Jimenez-Capdeville ME, Dufour L, Giordano M: **The effects of sodium arsenite exposure on behavioral parameters in the rat.** *Brain Res Bull* 2001, **55**:301–308.
34. Tabocova S, Hunter ES 3rd, Gladen BC: **Developmental toxicity of inorganic arsenic in whole embryo: culture oxidation state, dose, time, and gestational age dependence.** *Toxicol Appl Pharmacol* 1996, **138**:298–307.
35. Sama RR, Ward CL, Kaushansky LJ, Lemay N, Ishigaki S, Urano F, Bosco DA: **FUS/TLS assembles into stress granules and is a prosurvival factor during hyperosmolar stress.** *J Cell Physiol* 2013, **228**:2222–2231.
36. Kedersha N, Anderson P: **Mammalian stress granules and processing bodies.** *Methods Enzymol* 2007, **431**:61–81.
37. McDonald KK, Aulas A, Destroismaisons L, Pickles S, Beleac E, Camu W, Rouleau GA, Vande Velde C: **TAR DNA-binding protein 43 (TDP-43) regulates stress granule dynamics via differential regulation of G3BP and TIA-1.** *Human Mol Genet* 2011.
38. Cashman NR, Durham HD, Blusztajn JK, Oda K, Tabira T, Shaw IT, Dahrouge S, Antel JP: **Neuroblastoma x spinal cord (NSC) hybrid cell lines resemble developing motor neurons.** *Dev Dyn* 1992, **194**:209–221.
39. Huang C, Zhou H, Tong J, Chen H, Liu YJ, Wang D, Wei X, Xia XG: **FUS transgenic rats develop the phenotypes of amyotrophic lateral sclerosis and frontotemporal lobar degeneration.** *PLoS Genet* 2011, **7**:e1002011.
40. Ju S, Tardiff DF, Han H, Divya K, Zhong Q, Maquat LE, Bosco DA, Hayward LJ, Brown RH Jr, Lindquist S, *et al*: **A Yeast Model of FUS/TLS-Dependent Cytotoxicity.** *PLoS Biol* 2011, **9**:e1001052.
41. Lanson NA Jr, Maltare A, King H, Smith R, Kim JH, Taylor JP, Lloyd TE, Pandey UB: **A Drosophila model of FUS-related neurodegeneration reveals genetic interaction between FUS and TDP-43.** *Human Mol Genet* 2011, **20**:2510–2523.
42. Guil S, Long JC, Caceres JF: **hnRNP A1 relocalization to the stress granules reflects a role in the stress response.** *Mol Cell Biol* 2006, **26**:5744–5758.
43. Kedersha N, Stoecklin G, Ayodele M, Yacono P, Lykke-Andersen J, Fritzler MJ, Scheuner D, Kaufman RJ, Golan DE, Anderson P: **Stress granules and processing bodies are dynamically linked sites of mRNP remodeling.** *J Cell Biol* 2005, **169**:871–884.
44. Nickerson JA: **The biochemistry of RNA metabolism studied in situ.** *RNA Biol* 2009, **6**:25–30.
45. Quaresma AJ, Sievert R, Nickerson JA: **Regulation of mRNA Export by the PI3 kinase / AKT Signal Transduction Pathway.** *Mol Biol Cell* 2013.
46. Buchan JR, Parker R: **Eukaryotic stress granules: the ins and outs of translation.** *Mol Cell* 2009, **36**:932–941.
47. Tourriere H, Chebli K, Zekri L, Courselaud B, Blanchard JM, Bertrand E, Tazi J: **The RasGAP-associated endoribonuclease G3BP assembles stress granules.** *J Cell Biol* 2003, **160**:823–831.
48. Buchan JR, Yoon JH, Parker R: **Stress-specific composition, assembly and kinetics of stress granules in Saccharomyces cerevisiae.** *J Cell Sci* 2011, **124**:228–239.
49. Dewey CM, Cenik B, Sephton CF, Dries DR, Mayer P, Good SK, Johnson BA, Herz J, Yu G: **TDP-43 is directed to stress granules by sorbitol, a novel physiological osmotic and oxidative stressor.** *Mol Cell Biol* 2010, **31**:1098–1108.
50. De Leeuw F, Zhang T, Wauquier C, Huez G, Kruys V, Gueydan C: **The cold-inducible RNA-binding protein migrates from the nucleus to cytoplasmic stress granules by a methylation-dependent mechanism and acts as a translational repressor.** *Experimental Cell Res* 2007, **313**:4130–4144.
51. Kedersha NL, Gupta M, Li W, Miller I, Anderson P: **RNA-binding proteins TIA-1 and TIAR link the phosphorylation of eIF-2 alpha to the assembly of mammalian stress granules.** *J Cell Biol* 1999, **147**:1431–1442.
52. Rajyaguru P, She M, Parker R: **Scd6 targets eIF4G to repress translation: RGG motif proteins as a class of eIF4G-binding proteins.** *Mol Cell* 2012, **45**:244–254.
53. Iko Y, Kodama TS, Kasai N, Oyama T, Morita EH, Muto T, Okumura M, Fujii R, Takumi T, Tate S, Morikawa K: **Domain architectures and characterization of an RNA-binding protein, TLS.** *J Biol Chem* 2004, **279**:44834–44840.
54. Cansizoglu AE, Lee BJ, Zhang ZC, Fontoura BM, Chook YM: **Structure-based design of a pathway-specific nuclear import inhibitor.** *Nat Struct Mol Biol* 2007, **14**:452–454.
55. Rappsilber J, Friesen WJ, Paushkin S, Dreyfuss G, Mann M: **Detection of arginine dimethylated peptides by parallel precursor ion scanning mass spectrometry in positive ion mode.** *Anal Chem* 2003, **75**:3107–3114.
56. Bedford MT, Clarke SG: **Protein arginine methylation in mammals: who, what, and why.** *Molecular cell* 2009, **33**:1–13.
57. Grant AJ, Lerner LM: **Dialdehydes derived from adenine nucleosides as substrates and inhibitors of adenosine aminohydrolase.** *Biochemistry* 1979, **18**:2838–2842.
58. Colombrita C, Onesto E, Megiorni F, Pizzuti A, Baralle FE, Buratti E, Silani V, Ratti A: **TDP-43 and FUS RNA-binding proteins bind distinct sets of cytoplasmic messenger RNAs and differently regulate their post-transcriptional fate in motoneuron-like cells.** *J Biol Chem* 2012, **287**:15635–15647.
59. Hoell JI, Larsson E, Runge S, Nusbaum JD, Duggimpudi S, Farazi TA, Hafner M, Borkhardt A, Sander C, Tuschl T: **RNA targets of wild-type and mutant FET family proteins.** *Nat Struct Mol Biol* 2011, **18**:1428–1431.
60. Sun Z, Diaz Z, Fang X, Hart MP, Chesi A, Shorter J, Gitler AD: **Molecular Determinants and Genetic Modifiers of Aggregation and Toxicity for the ALS Disease Protein FUS/TLS.** *PLoS Biol* 2011, **9**:e1000614.
61. Rajyaguru P, Parker R: **RGG motif proteins: modulators of mRNA functional states.** *Cell Cycle* 2012, **11**:2594–2599.
62. Tradewell ML, Yu Z, Tibshirani M, Boulanger MC, Durham HD, Richard S: **Arginine methylation by PRMT1 regulates nuclear-cytoplasmic localization and toxicity of FUS/TLS harbouring ALS-linked mutations.** *Human Mol Genet* 2012, **21**:136–149.
63. Yamaguchi A, Kitajo K: **The Effect of PRMT1-Mediated Arginine Methylation on the Subcellular Localization, Stress Granules, and Detergent-Insoluble Aggregates of FUS/TLS.** *PloS One* 2012, **7**:e49267.

doi:10.1186/1750-1326-8-30
Cite this article as: Baron *et al.*: Amyotrophic lateral sclerosis-linked FUS/TLS alters stress granule assembly and dynamics. *Molecular Neurodegeneration* 2013 **8**:30.

BIBLIOGRAPHY

Aitken, C.E., and Lorsch, J.R. (2012). A mechanistic overview of translation initiation in eukaryotes. Nat Struct Mol Biol *19*, 568–576.

Akhmedov, A.T., Bertrand, P., Corteggiani, E., and Lopez, B.S. (1995). Characterization of two nuclear mammalian homologous DNA-pairing activities that do not require associated exonuclease activity. Proc. Natl. Acad. Sci. U.S.A. *92*, 1729–1733.

Alappat, J.J. (2007). Ethnic variation in the incidence of ALS: a systematic review. Neurology *69*, 711–711–2.

Anderson, P., and Kedersha, N. (2008). Stress granules: the Tao of RNA triage. Trends Biochem. Sci. *33*, 141–150.

Andersson, M.K., Ståhlberg, A., Arvidsson, Y., Olofsson, A., Semb, H., Stenman, G., Nilsson, O., and Åman, P. (2008). The multifunctional FUS, EWS and TAF15 proto-oncoproteins show cell type-specific expression patterns and involvement in cell spreading and stress response. BMC Cell Biol *9*, 37.

Antar, L.N. et al. (2005) Localization of FMRP-associated mRNA granules and requirement of microtubules for activity-dependent trafficking in hippocampal neurons. Genes Brain Behav. 4, 350–359.

Arai, T., Hasegawa, M., Akiyama, H., Ikeda, K., Nonaka, T., Mori, H., Mann, D., Tsuchiya, K., Yoshida, M., Hashizume, Y., et al. (2006). TDP-43 is a component of ubiquitin-positive tau-negative inclusions in frontotemporal lobar degeneration and amyotrophic lateral sclerosis. Biochem. Biophys. Res. Commun. *351*, 602–611.

Arimoto, K., Fukuda, H., Imajoh-Ohmi, S., Saito, H., and Takekawa, M. (2008). Formation of stress granules inhibits apoptosis by suppressing stress-responsive MAPK pathways. Nat. Cell Biol. *10*, 1324–1332.

Aulas, A., Caron, G., Gkogkas, C.G., Mohamed, N.-V., Destroismaisons, L., Sonenberg, N., Leclerc, N., Parker, J.A., and Vande Velde, C. (2015). G3BP1 promotes stress-induced RNA granule interactions to preserve polyadenylated mRNA. J. Cell Biol. *209*, 73–84.

Aulas, A., Stabile, S., and Vande Velde, C. (2012). Endogenous TDP-43, but not FUS, contributes to stress granule assembly via G3BP. Mol Neurodegener *7*, 54.

Åman, P., Panagopoulos, I., Lassen, C., Fioretos, T., Mencinger, M., Toresson,

H., Höglund, M., Forster, A., Rabbitts, T.H., Ron, D., et al. (1996). Expression Patterns of the Human Sarcoma-Associated Genes FUS and EWS and the Genomic Structure of FUS. Genomics *37*, 1–8.

Baechtold, H., Kuroda, M., Sok, J., Ron, D., Lopez, B.S., and Akhmedov, A.T. (1999). Human 75-kDa DNA-pairing protein is identical to the pro-oncoprotein TLS/FUS and is able to promote D-loop formation. Journal of Biological Chemistry *274*, 34337–34342.

Barber, S.C., and Shaw, P.J. (2010). Oxidative stress in ALS: key role in motor neuron injury and therapeutic target. Free Radic. Biol. Med. *48*, 629–641.

Barmada, S.J., Ju, S., Arjun, A., Batarse, A., Archbold, H.C., Peisach, D., Li, X., Zhang, Y., Tank, E.M.H., Qiu, H., et al. (2015). Amelioration of toxicity in neuronal models of amyotrophic lateral sclerosis by hUPF1. Proceedings of the National Academy of Sciences 112, 7821–7826.

Baron, D.M., Kaushansky, L.J., Ward, C.L., Sama, R.R.K., Chian, R.-J., Boggio, K.J., Quaresma, A.J., Nickerson, J.A., and Bosco, D.A. (2013). Amyotrophic lateral sclerosis-linked FUS/TLS alters stress granule assembly and dynamics. Mol Neurodegener *8*, 30.

Bartoli, K.M., Bishop, D.L., and Saunders, W.S. (2011). The Role of Molecular Microtubule Motors and the Microtubule Cytoskeleton in Stress Granule Dynamics. International Journal of Cell Biology *2011*, 1–9.

Bedford, M.T., and Clarke, S.G. (2009). Protein Arginine Methylation in Mammals: Who, What, and Why. Mol. Cell *33*, 1–13.

Bentmann, E., Neumann, M., Tahirovic, S., Rodde, R., Dormann, D., and Haass, C. (2012). Requirements for stress granule recruitment of fused in sarcoma (FUS) and TAR DNA-binding protein of 43 kDa (TDP-43). J. Biol. Chem. *287*, 23079–23094.

Bertrand, P., Akhmedov, A.T., Delacote, F., Durrbach, A., and Lopez, B.S. (1999). Human POMp75 is identified as the pro-oncoprotein TLS/FUS: both POMp75 and POMp100 DNA homologous pairing activities are associated to cell proliferation. Oncogene *18*, 4515–4521.

Bilsland, L.G., Sahai, E., Kelly, G., Golding, M., Greensmith, L., and Schiavo, G. (2010). Deficits in axonal transport precede ALS symptoms in vivo. Proceedings of the National Academy of Sciences *107*, 20523–20528.

Blechingberg, J., Luo, Y., Bolund, L., Damgaard, C.K., and Nielsen, A.L. (2012). Gene Expression Responses to FUS, EWS, and TAF15 Reduction and

Stress Granule Sequestration Analyses Identifies FET-Protein Non-Redundant Functions. PLoS ONE *7*, e46251.

Bordeleau, M.-E., Matthews, J., Wojnar, J.M., Lindqvist, L., Novac, O., Jankowsky, E., Sonenberg, N., Northcote, P., Teesdale-Spittle, P., and Pelletier, J. (2005). Stimulation of mammalian translation initiation factor eIF4A activity by a small molecule inhibitor of eukaryotic translation. Proc. Natl. Acad. Sci. U.S.a. *102*, 10460–10465.

Bordeleau, M.-E., Mori, A., Oberer, M., Lindqvist, L., Chard, L.S., Higa, T., Belsham, G.J., Wagner, G., Tanaka, J., and Pelletier, J. (2006). Functional characterization of IRESes by an inhibitor of the RNA helicase eIF4A. Nat Chem Biol *2*, 213–220.

Bosco, D.A., and Landers, J.E. (2010). Genetic determinants of amyotrophic lateral sclerosis as therapeutic targets. CNS Neurol Disord Drug Targets *9*, 779–790.

Bosco, D.A., Lemay, N., Ko, H.K., Zhou, H., Burke, C., Kwiatkowski, T.J., Sapp, P., McKenna-Yasek, D., Brown, R.H., and Hayward, L.J. (2010). Mutant FUS proteins that cause amyotrophic lateral sclerosis incorporate into stress granules. Hum. Mol. Genet. *19*, 4160–4175.

Bozaykut, P., Ozer, N.K., and Karademir, B. (2014). Regulation of protein turnover by heat shock proteins. Free Radic. Biol. Med. *77*, 195–209.

Bruijn, L.I., Beal, M.F., Becher, M.W., Schulz, J.B., Wong, P.C., Price, D.L., and Cleveland, D.W. (1997). Elevated free nitrotyrosine levels, but not protein-bound nitrotyrosine or hydroxyl radicals, throughout amyotrophic lateral sclerosis (ALS)-like disease implicate tyrosine nitration as an aberrant in vivo property of one familial ALS-linked superoxide dismutase 1 mutant. Proc. Natl. Acad. Sci. U.S.a. *94*, 7606–7611.

Bruijn, L.I., Houseweart, M.K., Kato, S., and Anderson, K.L. (1998). Aggregation and motor neuron toxicity of an ALS-linked SOD1 mutant independent from wild-type SOD1. Science.

Buchan, J.R., and Parker, R. (2009). Eukaryotic Stress Granules: The Ins and Outs of Translation. Mol. Cell *36*, 932–941.

Burgess, H.M., Richardson, W.A., Anderson, R.C., Salaun, C., Graham, S.V., and Gray, N.K. (2011). Nuclear relocalisation of cytoplasmic poly(A)-binding proteins PABP1 and PABP4 in response to UV irradiation reveals mRNA-dependent export of metazoan PABPs. J. Cell. Sci. 124, 3344–3355.

Bushell, M., Stoneley, M., Kong, Y.W., Hamilton, T.L., Spriggs, K.A., Dobbyn, H.C., Qin, X., Sarnow, P., and Willis, A.E. (2006). Polypyrimidine tract binding protein regulates IRES-mediated gene expression during apoptosis. Mol. Cell *23*, 401–412.

Calvio, C., Neubauer, G., Mann, M., and Lamond, A.I. (1995). Identification of hnRNP P2 as TLS/FUS using electrospray mass spectrometry. Rna *1*, 724–733.

Cansizoglu, A.E., Lee, B.J., Zhang, Z.C., Fontoura, B.M.A., and Chook, Y.M. (2007). Structure-based design of a pathway-specific nuclear import inhibitor. Nat Struct Mol Biol *14*, 452–454.

Chalupnikova, K. et al. (2008) Recruitment of the RNA helicase RHAU to stress granules via a unique RNA-binding domain. J. Biol. Chem. 283, 35186–35198

Chance, P.F., Rabin, B.A., Ryan, S.G., Ding, Y., Scavina, M., Crain, B., Griffin, J.W., and Cornblath, D.R. (1998). Linkage of the gene for an autosomal dominant form of juvenile amyotrophic lateral sclerosis to chromosome 9q34. Am. J. Hum. Genet. *62*, 633–640.

Charcot, J.M., and Joffroy, A. (1869). Deux cas d'atrophie musculaire progressive: avec lésions de la substance grise et des faisceaux antérolatéraux de la moelle épinière.

Chio, A., Benzi, G., Dossena, M., Mutani, R., and Mora, G. (2005). Severely increased risk of amyotrophic lateral sclerosis among Italian professional football players. Brain *128*, 472–476.

Clemens, M.J., Bushell, M., Jeffrey, I.W., Pain, V.M., and Morley, S.J. (2000). Translation initiation factor modifications and the regulation of protein synthesis in apoptotic cells. Cell Death Differ. *7*, 603–615.

Colombrita, C., Onesto, E., Megiorni, F., Pizzuti, A., Baralle, F.E., Buratti, E., Silani, V., and Ratti, A. (2012). TDP-43 and FUS RNA-binding proteins bind distinct sets of cytoplasmic messenger RNAs and differently regulate their post-transcriptional fate in motoneuron-like cells. J. Biol. Chem. *287*, 15635–15647.

Colombrita, C., Zennaro, E., Fallini, C., Weber, M., Sommacal, A., Buratti, E., Silani, V., and Ratti, A. (2009). TDP-43 is recruited to stress granules in conditions of oxidative insult. Journal of Neurochemistry *111*, 1051–1061.

Couthouis, J., Hart, M.P., Shorter, J., DeJesus-Hernandez, M., Erion, R.,

Oristano, R., Liu, A.X., Ramos, D., Jethava, N., Hosangadi, D., et al. (2011). A yeast functional screen predicts new candidate ALS disease genes. Proceedings of the National Academy of Sciences *108*, 20881–20890.

Couthouis, J., Hart, M.P., Erion, R., King, O.D., Diaz, Z., Nakaya, T., Ibrahim, F., Kim, H.J., Mojsilovic-Petrovic, J., Panossian, S., et al. (2012). Evaluating the role of the FUS/TLS-related gene EWSR1 in amyotrophic lateral sclerosis. Hum. Mol. Genet. *21*, 2899–2911.

Cox, P.A., and Sacks, O.W. (2002). Cycad neurotoxins, consumption of flying foxes, and ALS-PDC disease in Guam. Neurology *58*, 956–959.

Crozat, A., Åman, P., Mandahl, N., and Ron, D. (1993). Fusion of CHOP to a novel RNA-binding protein in human myxoid liposarcoma. Nature *363*, 640–644.

Czaplinski, K., Ruiz-Echevarria, M.J., Paushkin, S.V., Han, X., Weng, Y., Perlick, H.A., Dietz, H.C., Ter-Avanesyan, M.D., and Peltz, S.W. (1998). The surveillance complex interacts with the translation release factors to enhance termination and degrade aberrant mRNAs. Genes Dev. *12*, 1665–1677.

Da Cruz, S., and Cleveland, D.W. (2011). Understanding the role of TDP-43 and FUS/TLS in ALS and beyond. Curr. Op. Neurobiology *21*, 904–919.

Daigle, J.G., Lanson, N.A., Smith, R.B., Casci, I., Maltare, A., Monaghan, J., Nichols, C.D., Kryndushkin, D., Shewmaker, F., and Pandey, U.B. (2013). RNA binding ability of FUS regulates neurodegeneration, cytoplasmic mislocalization and incorporation into stress granules associated with FUS carrying ALS-linked mutations. Hum. Mol. Genet. *22*, 1193–1205.

Darnell, R.B. (2013). RNA Protein Interaction in Neurons. Annu. Rev. Neurosci. *36*, 243–270.

Davidson, Y.S., Robinson, A.C., Hu, Q., Mishra, M., Baborie, A., Jaros, E., Perry, R.H., Cairns, N.J., Richardson, A., Gerhard, A., et al. (2012). Nuclear Carrier and RNA Binding Proteins in Frontotemporal Lobar Degeneration associated with Fused in Sarcoma (FUS) pathological changes. Neuropathology and Applied Neurobiology *39*, 157–165.

De Chiara, G., Marcocci, M.E., Sgarbanti, R., Civitelli, L., Ripoli, C., Piacentini, R., Garaci, E., Grassi, C., and Palamara, A.T. (2012). Infectious Agents and Neurodegeneration. Mol. Neurobiol. *46*, 614–638.

De Leeuw, F., Zhang, T., Wauquier, C., Huez, G., Kruys, V., and Gueydan, C. (2007). The cold-inducible RNA-binding protein migrates from the nucleus to cytoplasmic stress granules by a methylation-dependent mechanism and acts as a translational repressor. Exp. Cell Res. *313*, 4130–4144.

Deigendesch, N., Koch-Nolte, F., and Rothenburg, S. (2006). ZBP1 subcellular localization and association with stress granules is controlled by its Z-DNA binding domains. Nucleic Acids Research *34*, 5007–5020.

DeJesus-Hernandez, M., Mackenzie, I.R., Boeve, B.F., Boxer, A.L., Baker, M., Rutherford, N.J., Nicholson, A.M., Finch, N.A., Flynn, H., Adamson, J., et al. (2011b). Expanded GGGGCC Hexanucleotide Repeat in Noncoding Region of C9ORF72 Causes Chromosome 9p-Linked FTD and ALS. Neuron *72*, 245–256.

Dewey, C., Cenik, B., and Sephton, C. (2011). TDP-43 is directed to stress granules by sorbitol, a novel physiological osmotic and oxidative stressor. … And Cellular Biology.

Dolzhanskaya, N., Merz, G., Aletta, J.M., and Denman, R.B. (2006). Methylation regulates the intracellular protein-protein and protein-RNA interactions of FMRP. J. Cell. Sci. *119*, 1933–1946.

Donnelly, C.J., Fainzilber, M., and Twiss, J.L. (2010). Subcellular communication through RNA transport and localized protein synthesis. Traffic *11*, 1498–1505.

Dormann, D., and Haass, C. (2011). TDP-43 and FUS: a nuclear affair. Trends in Neurosciences *34*, 339–348.

Dormann, D., Madl, T., Valori, C.F., Bentmann, E., Tahirovic, S., Abou-Ajram, C., Kremmer, E., Ansorge, O., Mackenzie, I.R.A., Neumann, M., et al. (2012). Arginine methylation next to the PY-NLS modulates Transportin binding and nuclear import of FUS. Embo J. *31*, 4258–4275.

Dormann, D., Rodde, R., Edbauer, D., Bentmann, E., Fischer, I., Hruscha, A., Than, M.E., Mackenzie, I.R.A., Capell, A., Schmid, B., et al. (2010). ALS-associated fused in sarcoma (FUS) mutations disrupt Transportin-mediated nuclear import. Embo J. *29*, 2841–2857.

Dutertre, M., Lambert, S., Carreira, A., Amor-Guéret, M., and Vagner, S. (2014). DNA damage: RNA-binding proteins protect from near and far. Trends Biochem. Sci. *39*, 141–149.

ErLin, S., WenJie, W., LiNing, W., BingXin, L., MingDe, L., Yan, S., and RuiFa,

H. (2015). Musashi-1 maintains blood-testis barrier structure during spermatogenesis and regulates stress granule formation upon heat stress. Mol. Biol. Cell *26*, 1947–1956.

Ernoult-Lange, M. et al. (2012) Multiple binding of repressed mRNAs by the P-body protein Rck/p54. RNA *18*, 1702–1715.

Fang, F., Kamel, F., Sandler, D.P., Sparén, P., and Ye, W. (2008). Maternal age, exposure to siblings, and risk of amyotrophic lateral sclerosis. Am. J. Epidemiol. *167*, 1281–1286.

Farg, M.A., Soo, K.Y., Warraich, S.T., Sundaramoorthy, V., Blair, I.P., and Atkin, J.D. (2012). Ataxin-2 interacts with FUS and intermediate-length polyglutamine expansions enhance FUS-related pathology in Amyotrophic Lateral Sclerosis. Hum. Mol. Genet. *22*, 717–728.

Ferguson, T.A., and Elman, L.B. (2007). Clinical presentation and diagnosis of amyotrophic lateral sclerosis. NeuroRehabilitation *22*, 409–416.

Fujii, R., Okabe, S., Urushido, T., Inoue, K., Yoshimura, A., Tachibana, T., Nishikawa, T., Hicks, G.G., and Takumi, T. (2005). The RNA binding protein TLS is translocated to dendritic spines by mGluR5 activation and regulates spine morphology. Current Biology *15*, 587–593.

Fujii, R., and Takumi, T. (2005). TLS facilitates transport of mRNA encoding an actin-stabilizing protein to dendritic spines. J. Cell. Sci. *118*, 5755–5765.

Fujita, K., Ito, H., Nakano, S., Kinoshita, Y., Wate, R., and Kusaka, H. (2008). Immunohistochemical identification of messenger RNA-related proteins in basophilic inclusions of adult-onset atypical motor neuron disease. Acta Neuropathol *116*, 439–445.

Fujita, Y., Fujita, S., Takatama, M., Ikeda, M., and Okamoto, K. (2011). Numerous FUS-positive inclusions in an elderly woman with motor neuron disease. Neuropathology *31*, 170–176.

Gal, J., Zhang, J., Kwinter, D.M., Zhai, J., Jia, H., Jia, J., and Zhu, H. (2011). Nuclear localization sequence of FUS and induction of stress granules by ALS mutants. Neurobiol. Aging *32*, 2323.e27–.e40.

Gallo, V., Bueno-De-Mesquita, H.B., Vermeulen, R., Andersen, P.M., Kyrozis, A., Linseisen, J., Kaaks, R., Allen, N.E., Roddam, A.W., Boshuizen, H.C., et al. (2009). Smoking and risk for amyotrophic lateral sclerosis: analysis of the EPIC cohort. Ann. Neurol. *65*, 378–385.

Garbuzova-Davis, S., Rodrigues, M.C.O., Hernandez-Ontiveros, D.G., Louis, M.K., Willing, A.E., Borlongan, C.V., and Sanberg, P.R. (2011). Amyotrophic lateral sclerosis: A neurovascular disease. Brain Research *1398*, 113–125.

Gardner, L.B. (2008). Hypoxic Inhibition of Nonsense-Mediated RNA Decay Regulates Gene Expression and the Integrated Stress Response. Mol. Cell. Biol. *28*, 3729–3741.

Gardner, L.B. (2010). Nonsense-mediated RNA decay regulation by cellular stress: implications for tumorigenesis. Mol. Cancer Res. *8*, 295–308.

Gavett, B.E., Stern, R.A., and McKee, A.C. (2011). Chronic traumatic encephalopathy: a potential late effect of sport-related concussive and subconcussive head trauma. Clin Sports Med *30*, 179–88–xi.

Gehring, N.H., Neu-Yilik, G., Schell, T., Hentze, M.W., and Kulozik, A.E. (2003). Y14 and hUpf3b form an NMD-activating complex. Mol. Cell *11*, 939–949.

Genestra, M. (2007). Oxyl radicals, redox-sensitive signalling cascades and antioxidants. Cell. Signal. *19*, 1807–1819.

Ghezzi, P., and Bonetto, V. (2003). Redox proteomics: identification of oxidatively modified proteins. Proteomics.

Gijselinck, I., Van Langenhove, T., van der Zee, J., Sleegers, K., Philtjens, S., Kleinberger, G., Janssens, J., Bettens, K., Van Cauwenberghe, C., Pereson, S., et al. (2012). A C9orf72 promoter repeat expansion in a Flanders-Belgian cohort with disorders of the frontotemporal lobar degeneration-amyotrophic lateral sclerosis spectrum: a gene identification study. Lancet Neurol *11*, 54–65.

Gilks, N., Kedersha, N., Ayodele, M., Shen, L., Stoecklin, G., Dember, L.M., and Anderson, P. (2004). Stress granule assembly is mediated by prion-like aggregation of TIA-1. Mol. Biol. Cell *15*, 5383–5398.

Goggin, K., Beaudoin, S., Grenier, C., Brown, A.-A., and Roucou, X. (2008). Prion protein aggresomes are poly(A)+ ribonucleoprotein complexes that induce a PKR-mediated deficient cell stress response. Biochim Biophys Acta *1783*, 479–491.

Goldstein, L.E., Fisher, A.M., Tagge, C.A., Zhang, X.-L., Velisek, L., Sullivan, J.A., Upreti, C., Kracht, J.M., Ericsson, M., Wojnarowicz, M.W., et al. (2012). Chronic traumatic encephalopathy in blast-exposed military veterans and a blast neurotrauma mouse model. Sci Transl Med *4*,

134ra60–134ra60.

Goodier, J.L., Zhang, L., Vetter, M.R., and Kazazian, H.H. (2007). LINE-1 ORF1 Protein Localizes in Stress Granules with Other RNA-Binding Proteins, Including Components of RNA Interference RNA-Induced Silencing Complex. Mol. Cell. Biol. *27*, 6469–6483.

Grant, A.J., and Lerner, L.M. (1979). Dialdehydes derived from adenine nucleosides as substrates and inhibitors of adenosine aminohydrolase. Biochemistry *18*, 2838–2842.

Gregersen, L.H., Schueler, M., Munschauer, M., Mastrobuoni, G., Chen, W., Kempa, S., Dieterich, C., and Landthaler, M. (2014). MOV10 Is a 5' to 3‘ RNA helicase contributing to UPF1 mRNA target degradation by translocation along 3’ UTRs. Mol. Cell *54*, 573–585.

Hadano, S., Hand, C.K., Osuga, H., Yanagisawa, Y., Otomo, A., Devon, R.S., Miyamoto, N., Showguchi-Miyata, J., Okada, Y., Singaraja, R., et al. (2001). A gene encoding a putative GTPase regulator is mutated in familial amyotrophic lateral sclerosis 2. Nat Genet *29*, 166–173.

Halliday, G., Bigio, E.H., Cairns, N.J., Neumann, M., Mackenzie, I.R.A., and Mann, D.M.A. (2012). Mechanisms of disease in frontotemporal lobar degeneration: gain of function versus loss of function effects. Acta Neuropathol *124*, 373–382.

Hallier, M., Lerga, A., Barnache, S., Tavitian, A., and Moreau-Gachelin, F. (1998). The transcription factor Spi-1/PU.1 interacts with the potential splicing factor TLS. Journal of Biological Chemistry *273*, 4838–4842.

Harding, H.P., Calfon, M., Urano, F., Novoa, I., and Ron, D. (2002). Transcriptional and translational control in the Mammalian unfolded protein response. Annu. Rev. Cell Dev. Biol. *18*, 575–599.

Hart, M.P., and Gitler, A.D. (2012). ALS-associated ataxin 2 polyQ expansions enhance stress-induced caspase 3 activation and increase TDP-43 pathological modifications. J. Neurosci. *32*, 9133–9142.

Harwood, C.A., McDermott, C.J., and Shaw, P.J. (2009). Physical activity as an exogenous risk factor in motor neuron disease (MND): a review of the evidence. Als *10*, 191–204.

Hoell, J.I., Larsson, E., Runge, S., Nusbaum, J.D., Duggimpudi, S., Farazi, T.A., Hafner, M., Borkhardt, A., Sander, C., and Tuschl, T. (2011). RNA targets of wild-type and mutant FET family proteins. Nat Struct Mol Biol *18*, 1428–

1431.

Hofmann, S., Cherkasova, V., Bankhead, P., Bukau, B., and Stoecklin, G. (2012). Translation suppression promotes stress granule formation and cell survival in response to cold shock. Mol. Biol. Cell *23*, 3786–3800.

Huang, E.J., Zhang, J., Geser, F., Trojanowski, J.Q., Strober, J.B., Dickson, D.W., Brown, R.H., Shapiro, B.E., and Lomen-Hoerth, C. (2010). Extensive FUS-immunoreactive pathology in juvenile amyotrophic lateral sclerosis with basophilic inclusions. Brain Pathol. *20*, 1069–1076.

Hüttelmaier, S., Zenklusen, D., Lederer, M., Dictenberg, J., Lorenz, M., Meng, X., Bassell, G.J., Condeelis, J., and Singer, R.H. (2005). Spatial regulation of beta-actin translation by Src-dependent phosphorylation of ZBP1. Nature *438*, 512–515.

Ichikawa, H., Shimizu, K., and Hayashi, Y. (1994). An RNA-binding protein gene, TLS/FUS, is fused to ERG in human myeloid leukemia with t (16; 21) chromosomal translocation. Cancer Res.

Iko, Y., Kodama, T.S., Kasai, N., Oyama, T., Morita, E.H., Muto, T., Okumura, M., Fujii, R., Takumi, T., Tate, S.-I., et al. (2004). Domain architectures and characterization of an RNA-binding protein, TLS. Journal of Biological Chemistry *279*, 44834–44840.

Ishigaki, S., Masuda, A., Fujioka, Y., Iguchi, Y., Katsuno, M., Shibata, A., Urano, F., Sobue, G., and Ohno, K. (2012). Position-dependent FUS-RNA interactions regulate alternative splicing events and transcriptions. Sci Rep *2*, 529.

Ito, D., Seki, M., Tsunoda, Y., Uchiyama, H., and Suzuki, N. (2011). Nuclear transport impairment of amyotrophic lateral sclerosis-linked mutations in FUS/TLS. Ann. Neurol. *69*, 152–162.

Ivanov, P., Kedersha, N., and Anderson, P. (2011). Stress puts TIA on TOP. Genes Dev. *25*, 2119–2124.

Jain, S., and Parker, R. (2013). The discovery and analysis of P Bodies. Adv. Exp. Med. Biol. *768*, 23–43.

Jamison, J.T., Kayali, F., Rudolph, J., Marshall, M., Kimball, S.R., and DeGracia, D.J. (2008). Persistent redistribution of poly-adenylated mRNAs correlates with translation arrest and cell death following global brain ischemia and reperfusion. Nsc *154*, 504–520.

Kabashi, E., Valdmanis, P.N., Dion, P., Spiegelman, D., McConkey, B.J., Velde, C.V., Bouchard, J.-P., Lacomblez, L., Pochigaeva, K., Salachas, F., et al. (2008). TARDBP mutations in individuals with sporadic and familial amyotrophic lateral sclerosis. Nat Genet *40*, 572–574.

Kaehler, C., Isensee, J., Nonhoff, U., Terrey, M., Hucho, T., Lehrach, H., and Krobitsch, S. (2012). Ataxin-2-like is a regulator of stress granules and processing bodies. PLoS ONE *7*, e50134.

Kanai, Y., Dohmae, N., and Hirokawa, N. (2004). Kinesin Transports RNA. Neuron *43*, 513–525.

Kasarskis, E.J., Lindquist, J.H., Coffman, C.J., Grambow, S.C., Feussner, J.R., Allen, K.D., Oddone, E.Z., Kamins, K.A., Horner, R.D., Als Gulf War Clinical Review Team (2009). Clinical aspects of ALS in Gulf War veterans. Als *10*, 35–41.

Kato, M., Han, T.W., Xie, S., Shi, K., Du, X., Wu, L.C., Mirzaei, H., Goldsmith, E.J., Longgood, J., Pei, J., et al. (2012). Cell-free Formation of RNA Granules: Low Complexity Sequence Domains Form Dynamic Fibers within Hydrogels. Cell *149*, 753–767.

Kayali, F., Montie, H.L., Rafols, J.A., and DeGracia, D.J. (2005). Prolonged translation arrest in reperfused hippocampal cornu Ammonis 1 is mediated by stress granules. Nsc *134*, 1223–1245.

Kedersha, N., and Anderson, P. (2002). Stress granules: sites of mRNA triage that regulate mRNA stability and translatability. Biochem. Soc. Trans. *30*, 963–969.

Kedersha, N.L., Gupta, M., Li, W., Miller, I., and Anderson, P. (1999). RNA-binding proteins TIA-1 and TIAR link the phosphorylation of eIF-2 alpha to the assembly of mammalian stress granules. J. Cell Biol. *147*, 1431–1442.

Kedersha, N., Cho, M.R., Li, W., Yacono, P.W., Chen, S., Gilks, N., Golan, D.E., and Anderson, P. (2000). Dynamic Shuttling of Tia-1 Accompanies the Recruitment of mRNA to Mammalian Stress Granules. J. Cell Biol. *151*, 1257–1268.

Kedersha, N., and Anderson, P. (2007). Mammalian stress granules and processing bodies. Meth. Enzymol. *431*, 61–81.

Kedersha, N., Stoecklin, G., Ayodele, M., Yacono, P., Lykke-Andersen, J., Fritzler, M.J., Scheuner, D., Kaufman, R.J., Golan, D.E., and Anderson, P. (2005). Stress granules and processing bodies are dynamically linked

sites of mRNP remodeling. J. Cell Biol. *169*, 871–884.

Keller, A., Nesvizhskii, A.I., Kolker, E., and Aebersold, R. (2002). Empirical statistical model to estimate the accuracy of peptide identifications made by MS/MS and database search. Anal Chem *74*, 5383–5392.

Kiernan, M.C., Vucic, S., Cheah, B.C., Turner, M.R., Eisen, A., Hardiman, O., Burrell, J.R., and Zoing, M.C. (2011). Amyotrophic lateral sclerosis. Lancet *377*, 942–955.

Kim, S.H., Dong, W.K., Weiler, I.J., and Greenough, W.T. (2006). Fragile X mental retardation protein shifts between polyribosomes and stress granules after neuronal injury by arsenite stress or in vivo hippocampal electrode insertion. J. Neurosci. *26*, 2413–2418.

Kimball, S.R., Horetsky, R.L., Ron, D., Jefferson, L.S., and Harding, H.P. (2003). Mammalian stress granules represent sites of accumulation of stalled translation initiation complexes. Am. J. Physiol., Cell Physiol. *284*, C273–C284.

King, O.D., Gitler, A.D., and Shorter, J. (2012). The tip of the iceberg: RNA-binding proteins with prion-like domains in neurodegenerative disease. Brain Research *1462*, 61–80.

Kino, Y., Washizu, C., Aquilanti, E., Okuno, M., Kurosawa, M., Yamada, M., Doi, H., and Nukina, N. (2011). Intracellular localization and splicing regulation of FUS/TLS are variably affected by amyotrophic lateral sclerosis-linked mutations. Nucleic Acids Research *39*, 2781–2798.

Kovar, H. (2011). Dr. Jekyll and Mr. Hyde: The Two Faces of the FUS/EWS/TAF15 Protein Family. Sarcoma *2011*, 837474–13.

Kwiatkowski, T.J.J., Bosco, D.A., Leclerc, A.L., Tamrazian, E., Vanderburg, C.R., Russ, C., Davis, A., Gilchrist, J., Kasarskis, E.J., Munsat, T., et al. (2009). Mutations in the FUS/TLS gene on chromosome 16 cause familial amyotrophic lateral sclerosis. Science *323*, 1205–1208.

Lagier-Tourenne, C., Polymenidou, M., Hutt, K.R., Vu, A.Q., Baughn, M., Huelga, S.C., Clutario, K.M., Ling, S.-C., Liang, T.Y., Mazur, C., et al. (2012). Divergent roles of ALS-linked proteins FUS/TLS and TDP-43 intersect in processing long pre-mRNAs. Nature Publishing Group *15*, 1488–1497.

LaMonte, B.H., Wallace, K.E., Holloway, B.A., Shelly, S.S., Ascano, J., Tokito, M., Van Winkle, T., Howland, D.S., and Holzbaur, E.L.F. (2002). Disruption of dynein/dynactin inhibits axonal transport in motor neurons

causing late-onset progressive degeneration. Neuron *34*, 715–727.

Lanson, N.A., Jr, and Pandey, U.B. (2012). FUS-related proteinopathies: Lessons from animal models. Brain Research *1462*, 44–60.

Lavut, A., and Raveh, D. (2012). Sequestration of highly expressed mRNAs in cytoplasmic granules, P-bodies, and stress granules enhances cell viability. PLoS Genet *8*, e1002527.

Lee, B.J., Cansizoglu, A.E., Süel, K.E., Louis, T.H., Zhang, Z., and Chook, Y.M. (2006). Rules for nuclear localization sequence recognition by karyopherin beta 2. Cell *126*, 543–558.

Lerga, A., Hallier, M., Delva, L., Orvain, C., Gallais, I., Marie, J., and Moreau-Gachelin, F. (2001). Identification of an RNA binding specificity for the potential splicing factor TLS. Journal of Biological Chemistry *276*, 6807–6816.

Leung,A.K., Calabrese,J.M. and Sharp,P.A. (2006) Quantitative analysis of Argonaute protein reveals microRNA-dependent localization to stress granules. Proc. Natl Acad. Sci. USA, *103*, 18125–18130.

Leung, A.K.L., Vyas, S., Rood, J.E., Bhutkar, A., Sharp, P.A., and Chang, P. (2011). Poly(ADP-ribose) regulates stress responses and microRNA activity in the cytoplasm. Mol. Cell *42*, 489–499.

Li, X., Thompson, D., Kumar, B., and DeMartino, G.N. (2014). Molecular and cellular roles of PI31 (PSMF1) protein in regulation of proteasome function. J. Biol. Chem. *289*, 17392–17405.

Li, Y.R., King, O.D., Shorter, J., and Gitler, A.D. (2013). Stress granules as crucibles of ALS pathogenesis. J. Cell Biol. *201*, 361–372.

Ling, S.-C., Fahrner, P.S., Greenough, W.T., and Gelfand, V.I. (2004). Transport of Drosophila fragile X mental retardation protein-containing ribonucleoprotein granules by kinesin-1 and cytoplasmic dynein. Proc. Natl. Acad. Sci. U.S.a. *101*, 17428–17433.

Ling, S.-C., Polymenidou, M., and Cleveland, D.W. (2013). Converging Mechanisms in ALS and FTD: Disrupted RNA and Protein Homeostasis. Neuron *79*, 416–438.

Liu, L., Wise, D.R., Diehl, J.A., and Simon, M.C. (2008). Hypoxic reactive oxygen species regulate the integrated stress response and cell survival. Journal of Biological Chemistry *283*, 31153–31162.

Liu-Yesucevitz, L., Bassell, G.J., Gitler, A.D., Hart, A.C., Klann, E., Richter, J.D., Warren, S.T., and Wolozin, B. (2011). Local RNA Translation at the Synapse and in Disease. Journal of Neuroscience *31*, 16086–16093.

Liu-Yesucevitz, L., Bilgutay, A., Zhang, Y.-J., Vanderweyde, T., Vanderwyde, T., Citro, A., Mehta, T., Zaarur, N., McKee, A., Bowser, R., et al. (2010a). Tar DNA binding protein-43 (TDP-43) associates with stress granules: analysis of cultured cells and pathological brain tissue. PLoS ONE *5*, e13250.

Liu-Yesucevitz, L., Bilgutay, A., Zhang, Y.-J., Vanderwyde, T., Citro, A., Mehta, T., Zaarur, N., McKee, A., Bowser, R., Sherman, M., et al. (2010b). Tar DNA Binding Protein-43 (TDP-43) Associates with Stress Granules: Analysis of Cultured Cells and Pathological Brain Tissue. PLoS ONE *5*, e13250.

Lloyd, R.E. (2012). How Do Viruses Interact with Stress-Associated RNA Granules? PLoS Pathog. *8*, e1002741.

Lo, K.W.-H., Kogoy, J.M., Rasoul, B.A., King, S.M., and Pfister, K.K. (2007). Interaction of the DYNLT (TCTEX1/RP3) light chains and the intermediate chains reveals novel intersubunit regulation during assembly of the dynein complex. Journal of Biological Chemistry *282*, 36871–36878.

Logroscino, G., Traynor, B.J., Hardiman, O., Chio, A., Mitchell, D., Swingler, R.J., Millul, A., Benn, E., Beghi, E., EURALS (2010). Incidence of amyotrophic lateral sclerosis in Europe. Journal of Neurology, Neurosurgery & Psychiatry *81*, 385–390.

Lomen Hoerth, C., Anderson, T., and Miller, B. (2002). The overlap of amyotrophic lateral sclerosis and frontotemporal dementia. Neurology *59*, 1077–1079.

Loschi, M., Leishman, C.C., Berardone, N., and Boccaccio, G.L. (2009). Dynein and kinesin regulate stress-granule and P-body dynamics. J. Cell. Sci. *122*, 3973–3982.

Low, W.K., Dang, Y., Schneider-Poetsch, T., Shi, Z., and Choi, N.S. (2005). Inhibition of eukaryotic translation initiation by the marine natural product pateamine A. Mol. Cell *20*, 709–722.

Lykke-Andersen, J., Shu, M.D., and Steitz, J.A. (2000). Human Upf proteins target an mRNA for nonsense-mediated decay when bound downstream of a termination codon. Cell *103*, 1121–1131.

Marko, M., Vlassis, A., Guialis, A., and Leichter, M. (2012). Domains involved in TAF15 subcellular localisation: Dependence on cell type and ongoing transcription. Gene *506*, 331–338.

Mastrocola A. S., Kim S. H., Trinh A. T., Rodenkirch L. A., & Tibbetts R. S (2013) The RNA binding protein fused in sarcoma (FUS) functions downstream of PARP in response to DNA damage. Journal of Biological Chemistry 288(34): 24731–24741.

Mazroui, R. et al. (2002) Trapping of messenger RNA by Fragile X Mental Retardation protein into cytoplasmic granules induces translation repression. Hum. Mol. Genet. *11*, 3007–30017

Mazroui, R., Di Marco, S., Kaufman, R.J., and Gallouzi, I.-E. (2007). Inhibition of the ubiquitin-proteasome system induces stress granule formation. Mol. Biol. Cell *18*, 2603–2618.

Mazroui, R., Sukarieh, R., Bordeleau, M.-E., Kaufman, R.J., Northcote, P., Tanaka, J., Gallouzi, I., and Pelletier, J. (2006). Inhibition of ribosome recruitment induces stress granule formation independently of eukaryotic initiation factor 2alpha phosphorylation. Mol. Biol. Cell *17*, 4212–4219.

McDonald, K.K., Aulas, A., Destroismaisons, L., Pickles, S., Beleac, E., Camu, W., Rouleau, G.A., and Vande Velde, C. (2011). TAR DNA-binding protein 43 (TDP-43) regulates stress granule dynamics via differential regulation of G3BP and TIA-1. Hum. Mol. Genet. *20*, 1400–1410.

Meissner, M., Lopato, S., Gotzmann, J., Sauermann, G., and Barta, A. (2003). Proto-oncoprotein TLS/FUS is associated to the nuclear matrix and complexed with splicing factors PTB, SRm160, and SR proteins. Exp. Cell Res. *283*, 184–195.

Meister G, Landthaler M, Peters L, Chen PY, Urlaub H, et al. (2005) Identification of novel argonaute-associated proteins. Curr Biol *15*: 2149–2155

Mendell, J.T., Sharifi, N.A., Meyers, J.L., Martinez-Murillo, F., and Dietz, H.C. (2004). Nonsense surveillance regulates expression of diverse classes of mammalian transcripts and mutes genomic noise. Nat Genet *36*, 1073–1078.

Mokas, S., Mills, J.R., Garreau, C., Fournier, M.-J., Robert, F., Arya, P., Kaufman, R.J., Pelletier, J., and Mazroui, R. (2009). Uncoupling stress granule assembly and translation initiation inhibition. Mol. Biol. Cell *20*, 2673–2683.

Morimoto, R.I. (2011). The heat shock response: systems biology of proteotoxic stress in aging and disease. Cold Spring Harb. Symp. Quant. Biol. *76*, 91–99.

Munoz, D.G., Neumann, M., Kusaka, H., Yokota, O., Ishihara, K., Terada, S., Kuroda, S., and Mackenzie, I.R. (2009). FUS pathology in basophilic inclusion body disease. Acta Neuropathol *118*, 617–627.

Nakaya, T., Alexiou, P., Maragkakis, M., Chang, A., and Mourelatos, Z. (2013). FUS regulates genes coding for RNA-binding proteins in neurons by binding to their highly conserved introns. Rna *19*, 498–509.

Nesvizhskii, A.I., Keller, A., Kolker, E., and Aebersold, R. (2003). A statistical model for identifying proteins by tandem mass spectrometry. Anal Chem *75*, 4646–4658.

Neumann, M., Rademakers, R., Roeber, S., Baker, M., Kretzschmar, H.A., and Mackenzie, I.R.A. (2009a). A new subtype of frontotemporal lobar degeneration with FUS pathology. Brain *132*, 2922–2931.

Neumann, M., Roeber, S., Kretzschmar, H.A., Rademakers, R., Baker, M., and Mackenzie, I.R. (2009b). Abundant FUS-immunoreactive pathology in neuronal intermediate filament inclusion disease. Acta Neuropathol *118*, 605–616.

Neumann, M., Sampathu, D.M., Kwong, L.K., Truax, A.C., Micsenyi, M.C., Chou, T.T., Bruce, J., Schuck, T., Grossman, M., Clark, C.M., et al. (2006). Ubiquitinated TDP-43 in Frontotemporal Lobar Degeneration and Amyotrophic Lateral Sclerosis. Science *314*, 130–133.

Neumann, M., Bentmann, E., Dormann, D., Jawaid, A., DeJesus-Hernandez, M., Ansorge, O., Roeber, S., Kretzschmar, H.A., Munoz, D.G., Kusaka, H., et al. (2011). FET proteins TAF15 and EWS are selective markers that distinguish FTLD with FUS pathology from amyotrophic lateral sclerosis with FUS mutations. Brain *134*, 2595–2609.

Nevins, T.A., Harder, Z.M., Korneluk, R.G., and Holcík, M. (2003). Distinct regulation of internal ribosome entry site-mediated translation following cellular stress is mediated by apoptotic fragments of eIF4G translation initiation factor family members eIF4GI and p97/DAP5/NAT1. Journal of Biological Chemistry *278*, 3572–3579.

Nishimura, A.L., Mitne-Neto, M., Silva, H.C.A., Richieri-Costa, A., Middleton, S., Cascio, D., Kok, F., Oliveira, J.R.M., Gillingwater, T., Webb, J., et al. (2004). A mutation in the vesicle-trafficking protein VAPB causes late-

onset spinal muscular atrophy and amyotrophic lateral sclerosis. Am. J. Hum. Genet. *75*, 822–831.

Onishi, H., Kino, Y., Morita, T., Futai, E., Sasagawa, N., and Ishiura, S. (2008). MBNL1 associates with YB-1 in cytoplasmic stress granules. J. Neurosci. Res. *86*, 1994–2002.

Piazza, O., Sirén, A.-L., and Ehrenreich, H. (2004). Soccer, neurotrauma and amyotrophic lateral sclerosis: is there a connection? Www.Informahealthcare.com/Cmo *20*, 505–508.

Puls, I., Jonnakuty, C., LaMonte, B.H., Holzbaur, E.L.F., Tokito, M., Mann, E., Floeter, M.K., Bidus, K., Drayna, D., Oh, S.J., et al. (2003). Mutant dynactin in motor neuron disease. Nat Genet *33*, 455–456.

Quaresma, A.J., Bressan,G.C., Gava,L.M., Lanza,D.C., Ramos,C.H., Kobarg,J. (2009) Human hnRNP Q re-localizes to cytoplasmic granules upon PMA, thapsigargin, arsenite and heat-shock treatments. Exp. Cell Res., *315*, 968-980.

Rabbitts, T.H., Forster, A., Larson, R., and Nathan, P. (1993). Fusion of the dominant negative transcription regulator CHOP with a novel gene FUS by translocation t(12;16) in malignant liposarcoma. Nat Genet *4*, 175–180.

Rademakers, R., Neumann, M., and Mackenzie, I.R. (2012). Advances in understanding the molecular basis of frontotemporal dementia. Nature Reviews Neurology *8*, 423–434.

Rajyaguru, P., and Parker, R. (2012). RGG motif proteins: Modulators of mRNA functional states. Cell Cycle *11*, 2594–2599.

Rajyaguru, P., She, M., and Parker, R. (2012). Scd6 targets eIF4G to repress translation: RGG motif proteins as a class of eIF4G-binding proteins. Mol. Cell *45*, 244–254.

Rand, T.A., Petersen, S., Du, F., and Wang, X. (2005). Argonaute2 Cleaves the Anti-Guide Strand of siRNA during RISC Activation. Cell *123*, 621–629.

Rappsilber, J., Friesen, W.J., Paushkin, S., Dreyfuss, G., and Mann, M. (2003). Detection of arginine dimethylated peptides by parallel precursor ion scanning mass spectrometry in positive ion mode. Anal Chem *75*, 3107–3114.

Ralser M, Albrecht M, Nonhoff U, Lengauer T, Lehrach H, et al. (2005) An integrative approach to gain insights into the cellular function of human

ataxin-2. J Mol Biol *346*: 203–214.

Renton, A.E., Majounie, E., Waite, A., Simón-Sánchez, J., Rollinson, S., Gibbs, J.R., Schymick, J.C., Laaksovirta, H., van Swieten, J.C., Myllykangas, L., et al. (2011). A Hexanucleotide Repeat Expansion in C9ORF72 Is the Cause of Chromosome 9p21-Linked ALS-FTD. Neuron *72*, 257–268.

Richter, J.D. (2007). CPEB: a life in translation. Trends Biochem. Sci. *32*, 279–285.

Rodríguez-Gabriel, M.A., Watt, S., Bähler, J., and Russell, P. (2006). Upf1, an RNA helicase required for nonsense-mediated mRNA decay, modulates the transcriptional response to oxidative stress in fission yeast. Mol. Cell. Biol. *26*, 6347–6356.

Rogelj, B., Easton, L.E., Bogu, G.K., Stanton, L.W., Rot, G., Curk, T., Zupan, B., Sugimoto, Y., Modic, M., Haberman, N., et al. (2012). Widespread binding of FUS along nascent RNA regulates alternative splicing in the brain. Sci Rep *2*, 603.

Rosen, D.R., Siddique, T., Patterson, D., Figlewicz, D.A., Sapp, P., Hentati, A., Donaldson, D., Goto, J., O'Regan, J.P., and Deng, H.X. (1993). Mutations in Cu/Zn superoxide dismutase gene are associated with familial amyotrophic lateral sclerosis. Nature *362*, 59–62.

Rotunno, M.S., and Bosco, D.A. (2013). An emerging role for misfolded wild-type SOD1 in sporadic ALS pathogenesis. Front Cell Neurosci *7*, 253.

Rotunno, M.S., Auclair, J.R., Maniatis, S., Shaffer, S.A., Agar, J., and Bosco, D.A. (2014). Identification of a misfolded region in superoxide dismutase 1 that is exposed in amyotrophic lateral sclerosis. J. Biol. Chem. *289*, 28527–28538.

Rulten S. L., Rotheray A., Green R. L., Grundy G. J., Moore D. A., Gomez-Herreros F., . . . Caldecott K. W (2013) PARP-1 depend- ent recruitment of the amyotrophic lateral sclerosis-associated protein FUS/TLS to sites of oxidative DNA damage. Nucleic Acids Research 42(1): 307–314.

Sama, R.R.K., Ward, C.L., Kaushansky, L.J., Lemay, N., Ishigaki, S., Urano, F., and Bosco, D.A. (2013). FUS/TLS assembles into stress granules and is a prosurvival factor during hyperosmolar stress. Journal of Cellular Physiology *228*, 2222–2231.

Sama, R.R.K., Ward, C.L., and Bosco, D.A. (2014). Functions of FUS/TLS from DNA repair to stress response: implications for ALS. ASN Neuro *6*.

Shevchenko, A., Tomas, H., Havli sbreve, J., Olsen, J.V., and Mann, M. (2007). In-gel digestion for mass spectrometric characterization of proteins and proteomes. Nat Protoc *1*, 2856–2860.

Schäffler, K., Schulz, K., Hirmer, A., Wiesner, J., Grimm, M., Sickmann, A., and Fischer, U. (2010). A stimulatory role for the La-related protein 4B in translation. RNA *16*, 1488–1499.

Schreiber, V., Dantzer, F., Ame, J.-C., and de Murcia, G. (2006). Poly(ADP-ribose): novel functions for an old molecule. Nat Rev Mol Cell Biol *7*, 517–528.

Schwanhäusser, B., Busse, D., Li, N., Dittmar, G., Schuchhardt, J., Wolf, J., Chen, W., and Selbach, M. (2011). Global quantification of mammalian gene expression control. Nature *473*, 337–342.

Seelaar, H., Rohrer, J.D., Pijnenburg, Y.A.L., Fox, N.C., and van Swieten, J.C. (2010). Clinical, genetic and pathological heterogeneity of frontotemporal dementia: a review. Journal of Neurology, Neurosurgery & Psychiatry *82*, jnnp.2010.212225–jnnp.2010.212486.

Shenton, D., Smirnova, J.B., Selley, J.N., Carroll, K., Hubbard, S.J., Pavitt, G.D., Ashe, M.P., and Grant, C.M. (2006). Global translational responses to oxidative stress impact upon multiple levels of protein synthesis. Journal of Biological Chemistry *281*, 29011–29021.

Shi, Y. (2012). Alternative polyadenylation: new insights from global analyses. Rna *18*, 2105–2117.

Solomon, S. et al. (2007) Distinct structural features of caprin-1 mediate its interaction with G3BP-1 and its induction of phosphorylation of eukaryotic translation initiation factor 2alpha, entry to cytoplasmic stress granules, and selective interaction with a subset of mRNAs. Mol. Cell Biol. *27*, 2324–2342

Somasekharan, S.P., El-Naggar, A., Leprivier, G., Cheng, H., Hajee, S., Grunewald, T.G.P., Zhang, F., Ng, T., Delattre, O., Evdokimova, V., et al. (2015). YB-1 regulates stress granule formation and tumor progression by translationally activating G3BP1. J. Cell Biol. *208*, 913–929.

Somasekharan, S.P., El-Naggar, A., Leprivier, G., Cheng, H., Hajee, S., Grunewald, T.G.P., Zhang, F., Ng, T., Delattre, O., Evdokimova, V., et al. (2015). YB-1 regulates stress granule formation and tumor progression by translationally activating G3BP1. J. Cell Biol. *208*, 913–929.

Spriggs, K.A., Bushell, M., and Willis, A.E. (2010). Translational regulation of gene expression during conditions of cell stress. Mol. Cell *40*, 228–237.

Sreedharan, J., Blair, I.P., Tripathi, V.B., Hu, X., and Vance, C. (2008). TDP-43 mutations in familial and sporadic amyotrophic lateral sclerosis. Science *319*, 1668–1672.

Sreedharan, J., and Brown, R.H., Jr. (2013). Amyotrophic lateral sclerosis: Problems and prospects. Ann. Neurol. *74*, 309-316.

Stöhr, N., Lederer, M., Reinke, C., Meyer, S., Hatzfeld, M., Singer, R.H., and Hüttelmaier, S. (2006). ZBP1 regulates mRNA stability during cellular stress. J. Cell Biol. *175*, 527–534.

Strambio-De-Castillia, C., Niepel, M., and Rout, M.P. (2010). The nuclear pore complex: bridging nuclear transport and gene regulation. Nat Rev Mol Cell Biol *11*, 490–501.

Sun, Z., Diaz, Z., Fang, X., Hart, M.P., Chesi, A., Shorter, J., and Gitler, A.D. (2011). Molecular determinants and genetic modifiers of aggregation and toxicity for the ALS disease protein FUS/TLS. Plos Biol *9*, e1000614.

Sutherland, B.W., Toews, J., and Kast, J. (2008). Utility of formaldehyde cross-linking and mass spectrometry in the study of protein–protein interactions. J. Mass Spectrom. *43*, 699–715.

Takahama, K., Arai, S., Kurokawa, R., and Oyoshi, T. (2009). Identification of DNA binding specificity for TLS. Nucleic Acids Symposium Series 247–248.

Takahama, K., Takada, A., Tada, S., Shimizu, M., Sayama, K., Kurokawa, R., and Oyoshi, T. (2013). Regulation of telomere length by G-quadruplex telomere DNA- and TERRA-binding protein TLS/FUS. Chem. Biol. *20*, 341–350.

Takahashi, M. et al. (2013) Stress granules inhibit apoptosis by reducing reactive oxygen species production. Mol. Cell. Biol. *33*, 815–829

Takarada, T., Tamaki, K., Takumi, T., Ogura, M., Ito, Y., Nakamichi, N., and Yoneda, Y. (2009). A protein-protein interaction of stress-responsive myosin VI endowed to inhibit neural progenitor self-replication with RNA binding protein, TLS, in murine hippocampus. Journal of Neurochemistry *110*, 1457–1468.

Talbot, K. (2009). Motor neuron disease: the bare essentials. Pract Neurol *9*,

303–309.

Tan, A.Y., and Manley, J.L. (2009). The TET Family of Proteins: Functions and Roles in Disease. Journal of Molecular Cell Biology *1*, 82–92.

Tan, A.Y., and Manley, J.L. (2010). TLS inhibits RNA polymerase III transcription. Mol. Cell. Biol. *30*, 186–196.

Ticozzi, N., Vance, C., Leclerc, A.L., Keagle, P., Glass, J.D., McKenna-Yasek, D., Sapp, P.C., Silani, V., Bosco, D.A., Shaw, C.E., et al. (2011). Mutational analysis reveals the FUS homolog TAF15 as a candidate gene for familial amyotrophic lateral sclerosis. Am. J. Med. Genet. B Neuropsychiatr. Genet. *156B*, 285–290.

Thakor, N., and Holcik, M. (2012). IRES-mediated translation of cellular messenger RNA operates in eIF2 - independent manner during stress. Nucleic Acids Research *40*, 541–552.

Thomas, M.G., Martinez Tosar, L.J., Desbats, M.A., Leishman, C.C., and Boccaccio, G.L. (2009). Mammalian Staufen 1 is recruited to stress granules and impairs their assembly. J. Cell. Sci. *122*, 563–573.

Tourrière, H., Chebli, K., Zekri, L., Courselaud, B., Blanchard, J.M., Bertrand, E., and Tazi, J. (2003). The RasGAP-associated endoribonuclease G3BP assembles stress granules. J. Cell Biol. *160*, 823–831.

Tradewell, M.L., Yu, Z., Tibshirani, M., Boulanger, M.-C., Durham, H.D., and Richard, S. (2012). Arginine methylation by PRMT1 regulates nuclear-cytoplasmic localization and toxicity of FUS/TLS harbouring ALS-linked mutations. Hum. Mol. Genet. *21*, 136–149.

Traxinger, K., Kelly, C., Johnson, B.A., Lyles, R.H., and Glass, J.D. (2013). Prognosis and epidemiology of amyotrophic lateral sclerosis: Analysis of a clinic population, 1997-2011. Neurol Clin Pract *3*, 313–320.

Tsai, N.-P., Tsui, Y.-C., and Wei, L.-N. (2009). Dynein motor contributes to stress granule dynamics in primary neurons. Neuroscience *159*, 647–656.

van der Laan, A.M.A., van Gemert, A.M.C., Dirks, R.W., Noordermeer, J.N., Fradkin, L.G., Tanke, H.J., and Jost, C.R. (2012). mRNA cycles through hypoxia-induced stress granules in live Drosophila embryonic muscles. Int. J. Dev. Biol. *56*, 701–709.

Vance, C., Scotter, E.L., Nishimura, A.L., Troakes, C., Mitchell, J.C., Kathe, C., Urwin, H., Manser, C., Miller, C.C., Hortobágyi, T., et al. (2013). ALS

mutant FUS disrupts nuclear localization and sequesters wild-type FUS within cytoplasmic stress granules. Hum. Mol. Genet. *22*, 2676–2688.

Vance, C., Rogelj, B., Hortobágyi, T., De Vos, K.J., Nishimura, A.L., Sreedharan, J., Hu, X., Smith, B., Ruddy, D., Wright, P., et al. (2009). Mutations in FUS, an RNA processing protein, cause familial amyotrophic lateral sclerosis type 6. Science *323*, 1208–1211.

Vanderweyde, T., Youmans, K., Liu-Yesucevitz, L., and Wolozin, B. (2013). Role of stress granules and RNA-binding proteins in neurodegeneration: a mini-review. Gerontology *59*, 524–533.

Vanderweyde, T., Yu, H., Varnum, M., Liu-Yesucevitz, L., Citro, A., Ikezu, T., Duff, K., and Wolozin, B. (2012). Contrasting pathology of the stress granule proteins TIA-1 and G3BP in tauopathies. J. Neurosci. *32*, 8270–8283.

Vessey, J.P., Vaccani, A., Xie, Y., Dahm, R., Karra, D., Kiebler, M.A., and Macchi, P. (2006). Dendritic localization of the translational repressor Pumilio 2 and its contribution to dendritic stress granules. J. Neurosci. *26*, 6496–6508.

Wang W. Y., Pan L., Su S. C., Quinn E. J., Sasaki M., Jimenez J. C., . . . Tsai L. H (2013) Interaction of FUS and HDAC1 regu- lates DNA damage response and repair in neurons. Nature Neuroscience 16: 1383–1391.

Wang, X., Arai, S., Song, X., Reichart, D., Du, K., Pascual, G., Tempst, P., Rosenfeld, M.G., Glass, C.K., and Kurokawa, R. (2008). Induced ncRNAs allosterically modify RNA-binding proteins in cis to inhibit transcription. Nature *454*, 126–130.

Wanschers, B., van de Vorstenbosch, R., Wijers, M., Wieringa, B., King, S.M., and Fransen, J. (2008). Rab6 family proteins interact with the dynein light chain protein DYNLRB1. Cell Motil. Cytoskeleton *65*, 183–196.

Weidensdorfer, D., Stohr, N., Baude, A., Lederer, M., Kohn, M., Schierhorn, A., Buchmeier, S., Wahle, E., and Huttelmaier, S. (2008). Control of c-myc mRNA stability by IGF2BP1-associated cytoplasmic RNPs. RNA *15*, 104–115.

Wicks, P., Ganesalingham, J., Collin, C., Prevett, M., Leigh, N.P., and Al-Chalabi, A. (2007). Three soccer playing friends with simultaneous amyotrophic lateral sclerosis. ALS *8*, 177–179.

Williamson, T.L., and Cleveland, D.W. (1999). Slowing of axonal transport is a

very early event in the toxicity of ALS-linked SOD1 mutants to motor neurons. Nat. Neurosci. *2*, 50–56.

Wippich, F., Bodenmiller, B., Trajkovska, M.G., Wanka, S., Aebersold, R., and Pelkmans, L. (2013). Dual Specificity Kinase DYRK3 Couples Stress Granule Condensation/Dissolution to mTORC1 Signaling. Cell *152*, 791–805.

Wolozin, B. (2012). Regulated protein aggregation: stress granules and neurodegeneration. Mol Neurodegener *7*, 56.

Woulfe, J., Gray, D.A., and Mackenzie, I.R.A. (2010). FUS-immunoreactive intranuclear inclusions in neurodegenerative disease. Brain Pathol. *20*, 589–597.

Yamaguchi, A., and Kitajo, K. (2012). The effect of PRMT1-mediated arginine methylation on the subcellular localization, stress granules, and detergent-insoluble aggregates of FUS/TLS. PLoS ONE *7*, e49267.

Yang, L., Embree, L.J., Tsai, S., and Hickstein, D.D. (1998). Oncoprotein TLS interacts with serine-arginine proteins involved in RNA splicing. Journal of Biological Chemistry *273*, 27761–27764.

Yang, R., Gaidamakov, S.A., Xie, J., Lee, J., Martino, L., Kozlov, G., Crawford, A.K., Russo, A.N., Conte, M.R., Gehring, K., et al. (2011). La-related protein 4 binds poly(A), interacts with the poly(A)-binding protein MLLE domain via a variant PAM2w motif, and can promote mRNA stability. Mol. Cell. Biol. *31*, 542–556.

Yang, Y., Hentati, A., Deng, H.X., Dabbagh, O., Sasaki, T., Hirano, M., Hung, W.Y., Ouahchi, K., Yan, J., Azim, A.C., et al. (2001). The gene encoding alsin, a protein with three guanine-nucleotide exchange factor domains, is mutated in a form of recessive amyotrophic lateral sclerosis. Nat Genet *29*, 160–165.

Yang, L., Gal, J., Chen, J., and Zhu, H. (2014). Self-assembled FUS binds active chromatin and regulates gene transcription. Proceedings of the National Academy of Sciences *111*, 17809–17814.

Yasuda, K., Zhang, H., Loiselle, D., Haystead, T., Macara, I.G., and Mili, S. (2013). The RNA-binding protein Fus directs translation of localized mRNAs in APC-RNP granules. J. Cell Biol. *203*, 737–746.

Yoshimura, A., Fujii, R., Watanabe, Y., Okabe, S., Fukui, K., and Takumi, T. (2006). Myosin-Va facilitates the accumulation of mRNA/protein complex

in dendritic spines. Current Biology *16*, 2345–2351.

Zakaryan, R.P., and Gehring, H. (2006). Identification and Characterization of the Nuclear Localization/Retention Signal in the EWS Proto-oncoprotein. Journal of Molecular Biology *363*, 27–38.

Zetterström, P., Stewart, H.G., Bergemalm, D., Jonsson, P.A., Graffmo, K.S., Andersen, P.M., Brannstrom, T., Oliveberg, M., and Marklund, S.L. (2007). Soluble misfolded subfractions of mutant superoxide dismutase-1s are enriched in spinal cords throughout life in murine ALS models. Proc. Natl. Acad. Sci. U.S.a. *104*, 14157–14162.

Zhang, Z.C., and Chook, Y.M. (2012). Structural and energetic basis of ALS-causing mutations in the atypical proline-tyrosine nuclear localization signal of the Fused in Sarcoma protein (FUS). Proceedings of the National Academy of Sciences *109*, 12017–12021.

Zinszner, H., Albalat, R., and Ron, D. (1994). A novel effector domain from the RNA-binding protein TLS or EWS is required for oncogenic transformation by CHOP. Genes Dev. *8*, 2513–2526.

Zinszner, H., Sok, J., Immanuel, D., Yin, Y., and Ron, D. (1997). TLS (FUS) binds RNA in vivo and engages in nucleo-cytoplasmic shuttling. J. Cell. Sci. *110 (Pt 15)*, 1741–1750.